U.PORTO
FEUP FACULDADE DE ENGENHARIA
UNIVERSIDADE DO PORTO

FACULDADE DA ENGENHARIA DA UNIVERSIDADE DO PORTO

TURBULENCE MODELS FOR VISCOELASTIC FLUIDS

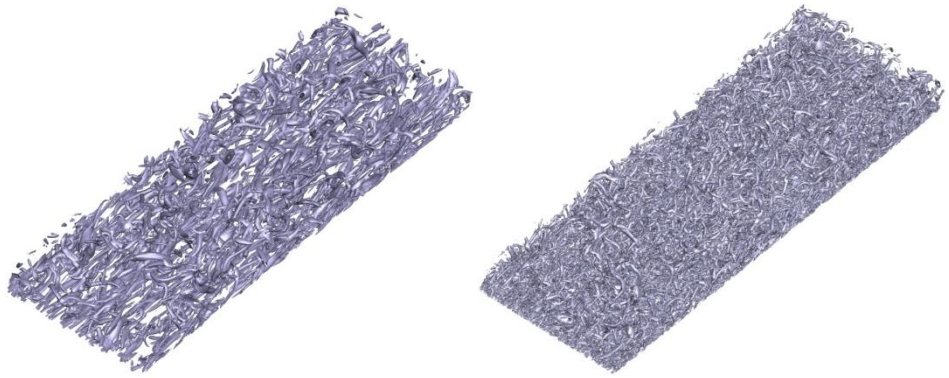

A Thesis submitted in partial fulfillment of the requirements for the degree of
Doctor of Philosophy in Mechanical Engineering by

Mohammadali Masoudian

Supervisor:
Professor Fernando T. Pinho

December 2015

To my family "Maman, Peyman and Marjan", for their fully developed, steady state support and love.

ABSTRACT

The main objectives of this thesis are the increase of our understanding and knowledge about turbulence in wall-dominated flows of viscoelastic homogeneous polymer solutions described by the Finitely Extensible Nonlinear Elastic-Peterlin (FENE-P) rheological constitutive model and the development of turbulence models for the prediction of their flows in the context of the Reynolds- averaged Navier-Stokes (RANS) philosophy. To fulfill these objectives extensive direct numerical simulations (DNS) of fully-developed channel flow were carried out for the whole range of drag reduction, i.e. from low (12%) to the high drag reduction (75%) and from very low (Re_τ=125) to high Reynolds numbers (Re_τ=590). This DNS database was used to develop RANS closures, to validate the performance of the developed RANS models and also to perform a *a-priori* analyses of the filtered governing equations, as explained next.

Using direct numerical simulation data of turbulent plane channel flow of homogeneous polymer solutions, the *a-priori* analyzes of the filtered momentum and FENE-P constitutive equations were performed for the first time for viscoelastic fluids. In this part of the work the influence of polymer additives on the subgrid scale (SGS) stress tensor was quantified, and it was found that polymers lead to a severe suppression of SGS stresses. Moreover, the budget of the filtered FENE-P constitutive equation was analyzed, and suggestions for development of the SGS closures for viscoelastic fluids, in the context of large eddy simulations (LES) closures were proposed. This part of the work provided us also with insight for developing SGS models for viscoelastic fluids in the near-future, but outside the scope of this thesis.

The same DNS database for fully developed channel flow was used to develop reliable turbulence closures for viscoelastic fluids in the context of RANS. This was accomplished via two different turbulence models: a second order Reynolds-Stress Model (RSM) and the simpler k-ε-$\overline{v^2}$-f model. These RANS single point turbulence closure developments extended and improved significantly the previous more limited models of Pinho et al (2008), Resende et al. (2011) and Iaccarino et al. (2010). In

particular, in both proposed models (RSM and k-ε-$\overline{v^2}$-f models), for the first time a Boussinesq type relation was suggested to model the non-linear term appearing in constitutive equation. Moreover, the non-linear terms appearing in the Reynolds stress tensor and turbulent kinetic energy transport equations, due to the presence of the polymer additives, were better modeled using an approximation over their exact definition, an approximation that was proved to be valid using the *a-priori* analyses of time-averaged and instantaneous DNS data base. All of the predicted polymer stresses, velocity profiles, and turbulent flow characteristics are in good agreement with the DNS data, apply to the whole range of drag reduction and show great improvement over previous RANS models.

Finally, direct numerical simulations were also carried out for passive scalar transport of FENE-P fluids in channel flow and the corresponding data used to devise the first Reynolds scalar flux closures for heat transfer of viscoelastic fluids that are capable of predicting heat transfer reduction in turbulent viscoelastic fluids. The closure of Kays (1993,1994) for calculating the turbulent Prandtl number for Newtonian fluids is extended to deal with heat transfer in turbulent viscoelastic fluids. Predictions of the time averaged statistics of temperature fluctuations, turbulent heat fluxes, thermal turbulent diffusivity, and budget terms of the temperature variance by the modeled equations are reported and compare very well with DNS data.

SUMÁRIO

Os principais objectivos desta tese são a sua contribuição para aumentar o conhecimento e a compreensão da turbulência de parede com soluções homogéneas de polímero, com reologia viscoelástica e descritos pela equação constitutiva reológica da extensão finita não linear elástica com fecho de Peterlin (FENE-P, do inglês Finitely Extensible Nonlinear Elastic-Peterlin) e o desenvolvimento de modelos de turbulência adequados á previsão das características dos escoamentos num contexto de equações de Reynolds (RANS, do inglês Reynolds-average Navier-Stokes). Para cumprir estes objectivos foi realizado um extenso conjunto de simulações numéricas diretas (DNS, do inglês direct numerical simulation) do escoamento desenvolvido entre placas paralelas e para toda a gama de redução de atrito, i.e., desde a redução de atrito baixa (12%) até à redução de atrito elevada (75%) e desde números de Reynolds baixos (Re_τ=125) até números de Reynolds elevados (Re_τ=590). Esta base de dados de DNS foi também utilizada para desenvolver fechos de turbulência para modelos tipo RANS, para validar o respectivo desempenho e ainda para efectuar uma análise *a-priori* das equações governativas filtradas, como se explica de seguida..

Utilizando dados das simulações DNS em escoamento turbulento entre placas paralelas, de soluções poliméricas homogéneas, faz-se uma análise a-priori das equações filtradas da quantidade de movimento e constitutiva reológica do modelo FENE-P, o que acontece pela primeira vez para fluidos viscoelásticos. Nesta parte do trabalho o trabalho analisa e quantifica a influência da adição dos polímeros no tensor das tensões submalha (SGS, do inglês subgrid scale), tendo verificado que os polímeros conduzem a uma severa redução dessas tensões. Além disso, foram quantificados todos os termos da equação constitutiva filtrada e são feitas sugestões para o desenvolvimento de fechos para as quantidades submalhas para fluidos viscoelásticos, no contexto de modelos do tipo simulação de grandes escalas (LES, do inglês large eddy simulation). Este trabalho providencia assim informação que é da maior relevância para o desenvolvimento, num futuro próximo, de fechos para termos submalha em escoamentos de fluidos viscoelásticos, mas que estão fora do âmbito desta tese.

A mesma base de dados DNS de escoamento desenvolvido entre placas paralelas foi também utilizado para desenvolver fechos turbulentos mais consistentes e simples no contexto de modelos do tipo RANS. Isto foi concretizado com dois modelos de turbulência diferentes: um modelo das tensões de Reynolds de segunda order (RSM, do inglês Reynolds stress model) e um modelo mais simples do tipo k-ε-$\overline{v^2}$-f. Eestes fechos de turbulência locais extendem e melhoram significativamente os modelos anteriores mais limitados de Pinho et al (2008), Resende et al. (2011) e Iaccarino et al. (2010). Em particular, em ambos os modelos propostos (RSM e k-ε-$\overline{v^2}$-f), uma relação do tipo Boussinesq é sugerida pela primeira vez para modelar o termo não-linear das equação constitutiva reológica. Além disso, os termos não lineares das equações de transporte das tensões de Reynolds e energia cinética turbulenta associados à presença de aditivos poliméricos são também melhor aproximados como também sugerido pela análise *a-priori* dos dados DNS das equações governativas instantânea e média. Todos os perfis previstos pelos modelos para as tensões poliméricas, velocidade e propriedades turbulentas comparem muito bem com os dados DNS e mostram uma melhoria significativa em relação as anteriores modelos do tipo RANS, sendo ainda aplicáveis a toda a gama de redução de atrito.

Finalmente, simulações numéricas diretas também foram executadas para estudar a transferência de calor em escoamento entre placas paralelas de fluidos FENE-P e os respectivos resultados utilizados para desenvolver o primeiro modelo para os fluxos escalares de Reynolds com fluidos viscoelásticos capazes de prever a redução da transferência de calor em escoamento turbulento deste tipo de fluidos. O fecho de Kays (1993,1994) utilizado para calcular o número de Prandtl turbulento para fluidos newtonianos foi extendido para lidar com transferência de calor de fluidos viscoelásticos em escoamento turbulento. As previsões das estatísticas de quantidades médias de Reynolds das flutuações de temperatura, fluxos escalares de Reynolds, difusividade térmica turbulenta, e dos termos da equação da variância da temperatura são apresentados, verificando-se a sua boa comparação com dados das simulações DNS.

ACKNOWLEDGMENT

I want to express my great appreciation to Professor Fernando Pinho, as my adviser, for his great support, guidance, and encouragement during my PhD. His deep knowledge in the field has been shedding light on the dark parts of the journey. He is a tremendous teacher for me, who takes care of his crew at the highest possible level.

I would also like to thank Prof. R. Sureshkumar and Prof. K. Kim for their guidance and comments on my work during this period of my life. I would like to extend my appreciation to Prof. Carlos da Silva for his comments and guidance during the last two years.

I thank all the members of the CEFT research center for useful discussions during my PhD, in particular, Prof. Manuel Alves. I gratefully thank my friends in M109 and FEUP for their warmth and support, In particular, Alex, Ali, Bahareh, Behdad, Curro, Laura, Mohsen, Negar, Romeu, and Sérgio. I also appreciate the financial support from FCT, FEDER, COMPETE, and ON2 through projects NORTE-07–0124-FEDER-000026-RL1-Energy, and PTDC/EMEMFE/113589/2009.

THESIS ORGANIZATION

The present dissertation is organized in four main parts:

Part I: Introduction (consists of one chapter, Chapter 1). The introduction to turbulence and drag reduction by the means of the polymer additives along with the mechanism of the drag reduction, and the introduction to turbulent viscoelastic flow modeling (RANS and LES) are presented in this part.

Part II: Direct Numerical Simulation (consists of two chapters, chapters 2 and 3). This part which deals with DNS data analyses is divided into two chapters. First, the details of the instantaneous governing equations appropriate for the polymeric solutions described by the FENE-P constitutive equation are presented, followed by a description of the numerical methods and the parallelization details for the DNS. This chapter also presents time averaged and, higher order turbulence statistics of FENE-P fluids and compares the data with those of Newtonian fluid data. In the second chapter of this part the *a-priori* analyzes of the filtered governing equations are performed. The findings of this chapter are fundamental to the understanding and developing reliable SGS models for the turbulent viscoelastic fluids in the context of LES.

Part III: Development of the closures in the context of RANS (consists of three chapters, chapters 4, 5, and 6). This part consists of three chapters; each presenting different viscoelastic turbulence models developed in this work.

Part IV: Conclusion remarks and suggestions of future work will be close the thesis (consists of one chapter, Chapter 7).

Table of contents

Table of contents

Table of contents

Latin symbols

a_1	Constant coefficient of polymer turbulent viscosity
a_2	Constant coefficient of NLT model
a_3	Constant coefficient of wall normal polymer stress work
C_L	Turbulent length scale constant
C_{ij}	Conformation tensor
C_p	Specific heat capacity
$C_{(u,v)}$	Correlation coefficient
C_1	Constant coefficient of redistribution function
C_2	Constant coefficient of redistribution function
C_η	Constant coefficient of turbulent length scale
C_L	Constant coefficient of turbulent length scale
C_s	Constant coefficient of dissipation equation RSM model
$C_{\varepsilon 1}$	Constant coefficient of dissipation equation RSM model
$C_{\varepsilon 2}$	Constant coefficient of dissipation equation RSM model
CT_{ij}	Advective transport of the conformation tensor
C_μ	Constant coefficient of turbulent eddy viscosity model
D	Diffusivity constant
$D_{ij,v}$	Molecular diffusion
$D_{ij,t}$	Turbulent transport
$D_{ij,p}$	Viscoelastic turbulent transport
DR	Drag reduction
Ep	Viscoelastic contribution of dissipation equation
$f(C_{kk})$	Peterlin function
$f(L^2)$	Peterlin function of polymer maximum length $f(L^2)=1$
f_w	RSM model damping function
f_{w2}	RSM model damping function
f_ε	RSM model damping function
f	Redistribution function
F	Flatness factor
FT_{ij}	Nonlinear term in filtered conformation tensor

h	Half width of the channel
H^*	Hookean dumbbell spring constant
HDR	High drag reduction
IDR	Intermediate drag reduction
κ	Isotropic artificial numerical diffusivity constant
k	Turbulent kinetic energy
L_t	Turbulence length scale
LDR	Low drag reduction
L^2	Polymer maximum extension length
M_{ij}	Mean flow distortion term
NLT_{ij}	Nonlinear term in time averaged conformation tensor
S_{ij}	Rate of strain tensor
P_{ij}	Turbulence production
Pe_t	Turbulent Peclet number
Pr	Molecular Prandtl number
Pr_t	Turbulent Prandtl number
$Pr_{t,extended}$	Extended Turbulent Prandtl number
q''	Heat flux
$\mathrm{Re}_{\tau 0}$	Reynolds number based on friction velocity
S	Skewness factor
ST_{ij}	Nonlinear term in filtered conformation tensor
u, v, w	Velocity components
T	*Temperature*
T_t	*Turbulence time scale*
Sc	Schmidt number
Wi_h	Weissenberg number
$Wi_{\tau 0}$	Weissenberg number based on friction velocity
U_τ	Friction velocity
U_m	Mean velocity

Greek symbols

α_t	Turbulent thermal diffusivity
β	Ratio of the solvent viscosity and the kinematic viscosity of the solution
ε_{ij}	Viscous dissipation by the solvent
$\varepsilon_{ij,p}$	Viscoelastic stress work
η_p	Polymer viscosity
η_s	Solvent viscosity
υ_T	Turbulent viscosity
$\upsilon_{T,P}$	Viscoelastic turbulent viscosity
ν_s	Solvent dynamic viscosity
ν_0	Solution dynamic viscosity
λ	Polymer relaxation time
Π_{ij}	Pressure–strain term
θ	Instantaneous temperature
θ^+	Normalized instantaneous temperature
Θ^+	Normalized mean temperature
ρ	Density
τ_w	Wall shear stress
<	Grid scale
>	Subgrid scale
+	Normalized by friction velocity

1

Chapter 1:
Introduction

Sonnet to turbulence

Shall we compare you to a laminar flow?
You are more lovely and more sinuous.
Rough winter winds shake branches free of snow,
And summer's plumes churn up in cumulus.
How do we perceive you? Let me count the ways.
A random vortex field with strain entwined.
Fractal? Big and small swirls in the maze
May give us paradigms of flows to find.
Orthonormal forms non-linearly renew
Intricate flows with many free degrees
Or, in the latest fashion, merely few
As strange attractor. In fact, we need Cray
Experiment and theory, unforgiving;
For serious searcher, fun ... and it's a living!

S. Corrsin

1.1 Turbulence

Leonardo da Vinci (1452-1519) was the first, who introduced the term "*la turbolenza*" for fluid motion. His drawings (see Figure 1.1) illustrate the earliest turbulent flow structures, which he observed around 500 years ago.

Figure 1.1: Leonardo da Vinci's observation of turbulent flow. (The royal collection, Queen Elizabeth II)

Unlike the laminar flow regime, in which fluid moves in smooth layers, in the context of fluid mechanics, when the fluid undergoes irregular fluctuations in different directions the

flow regime is called turbulent flow regime. Most kinds of fluid flow we experience in daily life are in the turbulent regime. Figure 1.2 shows some examples of turbulent flows, from our blood flowing in arteries to flow around aircraft.

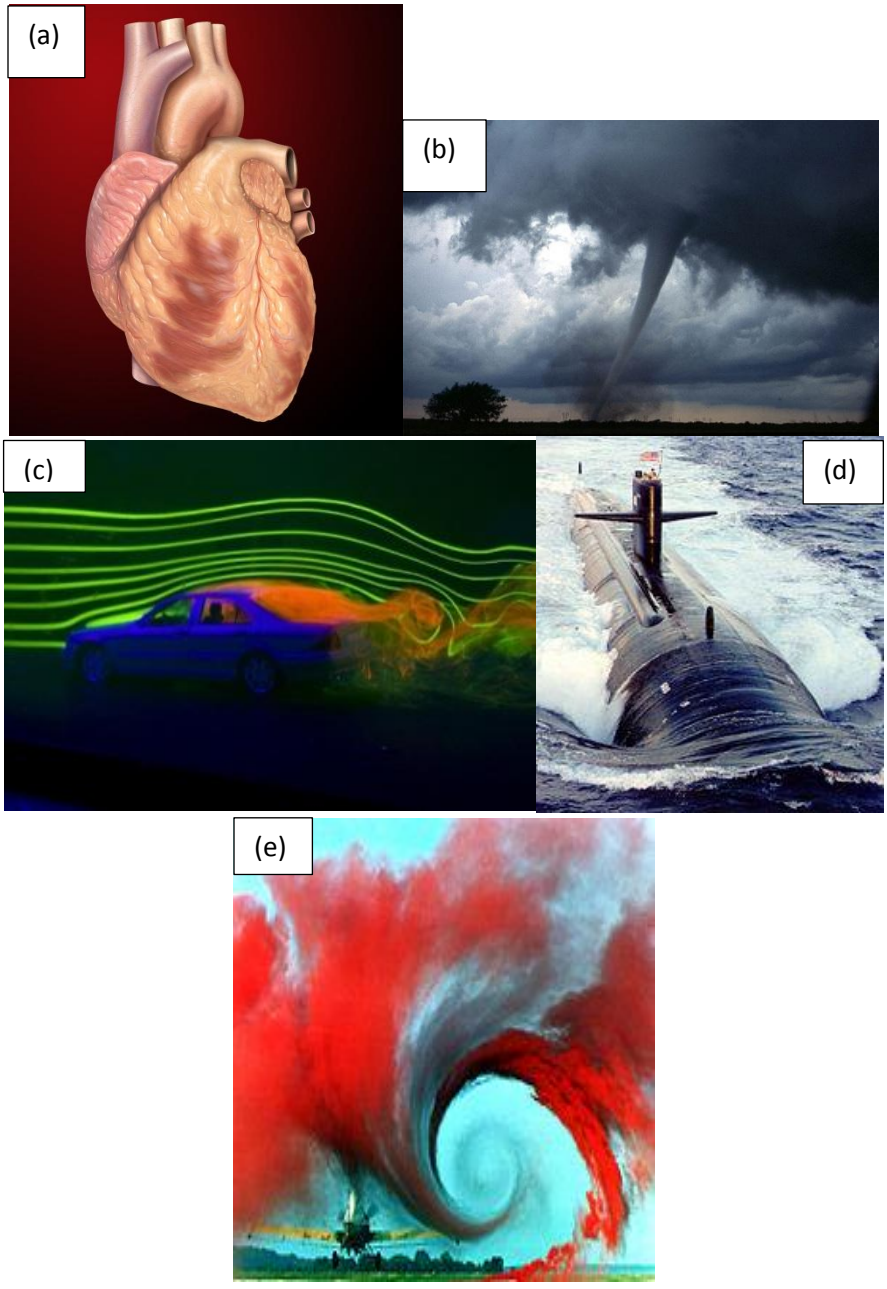

Figure 1.2: Examples of turbulent flows we experience in daily life. Photos by (a) Yale University Center for Advanced Instructional Media Medical Illustrations. (b) US national sever storm lab. (c) Eric James courtesy of NASA Ames Lab. (d) USS Los Angeles, US navy. (e) Langley Research Center of the United States National Aeronautics and Space Administration (NASA).

Although there is no exact definition of turbulent flow, it has a number of characteristic features such as:

- Irregularity: Turbulent flow is irregular, and chaotic but not random. Turbulent flow possesses a wide range of length and time scales and when these are considered as spatial structures, those spatial scales are named eddies. These eddies exist in a certain region of the flow in space for a certain time and after a while these eddies are destroyed. The size of the largest eddies is of the order of the flow geometry. At the other end of the spectrum we have the smallest eddies which are dissipated by viscous forces (stresses) into thermal energy. Although turbulence is chaotic, it is deterministic and is governed by the Navier-Stokes equation. The small eddies receive their kinetic energy from larger eddies. The slightly larger eddies receive their energy from even larger eddies and so on. The largest eddies extract their energy from the mean flow. This process of energy transferring from the largest eddies to the smallest is called the cascade process.
- Diffusivity: In turbulent flow we have a higher level of diffusivity.
- Large Reynolds Numbers: Turbulent flow most of the time occurs at high Reynolds number. For example, the transition to turbulent flow in pipes occurs at Reynolds number around 2300.
- Three-Dimensional: Turbulent flow is always three-dimensional and unsteady.
- Dissipation: Turbulent flow is dissipative, meaning that kinetic energy is transformed into thermal energy in the small (dissipative) eddies.
- Continuum: Although we have small turbulent scales in the flow they are much larger than the molecular scale and we can assume the flow as a continuum.

As mentioned above turbulence is the reason for formation of eddies of many different length scales. Most of the kinetic energy of the turbulent motion is carried by the large-scale eddies and then the energy "cascades" from these large-scale structures to smaller scale structures. This process keeps creating smaller and smaller structures which eventually form a hierarchy of structures (eddies). For the small structures/eddies molecular diffusion becomes important and finally viscous dissipation of energy takes place. The scale at which this happens is the Kolmogorov length scale.

Using this concept of energy cascade, turbulent flow can be characterized by a superposition of a spectrum of velocity fluctuations and eddies upon a mean flow. Turbulent flows may be assumed as an entire hierarchy of eddies over a wide range of length scales and the hierarchy can be described by the energy spectrum that measures the energy in flow velocity fluctuations for each length scale (wave number). Based on the length scales eddies can be divided into three categories.

- Integral length scales: Largest scales in the energy spectrum. These eddies obtain energy from the mean flow and also from each other. Thus, these are the energy

production eddies which contain most of the energy. They have the largest flow velocity fluctuations and are low in frequency. Integral scales are highly anisotropic. The maximum length of these scales is constrained by the characteristic length of the apparatus. For example, the largest integral length scale in a pipe flow has a magnitude of the order of the pipe diameter.

- Kolmogorov length scales: Smallest scales in the spectrum. In this range, the energy input from nonlinear interactions and the energy drain from viscous dissipation are in exact balance. The small scales are characterized by high frequencies of motion, causing turbulence to be locally isotropic.
- Taylor micro scales: The intermediate scales between the largest and the smallest scales form the inertial sub-range. Taylor microscales are not dissipative scales; however they transfer down the energy from the largest to the smallest scales without dissipation.

A more detailed explanation of turbulence at high-Reynolds number flow, intended for a general readership of physicists and applied mathematicians, is found in the textbooks by Frisch (1995), Cardy et al. (2008), Monin et al. (2007), and Pope (2013).

1.1.1. Direct Numerical Simulation (DNS)

Direct Numerical Simulation in computational fluid dynamics (CFD) is devoted to high-fidelity simulation of turbulent flows. A direct numerical simulation (Steven A. Orszag (1970)) is a simulation in CFD in which the Navier–Stokes equations are numerically solved without any turbulence model. This means that the whole range of spatial and temporal scales of the turbulence must be resolved. All the spatial scales of the turbulence must be resolved in the computational mesh, from the smallest dissipative scales (Kolmogorov microscales), up to the integral scale, associated with the motions containing most of the kinetic energy. Therefore, the computational cost of DNS is very high, even at low Reynolds number flows. For the Reynolds numbers encountered in most industrial applications, the computational resources required by a DNS would exceed the capacity of the most powerful computers currently available. However, direct numerical simulation is a useful tool in fundamental research in turbulence. Using DNS it is possible to perform "numerical experiments", and extract from them information difficult or impossible to obtain in the laboratory, allowing a better understanding of the physics of turbulence. Also, direct numerical simulations are useful in the development of turbulence models for practical applications, such as sub-grid scale models for Large eddy simulation (LES) and models for methods that solve the Reynolds-averaged Navier–Stokes equations (RANS). This is done by means of "a priori" tests, in which the input data for the model is taken from a DNS simulation, or by "a posteriori" tests, in which the results produced by the model are compared with those obtained by DNS.

1.1.2. Turbulent Flow Modeling Using LES (Large Eddy Simulation) Technique

LES is a turbulence model used in computational fluid dynamics. It was initially proposed by the meteorologists Lilly (1962) and Smagorinsky (1963) to simulate atmospheric air currents. Deardorff (1972,1974) tested the technique for channel flow and planetary flows in the early 70s. LES grew rapidly beginning with its invention in the 1960s and is currently applied in a wide variety of engineering applications, including combustion, incompressible flows, acoustics, and simulations of the atmospheric boundary layer. LES operates on the Navier–Stokes equations to reduce the range of length scales of the solution, reducing the computational cost. The principal operation in large eddy simulation is low-pass filtering. This operation is applied to the Navier–Stokes equations to eliminate small scales of the solution. The governing equations are thus transformed, and the solution is a filtered velocity field, in which the "small" length and time scales are selected according to turbulence theory and available computational resources. Large eddy simulation resolves large scales of the flow field solution allowing better fidelity than alternative approaches such as Reynolds-averaged Navier–Stokes (RANS) methods. It also models the smallest scales of the solution, rather than resolving them as direct numerical simulation (DNS) does. This makes the computational cost for practical engineering systems with complex geometry or flow configurations, such as turbulent jets, pumps, vehicles, and landing gear, attainable using supercomputers. Commonly used SGS models are those of Smagorinsky (1963) and Germano's dynamic model (1991), details of different SGS models can be found in Lesieur et al. (2005).

1.1.3. Turbulent Flow Modeling Using RANS (Reynolds-Averaged Navier–Stokes) Models

RANS models in the context of turbulent flow modeling offer the most economic approach for computing complex turbulent flows. Generally, a RANS turbulence model is a computational procedure to close the system of governing equations, using time averaged (mean) flow variables. The objective of the turbulence models for the RANS equations is to compute the Reynolds stresses, this can be done by three main categories of RANS-based turbulence models,

- Linear eddy viscosity models
- Nonlinear eddy viscosity models
- Reynolds stress model (RSM)

Linear eddy viscosity models: These kind of RANS models are turbulence models in which the Reynolds stresses, as obtained from a Reynolds averaging of the Navier-Stokes equations, are calculated by a linear relationship with the mean flow straining field. There

are three main categories for the linear eddy-viscosity models, depending on the number of transport equations solved to compute the eddy viscosity coefficient,

1. *Zero equation (algebraic) turbulence models,*

Algebraic turbulence models like Cebeci-Smith (1967) or Baldwin-Lomax (1978) are models that do not need the solution of any additional transport equations, and are calculated directly from the flow field variables. The advantages of these models are their simplicity and very low numerical cost of simulation; however these kinds of models do not account properly the history effects on the turbulence, for instance convection and diffusion of turbulent energy do not exist in these models. These models are commonly used in quick design iterations where robustness is more important than capturing all details of the flow physics. Note that, the dependency of the specification of the model on empirical data makes its use unfeasible in most of the applications.

2. *One equation turbulence models*

As an alternative to the algebraic (zero equation) model, one-equation models were developed (Prandtl (1945), and Spalart-Allmaras (1992)) to improve turbulent flow predictions by solving one additional transport equation. While several different turbulent scales have been used as the variable in the extra transport equation, the most popular method is to solve for the characteristic turbulent velocity scale proportional to the square root of the turbulent kinetic energy. The Reynolds stresses are then related to this scale. Although this family of the models is robust, the dependency of the specification of the model on empirical data, like the zero equation models, hinders its application for general turbulent flow simulations.

3. *Two equation turbulence models*

Two-equation models like *k-ε (Standard, RNG,* and *Realisable)* and *k-ω (Wilcox* and *SST)* are the commonly used RANS type models for a wide range of turbulent flows modeling. These models provide independent transport equations for both the turbulence length scale, and the turbulent kinetic energy. With the specification of these two variables, two-equation models are complete; no additional information about the turbulence is necessary to use the model for a given flow field. Although this is encouraging in that these models may appear to apply to a wide range of flows, it is instructive to understand the implicit assumptions made in formulating a two-equation model. While complete in that no new information is needed, the two-equation model is to some degree limited to flows in which its fundamental assumptions are not grossly violated. Specifically, most of the two-equation models make the same fundamental assumption of local equilibrium, where turbulent production and dissipation balance. This assumption further implies that the scales of the turbulence are locally proportional to the scales of the mean flow; therefore, most two equation models will be in error when applied to non-equilibrium flows. Though somewhat restricted, two-

equation models are still very popular and can be used to give results well within engineering accuracy when applied to appropriate cases.

Nonlinear eddy viscosity models: Unlike the linear eddy viscosity models, these are turbulence models in which the Reynolds stresses are modelled by a nonlinear constitutive relationship with the mean flow straining field.

1. *Explicit nonlinear constitutive relation model*
   An explicit nonlinear constitutive relation for the Reynolds stresses represents an explicitly-postulated expansion over the linear Boussinesq hypothesis. Such explicit and nonlinear expansion over the Boussinesq hypothesis proposed by Wallin and Johansson (2000).

2. $\overline{v^2}$*-f model,*
   The $\overline{v^2}$*-f* model is a modification of the Standard *k-epsilon* model. It incorporates also near-wall turbulence anisotropy as well as non-local pressure-strain effects. It is a general turbulence model for low Reynolds-number flows, that does not need to make use of wall functions because it is valid up to solid walls. Instead of turbulent kinetic energy *k*, the $\overline{v^2}$*-f* model uses a velocity scale $\overline{v^2}$*-f* (hence the name $\overline{v^2}$*-f* or the v2-f model) for the evaluation of the eddy viscosity. $\overline{v^2}$*-f* can be thought of as the velocity fluctuation normal to the streamlines. It can provide the right scaling for the representation of the damping of turbulent transport close to the wall. The anisotropic wall effects are modelled through the elliptic relaxation function *f*, by solving a separate elliptic equation of the Helmholtz type.

Reynolds stress model (RSM), The Reynolds Stress Model, also known as the Reynolds Stress Transport (RST) model, is a higher level, elaborate turbulence model. The method of closure employed is usually called a Second Order Closure. This modelling approach originates from the work by Launder (1975). In RSM, the eddy viscosity approach has been discarded and the Reynolds stresses are directly computed. The exact Reynolds stress transport equation accounts for the directional effects of turbulence on the Reynolds stress fields.

1.2 Homogeneous Polymeric Solutions

The term "polymer" stem from the ancient Greek word “πολύς” meaning "many" and “μέρος” meaning "parts", and refers to a molecule in which the structure is made of several repeating units, from which originates a characteristic of high relative molecular mass and attendant properties.

Polymers are studied in the fields of biophysics and macromolecular science, and polymer science (which includes polymer chemistry and polymer physics). In biological contexts, essentially all biological macromolecules i.e., proteins (polyamides), nucleic acids and polysaccharides are purely polymeric, or are composed in large part of polymeric.

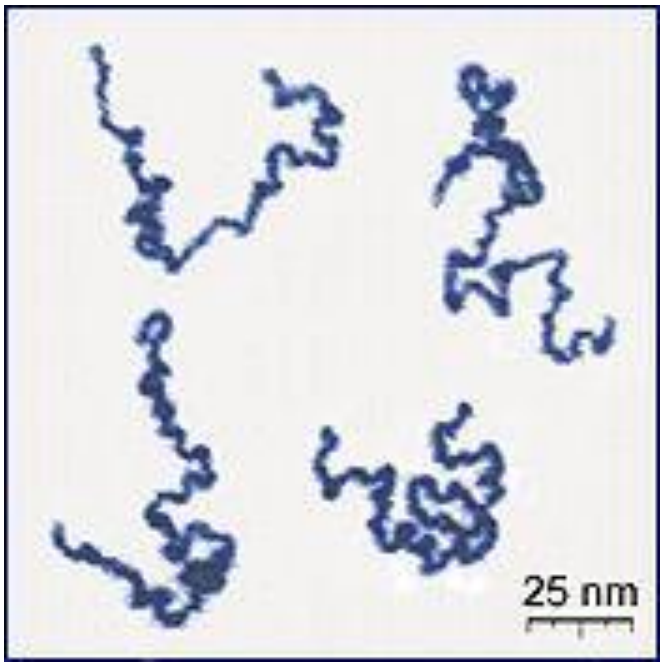

Figure 1.3: Real linear polymer chains. Recorded using an atomic force microscope on a surface, under liquid medium, Roiter et al. (2005).

Homogeneous polymeric solutions are solutions of polymer macromolecules in a solvent. Since the molecules are long they exhibit particularly strong viscoelastic effects because the molecules are easily distorted, even in rather slow flows. At high velocity, the polymer molecule is stretched to many times its undisturbed coiled state. Thus, a solution composed of stretchable molecules can be highly springy. On the other hand, fluids containing a high concentration of long polymer molecules become extremely viscous.

Constitutive equations are used to describe the complex rheological behavior of polymeric solutions relating the stress tensor with the kinematic quantities. Depending on the mathematical relationship, the equation can be linear, quasi-linear or non-linear, but mostly

are non-linear. The linear rheological constitutive equation is based on a simple principle where the response at any time is directly proportional to the value of the input signal, i.e., for example, for a fixed stress we obtain a directly proportional strain rate. The differential equations, in the linear viscoelasticity theory, are linear and the coefficients of the time differentials are defined by the material parameters. These material parameters such as, for example, the viscosity coefficient and the rigidity modulus, are constant not depending on variables such as strain or strain rate. The simplest constitutive equation used for non-Newtonian fluids is based on the generalized Newtonian fluids constitutive equation. In these kinds of models the viscosity is not constant and depends on the shear rate, capturing only the shear thinning/thickening effect of the polymeric solutions. This type of model is not viscoelastic because it is not able to predict the elastic contribution, i.e., it neither has memory effect nor normal stress effect, Bird et al. (1980). A more severe limitation of linear constitutive models is that they do not obey the principle of Oldroyd's material objectivity where they had to be formulated for general validity. The quasi-linear constitutive models solved this problem by replacing the material derivatives with Oldroyd's convected derivates. For example, both the Upper Convected Maxwell (UCM) and the Oldroyd-B models result from a substitution of the material derivatives by the contravariant convected derivate, and have the capacity to predict the first normal stress coefficient and are invariant to coordinate system changes.

The quasi-linear models are capable of describing time-dependent flows, however, these models are not able to portray well some rheological properties of some polymeric solutions. For example, the deficiencies of constant viscosity and normal stress coefficients in steady shear flow and the infinitive elongational viscosity at finite elongation rates.

In studying dilute polymeric solutions, the polymer molecules are often modeled simply as dumbbells consisting of two beads connected by a spring (Figure 1.4). In a flowing Newtonian solvent the dumbbells are convected and distorted by the viscous force exerted on the beads by the solvent. In the simplest physical model, the elastic force between the beads is taken to be proportional to the separation between the beads. This is the so-called Hookean dumbbell model. In addition to the forces mentioned above, the beads experience a randomly fluctuating force due to the thermal agitation by the surrounding solvent molecules. It can be shown that the constitutive equation associated with the Hookean dumbbell model is identical to the macroscopic Oldroyd-B equation. Due to its simplicity the model has some serious drawbacks, the most important being the fact that the shear viscosity is constant and that the dumbbells can be stretched infinitely. In elongational flow for example, this leads to an unbounded value of the elongational viscosity at a finite strain rate. A way to overcome these problems is to replace the Hookean spring by a non-linear spring to limit the dumbbell extension to a maximum value. An important example of such a non-linear spring is the finitely extensible non-linear elastic (FENE) spring introduced by Warner et al. (1972).

A major drawback of the FENE model is that it does not yield a closed-form constitutive equation for the polymer stress. For this reason it is not suited for a macroscopic flow calculation. However, if the expression for the connector force is replaced by its ensemble averaged value, it is possible to close the model. In this work we use the pre-averaging which is known as the Peterlin approximation and the resulting model as the FENE-P model.

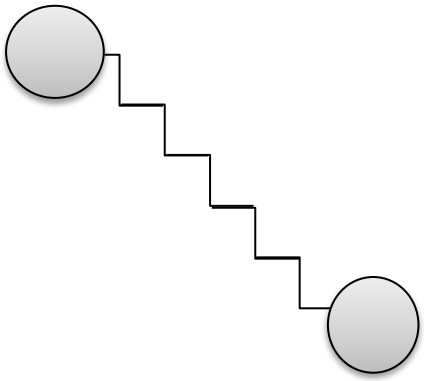

Figure 1-4: Viscoelastic dumbbell

The issue of whether a FENE-P is an adequate representation of the FENE model in the context of turbulent flow, and in particular turbulent channel flow, as also been investigated by Zhou et al. (2003), who concluded that the FENE-P dumbbell was accurate only in the steady state, incurring large errors at all phases of transient elongational flows. Contrasting to the FENE model demonstrated a good approximation in transient elongational flows. So, it is clear that an important step is the correct choice of the constitutive equation and as demonstrated they can be more or less complex, capturing more or less rheological properties. Sometimes a complex model is not the best choice, for example in channel turbulent flow without hysteretic behavior, both FENE-P and FENE-LS models predict with the same accuracy, but the numerical complexity of the FENE-LS model increases significantly, and so the FENE-P model should be preferred instead of the FENE-LS model, at least at this initial stage of turbulence modeling of viscoelastic fluids.

1.3 Drag Reduction and Turbulence Control

Over the last decades different strategies were developed to control the turbulence level in order to reduce the skin friction coefficient. A brief review of the different control techniques is summarized in this section. These methods of turbulent control divide into two main categories:

- **Active control:** Active flow control techniques are techniques which require direct energy input. These technics can be summarized as: near-wall flow excitement by

Lorentz forces (Berger et al., 2000; Pang and Choi, 2004), suction and blowing on the wall (Segawa et al., 2007), and cross-flow pressure gradients and wall motion (Jung et al., 1992) to disrupt the self-sustaining turbulence production mechanisms. The forcing takes place using different methods like spanwise-traveling waves (Du et al., 2002; Itoh et al., 2006), spanwise (Laadhari et al., 1994) or streamwise oscillations (Mito and Kasagi, 1998), and, more recently, of streamwise-traveling waves of spanwise wall velocity (Quadrio et al., 2009).

- **Passive control:** Passive flow control techniques are techniques which do not require direct energy input. These techniques are mainly characterized by non-smooth surfaces or additives. Well referenced examples are riblets, coating surfaces, bubbles and polymeric chains.

1.3.1. Drag Reduction by Polymer Additives

It has been known for quite sometime (Toms 1948) that the addition of small amount of polymers to turbulent flows of Newtonian fluids can dramatically reduce the turbulent friction coefficient with a concomitant effect upon all other associated quantities. It has been shown experimentally that very small amounts of polymers are sufficient to reduce drag up to 80%. Comprehensive reviews of the early literature in this area are given in Hoyt (1972), Lumley (1969,1973) and Virk (1971, 1975).

Although this phenomenon (perhaps a possible candidate for the title of the "most difficult open problem in classical mechanics" or in physics, according to McComb (1992)) has been known for almost sixty years, the underlying mechanisms, through which the introduction of polymers alter the fluid's rheological behavior in such a way that modify vortex structures and lead to drag reduction, have not yet been fully elucidated.

Several theories have been proposed to describe the complex mechanism of turbulent drag reduction (DR) with dilute polymer solutions. Lumley (1969) proposed a mechanism based on the extension of the polymers, suggesting that the stretching of coiled polymers, in regions with strong deformations such as the buffer layer, increases the effective extensional viscosity. This would dampen small eddies, thicken the viscous sublayer and consequently lead to drag reduction. Lumley also related the onset of drag reduction with the time scale of the polymers becoming larger than the time scale of the flow. A theory of polymer drag reduction should provide an explanation for the drag reduction onset, as well as the MDR law and its universality, which plays a significant fundamental role in understanding the phenomenon. Several theoretical concepts have been proposed but all have been subjected to criticism. The proposed theories mainly fall into two categories, that of viscous (Lumley, 1969; Procaccia et al., 2008) and that of elastic effects (Tabor and de Gennes, 1986; Saif et al. 1990; Sreenivasan and White, 2000). The principal phenomenology based on viscous explanation can be attributed to the time criterion/coil-

stretch transition by Lumley (1969, 1973), which basically claims that drag reduction occurs due to randomly coiled polymers that are fully stretched primarily in regions of highly fluctuating strain rates, like the buffer layer, and therefore strongly enhance the elongational viscosity. However, observations of drag reduction from polymer injection at the center of a pipe, where wall effects are not important (McComb and Rabie, 1979; Bewersdorff, 1982, 1984), prompted Tabor and de Gennes (1986); De Gennes (1990) to develop the elastic theory, a 'cascade theory' for three-dimensional turbulence without any wall effect, where polymer effects at small scales are described by elasticity and not by viscosity.

From the perspective of turbulence dynamics, both Lumley's mechanism and de Gennes's mechanism represent a drain of turbulence kinetic energy at the affected scales. The main difference between the two theories is the range of effective scales and the fate of the energy which has been redirected into the polymer. Lumley's theory predicts a shift of the peak of dissipation spectrum due to the enhanced dissipation introduced through the polymer, while de Gennes's theory predicts a truncation of the turbulent energy cascade for all turbulent eddies which have redirected all their turbulence kinetic energy into the elastic energy of the polymer. The energy spectra observed in viscoelastic flow in experiments (Wei et al. 1992; Warholic et al. 1999) and DNS (de Angelis, et al., 2003, 2005; Housiadas & Beris, 2003; Dubief, et al., 2005) show evidence of enhanced dissipation compared to Newtonian flows due to the enhanced elongational viscosity as suggested in Lumley's theory, but none of these show the truncation of the cascade which has been proposed by de Gennes. Furthermore, de Gennes' theory gives predictions for the criteria for onset and saturation which are orders of magnitude off from observations in both experiments and DNS. However, there are several features which are not explained by either theory. Specifically, the amount of energy redirected from turbulence to the polymer has been found to be minuscule in all numerical studies. Neither theory provides an explanation of how these energetically insignificant exchanges can result in the dramatic skin-friction drag reductions which have been observed with polymers. Furthermore, both experiments and DNS show a highly anisotropic state of turbulence near the buffer layer (Walker et al., 1990; Gampert et al., 1990; Gyr et al. 1990) and also in the viscous sublayer (Frohnapfel et al., 2007) in drag reduced flow. However, neither theory can explain how this anisotropic state is established through either elongational viscosity or elastic energy of the polymer.

1.3.2. Turbulence Models for Viscoelastic Fluids

DNS simulation of turbulent viscoelastic flow is significantly more expensive than Newtonian DNS for two reasons:

- The larger number of primary variables (tensorial constitutive equation to describe fluid rheology) in the governing equation.

- As DR increases, the near wall streaks become progressively stabilized and elongated, thus requiring the use of longer simulation boxes in particular for high DR value, Li et al. (2006).

Consequently, for a given Reynolds number, the CPU-time and memory requirements for DNS of viscoelastic flows are at least one order of magnitude larger as compared to the Newtonian case, so it is not feasible for most of the engineering purposes. Hence, Reynolds-averaged Navier–Stokes (RANS) or large eddy simulation (LES) type models have to be developed for modeling turbulent flows of dilute polymer solutions in engineering applications.

In the context of RANS models, in an attempt to incorporate fluid rheology into turbulence models for drag reducing fluids, Pinho et al. (2003), and Resende et al. (2006) developed several first-order turbulence models for a modified version of the generalized Newtonian fluid constitutive equation, where the dependence of strain hardening of the fluid on the third invariant of the rate of deformation tensor was included. This family of models also included an anisotropic version to capture the increased Reynolds stress anisotropy Resende et al. (2013), and a second order version, where the Reynolds stress tensor was computed from the corresponding transport equations Resende et al. (2013).

Leighton et al. (2003) proposed the first turbulence model for polymer flows based on the FENE-P dumbbell constitutive equation model. In their closure, transport equations for the Reynolds and the polymer stresses were added to the mean flow equation and closures for the unknown correlations were developed and the model tested in channel flow, but the model was not made available in the open literature. Pinho et al. (2008) devised a new RANS model for FENE-P fluids, which is an extension of the low Reynolds number k-ε closure for Newtonian fluids. This model provided closures for various terms of the governing equations, but only worked for low DR regime.

Iaccarino et al. (2010) introduced a k-ε -$\overline{v^2}$-f model for fully developed channel flow, which is capable of predictions over the whole range of DR. The concept of turbulent polymer viscosity (or viscoelastic eddy viscosity) was used to account for the combined effects of turbulence and viscoelasticity on the polymer extra stress tensor term in the momentum equation. The turbulent polymer viscosity was made to depend on the turbulent kinetic energy, the polymer relaxation time and the trace of conformation tensor an idea that is adopted here with a new improved closure. The model of the nonlinear terms in the conformation tensor equation relied on the turbulent dissipation rate, but the main characteristic of Iaccarino et al. (2010)'s model, imported from the corresponding Newtonian model, was the ability to incorporate into the Reynolds stress tensor closure the wall damping effect upon the wall normal turbulence via the scalar $\overline{v^2}$ and the role of pressure strain. Both of these quantities are significantly modified by polymer additives and enhance turbulence anisotropy. However, although their model predicts accurately the

amount of drag reduction, their predictions of the polymer shear stress in the Reynolds-averaged momentum, of the budgets of the turbulent kinetic energy and of the evolution equation for the conformation tensor are not in agreement with DNS results.
Subsequently, Resende et al. (2011) developed several sophisticated and exceedingly complex closures for the nonlinear turbulent term of the conformation tensor equation and improved previous closures of Pinho et al. (2008) for the viscoelastic stress work and the viscoelastic turbulent transport of the turbulent kinetic energy (k) extending the model to intermediate DR levels and showing the limitations of a simple k-ε approach to modeling polymer solutions up to high DR. In fact, since turbulence anisotropy increases with DR, the inherent turbulence isotropy of the k-ε model does not allow the simultaneous accurate prediction of mean velocity, turbulent kinetic energy and its rate of dissipation at increasingly higher DR.

Although presently the SGS models for large eddy simulations of turbulent drag-reducing flows with additives described by FENE-P constitutive equation are rare, the first LES of turbulent drag-reducing channel flow of viscoelastic fluid was done by Thais et al. (2011) in the context of temporal large eddy simulation. Using temporal large eddy simulation they predicted all turbulence statistics well and it has been proved to be comparable with fully resolved DNS. Later on, Wang et al. (2014) performed LES of forced homogeneous isotropic turbulence of FENE-P fluids using temporal approximate deconvolution method, and investigated the characteristics of turbulence structures and statistics.

Recently, Ohta et al. (2014) developed a modified Smagorinsky model for the turbulent channel flow of generalized Newtonian fluids, with viscosity described by the power-law model. They focused on low-Reynolds-number wall turbulence of non-Newtonian channel flow, and they demonstrated that the Smagorinsky model can be extended to be used for LES of turbulent channel flow of power-law fluids.

1.4. Contribution of This Thesis

Large number of DNS cases of fluid flow and heat transfer of turbulent viscoelastic channel flow were performed in this work to analyze the main characteristics of turbulent heat and fluid flow of polymer dilute solutions. These DNS cases encompass the whole range of drag reduction from low (12%) to high drag reduction (75%) at very low Reynolds number to high Reynolds numbers (Re_τ=590). In essence, a complete DNS database was generated to be used for validating the developed models in the context of RANS.

Furthermore, this DNS database is used (*a-priori* analyses) to understand the behavior of non-linear terms in the governing equations which is the key for the development of reliable turbulent viscoelastic models. In addition, as mentioned above (as far as we are aware of) there is no SGS model for turbulent viscoelastic fluids, hence using the DNS database the ground level analyses (fundamental study) of the filtered governing equations

is performed, which the findings can be used in future to develop reliable SGS models for the turbulent viscoelastic fluids in the context of LES.

In the context of RANS, several new models are proposed, First, a turbulence model is developed in the context of k-ε-$\overline{v^2}$-f, which shows major improvements in comparison with the previous attempts in development of viscoelastic RANS models (Pinho et al. (2008), Resende et al. (2011), and Iaccarino et al. (2010)). In particular, the model shows improvement in prediction of mean flow statistics. To be specific previous models of Pinho et al. (2008), and Resende et al. (2011) are valid only for low drag reduction, on the other hand the model developed in this work is valid up to the maximum drag reduction limit. Additionally, the closures developed for non-linear terms are robust and numerically stable, and in comparison with the model of Iaccarino et al. (2010) the model developed here uses a Boussinesq like relation to model the non-linear term in FENE-P constitutive equation. This specific feature has a significant improvement upon the prediction of mean polymer stresses.

The first robust Reynolds-Stress Model (RSM) valid up to high drag reduction regime is also developed for turbulent viscoelastic flows. An important contribution of this model is the development of a single closure for the nonlinear fluctuating terms appearing in the FENE-P constitutive equation. All the closures developed in this work are based on the mean and instantaneous analyses of DNS data. The polymer stresses, velocity profiles, turbulent flow statistics and the percentage of friction drag reduction predicted by the RSM model are in good agreement with present and previously published DNS data over a wide range of rheological and flow parameters.

Finally, as far as we are aware of, there is no RANS model to deal with heat transfer in turbulent flows of viscoelastic fluids, so in this work the closure of Kays (1993, 1994) is extended for the first time to cope with viscoelastic fluids. The DNS database for channel flow of viscoelastic fluids pertaining to low, intermediate and high drag reductions are used to quantify the heat transfer in viscoelastic turbulent flows and all predictions are in agreement with DNS data over a wide range of Prandtl numbers.

2

Chapter 2:
Direct numerical simulation

"It would be possible to describe everything scientifically, but it would make no sense; it would be without meaning, as if you described a Beethoven symphony as a variation of wave pressure."
—Albert Einstein

Abstract

Direct numerical simulations (DNS) of polymer induced drag reduction in turbulent channel flows up to the maximum drag reduction limit have been performed using a parallelized spectral method. All turbulent time averaged statistics like mean velocity, mean velocity fluctuations and overall shear stress balance along with correlation coefficients and higher order statistics are calculated and compared with those of Newtonian fluid flow to understand basic features of turbulent viscoelastic fluids. Moreover the budgets of the Reynolds stress tensor are calculated for all cases and compared with those of Newtonian fluid cases. In summary the simulations of this chapter lead to a DNS data base that helped in developing RANS closures, was used to perform a-priori analyses of grid scale and sub-grid scale interactions, and was used to valid the performance of developed closures presented in the next chapters.

2.1. Governing equations

2.1.1 Continuity and momentum equation

Figure 2.1.1 shows a schematic of the channel flow studied in this work, where the *x*-axis is chosen as the mean flow direction, and the *y* and the *z* axes are the wall-normal and spanwise directions, respectively. The conservation of mass and momentum equations appropriate for FENE-P fluid are:

$$\nabla.\vec{u} = 0 \tag{2.1}$$

$$\frac{\partial \vec{u}}{\partial t} + \vec{u}.\nabla\vec{u} = -\nabla p + \frac{1}{\mathrm{Re}_{\tau 0}}\left[\beta\nabla^2\vec{u} + (1-\beta)\nabla.\overline{\overline{\tau}}_v\right] \tag{2.2}$$

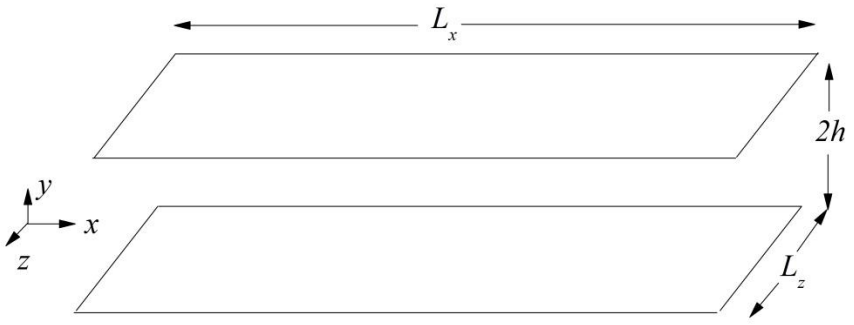

Figure 2.1.1 Schematic of the flow geometry, *x*: streamwise, *y*: wall normal, and *z:* spanwise directions.

where, $\vec{u}$, p and $\overline{\overline{\tau}}_v$ denote the instantaneous velocity vector, pressure and viscoelastic tensor contribution to the total extra stress tensor, respectively. The zero shear rate friction Reynolds number, $Re_{\tau 0}$, is defined as $Re_{\tau 0} = hU_\tau/\nu_0$, where ν_0 is the zero shear rate kinematic

viscosity of the solution, U_τ is the friction velocity, $U_\tau = (\tau_w/\rho)^{1/2}$, and h is the half-height of the channel, that together with the time scale, h/U_τ, are utilized to normalize the equations. The parameter β is the ratio of the solvent to the total solution zero shear-rate viscosity, $\beta = v_s/v_0$.

2.1.2. Constitutive equation

The additional viscoelastic stress tensor ($\overline{\overline{\tau}}_v$) in equation (2.2) arises due to the presence of polymer. The stress tensor for the FENE-P dumbbells is given by

$$\overline{\overline{\tau}}_v = \frac{f(c_{kk})\overline{\overline{c}} - I}{Wi_h} \tag{2.3}$$

where $Wi_h = \lambda U_\tau / h = Wi_{\tau 0} / Re_{\tau 0}$, is the dimensionless relaxation time, also known as Weissenberg number, $\overline{\overline{c}}$ is the conformation tensor, which quantifies the normalized polymer chain end-to-end distance vector, and I is the identity matrix. Function $f(c_{kk})$ is known as the Peterlin function, defined by

$$f(c_{kk}) = \frac{L^2}{L^2 - c_{kk}} \tag{2.4}$$

Note that $\overline{\overline{c}}$ and L^2 (polymer maximum extension length) are made dimensionless with respect to kT/H^*, where k, T and H^* denote the Boltzmann constant, the absolute temperature and the Hookean dumbbell spring constant, respectively. The polymer conformation tensor is obtained by solving the following evolution equation for the dimensionless conformation tensor,

$$\frac{\partial \overline{\overline{c}}}{\partial t} + \vec{u}.\nabla\overline{\overline{c}} - \left[\overline{\overline{c}}.\nabla\vec{u} + (\nabla\vec{u})^T.\overline{\overline{c}}\right] - D\nabla^2\overline{\overline{c}} = -\overline{\overline{\tau}}_v \tag{2.5}$$

2.1.3. Energy equation

The instantaneous thermal energy equation for incompressible flow can be written as,

$$\frac{\partial T}{\partial t} + u_j\frac{\partial T}{\partial x_j} = \frac{k}{\rho C_p}\frac{\partial^2 T}{\partial x_j^2} \tag{2.6}$$

The thermal boundary condition of uniform heat flux at the both walls is considered in this study to which corresponds a linear variation of the wall temperature in thermally fully-developed flow Kays et al. (1980). To impose the periodic boundary condition for temperature, the temperature is made dimensionless as following,

$$\theta = \frac{\langle T_w \rangle - T}{T^*}, \; T^* = \frac{q''}{\rho C_p U_m} \tag{2.7}$$

Using the normalized temperature, the non-dimensional governing equation becomes with velocity scale of the friction velocity and length scale of the channel half height. If the temperature is normalized by the friction temperature the governing equation becomes the same as Kasagi et al. (1992).

$$\frac{\partial \theta^+}{\partial t} + u_j \frac{\partial \theta^+}{\partial x_j} - \frac{u_1}{U_m} = \frac{1}{\mathrm{Re}_\tau \, \mathrm{Pr}} \frac{\partial^2 \theta^+}{\partial x_j^2} \tag{2.8}$$

In equation 2.8 θ^+ represents the instantaneous temperature; *Pr* denotes the molecular Prandtl number, defined as the ratio of kinematic viscosity to thermal diffusivity.

2.1.4. Parallelization

DNS of turbulent viscoelastic flow is significantly more expensive than Newtonian DNS and the CPU requirements for the DNS of viscoelastic flows are at least two orders of magnitude larger as compared to the corresponding Newtonian case (depending on the grid size), making it unfeasible to use single processing simulation. Hence in this work, the standardized and portable message-passing system named Message Passing Interface (MPI) was utilized to parallelization of the FORTRAN code. Simulations performed at most using 256 processors in FEUP cluster. This method results in good overall parallel performance and the speed up chart for the DNS of Newtonian and viscoelastic cases as the number of processors is increased from 1 to 128 processors on the FEUP's cluster is plotted in figure 2.1.2. It can be seen that the performance and speed up severely increased using the parallel code, which make it possible to perform DNS calculations in FEUP.

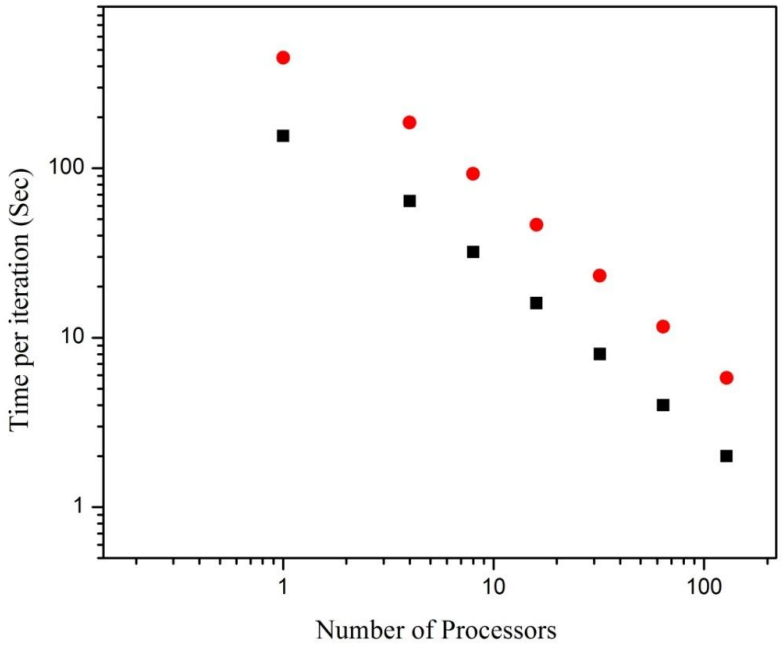

Figure 2.1.2 Comparison of the Newtonian (black) and Viscoelastic (Red) cases, simulation time.

2.1.5. Computational and physical parameters and validation with previous DNS data

In this study we investigate fully developed channel flow of FENE-P fluids over a wide range of conditions as described in Table (2.1), which lists the DNS data sets. The Reynolds number is defined as $Re_{\tau 0} \equiv hU_\tau/\nu_0$ where U_τ is the friction velocity, h is the channel half-height and ν_0 is the zero shear-rate kinematic viscosity of the solution, i.e., the sum of the kinematic viscosities of the solvent and polymer $\nu_0 = \nu_p + \nu_s$. The Weissenberg number based on the wall friction velocity is defined as $Wi_{\tau 0} \equiv \lambda {U_\tau}^2/\upsilon_0$ and a second Weissenberg number based on the channel half-height (h) is $Wi_h \equiv \frac{Wi_{\tau 0}}{Re_{\tau 0}} = \lambda U_\tau/h$.

Table 2.1. Summary of the physical and computational parameters for the DNS cases used in this chapter.

case	$Re_{\tau 0}$	Domain size $L_x \times L_y \times L_z$	$N_x \times N_y \times N_z$	L^2	$Wi_{\tau 0}$	β
DNS0	180	6.283h x 2h x 3.141h	128 x 129 x 128	0	0	0
DNS1	395	14.136h x 2h x 4.5h	384 x 257 x 192	0	0	0
DNS2	590	14.136h x 2h x 4.5h	512 x 257 x 256	0	0	0
DNS3	180	6.944h x 2h x 4.19h	128 x 129 x 128	3600	50	0.9
DNS4	395	14.136h x 2h x 4.5h	384 x 257 x 192	3600	50	0.9
DNS5	395	14.136h x 2h x 4.5h	384 x 257 x 192	10000	100	0.9
DNS6	590	25.136h x 2h x 4.5h	512 x 257 x 256	3600	50	0.9
DNS7	590	25.136h x 2h x 4.5h	512 x 257 x 256	10000	100	0.9

Another relevant independent dimensionless quantity is β, the ratio between the solvent viscosity and the zero shear-rate kinematic viscosity of the solution, ($\beta \equiv \nu_s/\nu_0$). In this work, as in Li et al. (2006), and Thais et al. (2012, 2014) a numerical diffusivity term $D\nabla^2 c$ was added to the FENE-P constitutive equation in order to perform stable numerical integration of the evolution equation for the conformation tensor, where D is a dimensionless number (equivalent to the inverse of a Schmidt number) defined as $D = \kappa/hU_\tau$, with κ denoting a constant isotropic artificial numerical diffusivity. The diffusivity is chosen in a way that it is large enough for the calculations to ensure the numerical stability of the calculations and the realizability of the conformation tensor values, while small enough that it does not affect the computational results. This follows on the steps of Sureshkumar et al. (2007) and the normalized artificial numerical diffusivity D was taken to be of $O(10^{-2})$ resulting in a numerical Schmidt number $Sc^+ = 1/Re_{\tau 0}D$ of the order $O(10^{-1})$.

Periodic boundary conditions were applied along the streamwise and spanwise directions. The channel size was chosen to adequately capture the streaky structures and the elongated vortical structures developed in the flow. In the two periodic directions, *x and z*, Fourier representations were used, whereas in the non-homogeneous shear direction a Chebyshev approximation was employed. As shown above, the flow and polymer stress fields can be fully characterized by dimensionless groups, namely, Re_τ, β, L^2 and Wi_h (or $Wi_{\tau 0}$). Further details of the numerical approaches used in this work can be found in Li et al. (2006), and Thais et al. (2012). Table 2.1 summarizes the computational parameters for the DNSs performed in the present study.

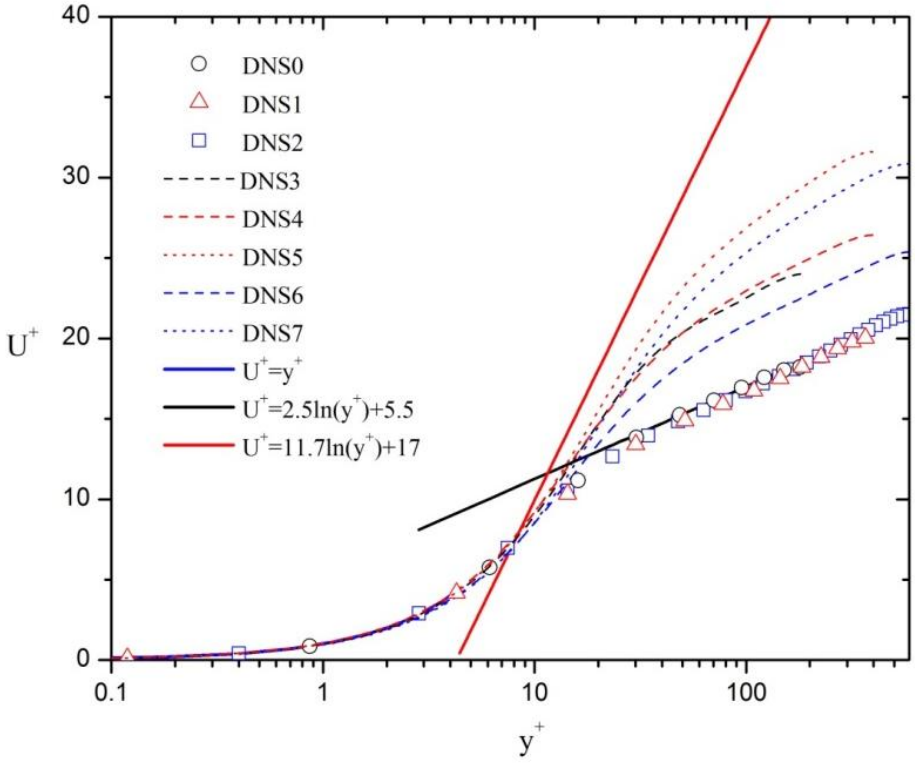

Figure 2.2. Mean streamwise velocity profiles as a function of distance from the wall, rheological and flow properties are described in table (2.1).

2.2. Flow statistics and DNS assessment

2.2.1 Mean velocity

Since the simulations are performed with a constant pressure gradient drag reduction is manifested via an increase in the flow rate (i.e., an increase in Re_{mean}). Typical mean streamwise velocity profiles as a function of the distance from the wall in logarithmic scale for wide range of flow and rheological parameters described in Table 2.1 are shown in

figure 2.2 For the sake of comparison the profiles for Virk's asymptote (Red solid line) and the Newtonian flow at each Reynolds number have also been included. For the Newtonian cases, excellent agreement with the linear distribution in the viscous sublayer, and well as the logarithmic layer is observed. In drag reduced flows, it can be seen that all profiles in the viscous sublayer also collapse on the linear distribution $U^+ = y^+$. Further away from the wall the mean velocity of the drag reduced flows increases as compared to that in Newtonian flows. The logarithmic profile is shifted upwards parallel to that of the Newtonian flow. The upward shift of the logarithmic profile can be interpreted as a thickening of the buffer layer. According to Lumley *et al.* (1969, 1973) the upward shift of the logarithmic profile is equivalent to drag reduction. The same behavior is found for the mean streamwise velocity in the channel flow experiments of Ptasinski *et al.* (2003) and in earlier DNS studies Li et al. (2006).

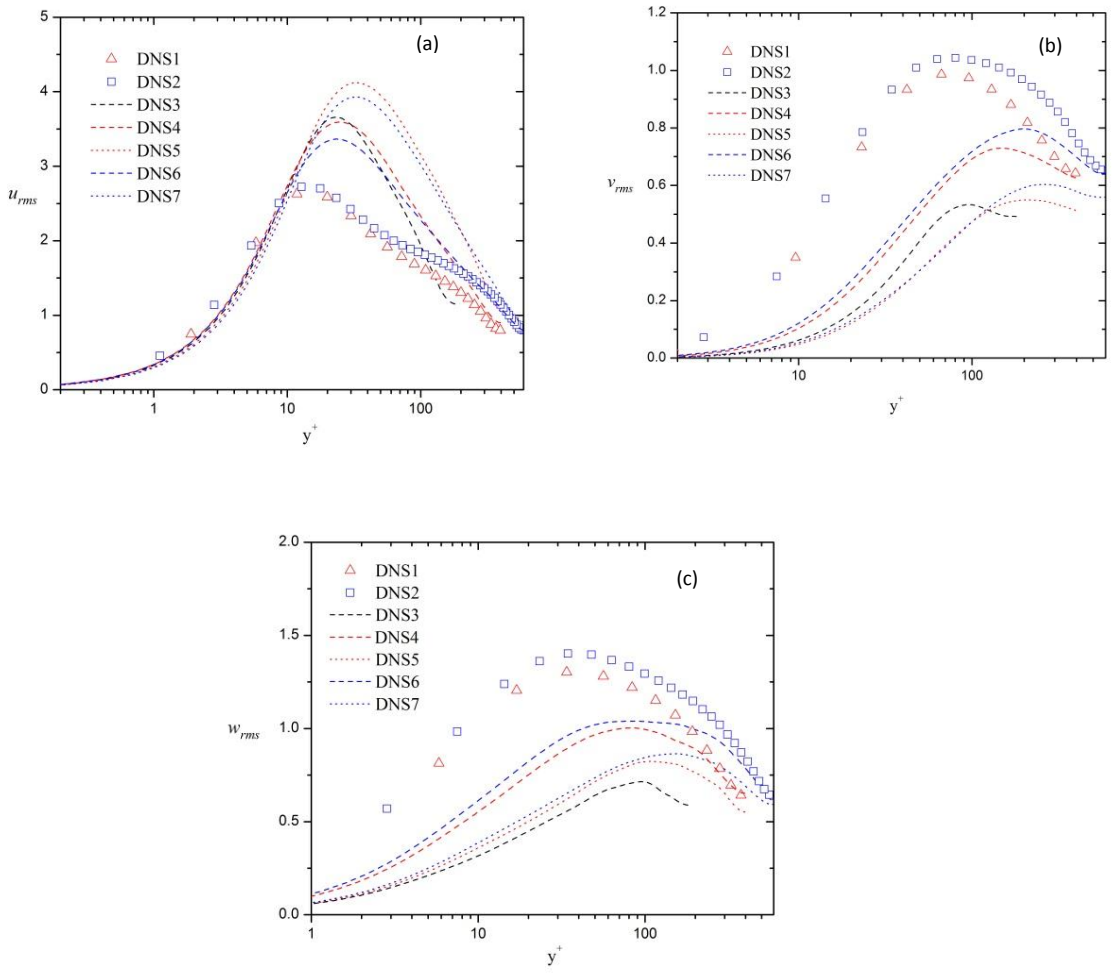

Figure 2.3. Velocity fluctuation components, (a) streamwise, (b) wall normal, and (c) spanwise , rheological and flow properties are described in table (2.1).

2.2.2. Velocity fluctuations

The root mean square of the streamwise velocity component fluctuations for viscoelastic fluid along with Newtonian data for a cases introduced in table 2.1 are shown in figure 2.3.(a). It is well known that the streamwise velocity fluctuations u_{rms} monotonically increase by enhancing the drag reduction (Ptasinski *et al.* (2003)), moreover the peak locations of the u_{rms} shift away from the wall as drag reduction increases. This is consistent with the shift of the logarithmic region in the mean velocity profile. The wall normal and spanwise components v_{rms} and w_{rms} are depicted in figure 2.3. (b,c), showing that v_{rms} and w_{rms} monotonically decrease as DR is enhanced. The peak values of v_{rms} and w_{rms} decrease to almost half of their Newtonian magnitude. Further note that the peak locations of the v_{rms} and w_{rms} also shift away from the wall as drag reduction increases. This is also consistent with the shift of the logarithmic region in the mean velocity profile.

2.2.3. Overall momentum balance

In figure 2.4 (a,b), different contributions to the overall shear stress balance as a function of the distance from the wall are shown for cases DNS4, DNS5. In both cases the total shear stresses follow the expected linear profiles over the channel height, indicating that a stationary fully developed state has been reached (for all cases in table (2.1) this behavior was checked). As shown and previously stated by others (Ptasinski *et al.* (2003)) the polymer stresses increase monotonically with increasing drag reduction, while the Reynolds stresses decrease. The polymer stress contributions are relatively small in low drag reduction and the peak location is close to the wall (i.e., the peak locations of polymer stress are in the buffer layer). However, as %DR in increased, the Reynolds stress is significantly reduced, and the polymer stress is increase. These observations are also consistent with experimental results by Ptasinski *et al.* (2003).

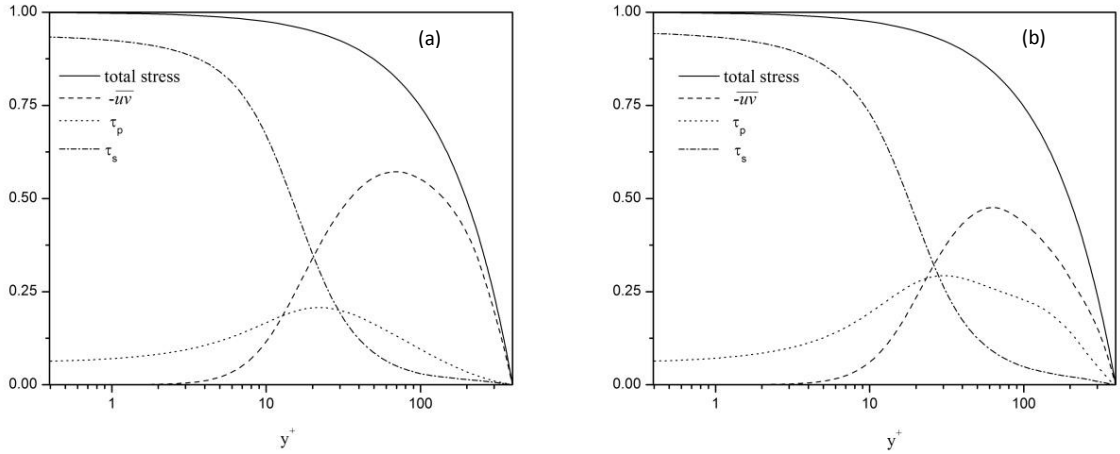

Figure 2.4. Overall momentum balance, (a) case DNS4 and (b) case DNS5 rheological and flow properties are described in table (2.1).

2.2.4. Correlation and higher order statistics

In this section, correlation coefficients and higher order statistics of velocity components of viscoelastic channel flow will be analyzed. This will be achieved through the statistical tools described below. In these equations T' is the fluctuating part of the instantaneous variable T, $T = \langle T \rangle + T'$. The skewness and flatness were made non-dimensional by the variance,

$$S = \frac{\langle T'^3 \rangle}{\left[\langle T'^2 \rangle^{0.5} \right]^3} \tag{2.9}$$

$$F = \frac{\langle T'^4 \rangle}{\left[\langle T'^2 \rangle^{0.5} \right]^4} \tag{2.10}$$

the correlation coefficients between two variables u and v is given by,

$$C_{(u,v)} = \frac{\langle u'v' \rangle}{\left[\langle u'^2 \rangle \langle v'^2 \rangle \right]^{0.5}} \tag{2.11}$$

The correlation coefficients for streamwise and wall normal components of the velocity for Newtonian and viscoelastic cases, DNS1, DNS4, and DNS5 are plotted in figure 2.5 As stated in Kim *et al.* (1987) the peak location of correlation coefficient for Newtonian case is located in the same location for the peak of maximum production and maximum streamwise velocity fluctuation. This is also true for viscoelastic fluids and as it can be seen in figure 2.5 by increasing the amount of drag reduction the peak of correlation coefficient slightly increases and shifts away from the wall same as the behavior of the production and streamwise fluctuation. Comparing correlation coefficients of the Newtonian and viscoelastic cases away from the wall, figure 2.5, shows a reduction of *u'* and *v'* correlation (around 30%) for viscoelastic cases in comparison to Newtonian case and this reduction increases by increasing the amount of drag reduction from case DNS4 to DNS5.

The skewness factors for the velocity components, except the skewness for *w*, which due to symmetry has to be zero, are shown in figures 2.6 for the Newtonian and the viscoelastic fluids, cases DNS1, DNS4, and DNS5, as a function of the distance from the bottom wall. Figure 2.6 shows the skewness of the streamwise and wall normal velocity components, *u* and *v*. We can see that the skewness of the streamwise velocity component of Newtonian case decreases dramatically as we move away from the wall, from a high positive value to an equally high in magnitude but negative value, right after the buffer layer, afterward we have a slight reduction throughout the log-law layer, and finally it increases slightly near

the center line. As it can be seen for the viscoelastic cases the reduction of the skewness of the *u'* is more extreme than the Newtonian case and it decreases more by increasing the amount of drag reduction from case DNS4 to DNS5, by moving more away from the wall for viscoelastic cases we have a plateau which skewness remains almost constant and it has a slight increase like Newtonian case close to the centerline. Skewness of the wall normal velocity component also plotted along with streamwise component in figure 2.6, as it can be seen the skewness of Newtonian fluid consist of three region, first it has an extreme reduction until minimum negative value around y^+=11 afterward it has a slight increase till y^+=300 and finally with an slight reduction it reaches channel centerline. Analyzing the viscoelastic cases, on the other hand, shows that instead of an extreme reduction very close to the wall, we have an almost slight reduction until y^+=37 for case DNS1 and until y^+=75 for case DNS4. Note that for the case DNS5 (high drag reduction regime) the profile does not have a negative region and it just decreases from the maximum value on the wall to 0 in the center line.

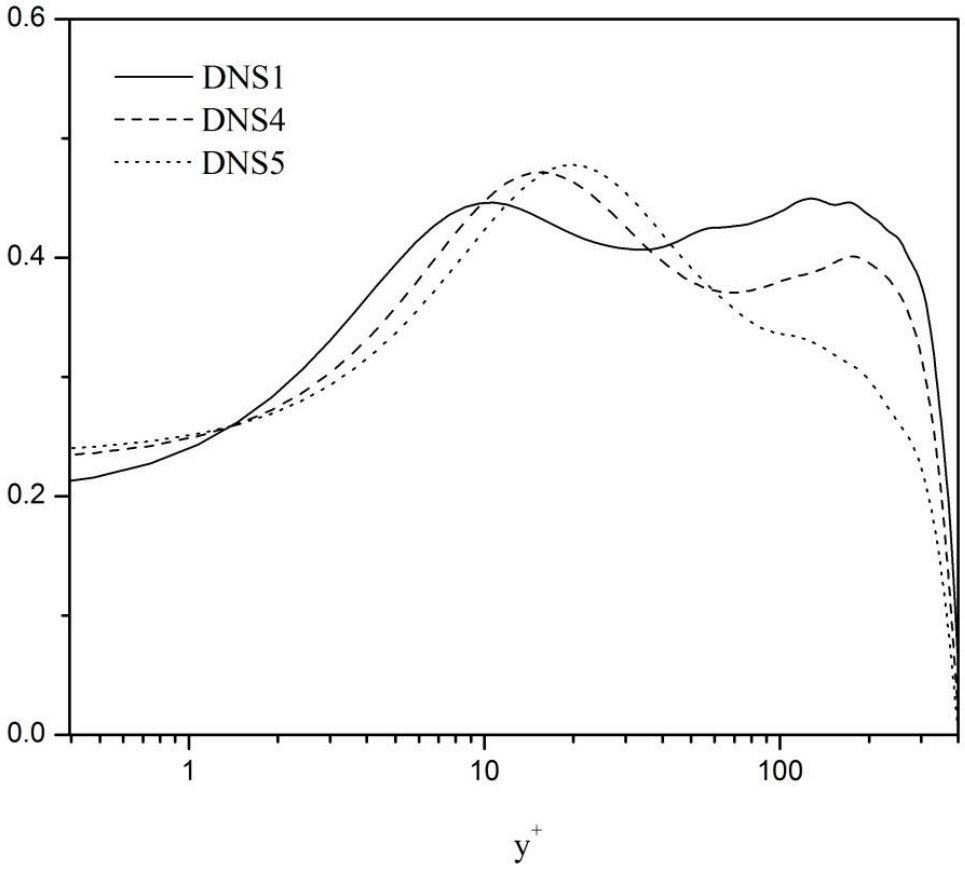

Figure 2.5 Correlation coefficient of *u',v'* ($-\langle uv\rangle/u_{rms}v_{rms}$) for cases DNS1, DNS4, and DNS5 rheological and flow properties are described in table (2.1).

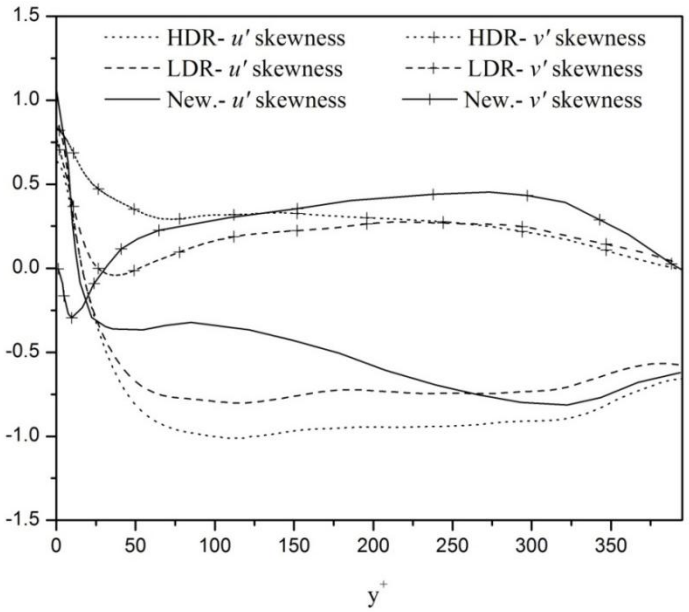

Figure 2.6. Skewness profiles of the velocity components as function of the distance from the wall for Newtonian flows: case DNS1, LDR: case DNS4, HDR: case DNS5, rheological and flow properties are described in table (2.1).

The flatness measures the intermittency of a quantity. A strongly intermittent signal at some point is dormant most of the time; there are periods with activity, but most of the time the activity is small. It is remarkable that the maximum intermittency of the velocity occurs near the wall. The flatness for all velocity components are plotted in figure 2.7. As expected for the streamwise components for all Newtonian and viscoelastic cases the maximum value is at the wall, and by moving away from the wall we have an extreme reduction in flatness coefficients. The main difference of the flatness for Newtonian and viscoelastic cases take place in y^+>50, in which Newtonian case has average value equal to 2.5, and the average flatness values are 3 and 3.7 for cases DNS4 and DNS5 respectively. Analyzing the flatness coefficient of the spanwise velocity shows that for both Newtonian and viscoelastic cases the rate of reduction close to the wall are same as each other, however away from the wall this coefficient increases by increasing the amount of drag reduction. In contrast with the flatness of streamwise and spanwise components which have same rate of reduction of Newtonian fluids, the rate of reduction of flatness of the wall normal component decreases by increasing the amount of drag reduction, as it can be seen from figure 2.7 for Newtonian case we have an extreme reduction until y+ around 25 but for case DNS4 this extreme reduction continues until y^+=5 and for high drag reduction case, DNS5, the reduction rate is much smaller and it continues until y^+=150.

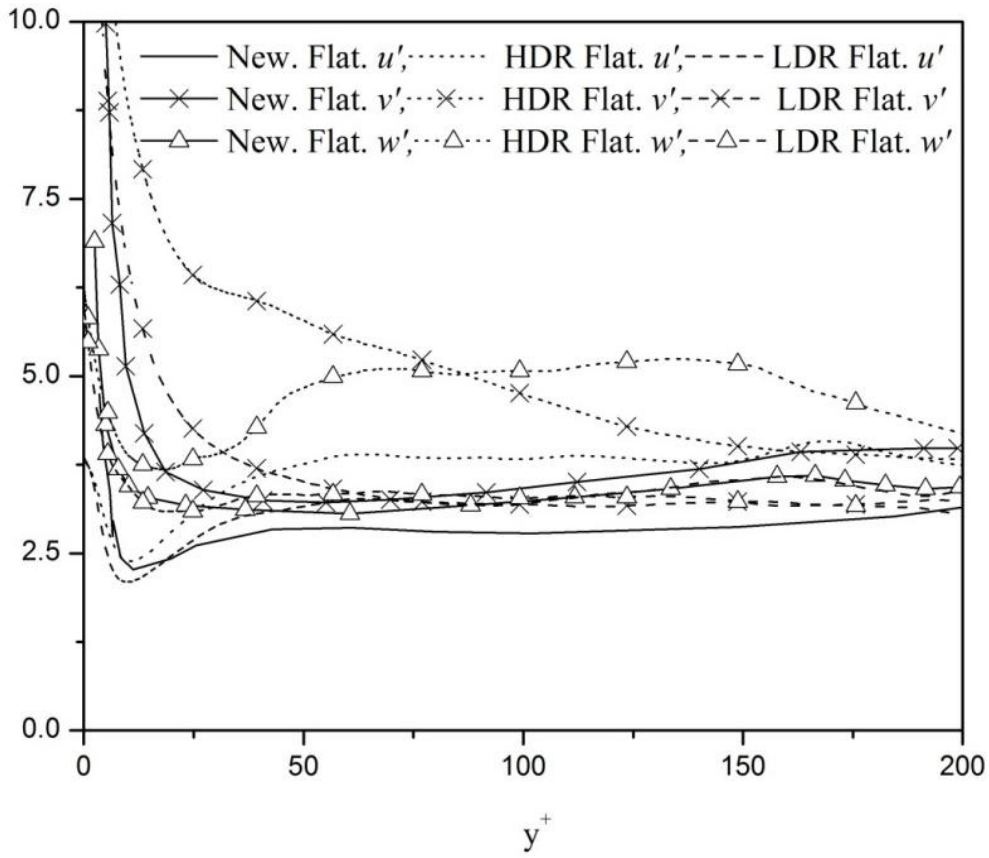

Figure 2.7. Flatness profiles of the velocity components as function of the distance from the wall for Newtonian flows: case DNS1, LDR: case DNS4, HDR: case DNS5, rheological and flow properties are described in table (2.1).

The most striking observation from the flatness profiles of Newtonian and viscoelastic cases is that *v'* is very intermittent near the wall. The behavior of the flatness profile of *v'* is illustrated by snapshots of *v'* in planes parallel to the wall (y^+=5) at (figures 2.8 a-c): regions with noticeable normal velocity fluctuation are scarce in the viscous sublayer of Newtonian case, however there regions increase by adding polymers to the fluid and keep increase by increasing drag reduction (DR), as it can be seen in figure (2.8 a-c). Snapshots of *v'* in planes parallel to the wall at maximum peak of the kinetic energy plotted at (figure 2.8 d-f) from these figures and also as it can be seen from the averaged flatness coefficient profiles, figure 2.8, the normal velocity is weakly intermittent at these regions in comparison to the *v'* intermittent behavior close to the wall. It is also interesting to see that by adding the polymers the flatness increases also in these regions (Newtonian flatness $\approx$ 3.4, LDR flatness $\approx$ 3.8, HDR flatness $\approx$ 5).

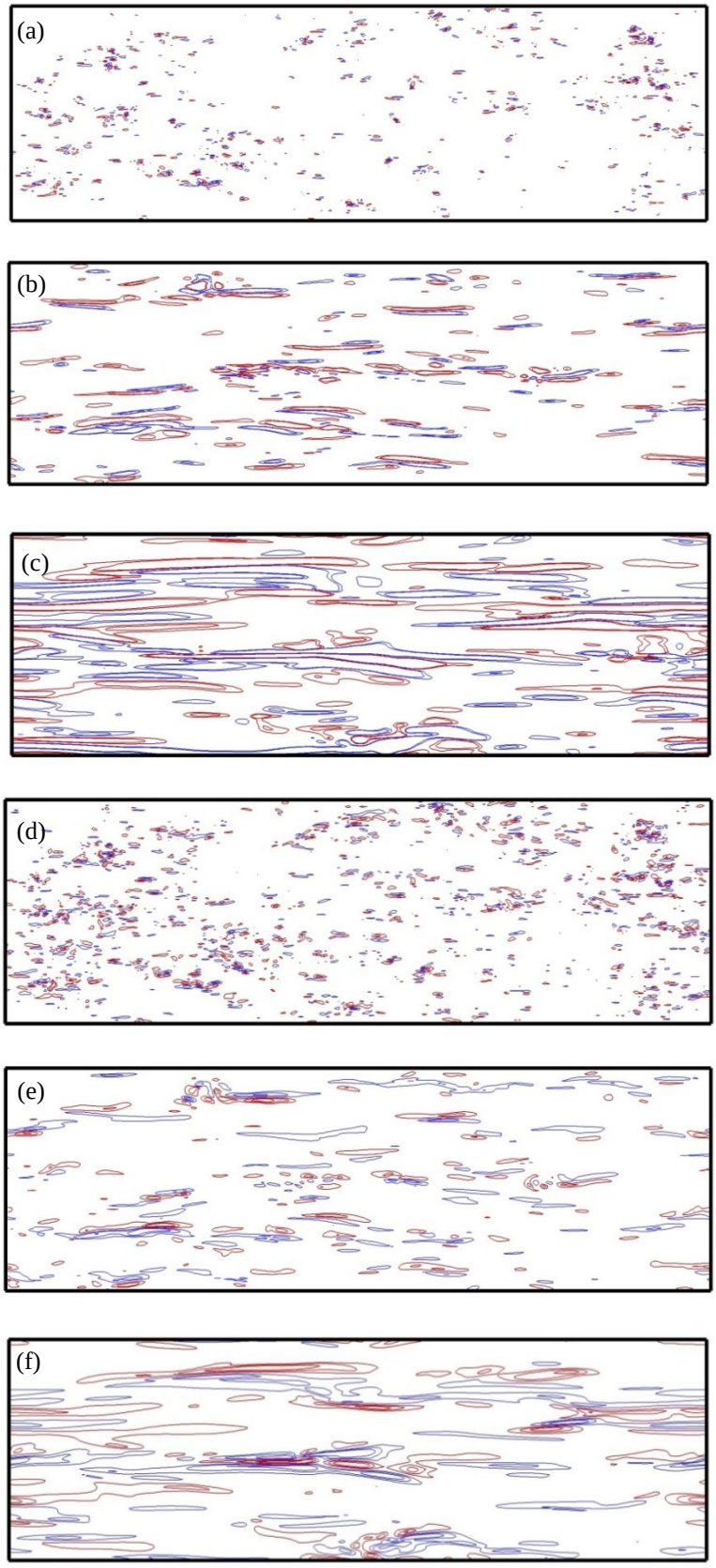

Figure. 2.8. Contours of a snapshot of *v'* normalized with the maximum |*v'*| in each plane, the blue lines contour levels are −0.2,−0.4, and −0.6, the red lines contour levels are 0.2, 0.4, and 0.6. (a): Newtonian (case DNS1) at y^+=5, (b): LDR (case DNS4) at y^+=5, (c): HDR (case DNS5) at y^+=5, (d): Newtonian (case DNS1) at y^+=15, (e): LDR (case DNS4) at y^+=24, (f): HDR (case DNS5) at y^+=34, rheological and flow properties are described in table (2.1).

2.2.5. Vortex identification and structure of turbulence

It is known that as DR is increased the intensity of near wall eddies is reduced and their size is increased. In this sub-section we shed some light on this phenomenon via vortex visualization using the Q-criteria ($Q = 1/2\left(\|\Omega\|^2 - \|S\|^2\right)$ where Ω and S are the antisymmetric and symmetric parts of ∇u). The vortical structures obtained for Newtonian, low, and high drag reduction cases are shown in figure 2.9. The figure illustrates the dramatic modification of coherent structures as drag reduction is increased. It can be observed that the number of vortices is severely reduced with increasing drag reduction.

This reduction is particularly significant at the high drag reduction regime. The observed reduction in the intensity of the wall eddies is in agreement with the proposed mechanism of drag reduction by polymer additives based on the inhibition of the near wall eddies.

2.3. Influence of viscoelasticity on Reynolds stress budgets

The objective of this section is to investigate the influence of viscoelasticity on the budgets of the Reynolds stress components using the instantaneous DNS data. Note that, as demonstrated above for the time averaged turbulence statistics, in order to have stationary time averaged statistics for low drag reduction the temporal averaging is performed over 10-15 computational units (h/U_τ), whereas for high drag reduction to obtain good statistics averaging is over 30–50 h/U_τ due to the significant variations in *xz* plane. The results of the Newtonian case also are included for comparison reasons.

An exact transport equation for the Reynolds stresses can be derived from the Navier-Stokes equation for FENE-P fluids. It is emphasized that this equation is exact or rather as exact as the Navier-Stokes equations. The Reynolds stress transport equation appropriate for FENE-P fluids can be written as:

$$\frac{\partial \overline{u_i u_j}}{\partial t} + U_k \frac{\partial \overline{u_i u_j}}{\partial x_k} =$$
$$\underbrace{\left(-\overline{u_i u_k}\frac{\partial U_j}{\partial x_k} - \overline{u_j u_k}\frac{\partial U_i}{\partial x_k}\right)}_{P_{ij}} + \underbrace{\frac{\partial}{\partial x_k}\left(\nu \frac{\partial \overline{u_i u_j}}{\partial x_k}\right)}_{D_{ij,\nu}} \underbrace{-\frac{\partial}{\partial x_k}\left(\overline{u_i u_j u_k} + \overline{\frac{p}{\rho}\left(\delta_{jk}u_i + \delta_{ik}u_j\right)}\right)}_{D_{ij,t}}$$
$$\underbrace{-2\nu\overline{\frac{\partial u_i}{\partial x_k}\frac{\partial u_j}{\partial x_k}}}_{\varepsilon_{ij}} + \underbrace{\overline{\frac{p}{\rho}\left(\frac{\partial u_i}{\partial x_j} + \frac{\partial u_j}{\partial x_i}\right)}}_{\Pi_{ij}} + \underbrace{\frac{\partial}{\partial x_k}\left(\overline{u_i \tau_{jk,p} + u_j \tau_{ik,p}}\right)}_{D_{ij,p}} \underbrace{-\overline{\left(\tau_{ik,p}\frac{\partial u_j}{\partial x_k} + \tau_{jk,p}\frac{\partial u_i}{\partial x_k}\right)}}_{\varepsilon_{ij,p}} \qquad (2.3.1)$$

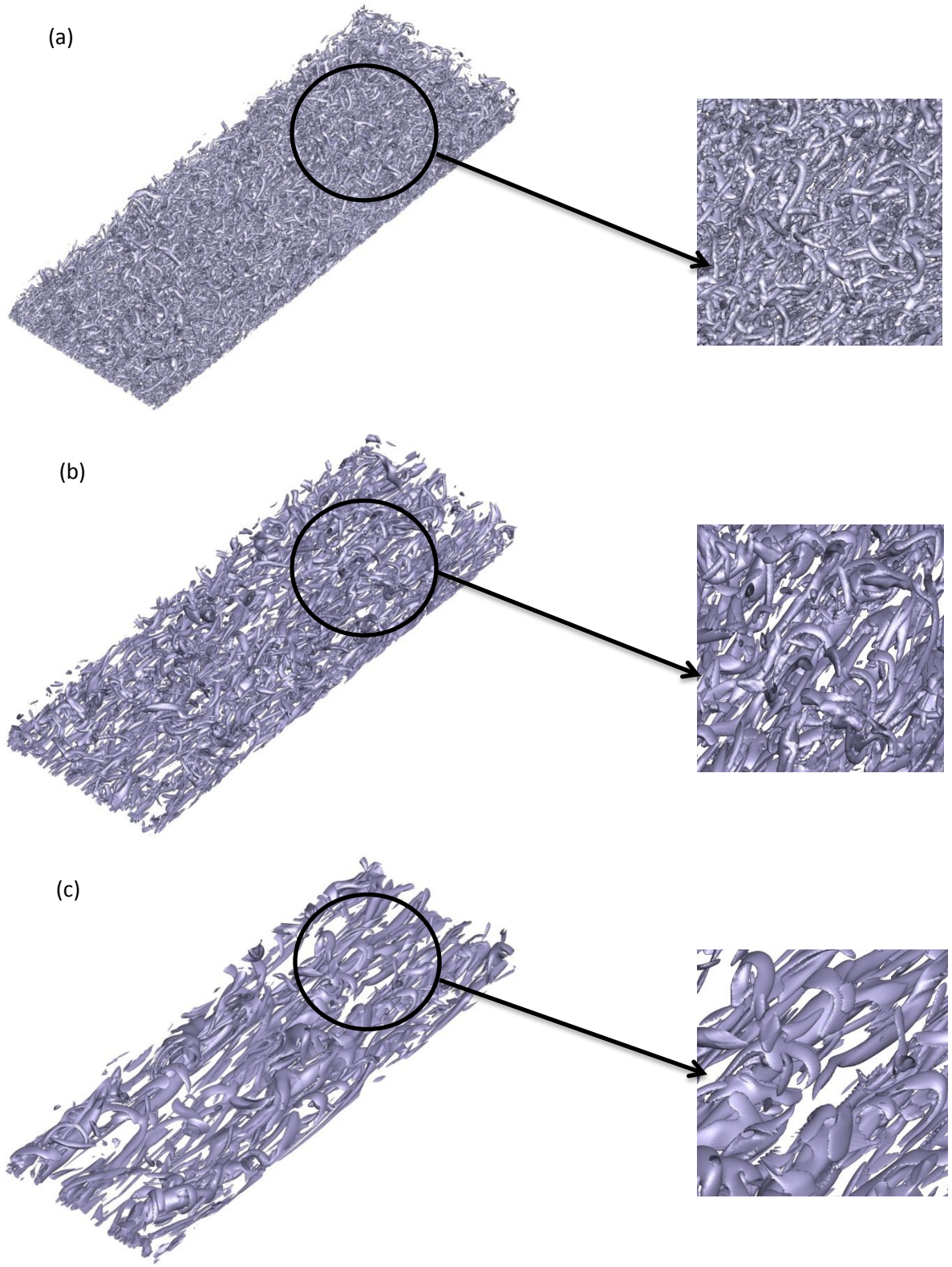

Figure 2.9. Vortex visualization using *Q*-criteria, (a): Newtonian, (b) LDR, (c) HDR cases.

Except for the last two terms on the right-hand-side, which involve the fluctuating polymer stresses, the other terms are classical terms appearing in the corresponding equation for

Newtonian fluids and represent the turbulence production by the mean strain (P_{ij}), molecular diffusion ($D_{ij,v}$), turbulent transport ($D_{ij,t}$), viscous dissipation by the solvent (ε_{ij}) and the pressure–strain term ($\Pi_{ij,v}$). The last two terms on the right-hand-side are viscoelastic terms representing the viscoelastic turbulent transport ($D_{ij,p}$) and the viscoelastic stress work ($\varepsilon_{ij,p}$).

In order to have an idea about the magnitude of the different terms of equation 2.3.1 in different directions, in figures 2.3.1 to 2.3.4 we plot the various terms, as a function of the wall distance. Although the overall shape and the behavior of the terms remains the same as for the Newtonian case, the maxima and minima associated with the different terms in equation 2.3.1 display a pronounced decrease and increase with increasing drag reduction.
It can be seen that the *xx* component of the viscoelastic stress work is negative all across the channel (except close to the wall) meaning that it behaves as a sink in the transport of the streamwise Reynolds stress. Figures also shows that although the viscoelastic stress work is small close to the wall, when compared with the other terms, far from the wall it has the same magnitude as the production and the solvent dissipation terms. Moreover, all the figures show that the viscoelastic turbulent transport has a small magnitude near the wall, and it is almost zero away from the wall.
The figures show that relative to their Newtonian values the most significant changes are taking place in the dissipation and production terms of the transport equation. It can be observed that the maximum peak of these terms reduces to almost half of the Newtonian value for high drag reduction case.

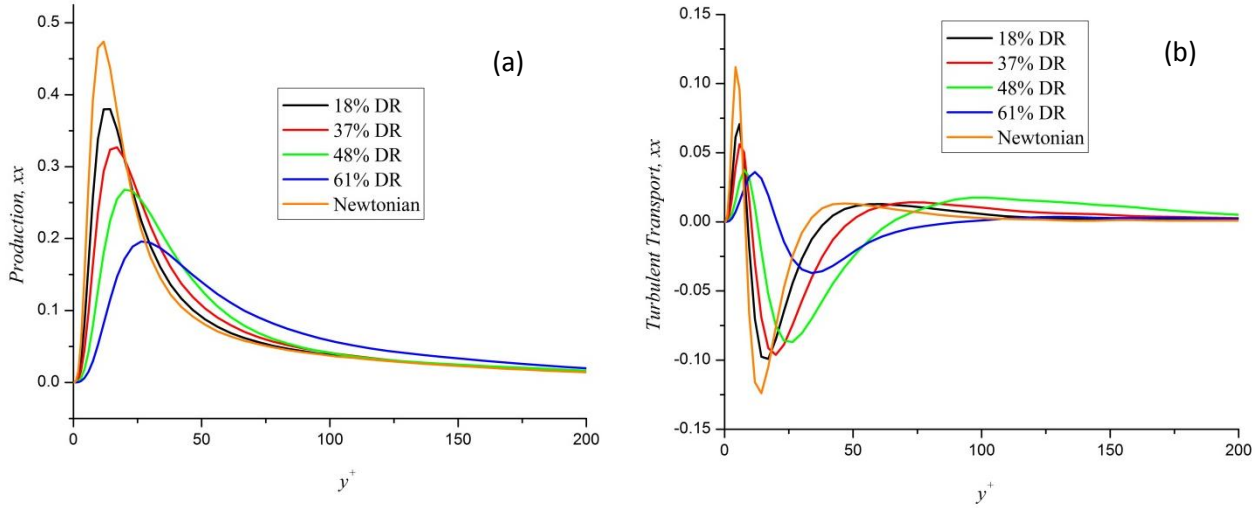

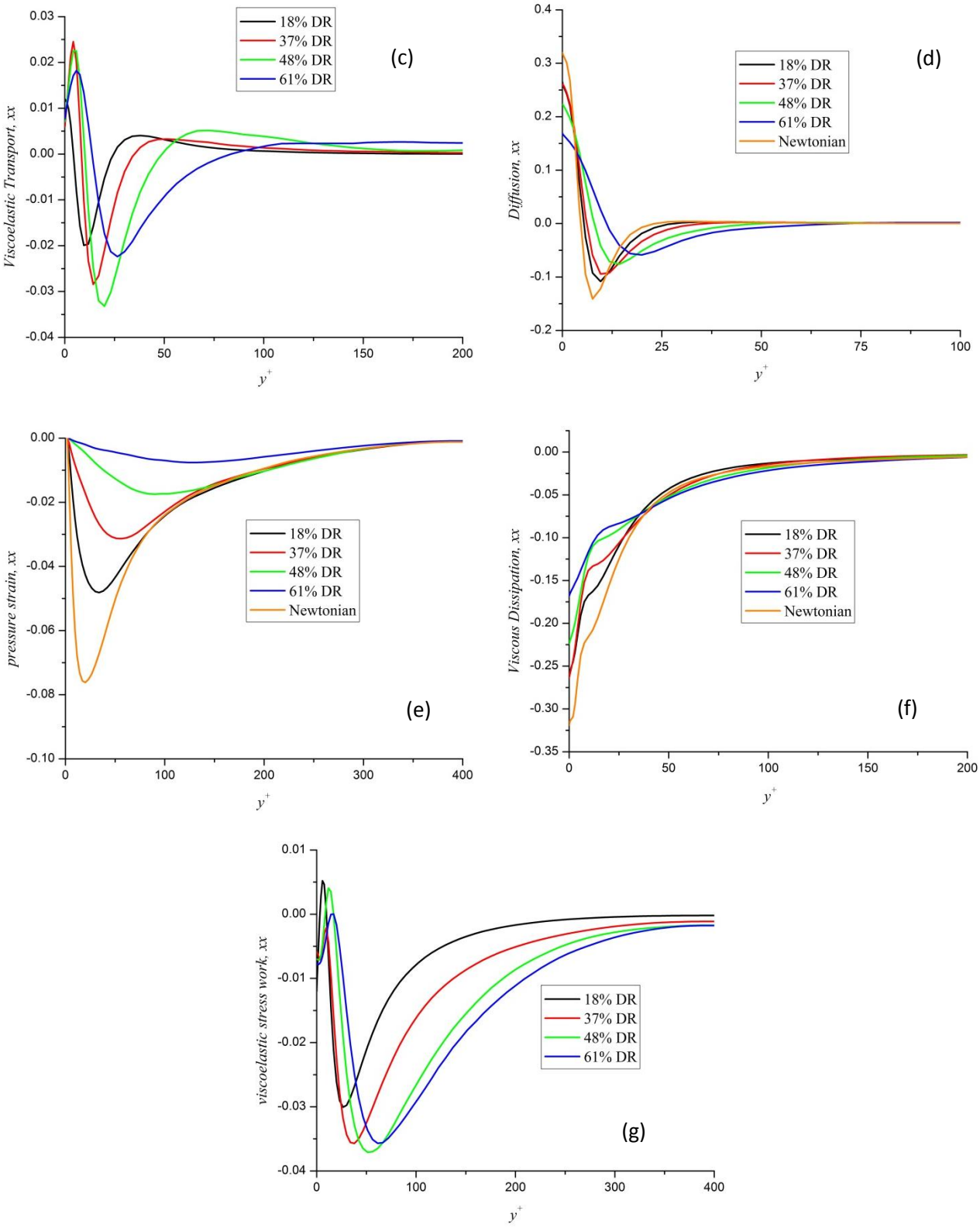

Figure. 2.3.1. Budgets of the xx component of Reynolds stress transport equation.

The budget terms of the *yy* and *zz* components of Reynolds stress transport are depicted in figures 2.3.2 and 2.3.3, it can be observed that the *yy* and *zz* components of the viscoelastic stress work is negative all across the channel, similar to *xx* component, meaning that it behaves as a sink in the transport of the streamwise Reynolds stress. The figures also show that the viscoelastic stress work dramatically decreases by increasing DR. Furthermore note that although the viscoelastic stress work is small close to the wall, when compared with the other terms, far from the wall it has the same magnitude as the solvent dissipation terms. Moreover, all the figures show that the viscoelastic turbulent transport has a small magnitude near the wall, and it is almost zero away from the wall.

The figures further indicate that relative to their Newtonian values the most significant changes are taking place in the dissipation and pressure strain terms of the transport equation. It can be observed that the maximum peak of these terms reduces to almost 10% of the Newtonian value for high drag reduction case.

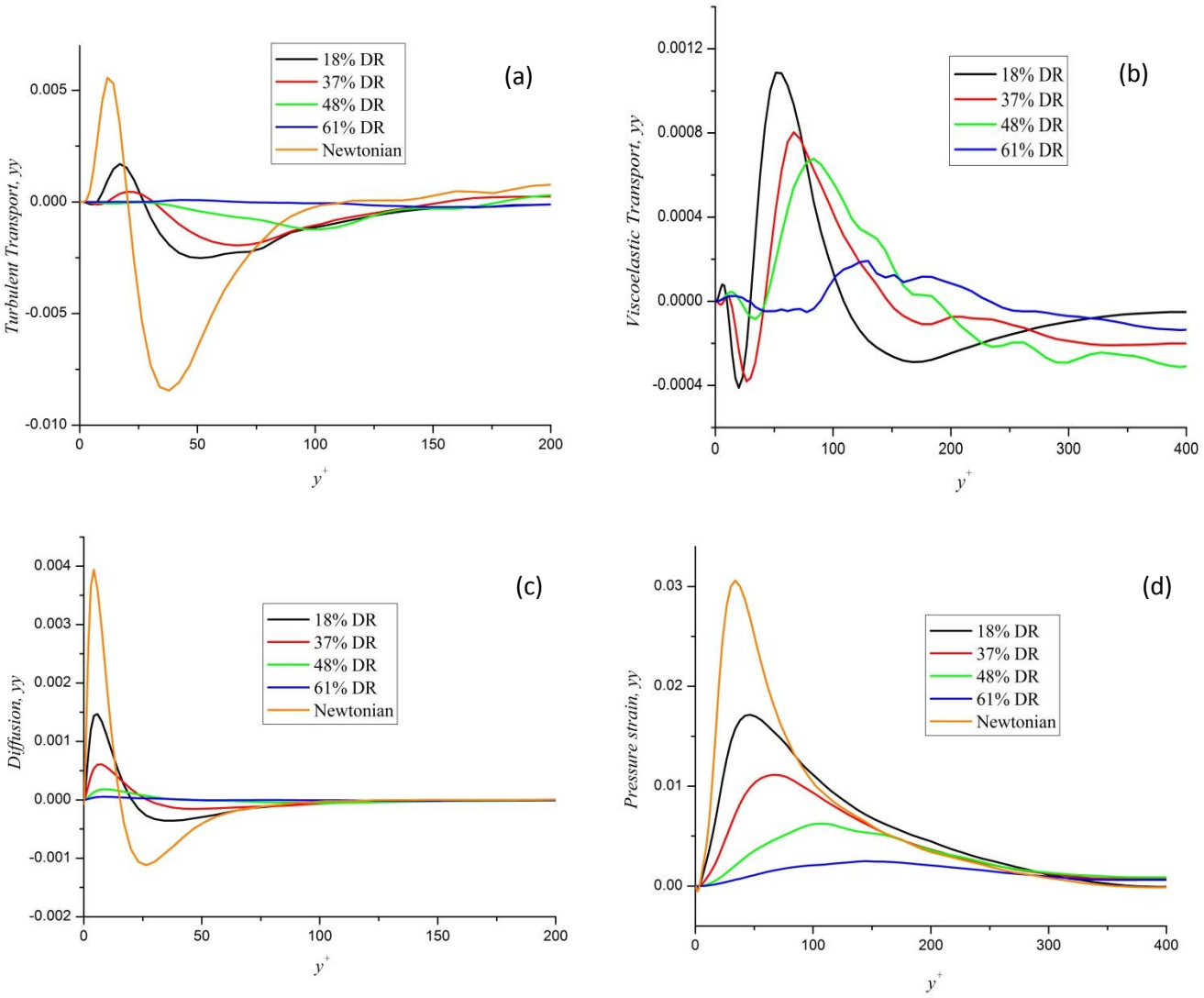

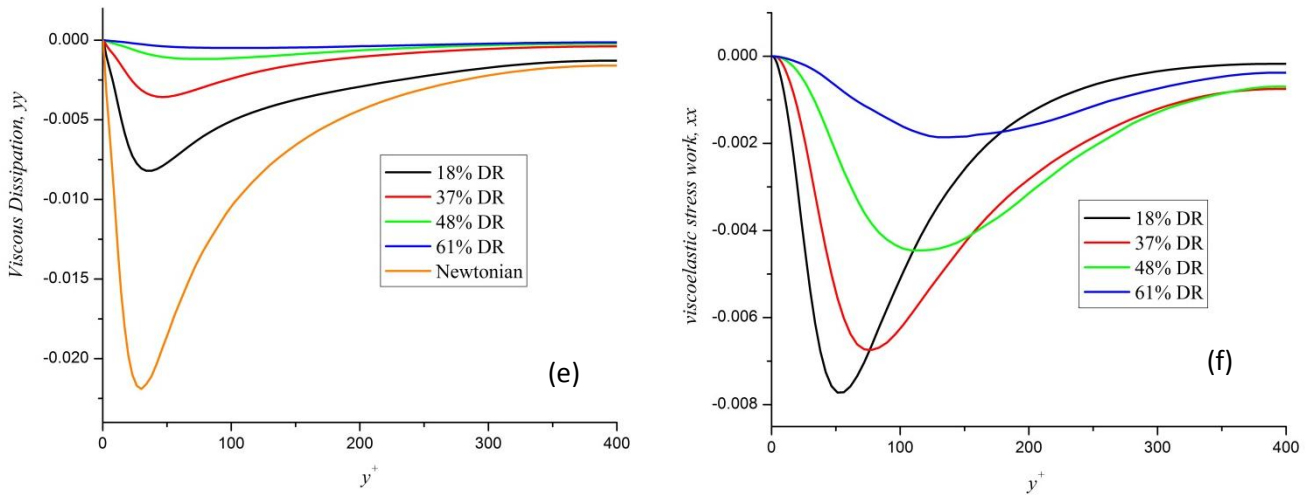

Figure. 2.3.2. Budgets of *yy* component of Reynolds stress transport equation.

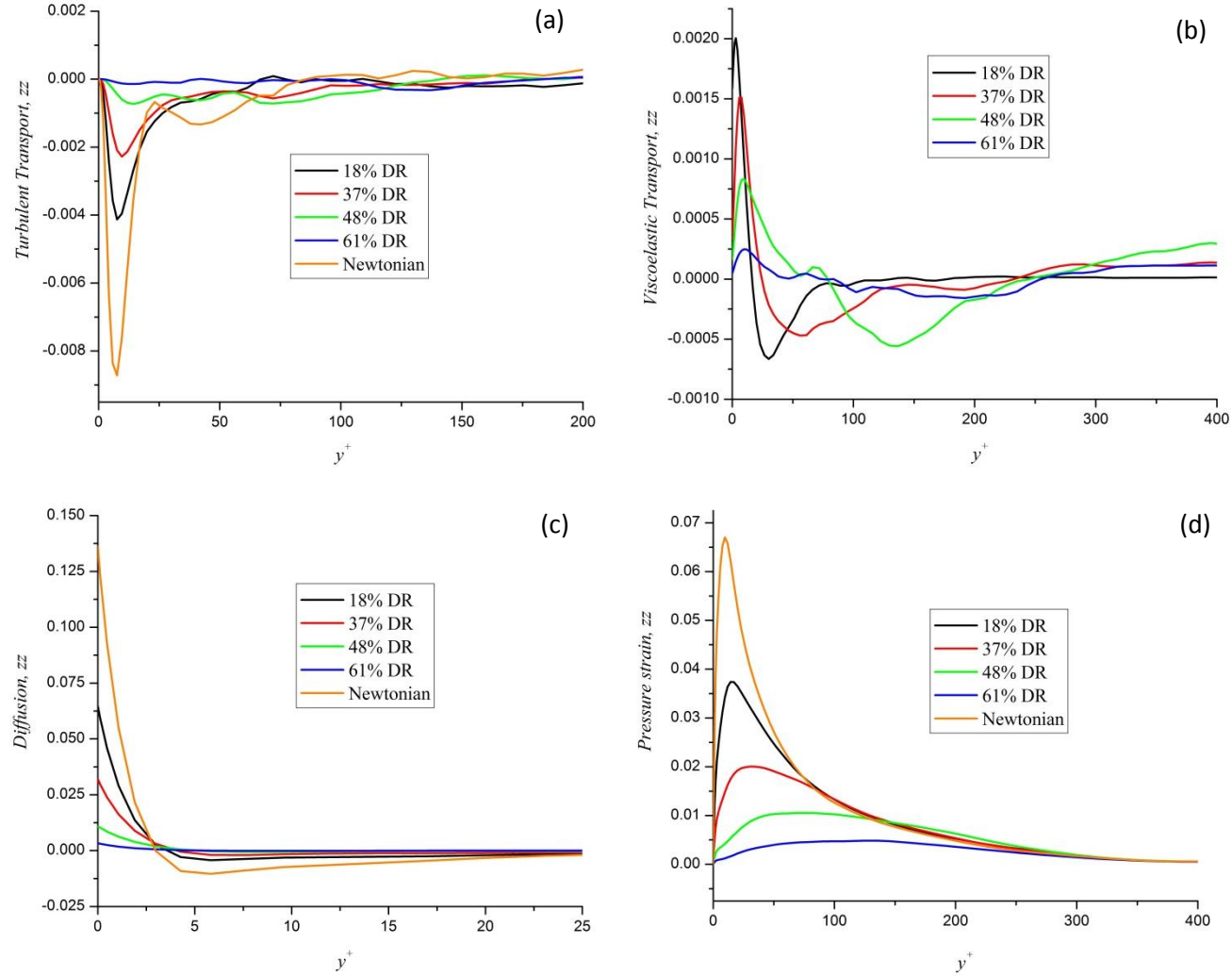

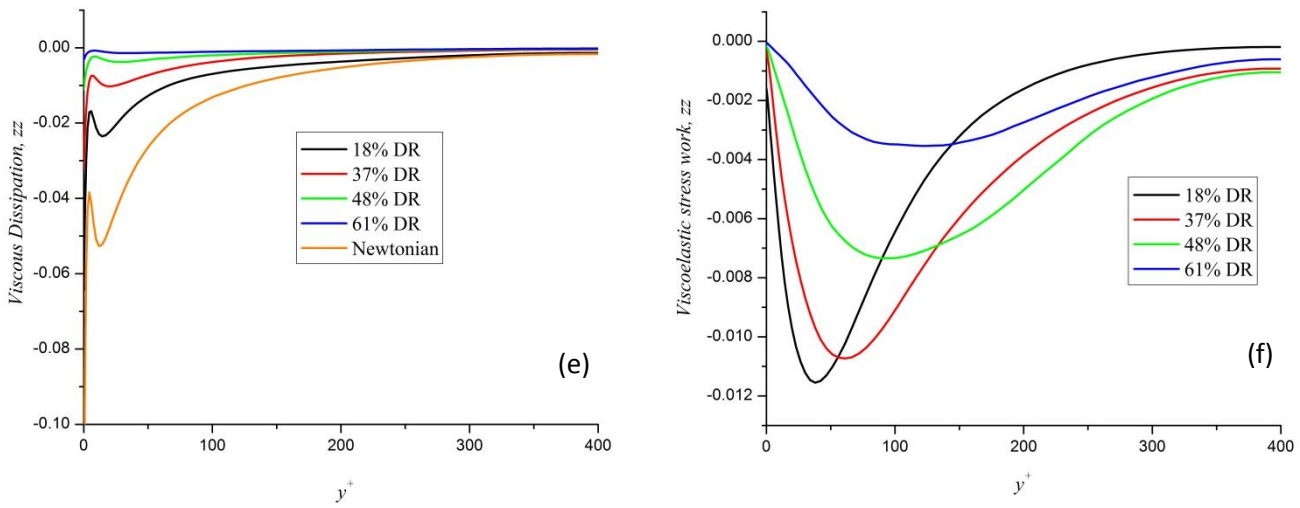

Figure. 2.3.3. Budgets of *zz* component of Reynolds stress transport equation.

It can be seen that the *xy* component of the viscoelastic stress work is positive all across the channel meaning that it behaves as a source in the transport of the streamwise Reynolds stress. Figures also shows that magnitude of the production term is decreasing by increasing DR. Also note that like other components although the viscoelastic stress work is small close to the wall, when compared with the other terms, far from the wall it has the same magnitude as the production and the solvent dissipation terms. Moreover, all the figures show that the viscoelastic turbulent transport has a small magnitude near the wall, and it is almost zero away from the wall.

The figures show that relative to their Newtonian values the most significant changes are taking place in the dissipation, pressure strain and production terms of the transport equation. It can be observed that the maximum peak of these terms reduces to almost 10% of the Newtonian value for high drag reduction case.

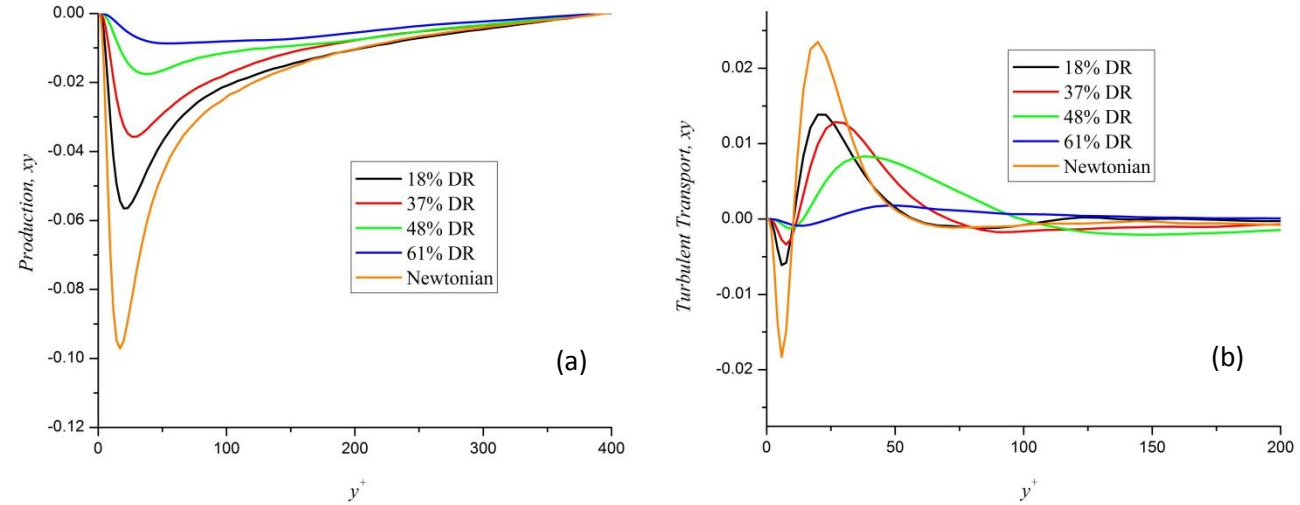

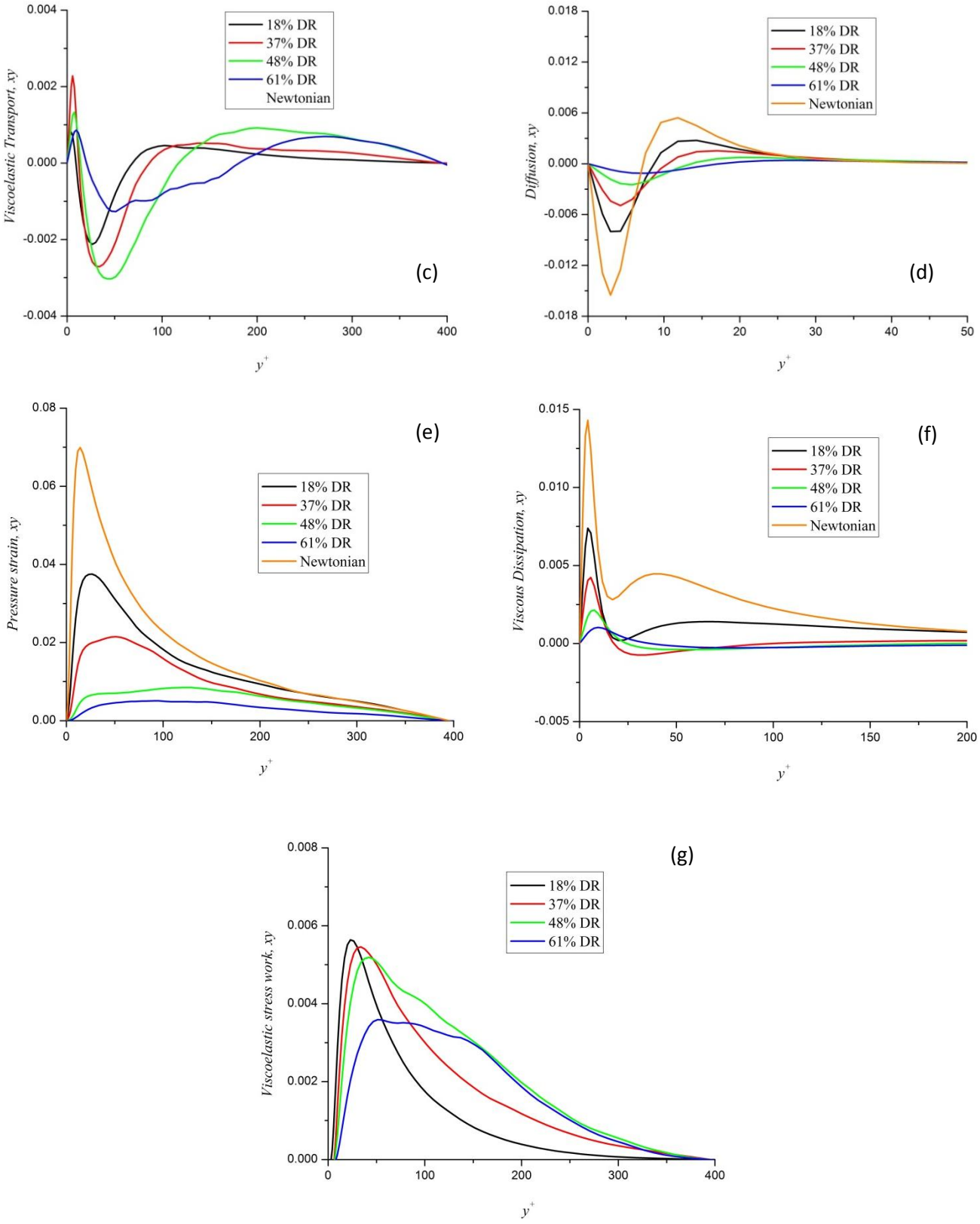

Figure 2.3.4. Budgets of *xy* component of Reynolds stress transport equation.

In this chapter DNS of polymer induced drag reduction in turbulent channel flows up to the maximum drag reduction limit was explained. All turbulent time averaged statistics like mean velocity, mean velocity fluctuations and overall shear stress balance along with correlation coefficients and higher order statistics are calculated and compared with those of Newtonian fluid flow to understand basic features of turbulent viscoelastic fluids. Moreover the DNS data was utilized to evaluate the budgets of Reynolds stresses in the turbulent channel flow of polymer solution. This part of the work contributes further information into the elucidation of the phenomenon of polymer-induced drag reduction and shows further results which are also consistent with previously proposed mechanisms in the literature.

These DNSs were generated to be used in following chapters to help understand the turbulent flow characteristics through a-priori analyses, and to help develop and validate new and better turbulence models in the context of RANS. The *a-priori* analyses focused on the behavior of non-linear terms in the instantaneous and averaged/filtered governing equations which is the key for development of reliable turbulent viscoelastic models in the context of RANS or LES.

3

Chapter 3:
Gs/sgs interactions in viscoelastic flows

M. Masoudian, C. B. da Silva, and F. T. Pinho, Journal of Turbulence, (In press-2015)

"An expert is a person who has made all the mistakes that can be made in a very narrow field."
– Niels Bohr

Abstract

Using direct numerical simulation (DNS) of turbulent plane channel flow of homogeneous polymer solutions, described by the Finitely Extensible Nonlinear Elastic-Peterlin (FENEP) rheological constitutive model, a-priori analyzes of the filtered momentum and FENE-P constitutive equations are performed. The influence of the polymer additives on the subgrid-scale (SGS) energy is evaluated by comparing the Newtonian and the viscoelastic flows, and a severe suppression of SGS tensor is observed in the viscoelastic flow. All the terms of the transport equation of the SGS kinetic energy for FENE-P fluids are analyzed, and an approximated version is suggested. The terms responsible for kinetic energy transfer between GS and SGS energy (including forward/backward energy transfer) are evaluated in the presence of polymers. It is observed that forward scatter events generated by the SGS dissipation decrease in the presence of polymers.

3.1. Introduction

DNS of turbulent viscoelastic flows has shed light on the mechanism and different aspects of drag reduction by polymer additives over the last two decades, however the DNS of the turbulent flows with homogenous polymer additives is much more expensive than the corresponding Newtonian turbulent flow, because of the existence of the constitutive equations which increases the number of primary variables, and these extra equations must be solved to account for the polymer contribution. Moreover, as DR increases, the near wall streaks become progressively stabilized and elongated, thus requiring the use of longer simulation boxes in particular for high DR cases Li et al. (2006). Consequently, for a given Reynolds number, the CPU-time and memory requirements for DNS of viscoelastic flows are at least one order of magnitude larger than for the corresponding Newtonian case, which is unfeasible for engineering applications. Hence, large eddy simulation (LES) and Reynolds-averaged Navier–Stokes (RANS) models need to be developed for modeling turbulent flows of dilute polymer solutions for engineering applications.

Recently, Ohta et al. (2014) developed a modified Smagorinsky model for turbulent channel flow of generalized Newtonian fluids, with viscosity described by the power-law model, and focused on low-Reynolds-number wall turbulence of non-Newtonian inelastic fluids.

Presently, subgrid scale (SGS) models for large eddy simulations of turbulent drag-reducing flows with additives described by differential viscoelastic constitutive equations, such as the FENE-P models, are rare. The present work is precisely motivated by the need to understand the effect of viscoelasticity on the filtered governing equations arising in LES. For this purpose, DNSs of turbulent channel flow of FENE-P fluids were carried out. The top filter is used to separate grid (GS) and subgrid scales (SGS). The additional terms appearing in the momentum equation for FENE-P fluids due to the filtering procedure are calculated and the influence of rheological parameters is investigated. Additionally, the

filtered FENE-P constitutive equation is also investigated and the resolved and unresolved terms are identified and assessed.

As suggested by Piomelli et al. (1991, 1996), and da Silva et al. (2002) for Newtonian turbulent flows, the accurate modeling of direct and inverse energy transfer between GS and SGS may be desirable, particularly for non-equilibrium flows. Although this issue has received attention for Newtonian fluids, no effort has actually been made to quantify this phenomenon in turbulent drag reducing flows described by the FENE-P constitutive equations, particularly in wall bounded flows. In this work we analyze for the first time the backward and forward scatter behavior of the terms incorporating the GS/SGS energy transfer by using the SGS kinetic energy transport equation appropriate for FENE-P fluids.

3.2. Filtering procedure

In LES all variables of the flow (φ) are decomposed into a grid scale ($\varphi^{<}$) and a subgrid scale part ($\varphi^{>}$). Using this notation the main flow variables are decomposed as:

$$u_i = u_i^{<} + u_i^{>},\ p = p^{<} + p^{>},\ \tau_{v,ij} = \tau_{v,ij}^{<} + \tau_{v,ij}^{>}$$

where the grid scales are identified by,

$$\varphi^{<}(x) = \int_{\Omega} \varphi(x') G_{\Delta}(x - x') dx \tag{3.1}$$

In this equation $G_{\Delta}(x)$ is the filter kernel of width Δ, which must satisfy $\int_{\Omega} G_{\Delta}(x) dx = 1$, $\varphi(x)$ is a given flow variable, and the integration is extended over the entire flow domain, Ω.

In *a priori* tests the resolved velocity fields obtained from DNS are explicitly filtered in order to obtain the exact quantities of interest. The filter kernel that is used here is the box or top-hat filter defined as,

$$G(x) = \begin{cases} 1/\Delta & if\ |x| \le \Delta/2 \\ 0 & otherwise \end{cases} \tag{3.2}$$

3.3. Filtered Navier-Stokes equation

Applying the filtering operation to the continuity and Navier-Stokes equations yields the so-called filtered Navier-Stokes tequation, which govern the evolution of the grid scales of motion:

$$\frac{\partial u_i^{<}}{\partial t} + \frac{\partial u_i^{<} u_j^{<}}{\partial x_j} = -\frac{\partial p^{<}}{\partial x_i} + \frac{\beta}{\mathrm{Re}_{\tau 0}} \frac{\partial}{\partial x_j}\left(\frac{\partial u_i^{<}}{\partial x_j} + \frac{\partial u_j^{<}}{\partial x_i}\right) - \frac{\partial \tau_{ij}}{\partial x_j} + (1-\beta)\frac{\partial \tau_{v,ij}^{<}}{\partial x_j} \tag{3.3}$$

$$\frac{\partial u_i^{<}}{\partial x_i} = 0 \tag{3.4}$$

τ_{ij} is the unknown subgrid-stress tensor defined by $\tau_{ij} = \left(u_i u_j\right)^{<} - u_i^{<} u_j^{<}$, and is responsible for the momentum exchanges between the grid and subgrid scales, and needs to be modeled in LES.

3.4. Filtered conformation tensor equation

The last term on the right-hand-side of the filtered Navier-Stokes equation is the filtered polymer extra stress tensor which arises by filtering Navier-stokes equation for FENE-P fluids, and can be expressed as:

$$\tau^{<}_{ij,v} = \frac{\eta_p}{\lambda}\left[f(c_{kk})c_{ij} - f(L)\delta_{ij} \right]^{<} = \frac{\eta_p}{\lambda}\left(f(c_{kk})c_{ij} \right)^{<} - \frac{\eta_p}{\lambda} f(L)\delta_{ij} \tag{3.5}$$

By applying the filtering operation described above, the filtered FENE-P constitutive equation is obtained,

$$\frac{\partial c_{ij}^{<}}{\partial t} + u_k^{<}\frac{\partial c_{ij}^{<}}{\partial x_k} - \left(c_{ik}^{<}\frac{\partial u_j^{<}}{\partial x_k} + c_{jk}^{<}\frac{\partial u_i^{<}}{\partial x_k} \right) + \frac{\tau_{ij,v}^{<}}{\eta_p} = FT_{ij} + ST_{ij} \tag{3.6}$$

where the two terms on the right-hand-side include the following subgrid scale contributions

$$FT_{ij} = u_k^{<}\frac{\partial c_{ij}^{<}}{\partial x_k} - \left(u_k \frac{\partial c_{ij}}{\partial x_k} \right)^{<}$$

$$ST_{ij} = \left(c_{ik}\frac{\partial u_j}{\partial x_k} + c_{jk}\frac{\partial u_i}{\partial x_k} \right)^{<} - \left(c_{ik}^{<}\frac{\partial u_j^{<}}{\partial x_k} + c_{jk}^{<}\frac{\partial u_i^{<}}{\partial x_k} \right)$$

FT_{ij}, and ST_{ij} are the unknown terms, and are subgrid scale contributions to the FENE-P constitutive equation.

3.5. Transport equations for the grid-scale and subgrid-scale kinetic energies

In order to study the interaction between grid (GS) and subgrid scales (SGS) kinetic energies, the GS and SGS kinetic energies for turbulent channel flow of viscoelastic fluids will be analyzed. The transport equation for (twice) the GS kinetic energy for viscoelastic fluids described by FENE-P is given by,

$$\underbrace{\frac{\partial u_i^{<} u_i^{<}}{\partial t}}_{(A)} + \underbrace{\frac{\partial u_i^{<} u_i^{<} u_j^{<}}{\partial x_j}}_{(B)} = -2\underbrace{\frac{\partial p^{<} u_i^{<}}{\partial x_i}}_{(C)} + \underbrace{\frac{\beta}{\mathrm{Re}_\tau}\frac{\partial}{\partial x_j}\left(\frac{\partial k}{\partial x_j}\right)}_{(D)} \underbrace{-\frac{2\beta}{\mathrm{Re}_\tau}\frac{\partial u_i^{<}}{\partial x_j}\frac{\partial u_i^{<}}{\partial x_j}}_{(E)} \tag{3.7}$$

$$\underbrace{-2\frac{\partial \tau_{ij} u_i^{<}}{\partial x_j}}_{(F)} + \underbrace{2\tau_{ij} S_{ij}^{<}}_{(G)} + \underbrace{2(1-\beta)\frac{\partial \tau_{v,ij}^{<} u_i^{<}}{\partial x_j}}_{(H)} \underbrace{-2(1-\beta)\tau_{v,ij}^{<} S_{ij}^{<}}_{(I)}$$

It is important to recall the physical meaning of this equation and its respective terms. Terms A and B account for the total (local and advection) variation of GS kinetic energy, respectively. Terms C and D represent the redistribution (diffusion) of GS kinetic energy by pressure/velocity interactions and molecular viscosity, respectively. Term E is the local GS kinetic energy dissipation associated to the molecular viscosity. The terms F and G are the only terms involving the subgrid-stress tensor τ_{ij} and they are directly related to the kinetic energy exchanges between GS and SGS. Term F (GS/SGS diffusion) represents a redistribution of GS kinetic energy by interactions between the GS velocity and the SGS stresses. The GS/SGS transfer (term G), also called subgrid-scale dissipation, represents the transfer of kinetic energy between GS and SGS. Terms H and I account for the interactions between GS and polymer. Term H, is hereafter called GS/polymer diffusion, and term I is the GS/polymer dissipation.

The transport equation for (twice) the SGS kinetic energy is given by,

$$\underbrace{\frac{\partial \tau_{ii}}{\partial t}}_{(J)} + \underbrace{\frac{\partial \tau_{ii} u_j^{<}}{\partial x_j}}_{(K)} = \underbrace{\frac{\partial}{\partial x_j}\left(\left(u_i u_i\right)^{<} u_j^{<} - \left(u_i u_i u_j\right)^{<}\right)}_{(L)} \underbrace{-2\frac{\partial}{\partial x_i}\left(p^{<} u_i^{<} - \left(p u_i\right)^{<}\right)}_{(M)} + \underbrace{\frac{\beta}{\mathrm{Re}_\tau}\frac{\partial}{\partial x_j}\left(\frac{\partial \tau_{ii}}{\partial x_j}\right)}_{(N)} \tag{3.8}$$

$$\underbrace{-\frac{2\beta}{\mathrm{Re}_\tau}\left(\left(\frac{\partial u_i}{\partial x_j}\frac{\partial u_i}{\partial x_j}\right)^{<} - \frac{\partial u_i^{<}}{\partial x_j}\frac{\partial u_i^{<}}{\partial x_j}\right)}_{(O)} + \underbrace{2\frac{\partial \tau_{ij} u_i^{<}}{\partial x_j}}_{(P)} \underbrace{-2\tau_{ij} S_{ij}^{<}}_{(Q)} +$$

$$\underbrace{2(1-\beta)\frac{\partial\left(\tau_{v,ij} u_i\right)^{<}}{\partial x_j}}_{(R)} \underbrace{-2(1-\beta)\frac{\partial \tau_{v,ij}^{<} u_i^{<}}{\partial x_j}}_{(S)} \underbrace{-2(1-\beta)\left(\tau_{v,ij} S_{ij}\right)^{<}}_{(T)} + \underbrace{2(1-\beta)\tau_{v,ij}^{<} S_{ij}^{<}}_{(U)}$$

Equation 3.8 expresses the mechanisms governing the evolution of the unresolved or subgrid scales kinetic energy (twice), in which terms *J* and *K* represent the local and advective variation of the SGS kinetic energy, respectively. The diffusion caused by the turbulence fluctuations of the SGS kinetic energy is represented by term *L* (SGS turbulent transport), term *M* represents the SGS pressure/velocity interactions and term *N* accounts for the SGS viscous diffusion. Term *O* is the SGS viscous dissipation, while terms P and Q are the only terms involving the subgrid-stress tensor τ_{ij} and are directly related to the kinetic energy exchanges between GS and SGS. These two terms represent the classical kinetic energy cascade, which also exists in viscoelastic turbulent flows. Term P (GS/SGS diffusion) represents a redistribution of SGS kinetic energy by interactions between the GS velocity and the SGS stresses, whereas the GS/SGS transfer (term Q) also often named subgrid-scale dissipation, represents the transfer of kinetic energy between GS and SGS. It is important to notice that terms P and Q are, respectively, the symmetric of terms F and G appearing in the GS equation. Since these terms appear in both equations with opposite signs, they represent the kinetic energy exchange between GS and SGS. Although the same happens mathematically with viscoelastic terms H, I and S, U, respectively, here the transfer of energy between GS and SGS is carried out through GS/polymer and SGS/polymer interactions. If term Q is positive, the kinetic energy cascades from GS to SGS (forward scatter), otherwise, SGS kinetic energy flows into the GS (backward scatter). In the presence of polymer additives, four new mechanisms must be accounted to study the SGS kinetic energy and the GS/SGS interactions, which are absent in Newtonian flows. These are terms R, S, T, and U accounting for the effects of polymer additives on the SGS transport equation. Term R represents additional diffusion prompted by polymer/velocity interactions, and at the end it does not involve net GS/SGS energy exchanges. In contrast, term S, which also represents a diffusion prompted by the polymer, but involves a net GS/SGS energy exchange. Terms T and U are similar to terms R and S but are associated with source/sinks prompted by the polymer. Term T does not involve net energy exchange between GS and SGS, while term U does indeed involve kinetic energy exchanges between GS and SGS induced by the presence of polymers in the solution. As with terms P and Q, positive values for terms U and S imply forward scatter, whereas negative values describe backward scatter events.

Table 3.1. Summary of the physical and computational parameters for the DNS cases used in this work.

case	$Re_{\tau 0}$	Domain size $L_x \times L_y \times L_z$	Grid size n_x, n_y, n_z	L^2	$Wi_{\tau 0}$	β
DNS0	395	14.136h× 2h× 4.5h	384× 257× 192	0	0	0
DNS1	395	14.136h× 2h× 4.5h	384× 257× 192	3600	50	0.9
DNS2	395	14.136h× 2h× 4.5h	384× 257× 192	10000	100	0.9

3.6. Results and discussions

In this section we analyze the grid/subgrid-scale interactions in turbulent channel flows with viscoelastic properties described in Table 3.1. The separation between grid and subgrid-scales is achieved through the application of a box filter, with filter sizes equal to $4\Delta x_i, 6\Delta x_i, 8\Delta x_i$. The averaged ratio of the SGS to GS kinetic energy for all chosen filter sizes are below 30% which indicates that all chosen filter sizes are representative of actual LES calculations Piomelli at al. (1991). Furthermore, all the conclusions and findings in this work were checked for all three filter sizes.

3.6.1. Subgrid scale terms in the momentum and conformation tensor equations

The subgrid-stress tensor, τ_{ij}, in the momentum equation is responsible for the momentum exchanges between the grid and subgrid scales. Most of SGS models are based on an artificial eddy viscosity approach, where the effects of the SGS turbulence are lumped into a turbulent or eddy viscosity. This approach treats the dissipation of kinetic energy at sub-grid scales as analogous to molecular diffusion,

$$\tau_{ij} - \frac{1}{3}\tau_{kk}\delta_{ij} = -2\upsilon_T S_{ij}^{<}$$

where υ_T is the turbulent eddy viscosity and $S_{ij}^{<}$ is the large scale rate of strain tensor. For instance, in the Smagorinsky model one assumes that the turbulent eddy viscosity is proportional to the rate of strain norm, $\left|S^{<}\right| = \sqrt{2(S_{ij}^{<}S_{ij}^{<})}$. In order to analyze the influence of viscoelasticity on the subgrid stresses tensor, the quantity $\tau_{xy} / (-S_{xy}^{<}\left|S^{<}\right|)$, which is equal to $\left(C_s\Delta_g\right)^2$ in LES of Newtonian turbulence, is plotted in figure 3.1-a using the *a priori* DNS data for viscoelastic (HRD: case DNS2 and LDR: case DNS1) and Newtonian cases.

As can be seen this quantity is severely suppressed by the addition of polymers to the solvent and keeps decreasing for increasing DR. In order to have an idea about the amount of suppression and the overall change in the shape of this quantity for viscoelastic cases in relation to the Newtonian flow case, the quantity $\left(\tau_{xy} / (-S_{xy}^{<}\left|S^{<}\right|)\right)_{LDR}$ and $\left(\tau_{xy} / (-S_{xy}^{<}\left|S^{<}\right|)\right)_{HDR}$ over $\left(\tau_{xy} / (-S_{xy}^{<}\left|S^{<}\right|)\right)_{New.}$ are plotted in figure 3.1-b. It is interesting to note that the ratios are almost constant, with values of circa 0.12 for low drag reduction and of about 0.03 for high drag reduction regimes, indicating that for FENE-P fluids the overall shape of $\left(C_s\Delta_g\right)^2$ remains similar to that for Newtonian fluid, suggesting that a simple

extension of the Newtonian closures may be effective to account for the influence of viscoelasticity on the SGS tensor.

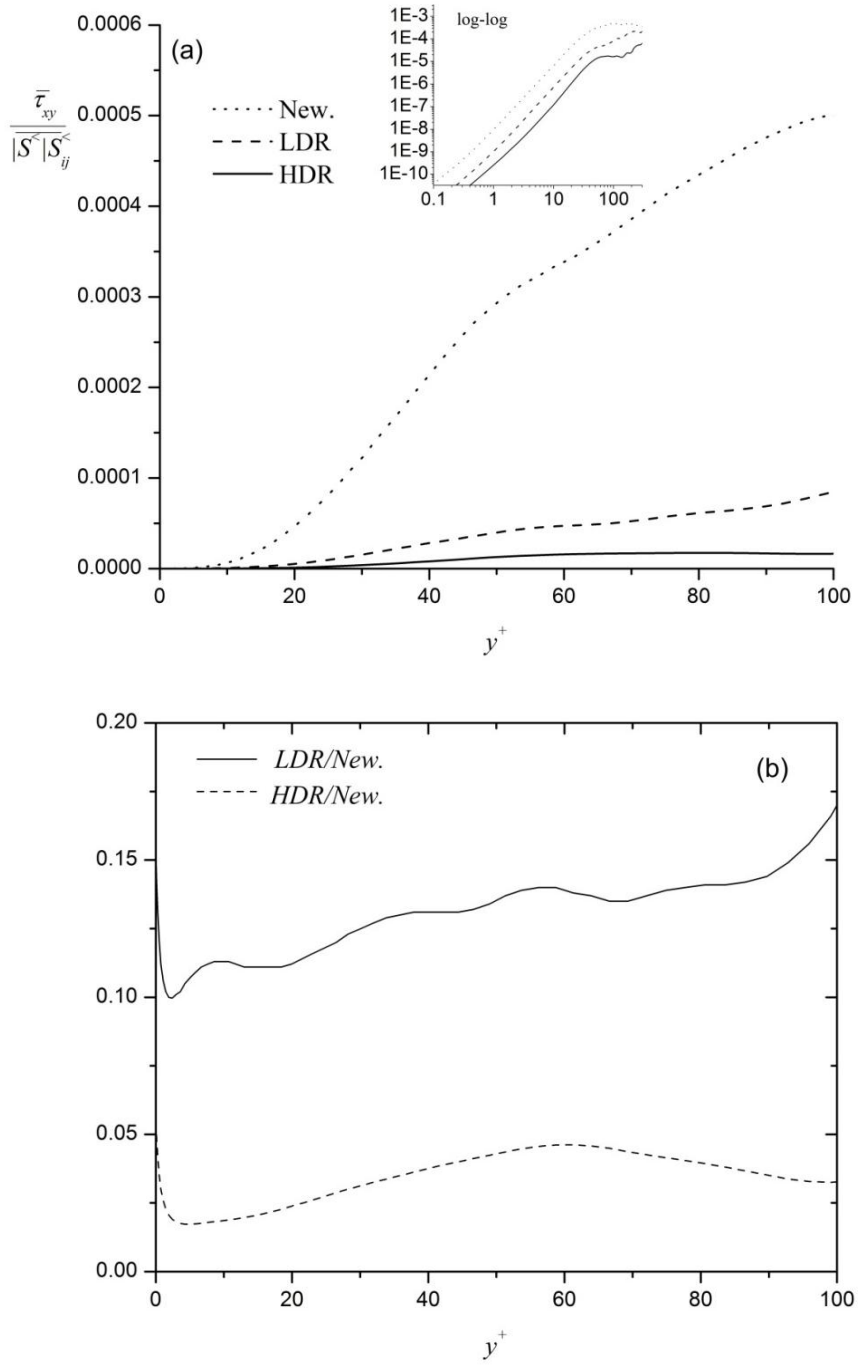

Figure 3.1. (a) Profiles of $\tau_{xy} / (-S^<_{xy}|S^<|)$ for New., LDR, and HDR cases. (b) Solid line: $\left(\tau_{xy} / (-S^<_{xy}|S^<|)\right)_{LDR} \Big/ \left(\tau_{xy} / (-S^<_{xy}|S^<|)\right)_{New.}$ dash line: $\left(\tau_{xy} / (-S^<_{xy}|S^<|)\right)_{HDR} \Big/ \left(\tau_{xy} / (-S^<_{xy}|S^<|)\right)_{New.}$, New., LDR, and HDR denote DNS0, DNS1, and DNS2 cases, respectively. Filter size is $4\Delta x$.

Another unknown term that appears in the filtered momentum equation is the filtered viscoelastic stress tensor, which can be split into,

$$\tau^{<}_{ij,v} = \underbrace{\left(\eta_p/\lambda\right)\left[\left(f(c_{kk})c_{ij}\right)^{<} - f(c_{kk})^{<}c_{ij}^{<}\right]}_{term\ 1} + \underbrace{\left(\eta_p/\lambda\right)\left[f(c_{kk})^{<}c_{ij}^{<} - f(L)\delta_{ij}\right]}_{term\ 2}$$

In this equation term 2 is exact and contains only large scale quantities, whereas term 1 accounts for the SGS influence and is unknown, and is the SGS contribution to the polymer stress. Both terms are compared in figure 3.2 in all directions for the smallest and largest filter sizes used in this study, and it is clear that regardless of the filter size in all directions $\left(\eta_p/\lambda\right)\left[\left(f(c_{kk})c_{ij}\right)^{<} - f(c_{kk})^{<}c_{ij}^{<}\right]$ is nearly 40 times smaller than $\left(\eta_p/\lambda\right)f(c_{kk})^{<}c_{ij}^{<}$ indicating that it is possible to safely approximate the filtered viscoelastic extra stress tensor in the filtered Navier-Stokes equation, $\tau^{<}_{ij,v}$, using only by its second GS term, i.e.

$$\tau^{<}_{ij,v} \simeq \frac{\eta_p}{\lambda}\left[f(c_{kk})^{<}c_{ij}^{<} - f(L)\delta_{ij}\right] \tag{3.9}$$

In the filtered conformation tensor equation (Eq. 3.6) there are also two unknown SGS terms, which need to be analyzed, terms FT_{ij} and ST_{ij}. FT_{ij} represents the SGS contribution to the advective transport of the filtered conformation tensor by the velocity field, and ST_{ij} represents the SGS contribution from the interaction between the components of the conformation tensor and the velocity gradient tensor, and is originated from the distortion term of the Oldroyd derivative of the filtered conformation tensor. Regardless of the filter size and the amount of drag reduction it was found that FT_{ij} is almost zero across the channel (see figure 3.3), hence the contribution from this term to the filtered conformation tensor can be safely neglected.

In figure 3.3 the trace and shear component of ST_{ij} are plotted using different filter sizes and compared with the corresponding GS exact term $\left(c_{ik}^{<}\,\partial u_j^{<}/\partial x_k + c_{jk}^{<}\,\partial u_i^{<}/\partial x_k\right)$. As can be observed ST_{kk} has a very small magnitude in comparison with $\left(c_{ik}^{<}\,\partial u_j^{<}/\partial x_k + c_{jk}^{<}\,\partial u_i^{<}/\partial x_k\right)$. It can be seen that ST_{kk} is almost independent of the filter size. On the other hand, its shear component is somehow comparable to $\left(c_{xk}^{<}\,\partial u_y^{<}/\partial x_k + c_{yk}^{<}\,\partial u_x^{<}/\partial x_k\right)$especially for larger filter sizes, where ST_{xy} is almost 15% of the corresponding GS term, $\left(c_{ik}^{<}\,\partial u_j^{<}/\partial x_k + c_{jk}^{<}\,\partial u_i^{<}/\partial x_k\right)$, hence ST_{ij} and in particular its shear component in our point of view is non-negligible especially for high drag reduction regimes, where the resolved polymer mean shear stress is comparable to the Reynolds shear stress. In summary, the term by term analysis of the

filtered conformation tensor in this work reveals that the filtered conformation equation can be approximated as,

$$\frac{\partial c_{ij}^{<}}{\partial t}+u_k^{<}\frac{\partial c_{ij}^{<}}{\partial x_k}-\left(c_{ik}^{<}\frac{\partial u_j^{<}}{\partial x_k}+c_{jk}^{<}\frac{\partial u_i^{<}}{\partial x_k}\right)+\frac{\tau_{ij,v}^{<}}{\eta_p}=ST_{ij}$$

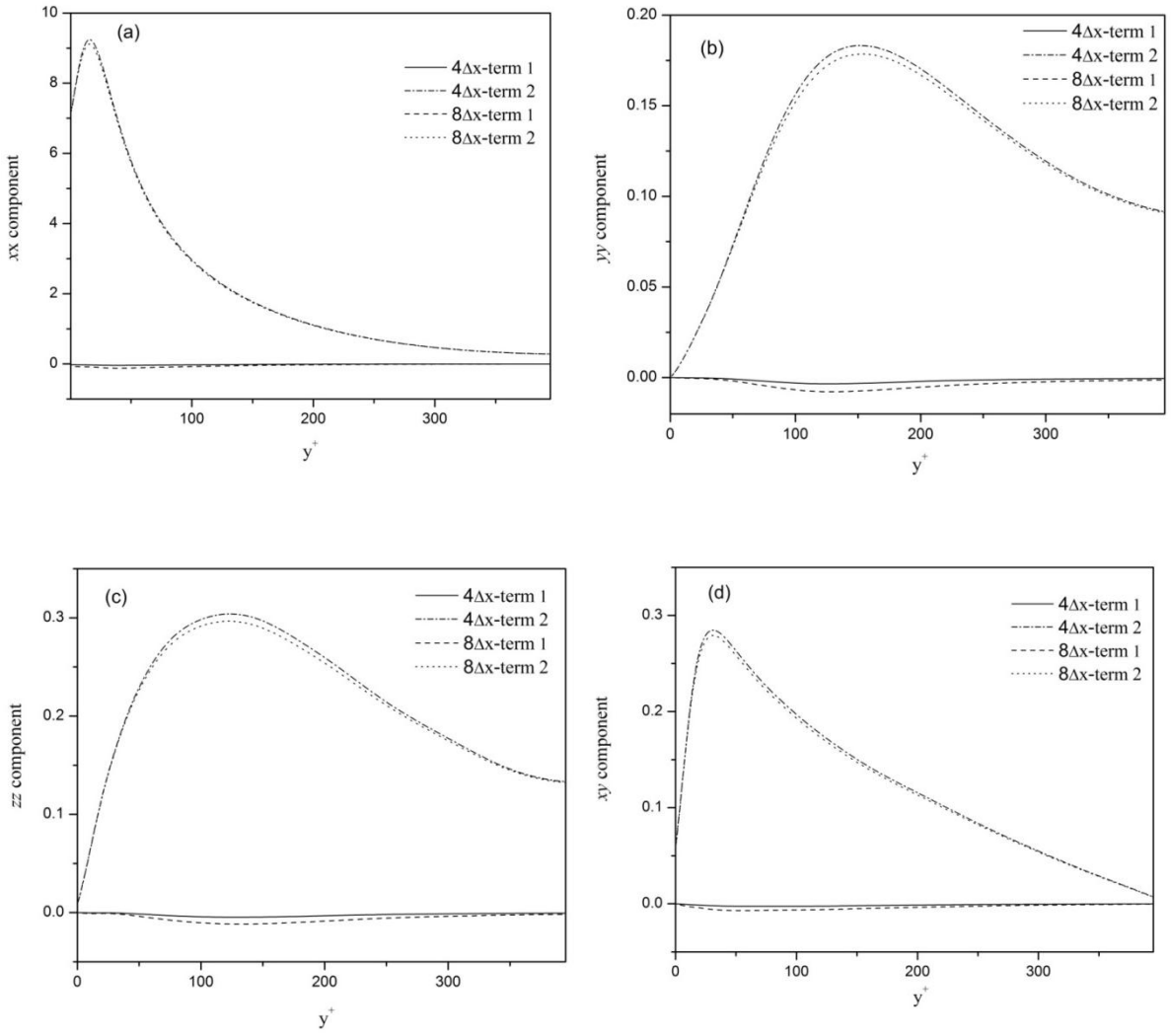

Figure 3.2. Profiles of components of terms $\left(\eta_p/\lambda\right) f(c_{kk})^{<} c_{ij}^{<}$ and $\left(\eta_p/\lambda\right)\left(f(c_{kk})c_{ij}\right)^{<}-\left(\eta_p/\lambda\right) f(c_{kk})^{<} c_{ij}^{<}$ (a) streamwise, (b) wall normal, (c) spanwise components, (d) shear components of HDR case (DNS2).

3.6.2. Analysis of the grid and subgrid-scale interactions

Figs. 3.4 (a-g) plot plane averaged profiles of the various terms in the budget of SGS kinetic energy transport equation, as a function of the dimensionless wall distance, y^+, for Newtonian and the low and high drag reduction viscoelastic cases (HDR: case DNS2 and LDR: case DNS1). As in all the results presented here, the number of realizations is sufficient to converge the budgets. In order to have an idea about instantaneous behavior of different terms the PDF of terms K, L, M, N, O, and P at y^+=5, and y^+=21 are plotted in figure 3.5 (a-b)).

The advection variation of the SGS kinetic energy, term K, is plotted in figure 3.4-a. The magnitude of the maxima is almost constant, and only weakly affected by the presence of the polymers and intensity of DR, although a shift of the peak location can be observed. This shift is consistent with the notion of the expansion of the buffer layer associated with drag reduction by polymer additives.

The terms involving only GS/SGS interactions within the solution, i.e. terms associated with SGS turbulent transport, SGS pressure/velocity interactions, SGS viscous diffusion, and SGS viscous dissipation are plotted in figures 3.4 (b-e), respectively. The magnitude of the maxima and minima of all these terms display a pronounced suppression with increasing DR especially close to the wall. The figures show that these quantities for LDR regime decrease around 60% relative to the Newtonian case, and for HDR case this reduction is around 80%. In addition, a shift farther from the wall of the peak value is observed with increasing DR, which is also conceptually consistent with the notion of the expansion of the buffer layer associated with drag reduction. It can be inferred that these terms show the most significant reduction relative to their Newtonian values and provide insight into the effects of polymer additives onto the SGS kinetic energy transport equation. Note that as for the Newtonian fluid, in the viscoelastic cases the advective term as well as all the diffusion-like terms, such as pressure-velocity, viscous, SGS diffusion, and turbulent transport, do not create or destroy energy but only redistribute it between adjoining volumes. The mean classical GS/SGS diffusion and SGS dissipation for the viscoelastic and Newtonian flows are plotted in figure 3.4-f. For the HDR case the peak value of the GS/SGS diffusion has decreased to 30% of the corresponding Newtonian value showing that polymer additives cause a severe reduction in the local energy transfer between the GS and SGS.

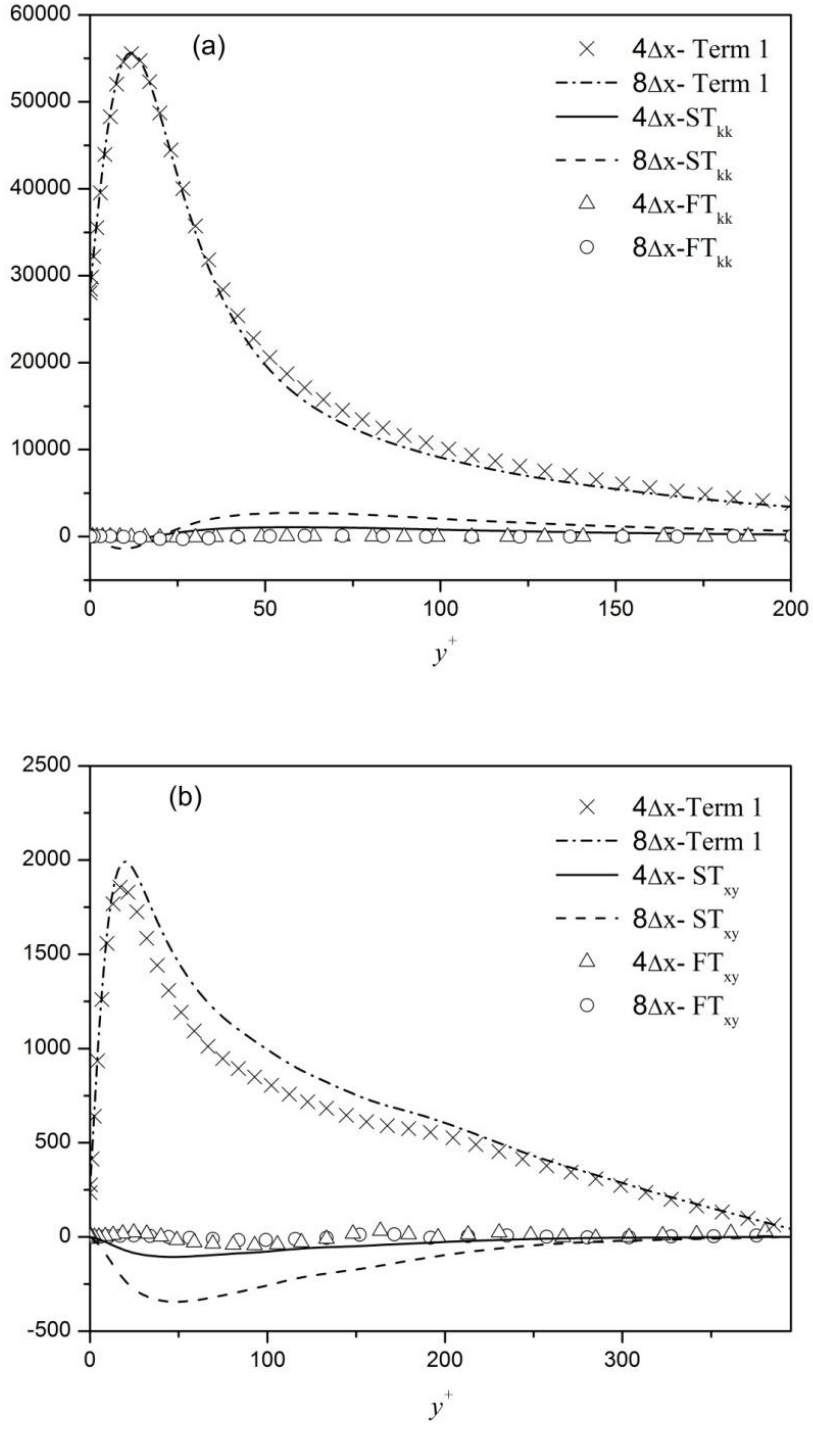

Figure 3.3. Comparison of FT_{ij}, ST_{ij}, and term1: $\left(c_{ik}^{<} \frac{\partial u_j^{<}}{\partial x_k} + c_{jk}^{<} \frac{\partial u_i^{<}}{\partial x_k} \right)$ (a) trace, (b) shear components of HDR case (DNS2).

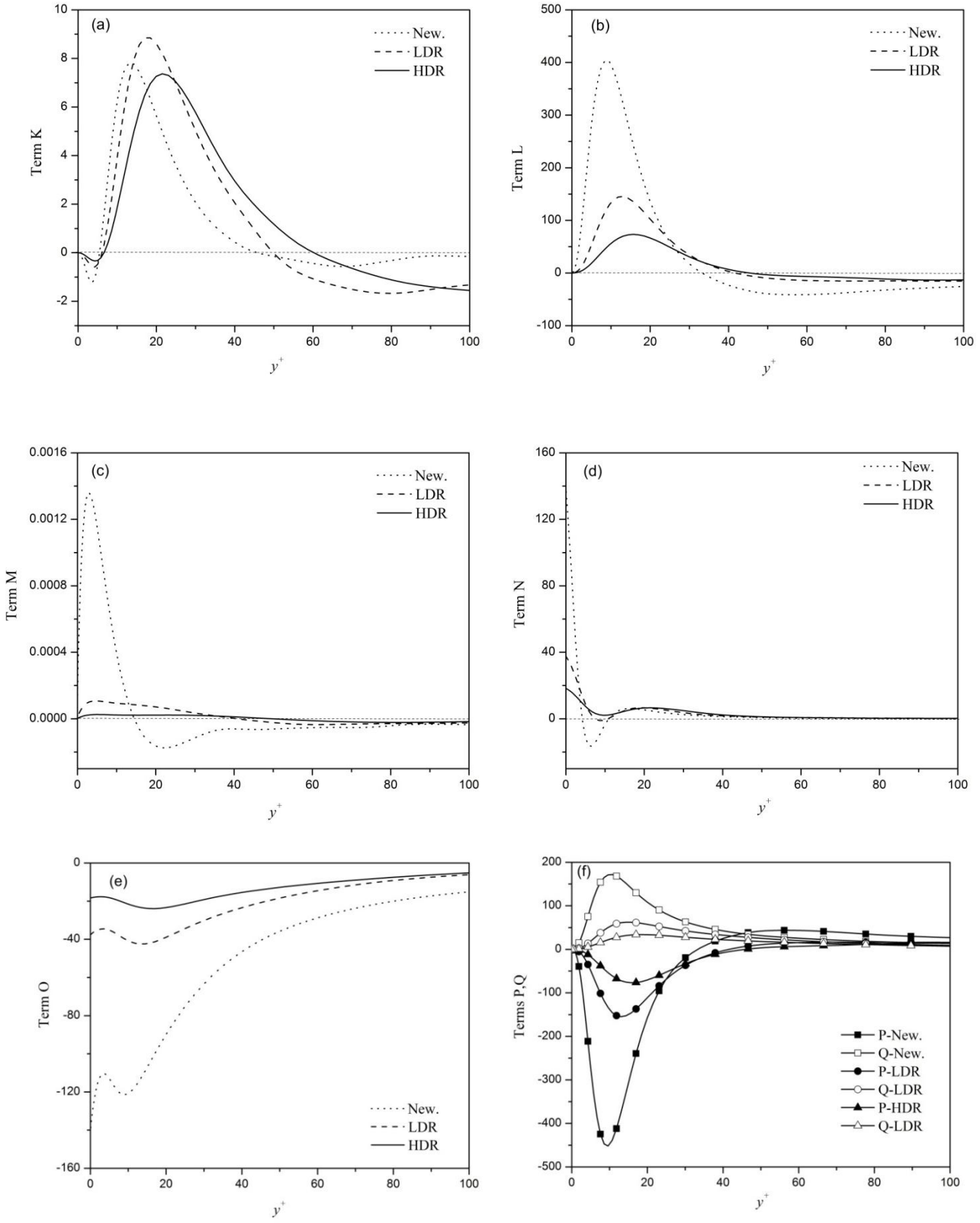
(a)
New.
LDR
HDR
Term K
y^+
(b)
New.
LDR
HDR
Term L
y^+
(c)
New.
LDR
HDR
Term M
y^+
(d)
New.
LDR
HDR
Term N
y^+
(e)
New.
LDR
HDR
Term O
y^+
(f)
P-New.
Q-New.
P-LDR
Q-LDR
P-HDR
Q-LDR
Terms P,Q
y^+

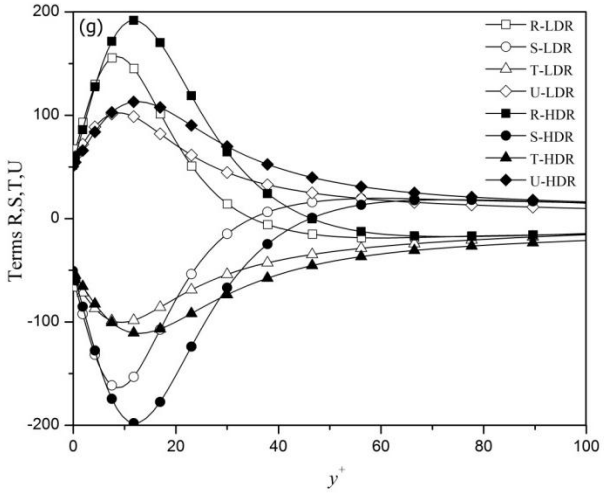

Figure. 3.4. Plane-averaged terms appearing in SGS transport equation. Newtonian, LDR, and HDR denote DNS0, DNS1, and DNS2 cases, respectively. Filter size is $8\Delta x$.

Comparing the magnitude of all the terms in figure 3.4 shows that term M is less than 1% of the magnitude of other terms for both Newtonian and viscoelastic flows, hence it is negligible in the budgets of SGS transport. This is also confirmed from its 1D PDF profile depicted in figure 3.5 (a-b). SGS turbulent transport (Term L), and SGS diffusion (term P) have a noticeable magnitude in the SGS transport equation. The joint probability density function for terms L and P for HDR case is plotted at y^+=17, the locus of its peak value, in figure 3.6, and it shows that for all events these quantities for viscoelastic cases as for Newtonian case are highly correlated regardless of the fluid. The correlation coefficient for these terms exceeds -98% all across the channel, indicating that terms L and P for viscoelastic cases as for Newtonian are in local and statistical equilibrium. This is important because it shows that for viscoelastic fluids as for Newtonian flows based on the findings of Piomelli at al. (1991) the SGS diffusion, although significant, cancels the turbulent transport term almost exactly. Consequently, as stated in Piomelli at al. (1991) for Newtonian flows if one wishes to model the SGS kinetic energy transport equation for viscoelastic fluids, the SGS diffusion may be lumped together with the other diffusion terms.

Another classical term that has a noticeable magnitude in the mean SGS kinetic energy transport is the SGS viscous diffusion (term N). Figure 3.4-d shows that this term for viscoelastic cases as for Newtonian case is active very close to the wall and drops to zero at around y^+=10 regardless of the fluid. Comparing figures 3.4-d, 3.4-e, and 3.5 (a,b) the SGS viscous diffusion (term N) has a similar magnitude, but an opposite sign to the SGS viscous dissipation (term O) at y^+<10. The joint PDF of both terms at y^+=5 is shown in figure 3.7, indicating that these terms not only in the mean but also instantaneously are highly correlated, their correlation coefficient close to the wall, where the viscous dissipation is

more active (y^+<10), is equal to -90% confirming that almost all the energy produced by term N, dissipates by the SGS viscous dissipation.

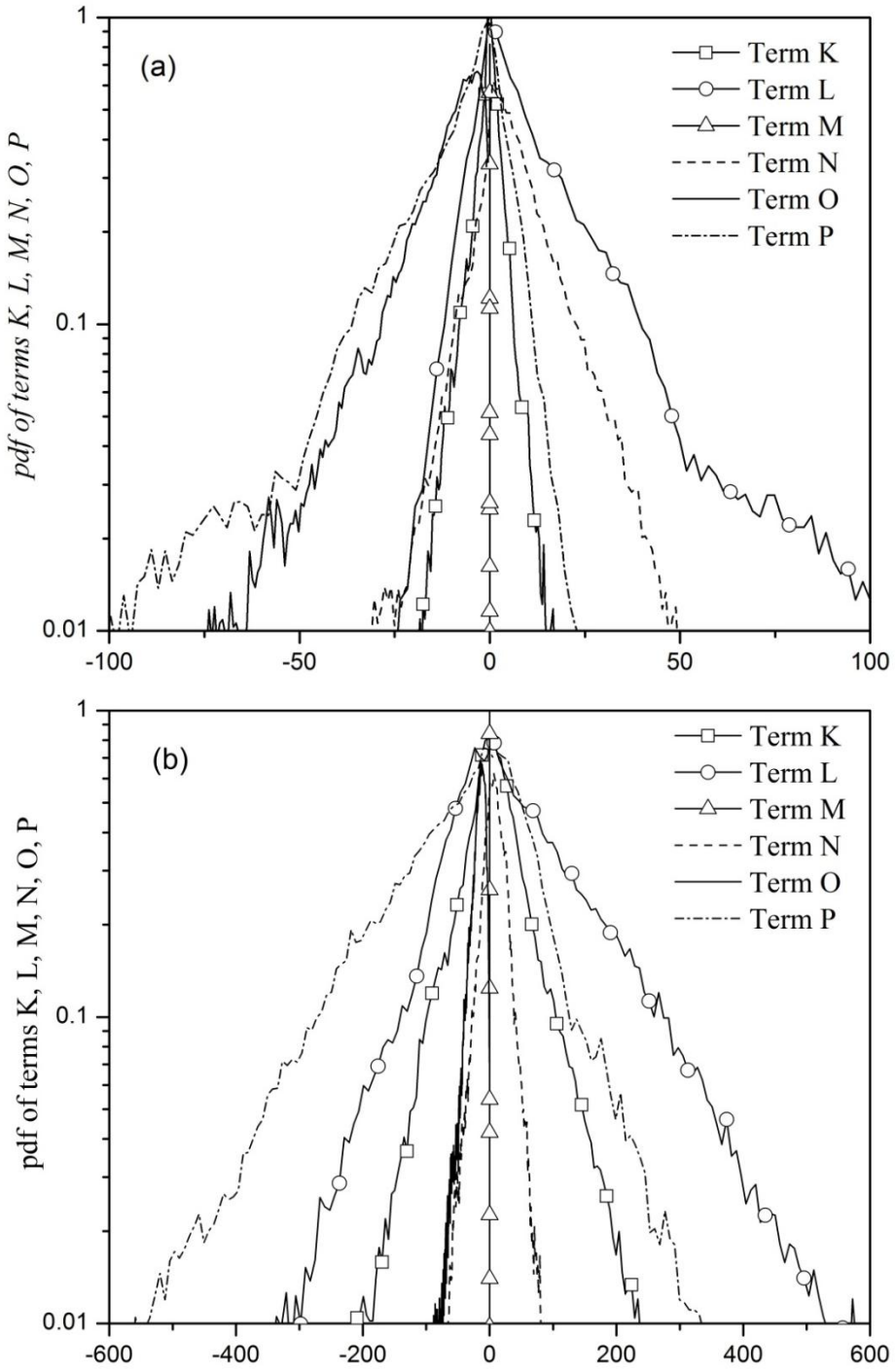

Figure. 3.5. Probability density function of terms K, L, M, N, O, and P, for case HDR (DNS2). Filter size is 8Δ*x*, a) at y^+=5, b) y^+=21.

The last four terms on the SGS kinetic energy transport equation are the new terms containing the viscoelastic stresses, and they are plotted in figure 3.4-g. The figure shows that by increasing DR the peak values associated with these terms display a slight increase, and move away from the wall. The terms R, S and T, U seem to be nearly symmetric in plane averaged budgets of SGS transport equation. For comparison purposes, in figure 3.8 the terms U+T and R+S are plotted, and for the sake of comparison the classical SGS dissipation, term Q, is also included in this figure. The two diffusion-like terms associated with the polymer stress, terms R and S, nearly cancel out across the channel and their sum has a small magnitude in comparison to the SGS dissipation term. The same happens for terms T and U close to the wall, for which the figure shows that their sum is very small in comparison to the SGS dissipation (around 5-15%), however as it can be seen far from the wall term T+U has same magnitude as term Q. In order to better assess the behavior of these two pairs of terms in the instantaneous form their joint probability density functions are plotted at y^+=17 (the place of its maximum value) for the HDR case (figure 3.9), showing that for all events these quantities, U,T and R,S, are highly correlated. Furthermore, the variation across the channel of the correlation coefficient for terms R, S and for terms T and U are calculated using the instantaneous field data for largest filter size and the plane-averaged correlation is plotted in figure 3.10.

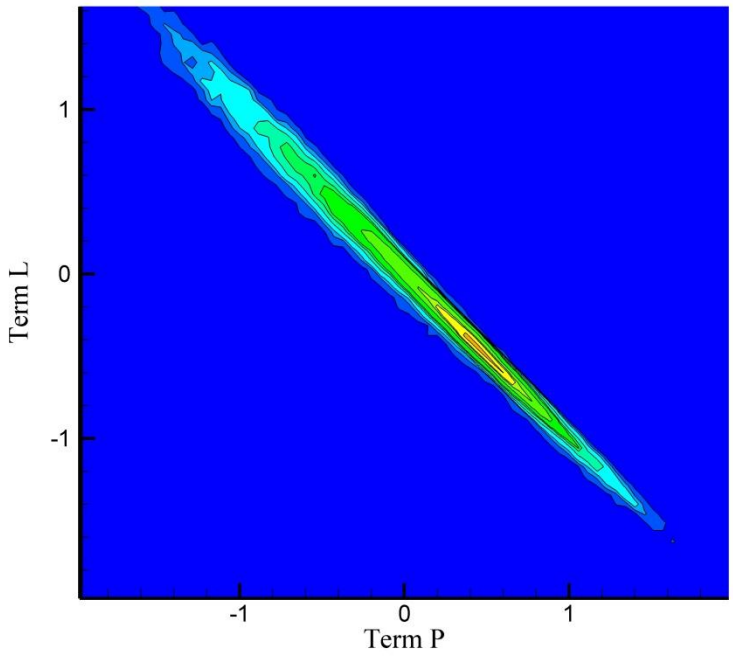

Figure 3.6. Joint probability density function of terms L, and P for case HDR (DNS2). Filter size is $8\Delta x$.

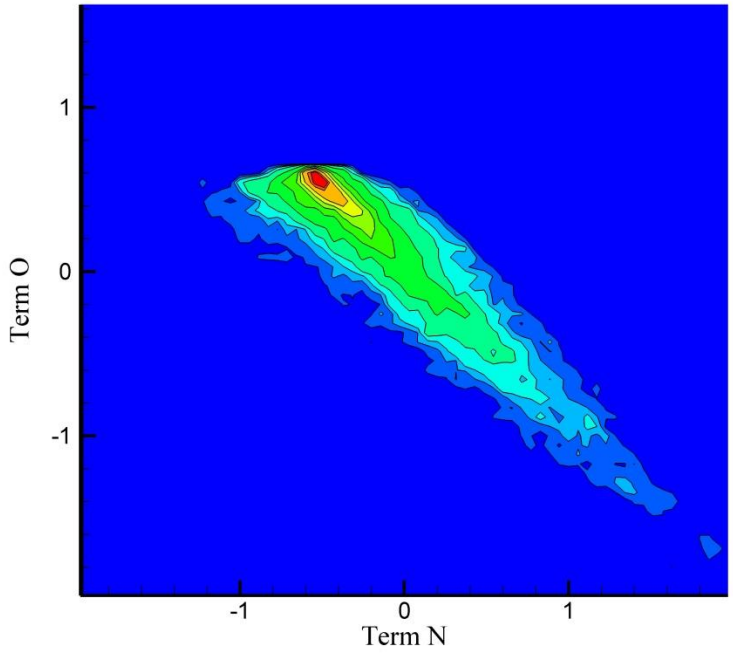

Figure 3.7. Joint probability density function of terms O, and N for case HDR (DNS2).Filter size is $8\Delta x$.

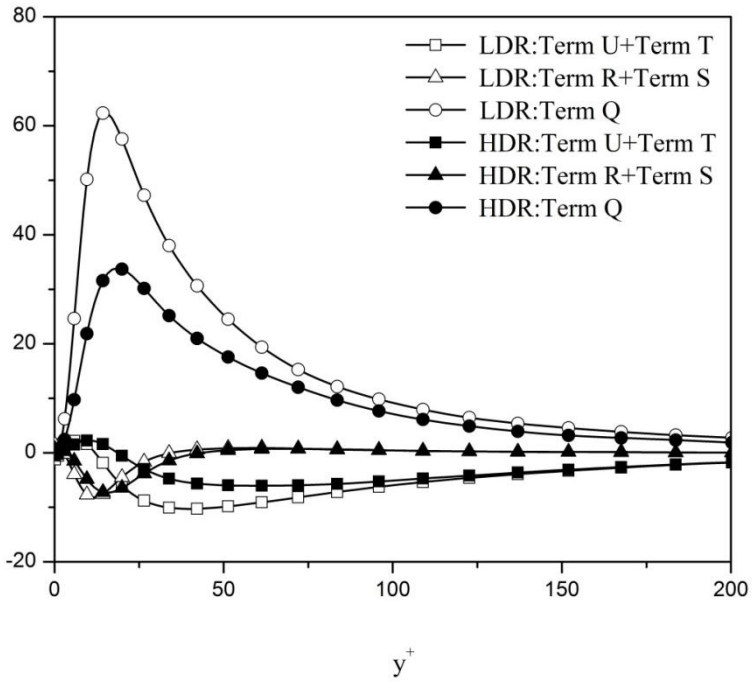

Figure 3.8. Mean U+T and R+S terms for case HDR (DNS2) using $8\Delta x$ filter. LDR, and HDR denote DNS1, and DNS2 respectively.

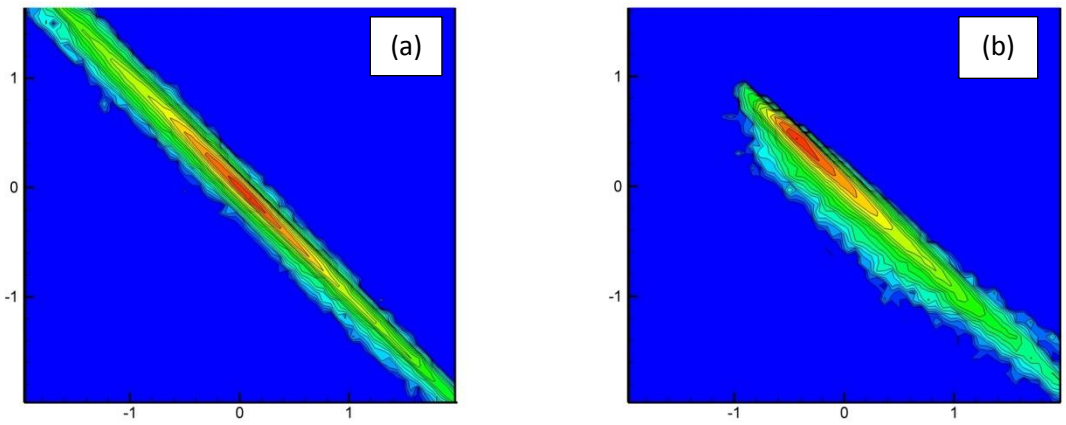

Figure 3.9. Joint probability density function of terms (a) R,S, (b) U,T for case HDR (DNS2). Filter size is 8Δ*x*.

The figure shows that terms R and S are highly correlated (their correlation coefficient is above -99%). whereas, the plane averaged correlation coefficient for terms T and U varies between –99% to -90% stating that although they are highly correlated for all events, some part of kinetic energy induced by the polymer plays a small role in the budget of SGS kinetic energy transport equation.

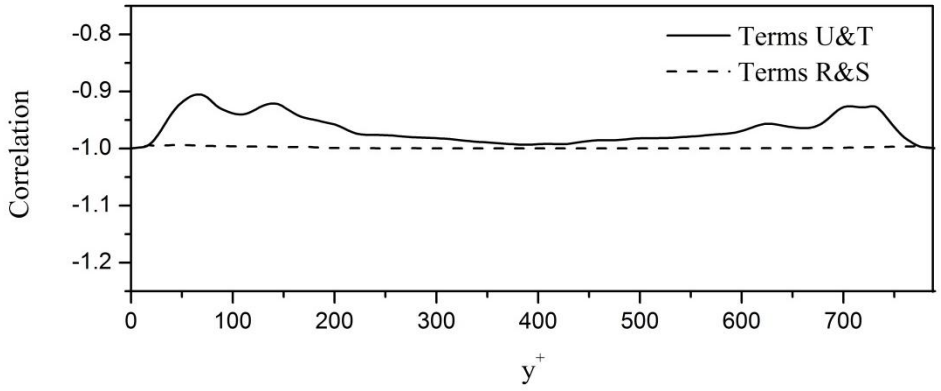

Figure 3.10. Correlation coefficient of terms U, T and R, S for case HDR (DNS2).Filter size is 8Δ*x*.

In summary, although term T+U has noticeable magnitude far from the wall, each pair of the new viscoelastic terms U, T and R,S, are in local and statistical equilibrium. Concerning the relevance (in terms of mean and instantaneous values) of the terms for the SGS kinetic energy transport equation in turbulent channel flow of FENE-P fluids, the most important terms are the classical SGS viscous diffusion (term N),viscous dissipation (term O), and SGS dissipation (term Q). On the other hand, the other terms investigated cancel each other e.g. terms P, L, R, S, or have small magnitude, term M. These observations suggest that the

SGS kinetic energy transport equation for viscoelastic fluids can be well approximated by the following relationship,

$$\underset{(J)}{\frac{\partial \tau_{ii}}{\partial t}} + \underbrace{\frac{\partial \tau_{ii} u_j^{<}}{\partial x_j}}_{(K)} \simeq \underbrace{\frac{\beta}{\mathrm{Re}_\tau}\frac{\partial}{\partial x_j}\left(\frac{\partial \tau_{ii}}{\partial x_j}\right)}_{(N)} \underbrace{-\frac{2\beta}{\mathrm{Re}_\tau}\left(\left(\frac{\partial u_i}{\partial x_j}\frac{\partial u_i}{\partial x_j}\right)^{<} - \frac{\partial u_i^{<}}{\partial x_j}\frac{\partial u_i^{<}}{\partial x_j}\right)}_{(O)} \underbrace{-2\tau_{ij}S_{ij}^{<}}_{(Q)}$$

$$\underbrace{-2(1-\beta)\left(\tau_{v,ij}S_{ij}\right)^{<}}_{(T)} + \underbrace{2(1-\beta)\tau_{v,ij}^{<}S_{ij}^{<}}_{(U)}$$

3.6.3. Influence of viscoelasticity on inverse transfer of kinetic energy (back-scattering)

The interaction between resolved and unresolved scales through the SGS dissipation (term Q) has received much attention in Newtonian turbulent flow (Piomelli et al. (1991, 1996), and da Silva st al. (2002)). In this section the influence of polymer additives on the kinetic energy transfer (backward as well as forward scatter) is investigated by analyzing the SGS dissipation in more detail. The probability density function of the SGS dissipation at y^+=30 (peak of turbulent kinetic energy) is plotted for the low and high drag reduction cases along with the Newtonian case in figure 3.11. It can be observed that although the forward scatter dominates for all flows at near wall regions, the increase in drag reduction severely reduces forward scatter while leaving the backscattering tail nearly unchanged. Hence, this implies that backscatter of SGS dissipation is more important for viscoelastic flows than for Newtonian flows and in particular for high drag reduction regimes, this also can be seen in the instantaneous field data plotted for Newtonian and viscoelastic case in figure (3.12). In order to better investigate this finding quantitatively, the backward and forward scatter part of ε_{SGS} are quantified as,

$$\varepsilon^{-} = \frac{1}{2}\left(\varepsilon_{sgs} - \left|\varepsilon_{sgs}\right|\right),\ \varepsilon^{+} = \frac{1}{2}\left(\varepsilon_{sgs} + \left|\varepsilon_{sgs}\right|\right) \tag{3.10}$$

where ε^- and ε^+ denote backward and forward scatter components of SGS dissipation, respectively. Using this definition, the fraction of points with backward scatter events are calculated and plotted in figure 3.13 all across the channel for all flows and for the three filter sizes. The figure shows that the backward scatter is almost independent of grid size (the maximum variation caused by filter size is around $\pm 5\%$) as was previously observed for Newtonian channel flow by Piomelli et al. (1991, 1996), and here we also confirmed same finding for viscoelastic fluids. Moreover, figure 3.13 indicates that the fraction of points experiencing the backward scatter increases by the addition of polymer to the fluid. Regardless of the filter size the average number of points/events experiencing backward scatter across the channel is 24%, 31%, and 35% for the Newtonian, LDR and HDR flows, respectively. The intensity of the plane-averaged forward and backward scatter contributions to SGS dissipation is also given by equation (3.10) are plotted in Figure 3.14

for the three flow cases. We observe the severe decrease in forward scatter with drag reduction, although it remains larger than backscatter. The figure shows that the ratio of backward scatter to forward scatter nearly doubles with enhancing drag reduction, and at the peak location this ratio is 0.15, 0.24, and 0.27 for the Newtonian, LDR, and HDR flows, respectively. Figures indicate that not only the number of backward scatter events increases by addition of polymer to the flow, but also the intensity of the backward scatter increases respective to the forward scatter.

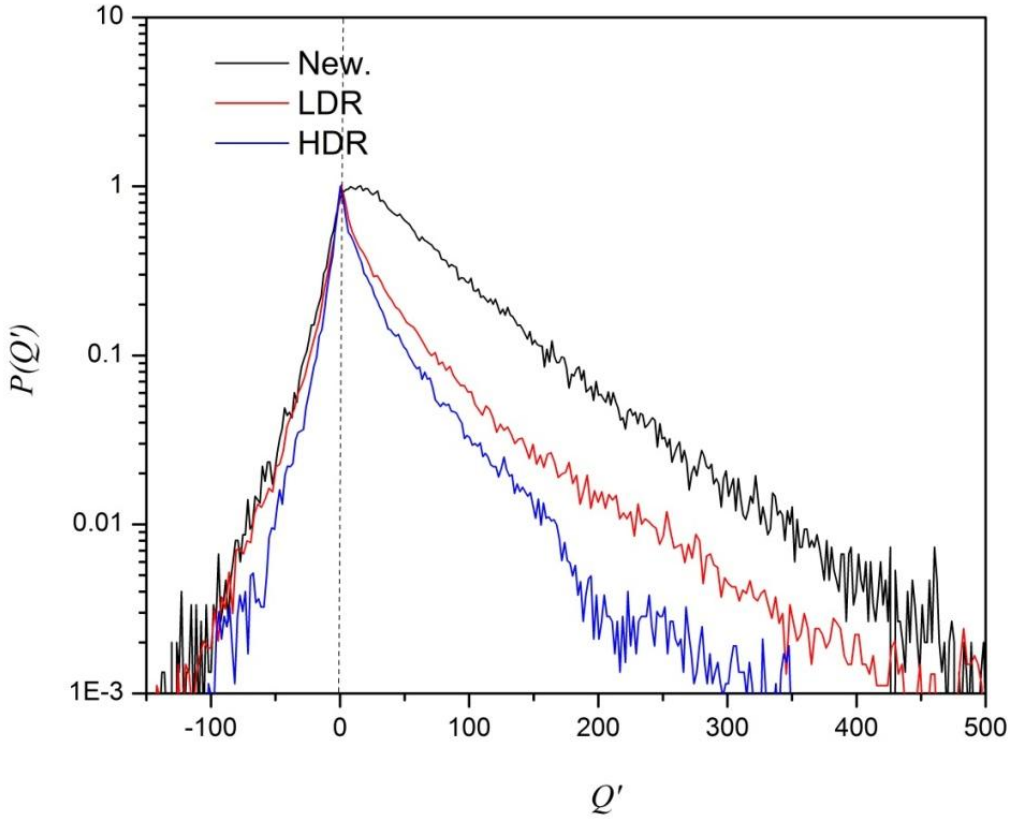

Figure 3.11. PDF of the SGS dissipation (term Q). New., LDR, and HDR denote DNS0, DNS1, and DNS2 respectively. Filter size is $8\Delta x$.

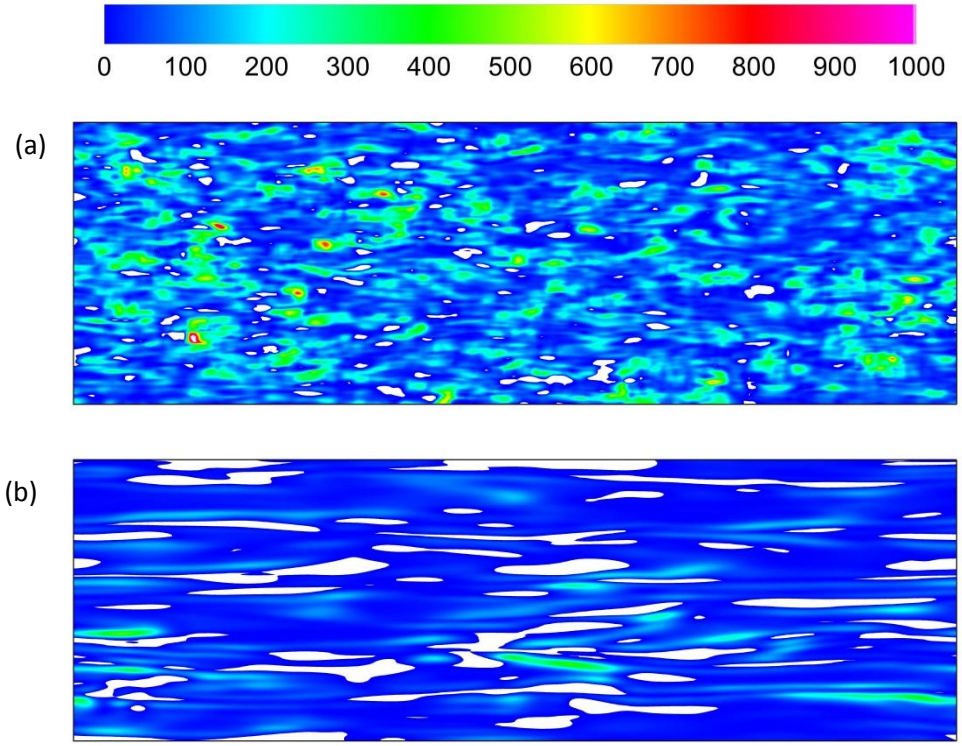

Figure 3.12. Contours of the SGS dissipation (term Q). (a) Newtonian, and (b) HDR, case DNS2. Filter size is $8\Delta x$. White spots are backward scattering events.

As mentioned before, the dissipation term prompted by the polymer (term U) is also responsible (indirectly) for the net kinetic energy exchange between resolved and unresolved scales. In order to investigate this specific mechanism the PDF of this term close to the wall (y^+=30) is plotted in figure 3.15, showing that this viscoelastic term is mostly responsible for forward-scatter. This is also confirmed by the fraction of points experiencing backward scatter due to the polymer induced dissipation, plotted in figure 3.16. This figure shows that as for the SGS dissipation the polymer induced backward scatter is almost independent of the filter size. Furthermore, the figure shows that close to the wall only 2% of the points are experiencing polymer induced indirect backward scatter and the maximum at the channel centerline region is of around 10% meaning that backward scatter events due to the polymer induced dissipation are rare.

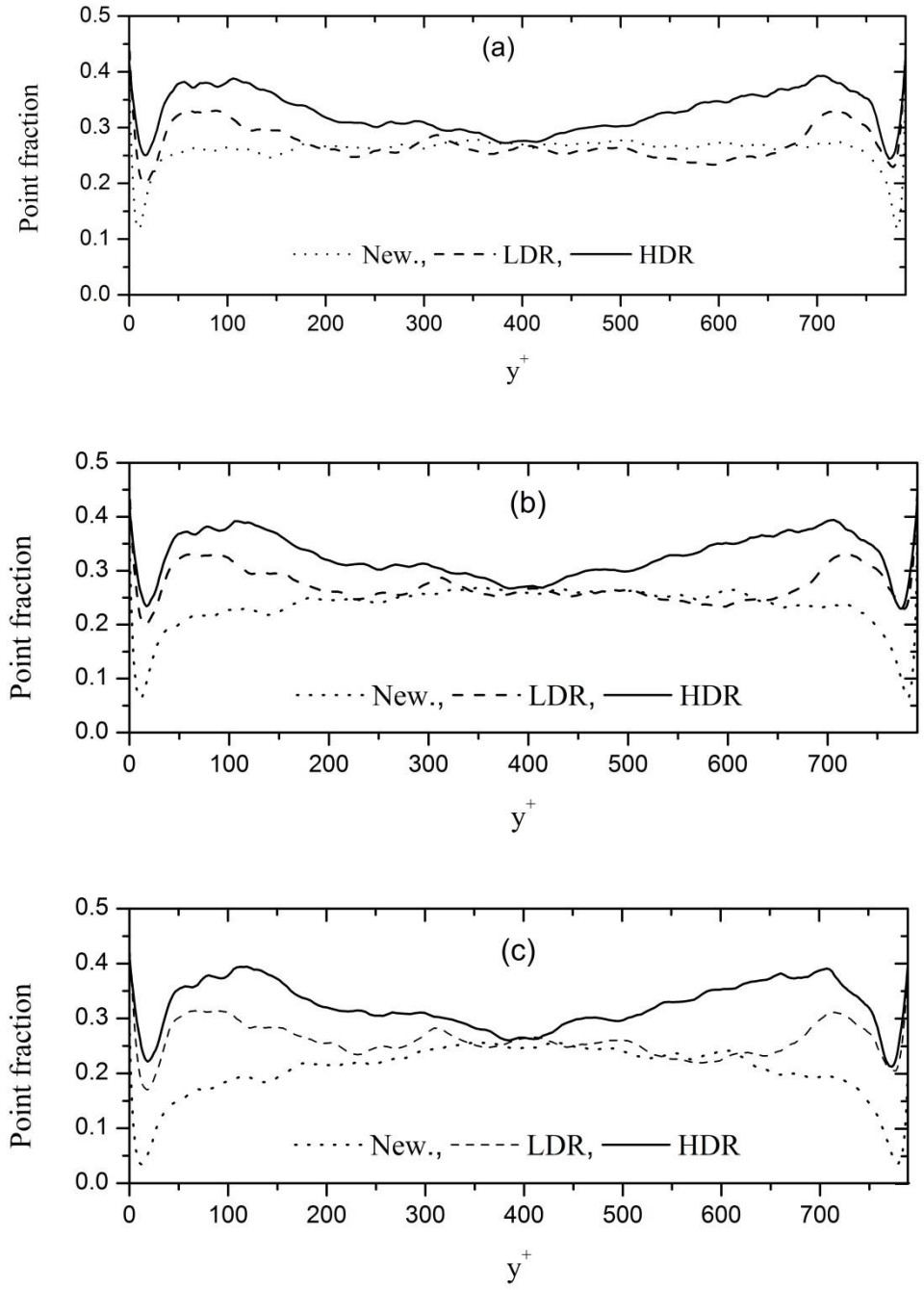

Figure 3.13. Fraction of points with backward scatter events with filter sizes defined as (a) 4Δx, (b) 6Δx, (c) 8Δx, New., LDR, and HDR denote DNS0, DNS1, and DNS2 respectively.

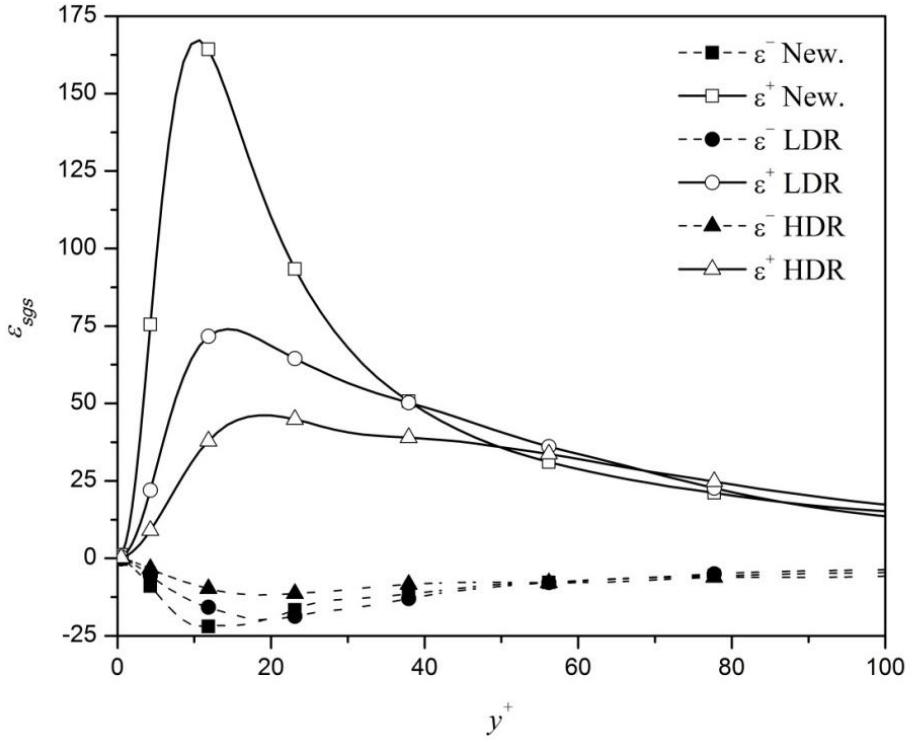

Figure 3.14. Mean backward and forward scatter of SGS dissipation. New., LDR, and HDR denote DNS0, DNS1, and DNS2 cases, respectively. Filter size is 8Δ*x*.

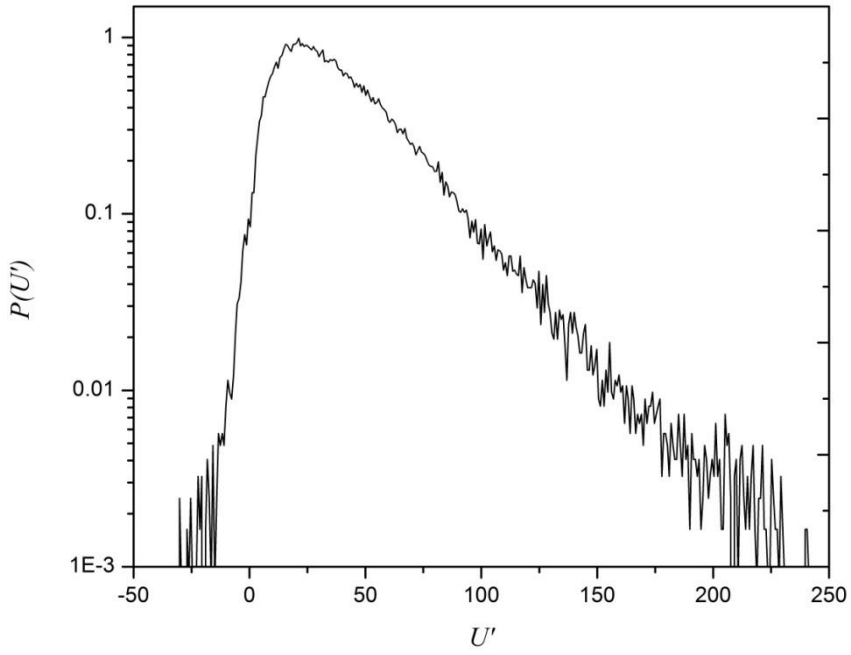

Figure 3.15. PDF of the dissipation term prompted by the polymer (term U) for case HDR (DNS2) using 8Δ*x*filter.

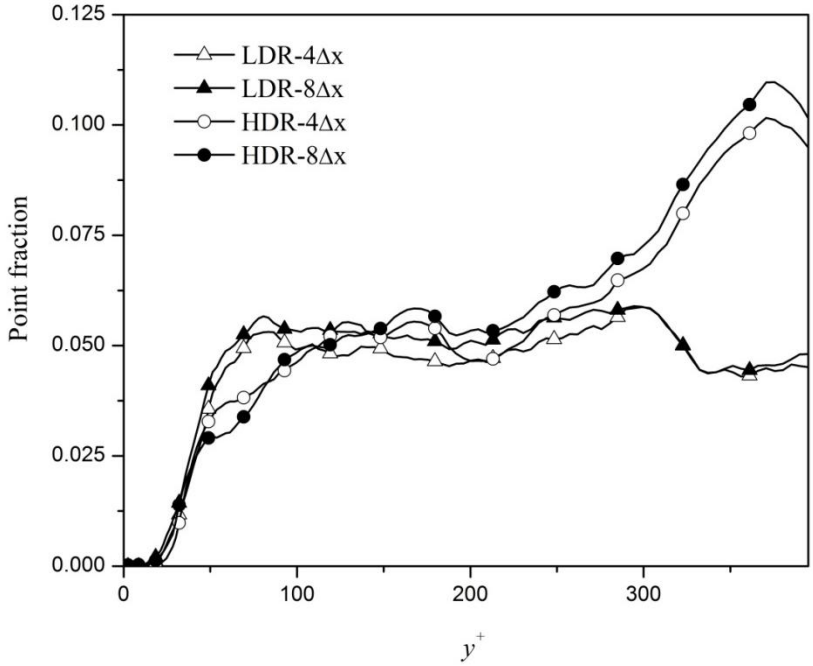

Figure 3.16. Fraction of points experiencing backward scatter due to the polymer induced dissipation. LDR, and HDR denote DNS1, and DNS2 respectively.

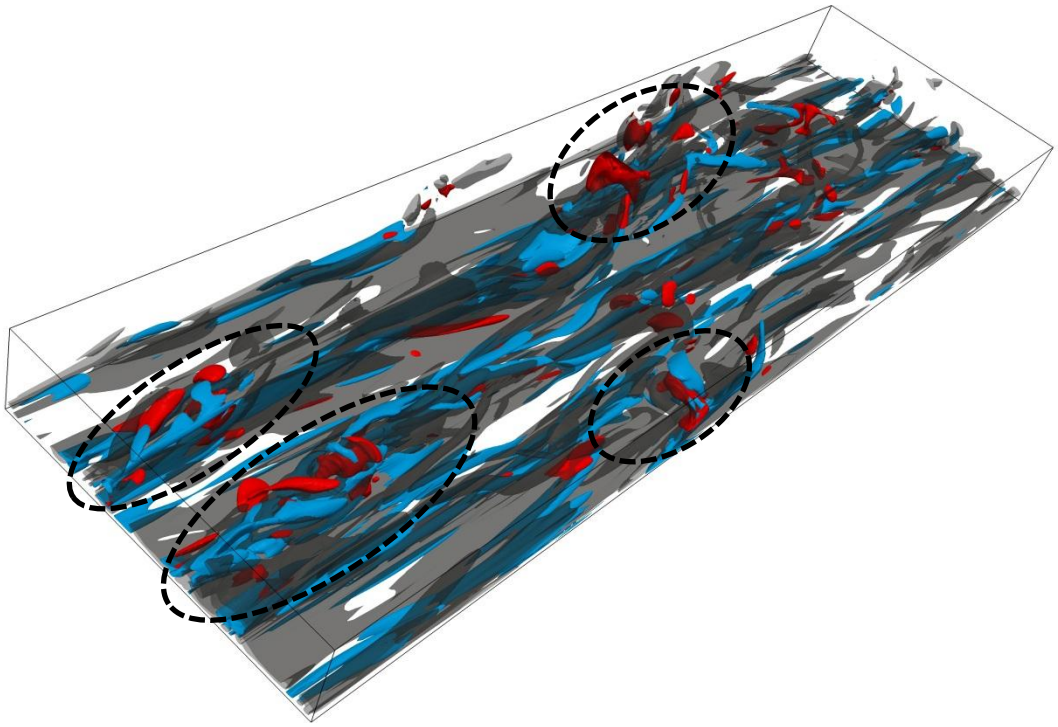

Figure 3.17. Iso-surface of backward (blue), forward (black) scatter of subgrid scale dissipation, red iso-surfaces denote backward scatter of SGS dissipation prompted by polymer. Using $\Delta=4\Delta x$ filter, for case DNS2.

Iso-surfaces of the backward scattering of the dissipation prompted by the polymer along with forward and backward scattering of classical SGS dissipation for the HDR case are plotted in figure 3.17. The figure shows that backward and forward scatter events of the SGS dissipation in turbulent viscoelastic fluids usually occur in close proximity to each other, with the backscatter event being generally surrounded by a region of significant forward scatter, as previously reported by Piomelli et al. (1996) for Newtonian fluids. Figure 3.17 also confirms that backward scatter events associated with polymer-induced SGS dissipation are very rare in comparison with the backward and forward scatter events of the SGS dissipation. Moreover it is interesting to note that the polymer induced backscatter event of dissipation also takes place in close proximity to backward and forward scatter events generated by the SGS dissipation (they are surrounded by a region of significant forward and backward scatter events of SGS dissipation). These regions are shown in figure 3.17 using dashed circles (Note that equal thresholds were chosen to illustrate iso-surfaces of the various quantities).

3.7. Conclusion of the *a-priori* analyses of GS/SGS interaction

The main goal of this chapter was to understand how the grid/subgrid-scale interactions are affected by the presence of the polymer additives in turbulent channel flow. This was achieved by the application of the top-hat filter to direct numerical simulations data of channel flow of viscoelastic fluids described by FENE-P rheological constitutive equation. The influence of rheological parameters on the SGS stress tensor show that in the presence of polymer additives the SGS stresses are considerably reduced compared to the Newtonian case. The ratio $\tau_{xy} / (-S^{<}_{xy} \left|S^{<}\right|)$, which is equal to $\left(C_s \Delta_g\right)^2$, the key parameter in classical closures for LES, was analyzed and it was observed that although this quantity severely decreases for viscoelastic fluids, the overall shape and behavior remains proportional to that for Newtonian fluids, and the ratio of this quantity for the viscoelastic cases and Newtonian fluid is almost constant, which is a useful result for future attempts to develop SGS modes for viscoelastic fluids.

The exact filtered polymer extra stress tensor arising in the filtered Navier-Stokes equation show that even for high drag reduction cases with the largest filter size this term can be safely approximated by its large-scale contribution and does not require modeling. The filtered evolution equation for the conformation tensor was also inspected in detail and an approximated form introduced after a quantitative assessment of its GS/SGS terms.

The energy transfer among grid and subgrid scales in the SGS kinetic energy transport equation appropriate for the FENE-P fluids was investigated. The budgets of all terms for Newtonian, low and high drag reduction cases exhibit severe suppression for the viscoelastic cases. It was also found that new terms appearing in this equation due to the presence of polymer additives are almost symmetric, and highly correlated, hence an approximated SGS kinetic energy transport equation was suggested for viscoelastic turbulent flows, which can be used for new SGS models based on an SGS kinetic energy

transport equation Fureby at al. (1994) and Davidson et al. (1997) for the purpose of LES computational methods.

Additionally, it was shown that the amount of points in the flow domain experiencing backward scatter events of the SGS dissipation is independent of the filter size for viscoelastic turbulent flows as for Newtonian fluid (Piomelli et al. (1991)). Moreover, it was observed that the amount of forward scattering events of SGS dissipation in the flow domain decreases significantly in the presence of polymer additives, indicating that backward scattering of SGS dissipation in viscoelastic fluids is proportionally more frequent than in Newtonian fluids and requires proper attention. Polymer induced dissipation, which is a polymeric term involved in GS/SGS energy transfer causes a very small amount of energy backward scatter, which is negligibly small close to the wall.

Finally, it was found that as for Newtonian fluid (Piomelli et al. (1996)), backward and forward scatter events of SGS dissipation for viscoelastic fluids occur in close proximity of each other, with the backward scatter event being generally surrounded by a region of significant forward scatter. Rather surprisingly it was also observed that the backward scatter events associated to the polymer induced dissipation although are very small, occur in close proximity of the backward and forward scatter events generated by SGS dissipation.

4

Chapter 4:
A viscoelastic k-ε-v^2-f model

M. Masoudian, K. Kim, F. T. Pinho, and R. Sureshkumar, Journal of Non-Newtonian Fluid Mechanics (2013) 202, 99-111.

"Heard melodies are sweet, but those unheard, are sweeter"
– John Keats,

Abstract

A tensorially consistent near-wall four equation model is developed to model turbulent flow of dilute polymer solutions. The model is validated up to the maximum drag reduction limit, by utilizing the data obtained from direct numerical simulations using the Finitely Extensible Nonlinear Elastic-Peterlin (FENE-P) constitutive model. Eight sets of direct numerical simulation (DNS) data are used to analyze budgets of relevant physical quantities, such as the nonlinear terms in the FENE-P constitutive equation, the turbulent kinetic energy, the wall normal Reynolds stress and dissipation transport. Closures were developed in the framework of the k-ε-$\overline{v^2}$-f model for the viscoelastic stress work, the viscoelastic destruction of the rate of dissipation, the viscoelastic turbulent viscosity, and the interactions between the fluctuating components of the conformation tensor and of the velocity gradient tensor terms. Predicted polymer stress, velocity profiles and turbulent flow characteristics are all in good agreement with the literature, from which six independent DNS data sets were used covering a wide range of rheological and flow parameters, including high Reynolds number flows, and showing significant improvements over the corresponding predictions of other existing models.

4.1 Introduction

It has been known for quite over 60 years that the addition of polymers to turbulent flows of Newtonian fluids can dramatically reduce the turbulent friction drag up to 80%. Comprehensive reviews of the early literature in this area are given in Hoyt (1972), Lumley (1963,1973) and Virk (1975). Several theories have been proposed to describe the complex mechanism of turbulent drag reduction (DR) in dilute polymer solutions. Lumley (1969) proposed a mechanism based on the extension of the polymers, suggesting that the stretching of coiled polymers, in regions with strong deformations such as the buffer layer, increases the effective extensional viscosity. This would dampen small eddies, thicken the viscous sublayer and consequently lead to drag reduction. Lumley also related the onset of drag reduction with the time scale of the polymers becoming larger than the time scale of the flow.

In his extensive experimental data analysis Virk (1971) introduced the concept of an "elastic sublayer" between the viscous sublayer and the logarithmic zone where crucial events in drag reduction take place. Virk (1971), Castro and Squire (1971), and Giles and Pettit (1967) observed an increase in the thickness of the elastic sublayer with drag reduction to eventually fill the whole logarithmic and outer layer regions at maximum drag reduction, thus introducing the concept of maximum drag reduction asymptote. On the other hand, Tabor and de Gennes (1986) postulated that drag reduction is caused by the elastic rather than the viscous properties of polymer additives. This idea is supported by experiments showing that drag reduction also occurs albeit by a different amount, when the polymers are injected at the centre of the pipe (heterogeneous drag reduction). Their explanation was that the shear waves, caused by the elasticity of the polymers prevented production of turbulent velocity fluctuations at the small scales.

Over the last 15 years, the development of accurate and efficient numerical and experimental methods has made it possible to investigate in detail turbulent DR in dilute polymer solutions (Xi et al. (2010), Sureshkumar et al. (1997), Dubief et al. (2014), and Ptasinski et al. (2003)). It is now generally accepted that DR is associated with inhibition of turbulent motion by the action of polymer additives; the high extensional viscosity of the viscoelastic polymer solutions leads to a reduction in the vortex dynamic activities that are characteristic of turbulence taking place near the wall in the viscous and buffer sublayers. This is essentially in agreement with the original proposals of Lumley (1969). More recently, Kim et al. (2007, 2008) proposed that weakening of hairpin vortices by polymer counter-torques as a key mechanism of DR. The torques created by straining the polymers inherently oppose the rotation of the legs and heads of the hairpin vortices in the log layer as well as the quasi-streamwise vortices in the buffer layer.

Several DNS investigations of fully-developed turbulent channel flow have been carried out to understand the effect of rheological parameters on turbulent structure and statistics Dimitropoulos et al. (2005). Most of these numerical simulations used constitutive equation based on the FENE-P (finitely extensible nonlinear elastic-Peterlin) model which allows one to probe the effect on the flow of the polymer relaxation time, the chain extensibility and the polymer to solution viscosity ratio on the flow.

DNS simulation of turbulent viscoelastic flow is significantly more expensive than Newtonian DNS for two reasons: first, because of the larger number of primary variables in the former than in the latter and secondly, as DR increases, the near wall streaks become progressively stabilized and elongated, thus requiring the use of longer simulation boxes in particular for high DR values, Li et al. (2006). Consequently, for a given Reynolds number, the CPU-time and memory requirements for DNS of viscoelastic flows are at least one order of magnitude larger as compared to the Newtonian case, and so it is not feasible for most of the engineering purposes. Hence, Reynolds-averaged Navier–Stokes (RANS) type or other computationally less demanding models have to be developed for modeling turbulent flows of dilute polymer solutions in engineering applications.

In an attempt to incorporate viscoelastic fluid rheology into turbulence models for drag reducing fluids, Pinho et al. (2003), and Resende et al. (2006) developed several first-order turbulence models for a modified version of the generalized Newtonian fluid constitutive equation, where the dependence of strain hardening of the fluid on the third invariant of the rate of deformation tensor was included. This family of models also included an anisotropic version to capture the increased Reynolds stress anisotropy (Resende et al. (2013)), and a second order version, where the Reynolds stress tensor was computed from the corresponding transport equations, Resende et al. (2013).

Leighton et al. (2003) proposed the first turbulence model for polymer flows based on the FENE-P dumbbell constitutive equation model. In their closure, transport equations for the Reynolds and the polymer stresses were added to the mean flow equation and closures for the unknown correlations were developed and the model tested in channel flow, but the model was not made available in the open literature. Pinho et al. (2008) and Resende et al. (2011) devised a new

RANS model for FENE-P fluids, which is an extension of the low Reynolds number *k-ε* closure for Newtonian fluids. This model provided closures for various terms of the governing equations, but only worked for low DR. Subsequently, Resende et al. (2011) developed several sophisticated and exceedingly complex closures for the nonlinear turbulent term of the conformation tensor equation and improved previous closures of Pinho et al. (2008) for the viscoelastic stress work and the viscoelastic turbulent transport of the turbulent kinetic energy (*k*) extending the model to intermediate DR levels and showing the limitations of a simple *k-ε* approach to modeling polymer solutions up to high DR. In fact, since turbulence anisotropy increases with DR, the inherent turbulence isotropy of the *k-ε* model does not allow the simultaneous accurate prediction of mean velocity, turbulent kinetic energy and its rate of dissipation at increasingly higher DR.

Iaccarino et al. (2010) introduced a *k-ε* - $\overline{v^2}$ -*f* model for fully developed channel flow, which is capable of predictions over the whole range of DR. The concept of turbulent polymer viscosity (or viscoelastic eddy viscosity) was used to account for the combined effects of turbulence and viscoelasticity on the polymer extra stress tensor term in the momentum equation. The turbulent polymer viscosity was made to depend on the turbulent kinetic energy, the polymer relaxation time and the trace of conformation tensor an idea that is adopted here with a new improved closure. The model of the nonlinear terms in the conformation tensor equation relied on the turbulent dissipation rate, but the main characteristic of Iaccarino et al. (2010)'s model, imported from the corresponding Newtonian model, was the ability to incorporate into the Reynolds stress tensor closure the wall damping effect upon the wall normal turbulence via the scalar $\overline{v^2}$ and the role of pressure strain. Both of these quantities are significantly modified by polymer additives and enhance turbulence anisotropy. However, although their model predicts accurately the amount of drag reduction, their predictions of the polymer shear stress in the Reynolds-averaged momentum, of the budgets of the turbulent kinetic energy and of the evolution equation for the conformation tensor are not in agreement with DNS results. In this work we aim to address these shortcomings by presenting a new *k-ε* - $\overline{v^2}$ -*f* model for FENE-P fluids and test it in fully-developed turbulent channel flow, which is essential to a future extension to other flows.

The single-point turbulence model developed here is based on the time-averaged governing equations for viscoelastic fluids presented by Dimitropoulos et al. (2001). An important contribution of the present work is the development of new closures for the nonlinear fluctuating terms appearing in the FENE-P rheological constitutive equation, and for the polymer stress work terms in the *k* and $\overline{v^2}$ transport equations. The model is assessed against different sets of DNS data covering a wide range of flow and fluid conditions quantified by the Weissenberg number (*We*), Reynolds number (*Re*) and maximum polymer extensibility (L^2). The paper is organized as follows: Section 4.2 introduces the instantaneous and time-averaged governing equations and identifies the viscoelastic terms requiring modeling. In Section 4.3, the turbulent

closures are developed and section 4.4 presents model predictions for fully developed turbulent channel flow over the whole range of DR. Conclusions are offered in section 4.5.

4.2. Governing equations

In what follows, upper-case letters or overbars denote Reynolds-averaged quantities and lower-case letters or primes denote fluctuating quantities. A hat denotes an instantaneous quantity. In this work steady flows are dealt with and the reader should be aware that the terms "time-averaging" and "Reynolds-averaging" are used indiscriminately to denote "Reynolds-averaging".

4.2.1. Continuity and momentum equations

The Reynolds-averaged equations appropriate for incompressible flow of FENE-P fluids are:
continuity:

$$\frac{\partial U_i}{\partial x_i} = 0 \tag{4.1}$$

and momentum:

$$\rho \frac{\partial U_i}{\partial t} + \rho U_k \frac{\partial U_i}{\partial x_k} = -\frac{\partial \overline{P}}{\partial x_i} - \frac{\partial}{\partial x_k}(\overline{\rho u_i u_k}) + \frac{\partial \overline{\tau}_{ik}}{\partial x_k} \tag{4.2}$$

where $\overline{\tau}_{ik}$ is the time-averaged extra stress tensor, U_i is the mean velocity, $\overline{P}$ is the mean pressure, ρ is the fluid density and $\overline{\rho u_i u_k}$ is the Reynolds stress tensor. The extra stress tensor $\overline{\tau}_{ij}$ describes the rheology of the fluid and is given in Eq. (4.3) as the sum of a Newtonian solvent contribution of viscosity η_s with a polymeric contribution $\overline{\tau}_{ij,p}$ described by the FENE-P rheological constitutive model:

$$\overline{\tau}_{ij} = 2\eta_s S_{ij} + \overline{\tau}_{ij,p} \tag{4.3}$$

where S_{ij} is the rate of strain tensor defined as:

$$S_{ij} = \frac{1}{2}\left(\frac{\partial U_i}{\partial x_j} + \frac{\partial U_j}{\partial x_i}\right) \tag{4.4}$$

In Eqs. (4.2) and (4.3) the Reynolds stress and the time-averaged polymer stress need approximations. The former can be calculated by models developed for Newtonian fluids but modified to account for the effects of viscoelasticity, whereas the latter must be calculated with the Reynolds-averaged rheological constitutive equation.

4.2.2. Constitutive equation

To develop a model for $\bar{\tau}_{ij,p}$, we start with the instantaneous FENE-P equation for the polymeric stress Bird et al. (1980,1987). The instantaneous polymeric contribution to the total extra stress is given as an explicit function of the instantaneous conformation tensor $\hat{c}_{ij}$

$$\hat{\tau}_{ij,p} = \frac{\eta_p}{\lambda}\left[f(\hat{c}_{kk})\hat{c}_{ij} - f(L)\delta_{ij} \right] \tag{4.5}$$

where the $f(\hat{c}_{kk})$ and $f(L)$ take here the forms used by Li et al. (2006) and are given by

$$f(\hat{c}_{kk}) = \frac{L^2 - 3}{L^2 - \hat{c}_{kk}} \qquad \text{and} \qquad f(L) = 1 \tag{4.6}$$

where L denotes the maximum dimensionless extensibility of the model dumbbell. Other functions are discussed in Beris et al. (1994). The required conformation tensor obeys a hyperbolic differential equation of the form:

$$f(\hat{c}_{kk})\hat{c}_{ij} + \lambda\left(\frac{\partial \hat{c}_{ij}}{\partial t} + \hat{u}_k \frac{\partial \hat{c}_{ij}}{\partial x_k} - \hat{c}_{jk}\frac{\partial \hat{u}_i}{\partial x_k} - \hat{c}_{ik}\frac{\partial \hat{u}_j}{\partial x_k} \right) = f(L)\delta_{ij} \tag{4.7}$$

Using Eq. (4.5), Eq. (4.7) can be alternatively written as

$$\left(\frac{\partial \hat{c}_{ij}}{\partial t} + \hat{u}_k \frac{\partial \hat{c}_{ij}}{\partial x_k} - \hat{c}_{jk}\frac{\partial \hat{u}_i}{\partial x_k} - \hat{c}_{ik}\frac{\partial \hat{u}_j}{\partial x_k} \right) = -\frac{\hat{\tau}_{ij,p}}{\eta_p} \tag{4.8}$$

The terms in the parenthesis in Eqs. (4.7) and (4.8) denote Oldroyd's upper convective derivative of the instantaneous conformation tensor. The first two terms represent the local and advective derivatives (together they form the material derivative) and the other two terms account for the distortion of c_{ij} by the instantaneous flow. The other parameters of the polymer constitutive equation are the relaxation time of the fluid λ and the polymer viscosity coefficient η_p.

Reynolds-averaging the above equations, the time-averaged polymer stress $\bar{\tau}_{ij,p}$ is obtained:

$$\bar{\tau}_{ij,p} = \frac{\eta_p}{\lambda}\left[f(C_{kk})C_{ij} - f(L)\delta_{ij} \right] + \frac{\eta_p}{\lambda}\overline{f(C_{kk} + c_{kk})c_{ij}} \tag{4.9}$$

where the last term on the right hand side also needs an approximation.

The time-averaged form of the conformation tensor evolution equation is:

$$\overset{\nabla}{C}_{ij} + \overline{u_k \frac{\partial c_{ij}}{\partial x_k}} - \left(\overline{c_{jk}\frac{\partial u_i}{\partial x_k}} + \overline{c_{ik}\frac{\partial u_j}{\partial x_k}} \right) = -\frac{\bar{\tau}_{ij,p}}{\eta_p} \tag{4.10}$$

which after substitution of Eq. (4.9), becomes:

$$\lambda \overset{\nabla}{C}_{ij} + \lambda\left(\overline{u_k \frac{\partial c_{ij}}{\partial x_k}} - \left(\overline{c_{jk}\frac{\partial u_i}{\partial x_k}} + \overline{c_{ik}\frac{\partial u_j}{\partial x_k}} \right) \right) = -\left[f(C_{kk})C_{ij} - f(L)\delta_{ij} + \overline{f(C_{kk} + c_{kk})c_{ij}} \right] \tag{4.11}$$

On the left hand side of Eqs. (4.10) and (4.11), the mean flow advective term contained within the Oldroyd derivative of C_{ij} (denoted by $\overset{\nabla}{C}_{ij}$) vanishes for fully developed channel flow. The mean flow distortion term of $\overset{\nabla}{C}_{ij}$ is M_{ij} and is given by:

$$M_{ij} = \left(C_{jk} \frac{\partial U_i}{\partial x_k} + C_{ik} \frac{\partial U_j}{\partial x_k} \right) \tag{4.12}$$

M_{ij} is non-zero, but it needs no closure. The remaining two terms are related to turbulence correlations and, following the analysis and nomenclature of Li et al. (2006) and Housiadas et al. (2005) and they are labeled as

$$CT_{ij} = -\overline{u_k \frac{\partial c_{ij}}{\partial x_k}} \tag{4.13}$$

which represents the contribution to the advective transport of the conformation tensor by the fluctuating velocity field, and

$$NLT_{ij} = \overline{c_{jk} \frac{\partial u_i}{\partial x_k}} + \overline{c_{ik} \frac{\partial u_j}{\partial x_k}} \tag{4.14}$$

which accounts for the interactions between the fluctuating components of the conformation tensor and of the velocity gradient tensor. This term originates from the Oldroyd derivative and is the fluctuating counterpart of M_{ij}. Both CT_{ij} and NLT_{ij} require closure approximations.

In this study we investigate fully developed channel flow of FENE-P fluids over a wide range of conditions as described in Table (4.1), which lists the DNS data sets. All DNS cases correspond to β = 0.9, the Reynolds number $Re_{\tau 0}$ is defined as $Re_{\tau 0} \equiv hU_\tau/\nu_0$ based on the friction velocity (U_τ), the channel half-height (h) and the zero shear-rate kinematic viscosity of the solution, i.e., the sum of the kinematic viscosities of the solvent and polymer $\nu_0 = \nu_p + \nu_s$. All kinematic viscosities are defined with the total solution density. The Weissenberg number is $Wi_{\tau 0} \equiv \lambda U_\tau{}^2/\nu_0$ and β is the ratio between the solvent viscosity and the zero shear-rate kinematic viscosity of the solution, ($\beta \equiv \nu_s/\nu_0$). A semi-implicit method is used for time-integration of the governing equations. In space, a spectral method is used with Fourier representations in the streamwise and spanwise directions, and Chebyshev expansion in the wall-normal direction. To achieve stable numerical integration of Eq. (4.8), a stress diffusion term ($\kappa \partial^2 \hat{c}_{ij} / \partial x_k^2$) is introduced, where κ denotes a constant, isotropic, artificial numerical diffusivity. As in earlier studies Sureshkumar et al. (1997), and Kim et al. (2007), the dimensionless artificial numerical diffusivity is taken to be $\kappa / hu_\tau \sim O(10^{-2})$. Periodic boundary conditions are applied in the streamwise (x) and spanwise (z) directions, and the no-slip boundary condition is imposed on velocity at the solid walls. Details of the numerical approaches used in this work can be found in Li et al. (2006).

In normalizing the governing equations and inherently the various physical quantities, the velocity scale is taken to be the friction velocity (leading to the use of superscript +), the length scale is either the channel half-height ($x_i = x_i^* h$) or the viscous length ($x_i = x_i^+ \nu_0/U_\tau$), leading to superscripts * and +, respectively. When mixing the two types of normalization, i.e. using wall/viscous and physical quantities, the superscript used is *, e.g. $M_{ij} = M_{ij}^* U_\tau^2/\nu_0$. The conformation tensor is already in dimensionless form.

4.2.3. Reynolds stresses

To compute the Reynolds stress tensor, we adopt Boussinesq's turbulent stress–strain relationship:

$$-\rho\overline{u_i u_j} = 2\rho\nu_T S_{ij} - \frac{2}{3}\rho k\delta_{ij} \qquad (4.15)$$

Table 4.1. DNS Parameters

case	$Re_{\tau 0}$	Domain size	Nodes (N_x, N_y, N_z)	Artificial diffusivity (κ / hu_τ)	L^2	$Wi_{\tau 0}$	DR
(A)	395	L_x:8πh, L_z:πh	512x129x128	0.02	900	25	18%
(B)	395	L_x:8πh, L_z:πh	512x129x128	0.02	900	100	37%
(C)	395	L_x:16πh, L_z:πh	1024x129x128	0.025	3600	100	51%
(D)	395	L_x:16πh, L_z:πh	1024x129x128	0.025	14400	100	63%
(E)	180	L_x:7h, L_z:πh	64x97x64	0.02	900	25	19%
(F)	180	L_x:14h, L_z:πh	128x97x64	0.02	900	100	38%
(G)	180	L_x:14h, L_z:πh	128x97x64	0.02	3600	100	54%
(H)	180	L_x:28h, L_z:πh	128x97x64	0.02	14400	100	71%

where υ_T is the eddy viscosity and *k* is the turbulent kinetic energy, $\overline{u_i u_i}/2$. The eddy viscosity is modeled according to the $k-\varepsilon-\overline{v^2}-f$ model Lien and Durbin (1996). This particular choice is justified by the fact that the polymer drag reduction is mostly a near wall phenomenon, and it requires a modification to the turbulence redistribution mechanism. This model of Lien and Durbin (1996) represents a comprehensive and accurate approach to capture these aspects of turbulent boundary layers within a Boussinesq framework. Durbin's original proposal (1991) for a near-wall eddy viscosity model is inspired by the physics of the full Reynolds stress transport model, but retains only the wall-normal fluctuating velocity variance, $\overline{v^2}$, and its source, *kf*, representing the redistribution by pressure fluctuations. Then, in the classical closure for the

eddy viscosity ($\nu_T \propto k^2/\varepsilon$) the wall damping effect is obtained by substituting one instance of *k* by $\overline{v^2}$ as:

$$\nu_T = C_\mu \overline{v^2} T_t \tag{4.16}$$

where T_t is turbulent time scale defined as:

$$T_t = \max\left\{\frac{k}{\varepsilon}, 6\sqrt{\frac{\nu}{\varepsilon}}\right\} \tag{4.17}$$

Thus, the turbulence model for Newtonian fluids has three transport equations for *k*, ε and $\overline{v^2}$, and one elliptic equation for *f*, and it accurately reproduces the parabolic decay of $\overline{v^2}/k$ down to the solid wall without introducing the wall-distance or low-Reynolds number damping functions in the eddy viscosity and *k*-ε equations, which would then need to be modified to account for viscoelastic fluids. The absence of these damping functions is a major strength of this type of closures. However, most $\overline{v^2}$ - *f* variants suffer from numerical stiffness making them impractical for industrial or unsteady RANS applications, while the one version available in major commercial codes often tends to lead to unrealistic solutions. Lien and Durbin (1996) proposed a variant to address these shortcomings.

In the $\overline{v^2}$ - *f* model suggested by Lien and Durbin (1996), the scalar $\overline{v^2}$, and its source term f, are retained as variables in addition to the traditional *k* and ε quantities. The turbulent kinetic energy transport equation is derived formally from the Reynolds-averaged momentum equation and, therefore, in this case contains extra terms originating from the polymer stresses.

The transport equations for the turbulent kinetic energy and its dissipation rate share similarities with the classical *k*–ε model equations, but contain additional terms for viscoelastic fluids, as reported by Pinho *et al*. (2008). The transport equation of *k* for turbulent flow of viscoelastic fluids is

$$U_j \frac{\partial k}{\partial x_j} = P_k - \varepsilon + \frac{\partial}{\partial x_j}\left(\left(\nu + \frac{\nu_T}{\sigma_k}\right)\frac{\partial k}{\partial x_j}\right) - \left(\overline{\tau_{ij}^p \frac{\partial u_i}{\partial x_j}}\right) + \frac{\partial}{\partial x_j}\left(\overline{\tau_{ij}^p u_i}\right) \tag{4.18}$$

Except for the last two terms on the right hand side, the other terms are classical terms appearing in Newtonian fluid models and represent the advection of *k*, turbulence production by the mean strain ($P_k = 2\upsilon_T S_{ij}^2$), viscous dissipation by the solvent, molecular diffusion and turbulent diffusion. The two viscoelastic terms require closure and represent the viscoelastic turbulent transport ($Q_p \equiv \partial\left(\overline{\tau_{ij}^p u_i}\right)/\partial x_j$) and the viscoelastic stress work ($\varepsilon_p \equiv \overline{\tau_{ij}^p \partial u_i / \partial x_j}$).

The balance of turbulent kinetic energy is plotted in Figure (4.1) for low (18%) and high (63%) drag reductions using normalization by wall quantities (e.g. $\varepsilon = \varepsilon^+ u^4_\tau / \nu_0$). The turbulent kinetic energy budgets in Figure (4.1) show that the qualitative behavior of the various terms is not affected by the level of drag reduction, although the thickening of the sublayer is clearly

noticeable from the shift of the peak of kinetic energy production away from the wall. As for a Newtonian fluid, the main contributions in the log-law region are from the production of *k* on one side, and the dissipations by the Newtonian solvent and the viscoelastic stress work on the other. This is why the viscous dissipation due to the solvent is lower in the viscoelastic case than for a Newtonian fluid at the same Reynolds number. Well inside the viscous sublayer molecular diffusion takes over the role of production, and dissipation by the solvent is greater than the viscoelastic stress work. The viscoelastic turbulent transport term is usually small and only relevant within the buffer layer, but even there smaller than the turbulent diffusion (D_N), hence this term will not have a dramatic impact on model predictions.

The dissipation by the Newtonian solvent (ε) appearing on the right hand side of Eq. (4.18), is obtained from its own transport equation:

$$U_j \frac{\partial \varepsilon}{\partial x_j} = \frac{C_{\varepsilon 1} P_k - C_{\varepsilon 2} \varepsilon}{T_t} + \frac{\partial}{\partial x_j}\left(\left(\nu + \frac{\nu_T}{\sigma_\varepsilon}\right)\frac{\partial \varepsilon}{\partial x_j}\right) - E_p \tag{4.19}$$

Here, all terms are conceptually identical to those for a Newtonian fluid except for the last term (E_p) representing the viscoelastic contribution to the transport equation of ε. The definition of E_p was derived by Pinho et al. (2008) and is given by:

$$E_p = 2\nu_s \frac{\eta_p}{\lambda\left(L^2 - 3\right)} \overline{\frac{\partial u_i}{\partial x_m}\frac{\partial}{\partial x_k}\left\{\frac{\partial}{\partial x_m}\left[f\left(C_{mm}\right) f\left(\hat{c}_{pp}\right) c'_{qq}\, C_{ik}\right]\right\}} \tag{4.20}$$

This term is clearly nonlinear and a closure is needed for its calculation.

The other two equations needed to compute the eddy viscosity (cf. Eq. (4.16)) are the transport equation for the scalar $\overline{v^2}$, which is derived from the transport equation for the wall normal turbulent fluctuations according to Iaccarino et al. (2010), and the equation for the turbulence energy redistribution process (*f*) that plays a crucial role in producing $\overline{v^2}$ (cf. Eq. (4.22)).

In the context of a second order model for the full Reynolds stress tensor such role is played by the pressure-strain correlations from which the *f*-equation gets derived. The equations for $\overline{v^2}$ and *f* are given below:

$$U_j \frac{\partial \overline{v^2}}{\partial x_j} = kf + \frac{\partial}{\partial x_j}\left(\left(\nu + \frac{\nu_T}{\sigma_k}\right)\frac{\partial \overline{v^2}}{\partial x_j}\right) - 6\frac{\varepsilon}{k}\overline{v^2} - \varepsilon_{p,yy} + Q_{p,yy} \tag{4.21}$$

$$f - L_t^2 \frac{\partial^2 f}{\partial x_j \partial x_j} = C_1 \frac{\left(\frac{2}{3} - \frac{\overline{v^2}}{k}\right)}{T_t} + C_2 \frac{P_k}{k} - 5\varepsilon \frac{\overline{v^2}}{k} + \Phi_{yy}^p \tag{4.22}$$

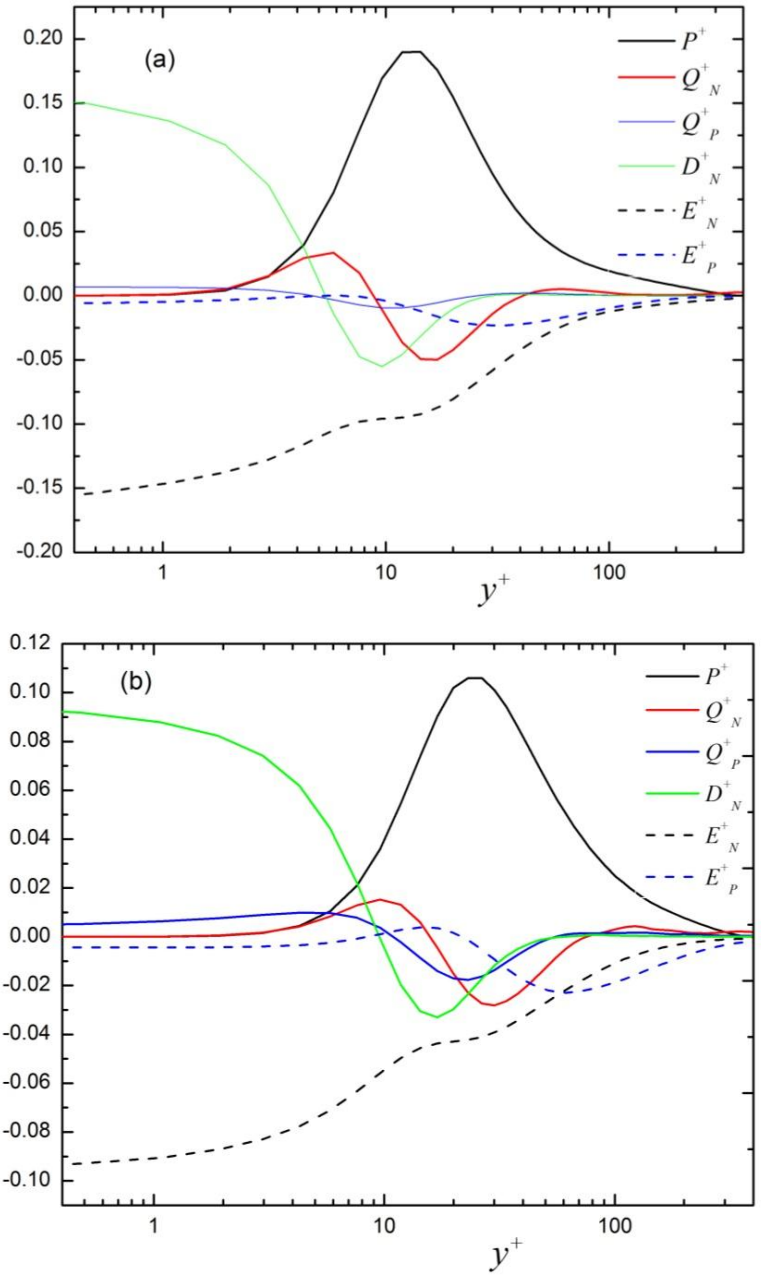

Figure 4.1. Balance of turbulent kinetic energy at $Re_{\tau 0}$ = 395 (a) case A, (b) case D.

where the eddy viscosity and time scale are given in Eqs. (4.16) and (4.17), and the length scale is defined as:

$$L_t^2 = C_L \max\left\{\frac{k^3}{\varepsilon^2}, C_\eta^2\sqrt{\frac{\nu^3}{\varepsilon}}\right\} \tag{4.23}$$

As reported in Durbin et al. (1996) the coefficients appearing in the above equations are : $C_\mu = 0.19,\ \sigma_k = 1,\ \sigma_\varepsilon = 1.3,\ C_{\varepsilon 1} = 1.4\left[1 + 0.05\sqrt{k/\bar{v}^2}\right],\ C_{\varepsilon 2} = 1.9,\ C_1 = 1.4,\ C_2 = 0.3,\ C_L = 0.23, C_\eta = 70.$

The transport equation for $\overline{v^2}$, a scalar representing the local wall normal Reynolds stress, is also modified relative to the corresponding Newtonian equation due to the presence of polymer additives in a similar manner to the *k* transport equation. The last two terms in Eq. (4.21) are the viscoelastic turbulent transport of $\overline{v^2}$ ($Q_{p,yy}$) and the viscoelastic stress work of $\overline{v^2}$ ($\varepsilon_{p,yy}$), and correspondingly they also need closures. The qualitative behavior of $\varepsilon_{p,yy}$, $Q_{p,yy}$, and *kf* depicted in Figure (4.2) shows that for the low drag reduction case the peaks of *kf* and $\varepsilon_{p,yy}$ occur close to the wall, and then the quantities fall significantly by moving away from the wall. On the other hand for the high drag reduction case the maximum values of the dimensionless quantities are much lower than at low DR and sharp peaks are no longer observed near the wall. Instead, there is a wide region where those quantities are close to the maximum. In addition, when increasing DR the ratio $\varepsilon_{p,yy}/(kf)$ increases, i.e., the wall normal viscoelastic stress work becomes an increasing proportion of *kf* and this suggest that wall normal velocity fluctuations tend to decrease as DR increases. Φ^p_{yy} is representing the viscoelastic contribution to the *f* equation. Note that indices *yy* used in this work denotes wall normal direction.

4.3. Development of closures

In this section closures are developed for all unknown turbulent cross-correlations identified in the previous section. All closures are developed on the basis of the DNS data case (B) ($Re_{\tau 0}$=395 and *DR*=37% in Table (4.1)) and subsequently compared with the other DNS data sets.

4.3.1. A model for the time-averaged polymer constitutive equation

For fully developed channel flow the polymer shear stress given by the FENE-P constitutive equation reduces to:

$$\bar{\tau}_{xy,p} = \frac{\eta_p}{\lambda}\left[f(C_{kk})C_{xy} - f(L)\delta_{ij}\right] + \frac{\eta_p}{\lambda}\overline{f(C_{kk}+c_{kk})c_{xy}} \qquad (4.24)$$

which contains a nonlinear term, $\overline{f(C_{kk}+c_{kk})c_{xy}}$. This quantity is compared with its mean value $f(C_{kk})C_{xy}$ in Figure (4.3) for both low (case A) and high (case D) drag reductions, and confirms the assertion that, in Eq. (4.24), it is justifiable to neglect the last term on the right-hand-side by comparison with the first term, as also found previously Pinho et al. (2008), and Iaccarino et al. (2010). Consequently for fully developed channel flow the polymer shear stress can in principle be calculated by:

$$\bar{\tau}_{xy,p} = \frac{\eta_p}{\lambda} f(C_{kk})C_{xy} \qquad (4.25)$$

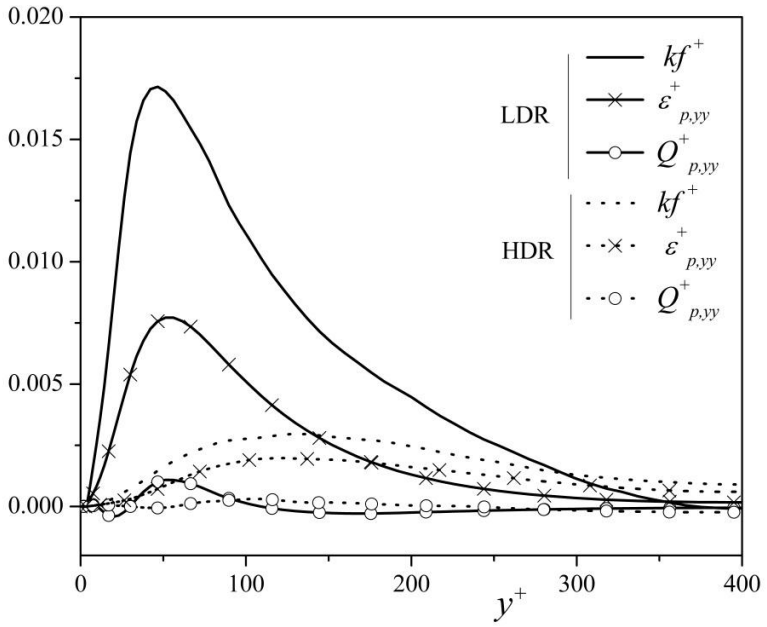

Figure 4.2. DNS data for the normalized budgets of the $\overline{v^2}$ for cases A (LDR, DR= 18%) and D (HDR, DR= 63%) at $Re_{\tau 0}$ = 395.

Eq. (4.25) implies that in fully-developed turbulent channel flow of viscoelastic fluids described by the FENE-P model we need the trace of conformation tensor (C_{kk}) and the mean shear polymer conformation component (C_{xy}) to calculate the polymer shear stress.

Still the polymer stress depends on turbulent quantities since the conformation tensor is highly dependent on turbulent flow characteristics as shown by Eqs. (4.11) to (4.14). The consequence of that cascade of dependencies is that small differences in the closures of those quantities result in inaccurate prediction of the polymer stress. Hence, instead of using eq. (4.25) Iaccarino et al. (2010) introduced the concept of viscoelastic kinematic viscosity ($\nu_{T,p}$) in order to directly account for the effect of turbulence on C_{ij}. They related the viscoelastic kinematic viscosity to the turbulent kinetic energy, and proposed a closure for $\nu_{T,p}$ and $\bar{\tau}_{xy,p}$ as:

$$\bar{\tau}_{xy,p} = \frac{\rho}{f(C_{kk})}\left(\nu_p + \nu_{T,p}\right)S_{xy} \quad \text{where} \quad \nu_{T,p} = b\lambda k,\ b = 0.1 \tag{4.26}$$

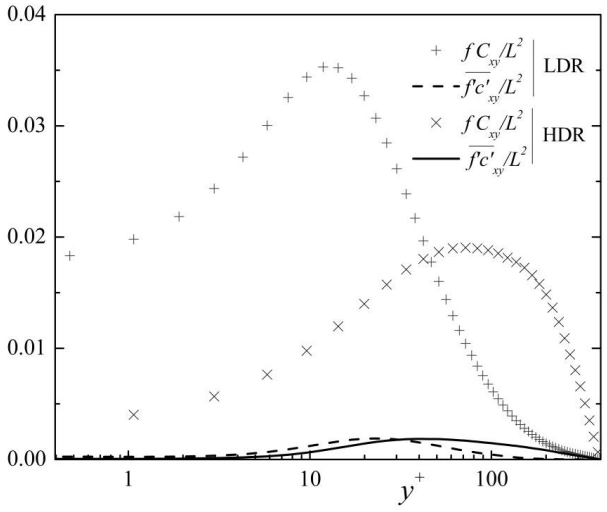

Figure 4.3. Comparison between $\overline{f(C_{kk}+c_{kk})c_{xy}}$ and $f(C_{kk})C_{xy}$ for cases A (LDR, DR= 18%) and D (HDR, DR= 63%) at $Re_{\tau 0}$ = 395.

We follow some of those ideas, but model the Reynolds-averaged polymer shear stress differently and as follows. In order to account for the variations in the mean polymer shear stress we utilized the trace of the C_{ij} tensor, as in Eq. (4.25). However, to capture the effect of turbulence upon C_{ij} we followed the concept of turbulent kinematic viscosity ($\nu_{T,p}$) introduced by Iaccarino et al. (2010). This is something like introducing a concept of viscoelastic turbulent Prandtl number, which is a dimensionless number quantifying the ratio between the viscoelastic eddy diffusivity of momentum and the classical momentum eddy diffusivity. The turbulent viscoelastic kinematic viscosity ($\nu_{T,p}$) describes the effect of the turbulent fluctuations on the polymer stresses, and relies on a Boussinesq-like relationship meaning an alignment of the viscoelastic stresses with the mean strain (consistent with a dumbbell spring). Figure(4.4) compares DNS data for the kinematic eddy viscosity, the viscoelastic kinematic viscosity ($\nu_{T,p} = \bar{\tau}_{xy,p} / (\rho dU_x/dy)$) and the closure developed in Iaccarino et al (2010). The behavior of the turbulent viscoelastic kinematic viscosity ,$\nu_{T,p}$, can be rationalized as follows. In the viscous sublayer ($y^+ < 5$), where the turbulence is severely dampened, it is possible to calculate the polymer stress neglecting any effect of turbulence upon the constitutive equation, i.e., by using the laminar constitutive equation. The polymer stress in fully-developed laminar channel flow has the exact solution given by Pinho et al. (2008) as:

$$\tau_{xylam,p} = \frac{\rho \nu_p}{f(C_{kk})} \frac{dU_x}{dy} \tag{4.27}$$

Eq. (4.27) is sufficient to describe the polymer stress in the viscous sublayer ($y^+ < 5$ region) while ensuring the compatibility of the polymer stresses in laminar flows. As depicted in Figure (4.4) the turbulent viscoelastic viscosity attains its maximum away from the wall and then decreases slowly towards the centerline as is the case also with the eddy viscosity (ν_T). Moreover, a correct closure for the polymer shear stress should naturally follow the dynamics imposed by the constitutive FENE-P Eq. (4.25) in regard to $f(C_{kk})$ and the polymer relaxation time. Analyzing carefully the DNS data and experimental results of Ptasinski et al. (2003) we observed that away from the wall there is a partial correspondence between the eddy viscosity and the viscoelastic eddy viscosity and consequently we propose a closure for the viscoelastic turbulent viscosity in the whole domain as:

$$\nu_{T,p} = \left(\frac{\nu_p}{f(C_{kk})} + a_1 \sqrt{L^2 / Wi_{\tau o}}\ f(C_{kk}) \nu_T \right) \tag{4.28}$$

and the time averaged polymer shear stress becomes:

$$\bar{\tau}_{xy,p} = \rho \left(\frac{\nu_p}{f(C_{kk})} + a_1 \sqrt{L^2 / Wi_{\tau o}}\ f(C_{kk}) \nu_T \right) \frac{dU_x}{dy} \tag{4.29}$$

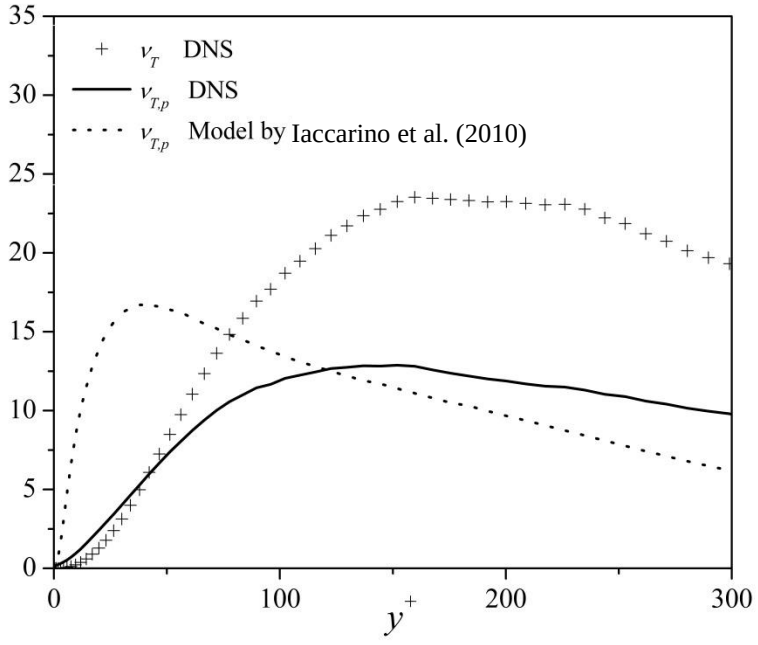

Figure 4.4. Variation of $\nu_{T,p}$ and ν_T for *DR*= 37% (case B in table 1) across the channel and comparison with the model of $\nu_{T,p}$ developed by Iaccarino et al. (2010).

where the first term on the right hand side dominates in the near wall region and the second term captures the effect of turbulence far from the wall. By utilizing the turbulent term of $\nu_{T,p}$, the turbulent viscoelastic Prandtl number ($\mathrm{Pr}_{T,p}$) is defined as: $\mathrm{Pr}_{T,p} = a_1\sqrt{L^2/Wi_{\tau o}}\, f(C_{kk})$. The model for the kinematic turbulent viscoelastic viscosity developed with data for case B (DR=37%) is compared in Figure (4.5), in terms of the polymer stress, with DNS data and the model of Eq. (4.26) previously proposed by Iaccarino et al. (2010). While this latter model describes well the rise of the shear stress very close to the wall it severely underpredicts the polymer stress away from the wall, a feature corrected by the proposed closure.

To compute the polymer stress according to the model of Eq. (4.29) we also need the extension of the chains via C_{kk} and this can be computed directly via the corresponding Reynolds-averaged equation, which is obtained as the trace of the Reynolds-averaged conformation Eq. (4.11):

$$M_{kk} + NLT_{kk} + CT_{kk} + \frac{1}{\lambda}\left(3 - f(C_{kk})C_{kk}\right) = 0 \qquad (4.30)$$

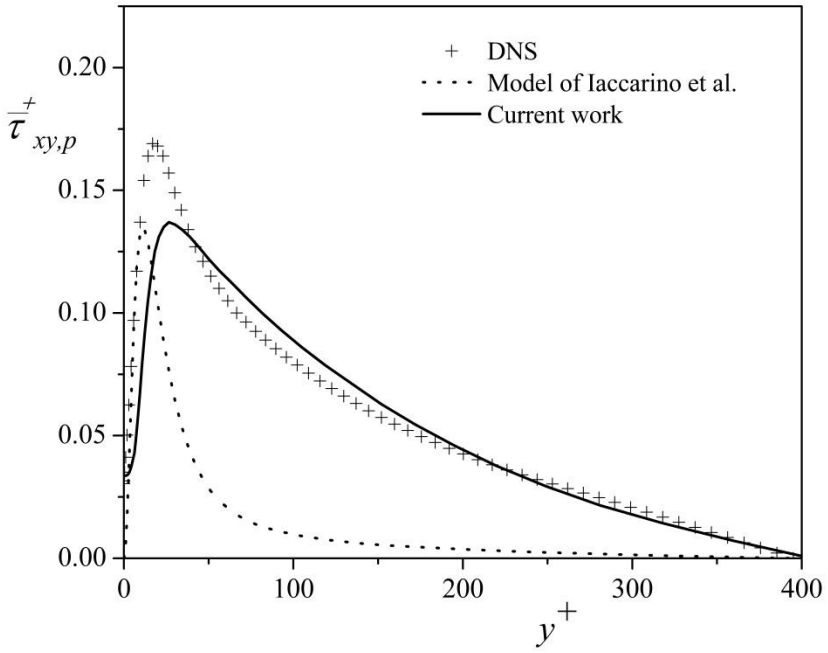

Figure 4.5. Comparison between current model for the polymer mean shear stress, the model of Iaccarino et al. (2010) and DNS data for case B (DR=37% and $Re_{\tau 0}$ = 395)

In Eq. (4.30) M_{kk} is the trace of the mean flow distortion term of $\overset{\nabla}{C}_{ij}$, NLT_{kk} accounts for the interactions between the fluctuating components of the conformation and velocity gradient tensors, and CT_{kk} is the contribution to the transport of the conformation tensor by the fluctuating advection.

Figure (4.6) compares the first three terms on the left-hand-side of Eq. (4.30) for low (case A) and high (case D) drag reductions, showing CT_{kk} to be negligible regardless of the amount of DR, in agreement with the findings of Housiadas et al. (2005) and Li et al. (2010). In contrast, NLT_{kk} is not negligible, and its closure constitutes a main task in this work. Apart from NLT_{kk}, the other main contribution comes from the exact mean flow term (M_{kk}), especially in the viscous sublayer and buffer layer.

Provided the model for $\nu_{T,p}$ is robust, M_{kk} is easily computed from its definition. For fully-developed flow we have $M_{yy}=M_{zz}=0$ and

$$M_{xx} = 2C_{xy}\frac{dU}{dy} \quad \longrightarrow M_{kk} = 2\left(\frac{\lambda\bar{\tau}_{xy,p}}{\eta_p f(C_{kk})}\frac{dU}{dy}\right) \tag{4.31}$$

Fig (4.6) shows that this term is an important term in Eq. (4.30). Although M_{kk} is exact, Iaccarino et al. (2010) proposed the following model to compute it:

$$M_{kk} = \frac{2\lambda}{f^2(C_{kk})}\left(\frac{dU_x}{dy}\right)^2 \tag{4.32}$$

which is the exact solution for laminar channel flow. Figure (4.7) compares the predictions of M_{kk} using our method (Eq. (4.31)) and the model of Iaccarino et al. (2010) (Eq.(4.32)) and includes also the corresponding DNS data. The use of the exact definition of the M_{kk} , based on our model for the turbulent polymer viscosity is able to predict better M_{kk} all across the channel.

NLT_{kk} accounts for the interactions between the fluctuating components of the conformation tensor and of the velocity gradient tensor. For low and intermediate DR a closure for NLT_{ij} was derived by Resende et al. (2011), but that is a very complex model. An alternative simpler closure had been previously derived by Pinho et al. (2008,2012), but in this work we develop a specific model for the trace NLT_{kk}, simpler than any of the previous existing closures, and here NLT_{kk} is related to its mean value (M_{kk}) and the eddy viscosity via:

$$NLT_{kk} = a_2 M_{kk}\frac{\nu_T}{\nu_o} \tag{4.33}$$

Mathematically NLT_{kk} originates from the Oldroyd derivative and it is the fluctuating counterpart of M_{kk}. The closure of Eq. (4.33) was developed after an extensive analysis of DNS data and the constant coefficient appearing in it was fixed on the basis of the data for case B (DR=37%, Table (4.1)).

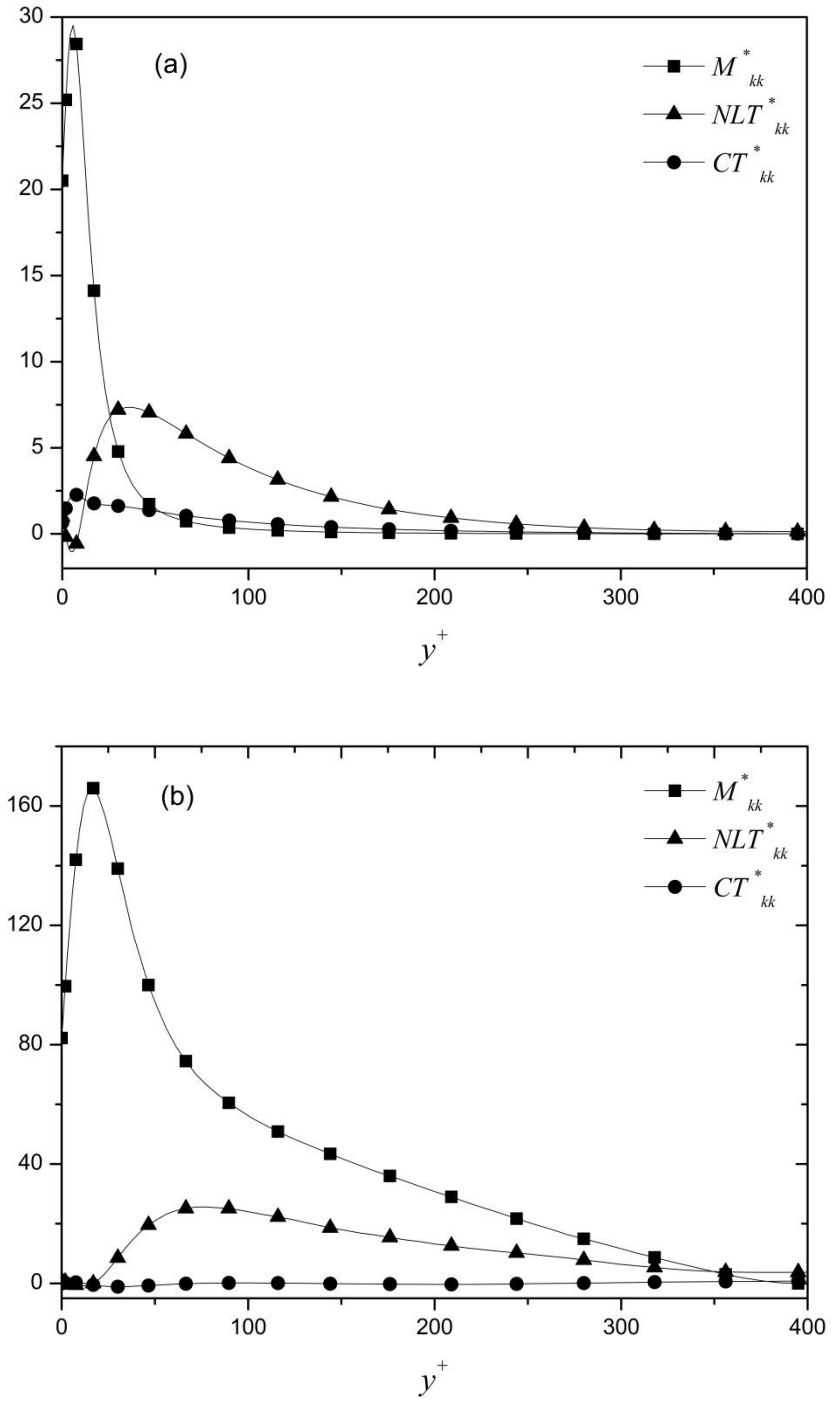

Figure 4.6. Contributions to the trace of the conformation tensor (eq. (31)) in fully developed channel flow for (a) case A, (b) case D.

Figure (4.8) compares its predictions and performance against DNS data. The model developed by Iaccarino et al. (2010) relates NLT_{kk} with ε, which according to Fig (4.1), on account of the location of the peak in ε and its behavior far from the wall is less accurate compared with DNS.

As a result of the developed closures for M_{kk}, and NLT_{kk} the trace of the polymer stress (τ_{kk}) is depicted in Figure (4.9), which is calculated from Eq. (4.30) while neglecting CT_{kk} .
The proposed closure for NLT_{kk} is always positive, whereas the DNS data of Figure (4.8) shows a small incursion of NLT_{kk} into negative values near the wall. However, Fig 4.6 (a,b) also shows this negative peak in NLT_{kk} to be negligible in relation to M_{kk}, which is nearly 100 times bigger than NLT_{kk} close to the wall, so that neglecting the negative peak of NLT_{kk} is of no consequence to the predictions of C_{kk}, as seen in Figure (4.9), and in addition it prevents possible numerical divergence.

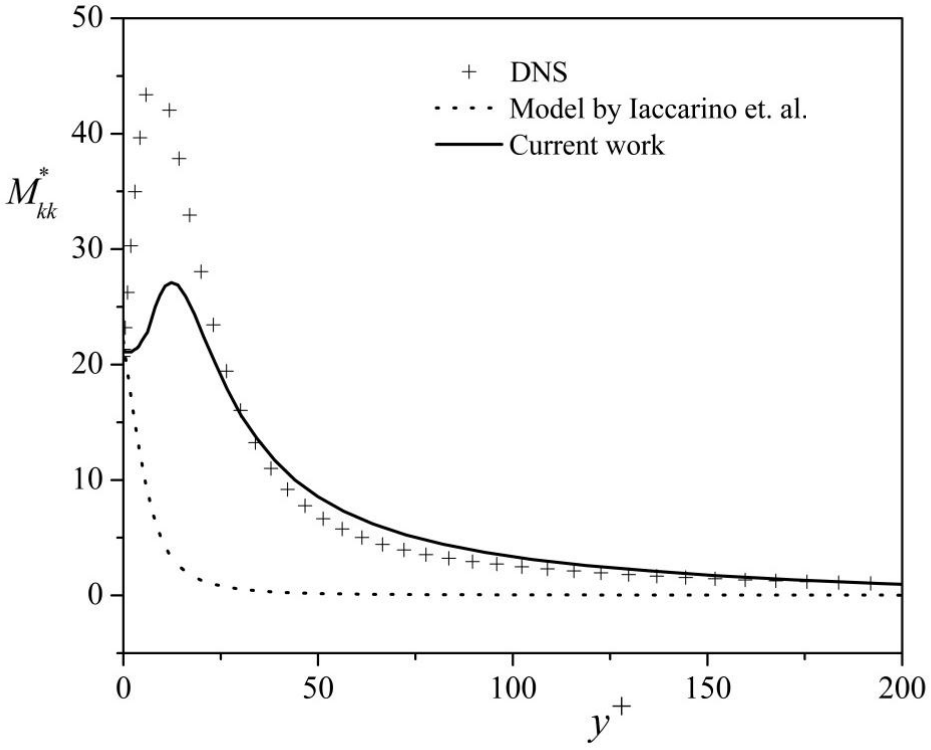

Figure 4.7. Comparison between the predicted M_{kk}, by current method with the model of Iaccarino et al. (2010), and DNS data for case B.

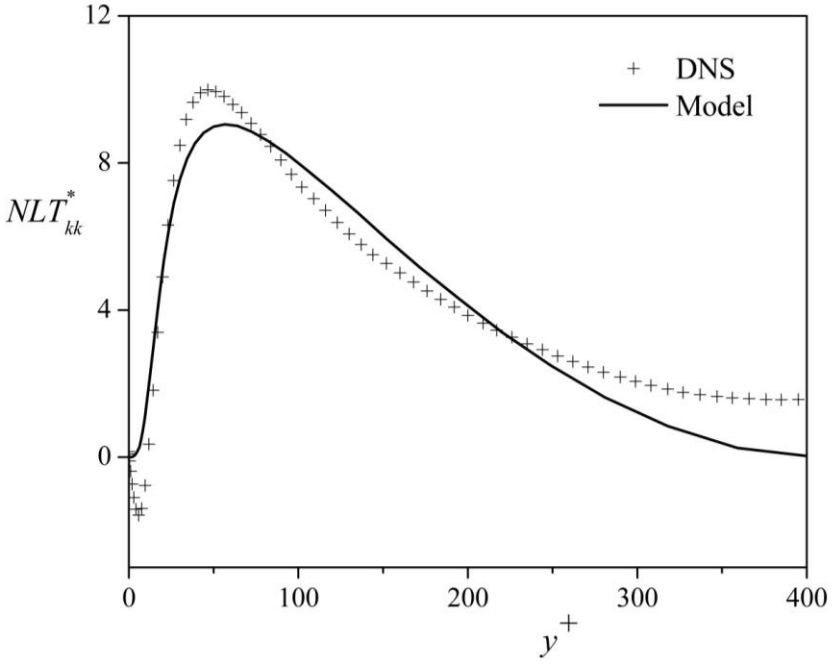

Figure 4.8. Comparison between predicted NLT_{kk} and DNS data for case B.

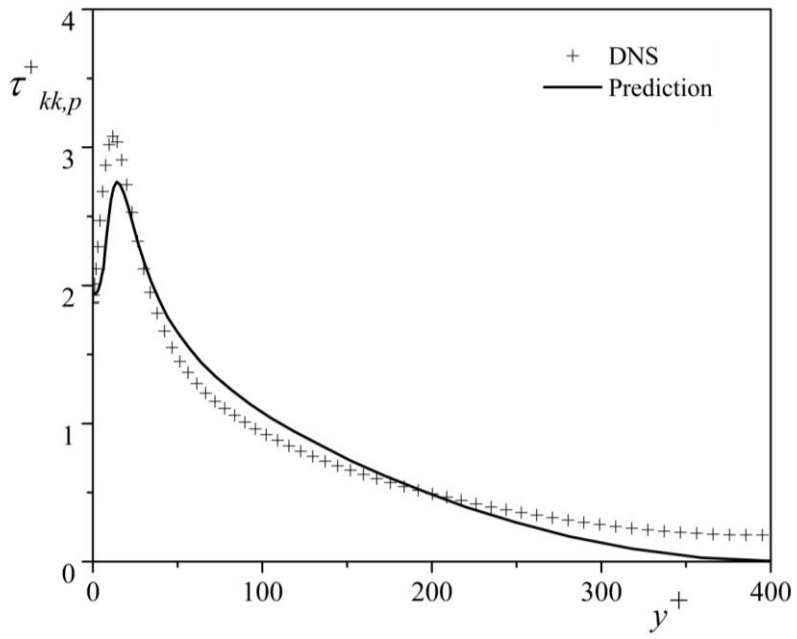

Figure 4.9. Comparison between predicted and DNS data of $\tau_{kk,p}$ for case B.

4.3.2. Development of closures needed by k , ε , *and* $\overline{v^2}$ equations

Closures are required for two terms in the transport equation of *k*, namely for the viscoelastic turbulent transport (Q_p) and the viscoelastic stress work (ε_p). Similarly, the corresponding terms need to be modeled in the transport equation of $\overline{v^2}$, namely the transverse viscoelastic turbulent transport ($Q_{yy,p}$) and the transverse viscoelastic stress work ($\varepsilon_{yy,p}$). Finally, it is also necessary to provide a closure for the term accounting for the viscoelastic contribution to the transport equation of ε denoted by E_p. Figures (4.1) and (4.2) showed the budgets of *k* and $\overline{v^2}$ obtained from DNS data, respectively. In both cases the viscoelastic turbulent transport is negligible as also found previously Pinho et al. (2008) and in particular also by the independent DNS data of Iaccarino et al. (2010), and Thais et al. (2013).

The viscoelastic stress work (ε_p) appearing in the transport equation of *k* is defined as

$$\varepsilon_p = \frac{1}{\rho}\overline{\tau_{ij}^p \frac{\partial u_i}{\partial x_j}} = \frac{\eta_p}{\rho\lambda}\left[C_{ij}\overline{f(C_{mm}+c_{mm})\frac{\partial u_i}{\partial x_j}} + \overline{c_{ij} f(C_{mm}+c_{mm})\frac{\partial u_i}{\partial x_j}} \right] \tag{4.34}$$

Pinho and co-workers (2008, 2011) showed that in low drag reduction the triple correlation can be decoupled into a product of function $f(C_{kk})$ by the remaining double correlation, which is $NLT_{kk}/2$, therefore they approximated the viscoelastic stress work by

$$\varepsilon_p \approx \frac{\eta_p}{2\rho\lambda} f(C_{mm})\left[\overline{c_{ij}\frac{\partial u_i}{\partial x_j}} \right] = \frac{\eta_p}{2\rho\lambda} f(C_{mm}) NLT_{kk} \tag{4.35}$$

Figure (4.10) shows that this closure remains valid for intermediate and high drag reductions without the need for the coefficient of 1.076 in Pinho et al. (2008).

By contrast Iaccarino et al. (2010) modeled the viscoelastic stress work by

$$\varepsilon_p = b\lambda k S^2 \tag{4.36}$$

where *b* is a constant, λ is the polymer relaxation time, *k* is the turbulent kinetic energy, and *S* represents the magnitude of the strain rate. Figure (4.10) compares performance of both closures with DNS data for intermediate and high drag reduction. Clearly the model of Iaccarino et. al. (2010) excessively dampens ε_p far from the wall, whereas the current model (Eq. (4.35)) is a better representation of DNS data all across the channel.

The other term that needs closure is the transverse component of the viscoelastic stress work $\varepsilon_{yy,p}$. Figure (4.2) shows the budgets of different terms in $\overline{v^2}$ equation. For Newtonian fluids, Durbin (1996) modeled the transverse component of the velocity-pressure gradient term by the source term (*kf*) in the $\overline{v^2}$ transport equation. The true closure for $\varepsilon_{yy,p}$ must be a function of NLT_{yy} as presented in equation (4.34), however due to the fact that in this work we only considered the trace of the time averaged constitutive equation in the following an alternative approach is introduced. The DNS data plotted in Figure 4.2 include the source term (*kf*) and the

transverse component of the polymer stress work for LDR and HDR. Regardless of the amount of drag reduction the transverse component of the polymer stress work follows the shape of the source term (*kf*), so this behavior suggests that the largest positive quantity in the $\overline{v^2}$ transport equation, i.e. the pressure strain term (here *kf*), is the main responsible for accounting for the energy absorbed by the polymers. Therefore, to close the transverse component of the polymer stress work the source term (*kf*) in the $\overline{v^2}$ transport equation was used together with the turbulent viscoelastic Prandtl number ($\mathrm{Pr}_{T,p}$) as:

$$\varepsilon_{p,yy} = a_3 \sqrt{Wi_{\tau 0}}\, \mathrm{Pr}_{T,p}\, kf \tag{4.37}$$

The last term in Eq. 4.22 (Φ_{22}^{p}) represents the viscoelastic contribution to the *f* equation. Leighton et al. (2003) introduced an explicit modification to the pressure–strain correlation to account for the polymer-induced turbulence energy redistribution, but Iaccarino et al. (2010) tested this formulation and found that it did not produce acceptable results for high drag reduction. Similarly, we tested this term and found that by using it there is an excessive damping of the wall normal fluctuations leading to a complete flow laminarization. Therefore, this term was neglected as was also previously the case in Iaccarino et al. (2010). Figure (4.11) compares DNS and predicted *k* and $\overline{v^2}$ by using developed closures above, all across the channel.

The last quantity that needs to be modeled is the viscoelastic contribution to the transport equation of ε, denoted as E_p. A closure was developed by Resende et al. (2011), but here we adopt a much simpler approach. E_p is assumed to be a destruction term Resende et al. (2011) and to devise its closure we followed the same approach as for the classical Newtonian destruction term in the ε equation, but involving a viscoelastic quantity, i.e., we assumed that it is proportional to the viscoelastic stress work (usually acting as a viscoelastic dissipation of *k*, cf. Figure 4.1) and to the time scale $\frac{1}{T_t}$. The viscoelastic destruction term is therefore modeled as equation (4.38).

$$E_p = \frac{C_{\varepsilon 1}\varepsilon_p}{T_t} \tag{4.38}$$

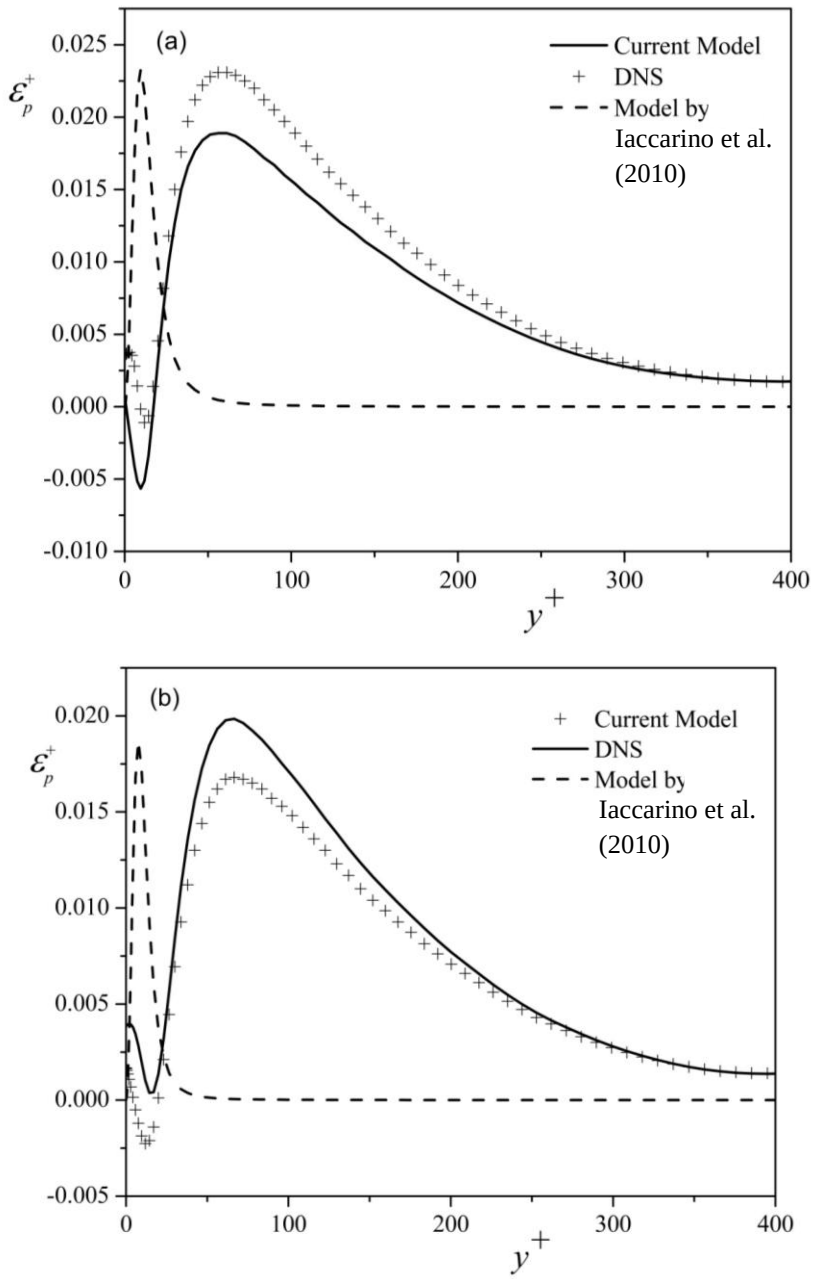

Figure 4.10. Comparison between current model for ε_p against DNS data and the model of Iaccarino et al. (2010) for (a) case C, (b) case D

Consequently the solvent dissipation rate transport equation is closed as

$$U_j \frac{\partial \varepsilon}{\partial x_j} = \frac{C_{\varepsilon 1}(P_k - \varepsilon_p) - C_{\varepsilon 2}\varepsilon}{T_t} + \frac{\partial}{\partial x_j}\left(\left(\nu + \frac{\nu_T}{\sigma_\varepsilon}\right)\frac{\partial \varepsilon}{\partial x_j}\right) \tag{4.39}$$

Figure (4.12) shows the performance of the model in predicting the dissipation rate. We next compare in Figure 4.13 the overall shear stress balance for case B (Table 4.1) as predicted by this

model with the corresponding DNS balance. It includes the Reynolds stress, the solvent stress, and the polymer stress.

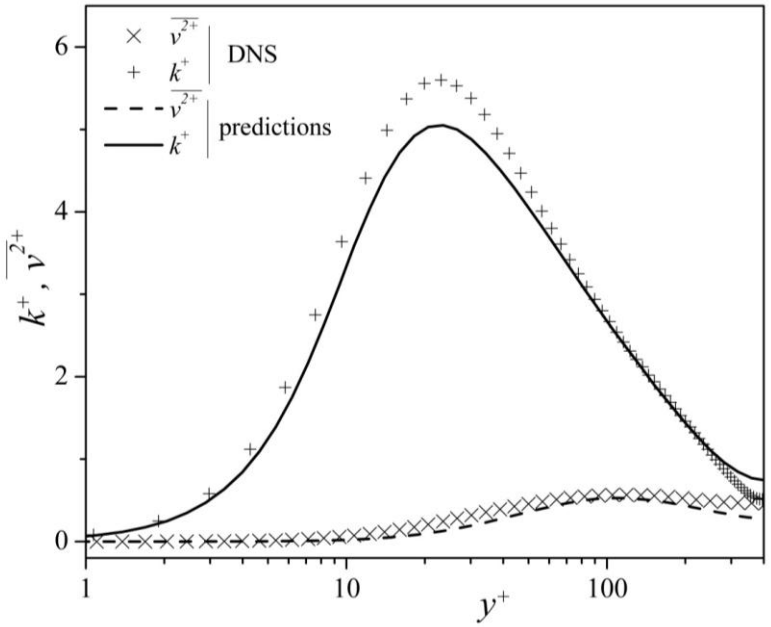

Figure 4.11. Comparison between predicted and DNS data of k^+, $\overline{v^2}$ for case B.

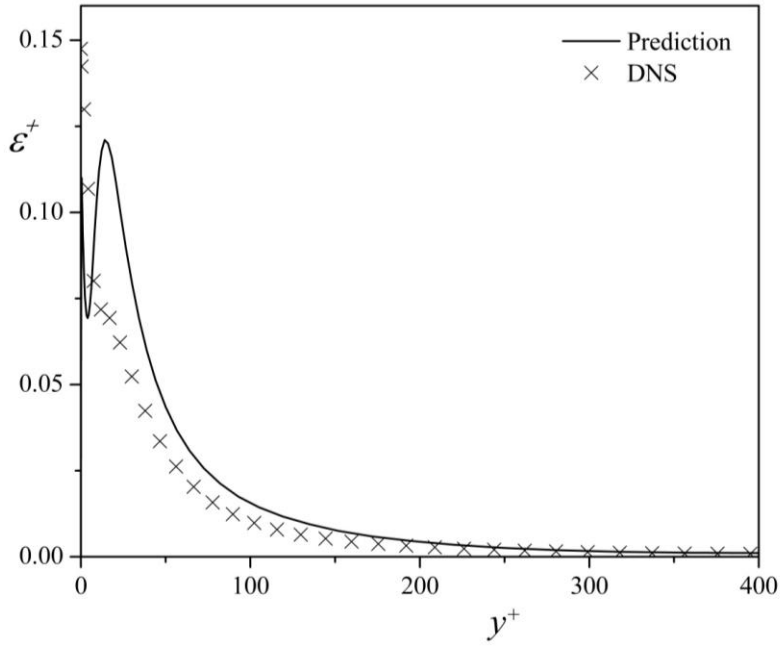

Figure 4.12. Comparison between predicted and DNS data of ε^+, for case B.

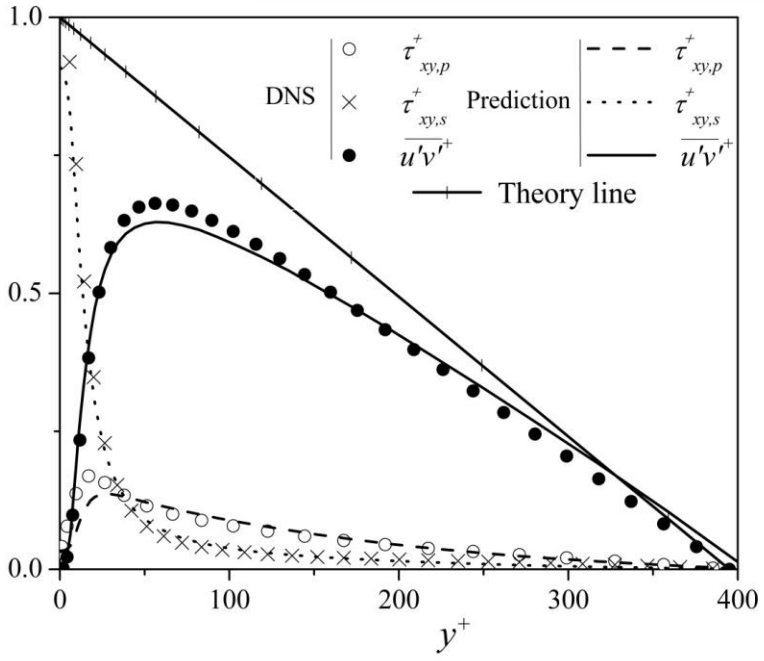

Figure 4.13. Comparison between predictions (lines) and DNS data (symbols) of normalized shear stresses for case B.

4.3.3. Summary of the model

Utilizing the closures developed in the previous section, the model equations are given below.

$$\rho\frac{\partial U_i}{\partial t}+\rho U_k\frac{\partial U_i}{\partial x_k}=-\frac{\partial \overline{P}}{\partial x_i}+\rho\frac{\partial}{\partial x_k}\left[\left(\nu_s+\nu_T+\nu_{T,p}\right)\frac{\partial U_i}{\partial x_k}\right] \tag{4.40}$$

$$U_j\frac{\partial k}{\partial x_j}=P_{kk}-\varepsilon+\frac{\partial}{\partial x_j}\left(\left(\nu_s+\frac{\nu_T}{\sigma_k}\right)\frac{\partial k}{\partial x_j}\right)-\varepsilon_p \tag{4.41}$$

$$U_j\frac{\partial \varepsilon}{\partial x_j}=\frac{C_{\varepsilon 1}P_k-C_{\varepsilon 2}\varepsilon}{T_t}+\frac{\partial}{\partial x_j}\left(\left(\nu_s+\frac{\nu_T}{\sigma_\varepsilon}\right)\frac{\partial \varepsilon}{\partial x_j}\right)-E_p \tag{4.42}$$

$$U_j\frac{\partial \overline{v^2}}{\partial x_j}=kf+\frac{\partial}{\partial x_j}\left(\left(\nu_s+\frac{\nu_T}{\sigma_k}\right)\frac{\partial \overline{v^2}}{\partial x_j}\right)-6\frac{\varepsilon}{k}\overline{v^2}-\varepsilon_{p,yy} \tag{4.43}$$

$$f - L_t^2 \frac{\partial^2 f}{\partial x_j \partial x_j} = C_1 \frac{\left(\frac{2}{3} - \frac{\overline{v^2}}{k}\right)}{T_t} + C_2 \frac{P_k}{k} - 5\varepsilon \frac{\overline{v^2}}{k} \tag{4.44}$$

$$M_{kk} + NLT_{kk} + \frac{1}{\lambda}\left(3 - f(C_{kk})C_{kk}\right) = 0 \tag{4.45}$$

where

$$\nu_{T,p} = \left(\frac{\nu_p}{f(C_{kk})} + a_1 \sqrt{L^2 / Wi_{\tau o}}\ f(C_{kk})\nu_T \right) \tag{4.46}$$

$$M_{kk} = 2\left\{ \frac{\lambda}{f(C_{kk})} \frac{\nu_{T,p}}{\nu_p} \left(\frac{dU}{dy} \right)^2 \right\} \tag{4.47}$$

$$NLT_{kk} = a_2 M_{kk} \frac{\nu_T}{\nu_o} \tag{4.48}$$

$$\varepsilon_p = \frac{\eta_p}{2\rho\lambda} f(C_{mm}) NLT_{kk} \tag{4.49}$$

$$\varepsilon_{p,yy} = a_3 \sqrt{Wi_{\tau 0}}\ \mathrm{Pr}_{T,p}\, kf \tag{4.50}$$

$$E_p = \frac{C_{\varepsilon 1}\varepsilon_p}{T_t} \tag{4.51}$$

Relative to the model of Lien and Durbin (1996) this model has 3 extra coefficients to incorporate the polymer effects, $a_1 = 0.02$, $a_2 = 0.16$ and $a_3 = 0.15$. Other coefficients arise from the Newtonian model and take the same numerical values as reported in Lien and Durbin (1996), the coefficient C_μ also exists in the context of Newtonian fluid models, but here it was modified to take the numerical value of 0.16 instead of the original value of 0.19. The boundary conditions are those of no slip for velocities, *k* and v^2, whereas for the dissipation by the solvent and *f* we used the standard conditions of Newtonian fluids described in Lien and Durbin (1996).

4.4. Results and Discussion

In this section, results from several predictions of fully-developed channel flow using this model are presented and assessed against other sets of DNS data for FENE-P fluids as in Table (4.1). All viscoelastic flow calculations were carried out using the same channel dimensions and friction velocity as for the DNS. Note that some comparisons involve DNS data for $Re_{\tau 0}$ = 180, and also the independent DNS results of Iaccarino et al. (2010), and Thais et al. (2012, 2013).

The predicted *k* and $\overline{v^2}$ profiles are shown in Figure 4.14 for cases A and D. It is well known Housiadas et al. (2005), Oldaker et al. (1977), and Tiederman et al. (1985) that streamwise

velocity fluctuations $\overline{u^2}$ increase with DR, while the wall normal and spanwise components $\overline{v^2}$ and $\overline{w^2}$ monotonically decrease. The increase of $\overline{u^2}$ is larger than the decrease of $\overline{v^2}$ and $\overline{w^2}$ and as a consequence the turbulent kinetic energy slightly increases. Moreover the peak location of *k* shifts away from the wall as DR increases, which is consistent with the upward shift of the logarithmic region in the mean velocity profile. As it is shown in Figure 4.14 the predictions have a satisfactory agreement with DNS data and the model captures both the physical characteristics of turbulent channel flow of dilute polymer solutions in terms of the slight increase in *k* and the upward shift of its peak location by increasing DR, as reported in the DNS results and in the experimental findings of Ptasinski et al. (2003). Nevertheless, at HDR (case D in Figure 4.14) the model under-predicts the peak value of k^+. As is well known from experiments Ptasinski et al. (2003), DR is associated with a decoupling between the streamwise and transverse turbulence accompanied by a reduction in $\overline{v^2}$ and this causes a decrease in the Reynolds shear stress, whereas the streamwise turbulence may even increase slightly before a decrease at very high DR. In the model the reduction in the $\overline{uv}$ is accomplished by the eddy viscosity and by adopting Durbin's model of Eq. (4.16) this reduction can be achieved via a decrease in turbulent time scale and/or wall normal Reynolds stress. The reduction of the predicted v^2 is accurately predicted for all cases, but is insufficient to reduce $\overline{uv}$ as much as needed at HDR, so the turbulent time scale must also decrease and this can be achieved via a decrease in *k* and/or an increase in ε. However, since ε is also reduced (cf. Figure (4.1-a, 4.1-b)), there is still the need for a reduction in *k* at HDR and this explains the discrepancy. One remedy in the context of this model is the use of a damping function for the eddy viscosity, which we decided not to do in order to maintain the original idea of Durbin's theory (the elimination of damping functions). The other remedy is the use of a higher level turbulence model, but this is beyond the scope of this work.

We should add that this problem is here limited to HDR and is much more alleviated than with two equation models that do not rely on v^2, as discussed in Resende et al. (2011) where a severe reduction in *k* was observed already at intermediate DR even when using damping functions.

Finally, we should also say that the discrepancy may be somewhat fictitious: in the experiments of Ptasinski et. al. (2003) the stream wise turbulence ($\overline{u^2}$) increases slightly by increasing DR with a peak of $\sqrt{\overline{u^2}}$ reaching around 3.2 corresponding to a peak for *k* of around 5.5. On the other hand their corresponding DNS calculations over-predict those peak values (maximum *u*' of around 4.5, and maximum *k* of around 8.5). They extensively discuss this difference and state that this might be due to shortcomings in the FENE-P model.

Predictions of the trace of the polymer stress and of the conformation tensor are compared with DNS data in Figure 4.15-(a), 4.15-(b), respectively for case A (LDR) and D (HDR). Note that the region of high chain dumbbell extension is limited to the near wall region ($y^+ < 50$), which is in agreement with findings of Li et al. 2006-b.

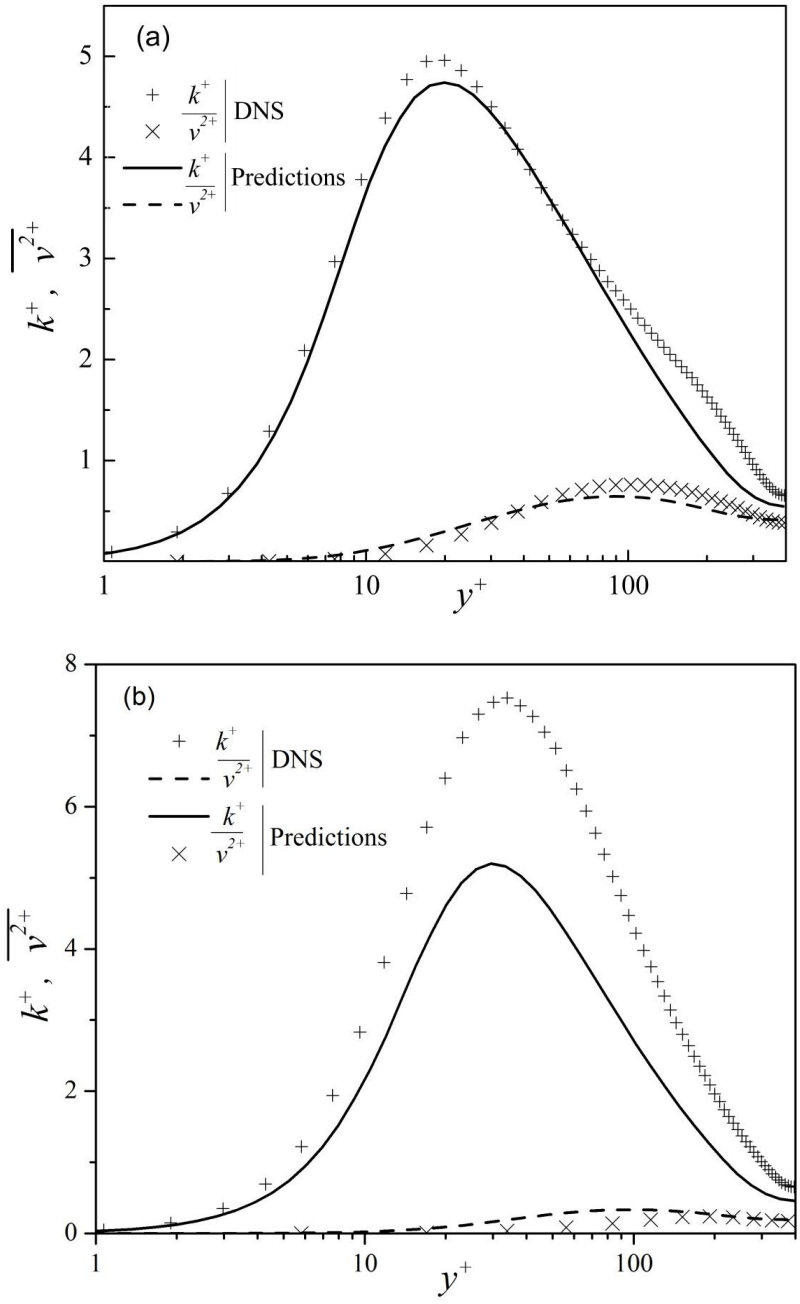

Figure 4.14. Turbulent kinetic energy and $\overline{v^2}$, (a) case A (LDR), (b) case D (HDR).

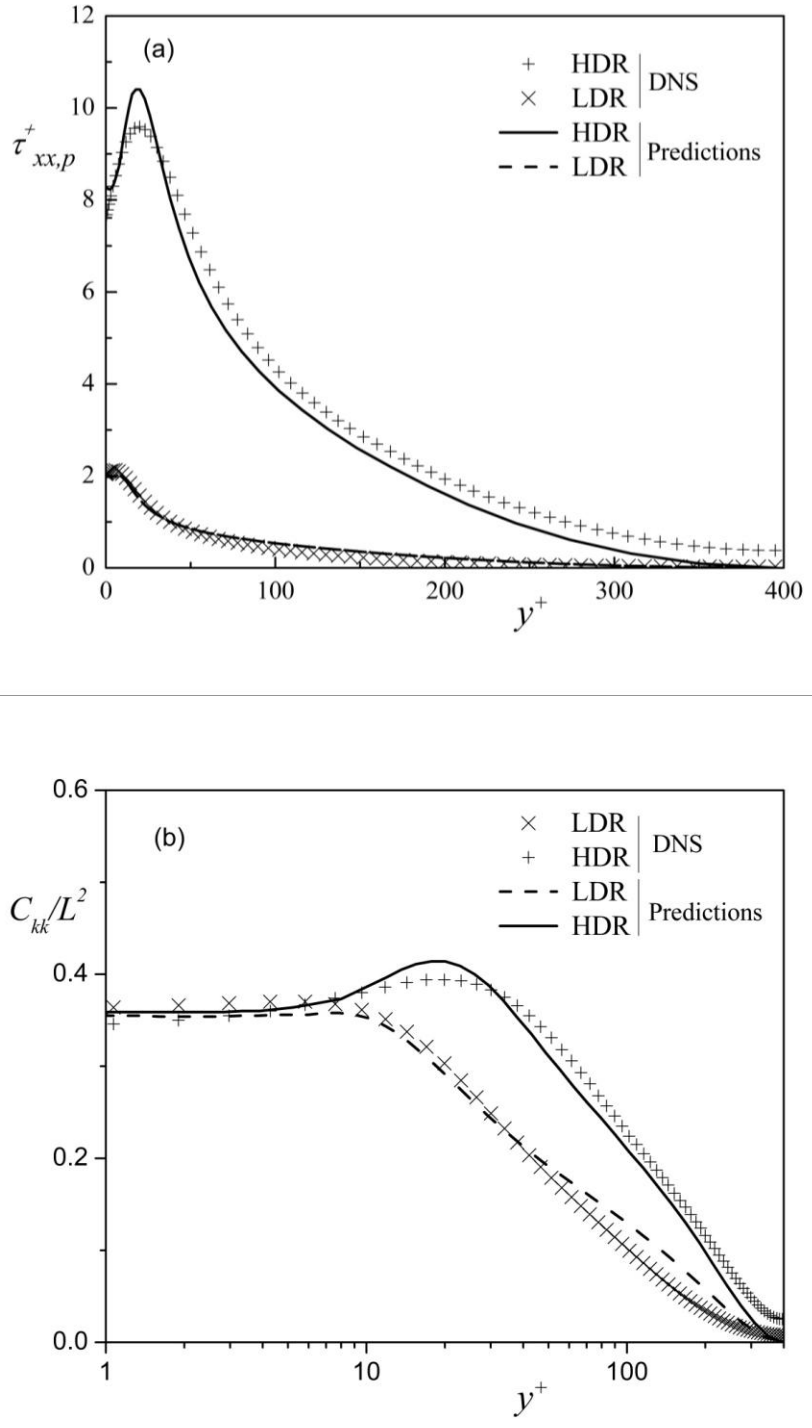

Figure 4.15. (a): Polymer Stress, (b) Polymer length normalized by Polymer maximum length , at $Re_{\tau 0}$ = 395

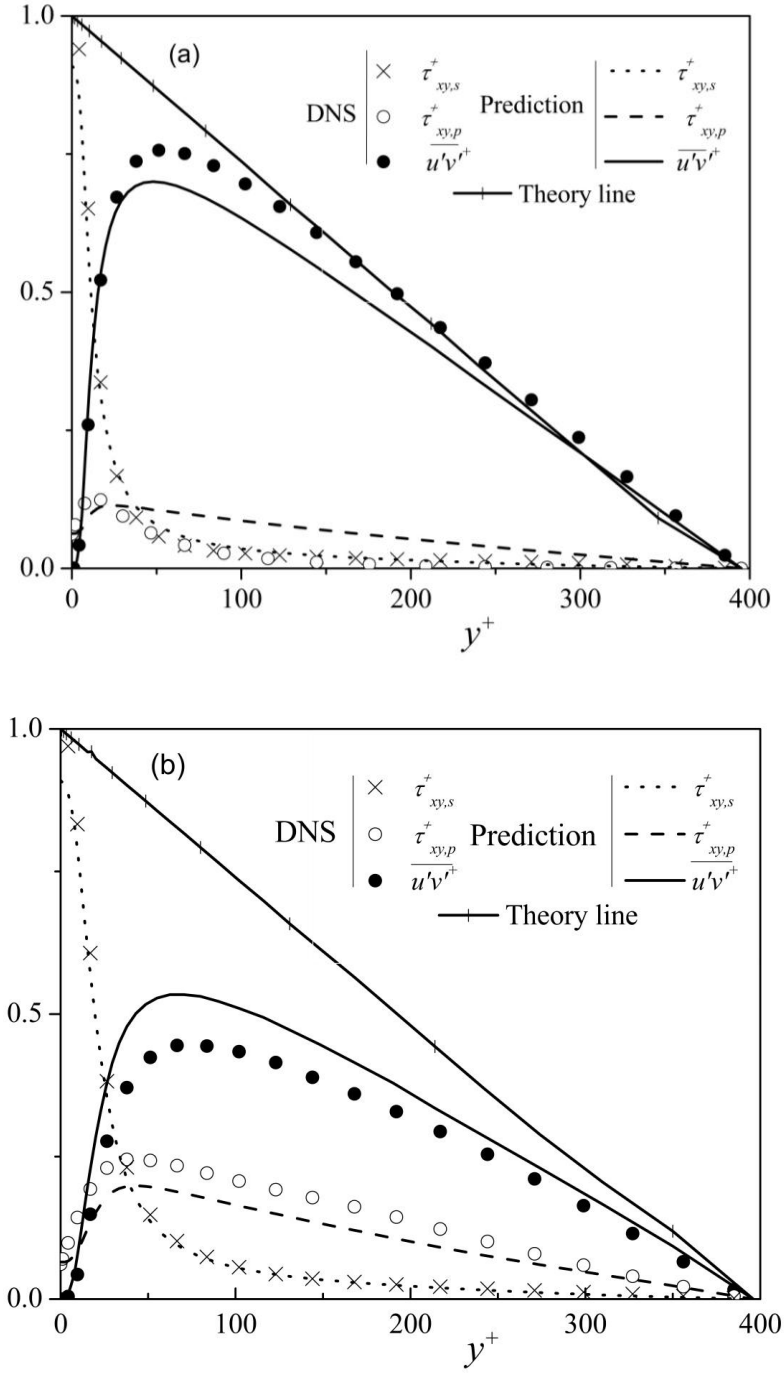

Figure 4.16. Comparison between predictions (lines) and DNS data (symbols) for normalized shear stresses (a) case A (LDR), (b) case D (HDR).

In a fully developed state, the total shear stress must follow a straight line across the channel varying from zero at the centerline to the wall shear stress (τ_w) at the wall. Here the total shear stress is the sum of three contributions, namely, the Reynolds stress, the viscous stress of the

solvent and the polymer stress. The total shear stress profile and its three components are plotted in Figure 4.16 normalized by the wall shear stress for low and high drag reduction (cases A and D) and compared with the corresponding DNS. In both cases the total shear stress follows the expected linear profiles over the channel height, indicating that a stationary fully developed state has been reached. In low drag reduction case the polymer stress contribution is relatively small, and it occurs mainly in the near wall region. However, as DR increases, the Reynolds stress is significantly reduced, and correspondingly the polymer stress increases to ensure the balance and becomes comparable to the Reynolds stress. Specifically, at HDR the Reynolds stress is significantly reduced as compared to the LDR regime, but it remains non-zero. In the LDR case the proposed model predicts the peak and the general trend of all stresses very well. In HDR case the polymer contribution becomes important and clearly the prediction of the proposed closure is good. These observations are consistent with the numerical findings of Li et al. (2006-b) and the experimental results of Ptasinski et al. (2003).

In Figure 4.17 the predictions of the dissipation rate are compared with the DNS data for both LDR (case A) and HDR (case D). At LDR the predictions are accurate near and far from the wall, while at HDR the predictions are accurate far from the wall, but overpredicted close to the wall.

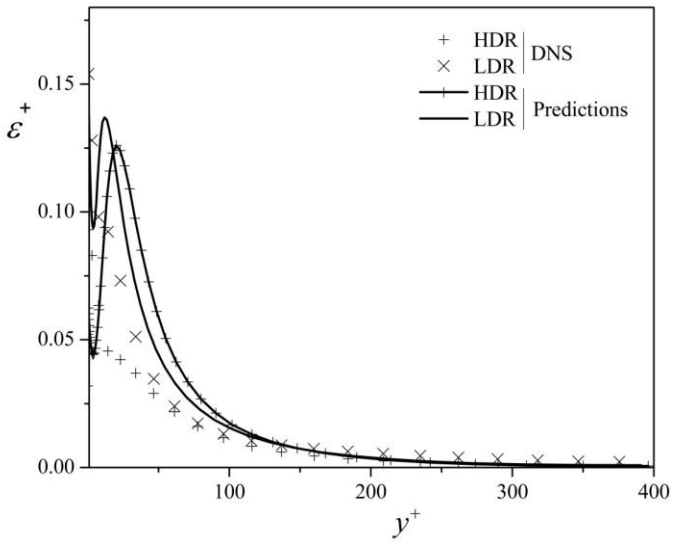

Figure 4.17. Comparison between predictions and DNS data of ε^+ for case A (LDR), and case D (HDR).

We present predicted transverse profiles of the mean streamwise velocity for a large set of data covering the whole range of DR, different values of L^2, Reynolds numbers, and Weissenberg numbers in Figs. 4.18 to 4.20, and comparing the profiles with the corresponding DNS data. For the sake of comparison the profiles for Newtonian flow at each Reynolds number have also been included. All profiles in the viscous sublayer collapse on the linear distribution $U^+ = y^+$. Further away from the wall the mean velocity of the drag reduced flows increases as compared to that in

Newtonian flows. Specifically in the LDR regime, the logarithmic profile is shifted upwards but remains parallel to that of the Newtonian flow as is also found in the DNS results. The upward shift of the logarithmic profile can be interpreted as a thickening of the buffer layer. In the HDR regime, the slope of the mean velocity has augmented as the thickened buffer layer occupies nearly the whole channel. In addition, the slope increases as a function of DR and the predictions and DNS are consistent and this is seen to be the case at both high and low Reynolds numbers in Figs. 4.18 and 4.19.

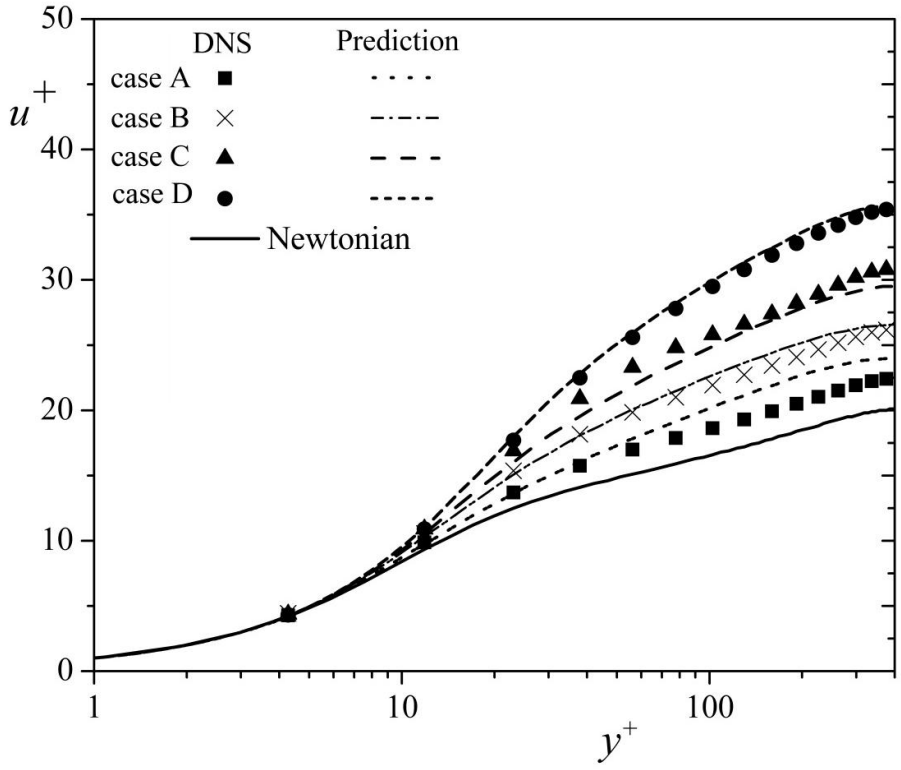

Figure 4.18. Transverse profiles of the normalized mean velocity in wall coordinates for Newtonian and FENE-P fluids with rheological parameters defined in table (1), at $Re_{\tau 0}$ = 395

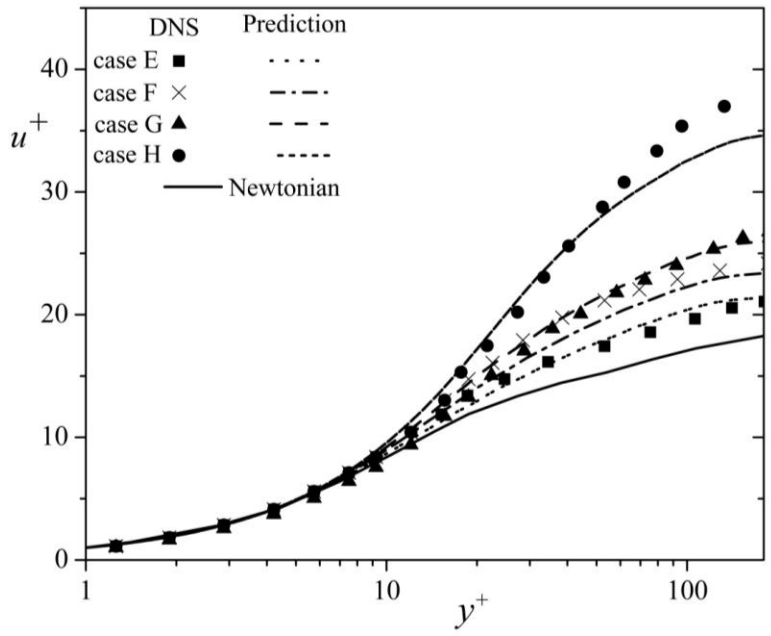

Figure 4.19. Transverse profiles of the normalized mean velocity in wall coordinates for Newtonian and FENE-P flows with rheological parameters defined in table (1), at $Re_{\tau 0}$ = 180

We also assessed the model performance in predicting drag reduction against independent DNS data provided by Iaccarino et al. (2010), and Thais et al. (2012, 2013), which corresponds to $Re_{\tau 0}$ = 300,395,590,1000, i.e., including high Reynolds number flows. As seen in Figure 4.20, the agreement between the predictions and the DNS profiles of the mean velocity for the cases in Table (4.2) is fairly good regardless of the Reynolds number. The comparisons between the DNS data and the predictions in terms of k, v^2, and C_{kk} for the high Reynolds number flow case (e) (Re_τ= 1000) are presented in Figs. 4.21 and 4.22 and show again a good agreement, similar to that observed at lower Reynolds number flows.

Table 4.2. Independent DNS data

DNS data	case	$Re_{\tau 0}$	L^2	$Wi_{\tau 0}$
Iaccarino *et al.* (2010)	(a)	300	10000	36
Iaccarino *et al.* (2010)	(b)	300	10000	120
Thais *et al.* (2012)	(c)	395	10000	116
Thais *et al.* (2012)	(d)	590	10000	116
Thais *et al.* (2013)	(e)	1000	900	50
Thais *et al.* (2013)	(f)	1000	10000	115

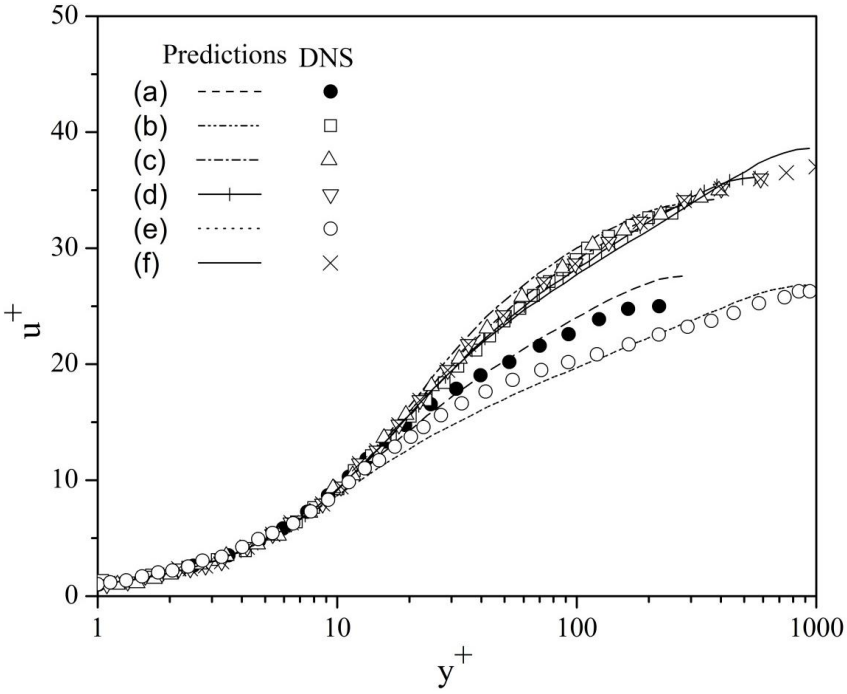

Figure 4.20. Transverse profiles of the normalized mean velocity in wall coordinates for turbulent FENE-P flows with rheological parameters define in table (2),

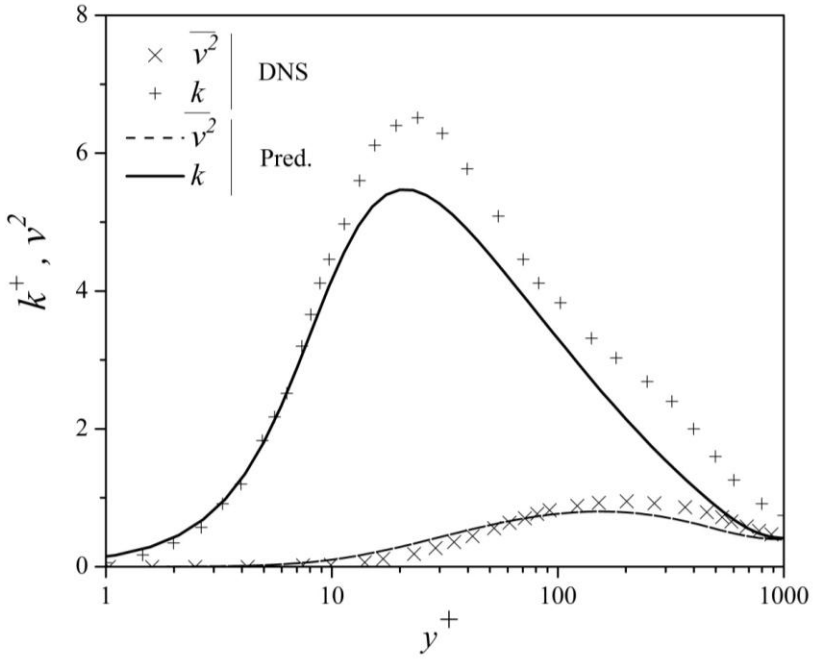

Figure 4.21. Comparison between predictions and DNS for the transverse profiles of k^+ and $\overline{v^2}$ for $Re_{\tau 0} = 1000$, $We_{\tau 0} = 50$, and L^2= 900 (case (e) Table 4.2).

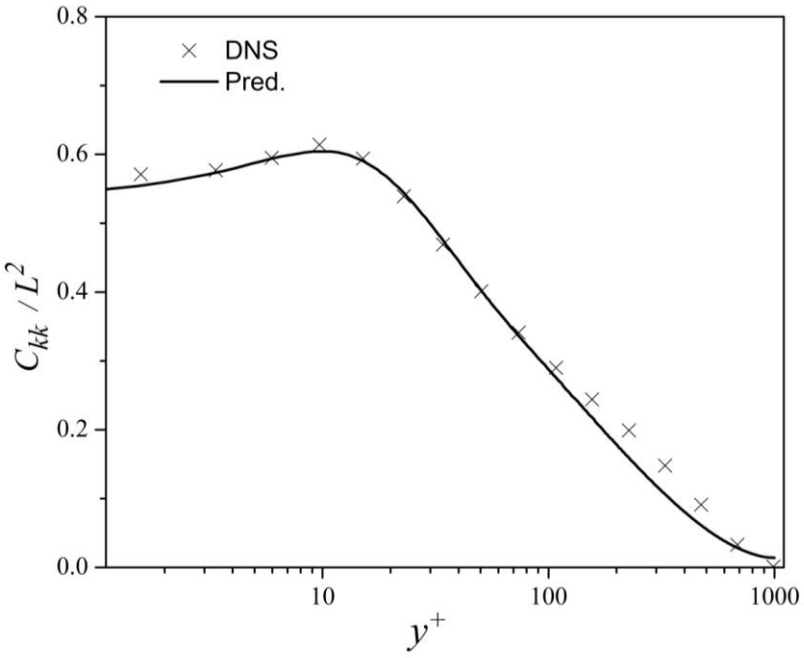

Figure 4.22. Comparison between predictions and DNS for the Polymer length normalized by Polymer maximum length,$Re_{\tau 0} = 1000$, $We_{\tau 0} = 50$, and L^2= 900 (case (e) Table 4.2).

4.5. Conclusions

The *k-ε* -$\overline{v^2}$ *-f* model of Lien and Durbin (1996) is modified for modeling turbulent channel flow of dilute polymer solutions up to the maximum drag reduction. Fluid rheology is described by the finitely extensible nonlinear elastic-Peterlin (FENE-P) constitutive equation and to help develop the model eight sets of recent direct numerical simulations (DNS) data are analyzed. To account for the polymer shear stress term in the Reynolds averaged momentum equation the procedure proposed by Iaccarino et. al (2010) is used and a turbulent viscoelastic viscosity is introduced in order to calculate the polymer shear stress via a Boussinesq-like relationship which is consistent with current DNS and independent DNS simulation.

Analysis of the DNS results confirms the previously developed closure Pinho et al. (2008) for the viscoelastic stress work on the basis of NLT_{kk}, which is a new contribution to the transport equation of *k*. A simple closure for NLT_{kk} is proposed by using M_{kk} and the turbulent eddy viscosity. A closure was also proposed for the transverse polymer stress work in the $\overline{v^2}$ transport equation leading to a modification of the original Newtonian source term developed by Lien and Durbin (1996) to account for the reduction of the pressure-strain redistribution term. The f equation remained the same as for Newtonian fluids. Finally, the closure for the viscoelastic destruction of the rate of dissipation by the solvent has similarities with the classical Newtonian destruction term.

All closures were developed on the basis of DNS data for 37% drag reduction at $Re_{\tau 0} = 395$ and the performance assessed against sets of DNS data for a wide range of Reynolds numbers ($Re_{\tau 0} = 180, 300, 395, 590$ and 1000) over a wide range of Weissenberg numbers together with different values of L^2 and β and also against independent DNS results.

The predictions in fully-developed channel flow compare very well with DNS data in terms of mean velocity, turbulent kinetic energy and viscoelastic stresses at all ranges of drag reduction. The turbulence model here developed does not require wall damping functions as the original model of Lien and Durbin (1996) and the new closures required to account for viscoelastic fluid behavior are simple and numerically inexpensive with the model showing effectively a better predictive capability than existing models for FENE-P fluids.

5

Chapter 5:
A viscoelastic RSM model

M. Masoudian, K. Kim, F. T. Pinho, and R. Sureshkumar, International Journal of Heat and Fluid Flow (2015) 54, 220-235

"If the facts don't fit the theory, change the facts."
– Albert Einstein

Abstract

Using *a priori* analyses of direct numerical simulation (DNS) data, a Reynolds stress model (RSM) is developed to account for the influence of polymer additives on turbulent flow over a wide range of flow conditions. The Finitely Extensible Nonlinear Elastic-Peterlin (FENE-P) rheological constitutive model is utilized to evaluate the polymer contribution to the stress tensor. Thirteen DNS data sets are used to analyze the budgets of elastic stress-velocity gradient correlations as well as Reynolds stress and dissipation transport. Closures are developed in the framework of the RSM model for all the required unknown and non-linear terms. The polymer stresses, velocity profiles, turbulent flow statistics and the percentage of friction drag reduction predicted by the RSM model are in good agreement with present and those obtained from independent DNS data over a wide range of rheological and flow parameters.

5.1. Introduction

The addition of a small amount of polymers to turbulent flows of Newtonian fluids can dramatically reduce the turbulent friction drag compared to that of the original Newtonian flow. It has been shown experimentally that very small amounts of polymers are sufficient to reduce drag by up to 80%. The phenomenon was found by Toms (1948), and it has been exploited in several applications, e.g. firefighting and irrigation systems among others. Comprehensive reviews of the early literature on this topic are reported in Hoyt (1972), Lumley (1969,1973), Virk (1971,1975).

Two early prominent proposals by Lumley (1969) and Tabor and De Gennes et al. (1986) describe the mechanism of turbulent drag reduction (DR) with dilute polymer solutions. Lumley proposed that flow-induced polymer stretching would increase the effective elongational viscosity in a region outside of the viscous sublayer and in the buffer layer. This in turn can inhibit turbulence-producing vortex stretching events. Tabor and De Gennes studied the drag reduction by polymer additives in the context of homogeneous isotropic turbulence, and related drag reduction to storage and release of energy by the polymer molecules.

Over the last 20 years, the development of accurate and efficient numerical and experimental methods have made it possible to investigate in detail turbulent DR of dilute polymer solutions Poole et al. (2003), Dubief et al. (2004), Ptasinski et al. (2003), Dimitropoulos et al. (2005), and Li et al. (2006). Direct numerical simulations (DNSs) of turbulent channel flow of homogeneous polymer solutions have been carried out over the last two decades in order to understand various aspects of DR by investigating the effects of rheological parameters on DR mechanisms Dimitropoulos et al. (2005), and Li et al. (2006). Most of these numerical simulations have used constitutive equations based on the finitely extensible nonlinear elastic model with Peterlin's closure (FENE-P), which accounts for polymer stretching and relaxation effects as well as finite chain extensibility.

DNS of turbulent viscoelastic flow is significantly more expensive than Newtonian DNS and the CPU requirements for the DNS of viscoelastic flows are at least two orders of magnitude larger as compared to the corresponding Newtonian case, making it unfeasible for the simulation of turbulent flow in complex geometries encountered in engineering applications. Hence, Reynolds-Averaged Navier–Stokes (RANS) Poreh et al. (1978), Malin (1998), Pinho et al. (2003, 2008, 2011,2013), Leighton et al. (2003), Iaccarino et al. (2010), Tsukahara et al. (2013) and Large Eddy Simulation (LES) models Thais et al. (2010) have been developed over the last decade.

The first models for turbulent DR of polymer solutions relied on modifications of the numerical values of the coefficients for Newtonian fluid closures as done by Hassid and Poreh (1978), who devised an empirical correlation to determine the constant coefficients in the standard k–ε model in order to control the behavior of the mean velocity profile in the buffer layer. Apart from the obvious consideration of lack of universality of such a closure, the major limitation is the lack of a minimal molecular representation of the behavior of the polymer solutions.

Later on, turbulence closures for non-Newtonian fluids started by modifying the von-Kármán coefficient in order to predict DR. Subsequent turbulence models were developed for inelastic fluids and included only variable viscosity effects, described by such rheological constitutive equations as the power law or Bingham law for yield stress fluids. Several first-order turbulence models were also developed for a modified version of the generalized Newtonian fluid constitutive equation in Malin (1998), and Pinho (2003) in an attempt to capture through a simple constitutive equation the effects of viscoelasticity upon turbulent friction drag.

The first turbulence model for turbulent flows of dilute polymer solutions described by a viscoelastic equation, such as the FENE-P model was developed by Leighton et al. (2003). In their approach, transport equations for the Reynolds and the polymer stresses were added to the mean flow equation and closures introduced to determine the unknown new correlations. Encouraging results were presented for the fully-developed flow in channel, but limited to the low drag reduction regime.

A low-Reynolds-number k-ε closure for FENE-P fluids was developed independently by Pinho et al. (2008), who relied on *a priori* analyses of DNS data. Even though the model was simpler and the Reynolds-averaged flow and conformation quantities were predicted well, the model was still limited to applications in the low DR regime (DR <20%). Subsequently, Resende et al. (2011) developed an alternative closure for the nonlinear turbulent term of the conformation tensor equation and improved the previous closures of Pinho et al. (2008) for the viscoelastic stress work and the viscoelastic turbulent transport of the turbulent kinetic energy (k).These modifications extended the turbulence model to intermediate DR levels and in this investigation the authors also showed the limitations of a simple k-ε approach to model the flow of viscoelastic fluids. In fact, since turbulence

anisotropy increases with DR, the inherent turbulence isotropy of the k-ε model leads to some conflicting variations. Hence, their model Resende et al. (2011) is not accurate in the high DR regime. Furthermore, the model has an excessive number of damping functions and coefficients, which makes it unattractive to use, but still in a significantly less number than in Leighton et al. (2003).

Iaccarino et al. (2010) developed a k-ε -$\overline{v^2}$ -f model for fully developed channel flow, which is capable of predictions over the whole range of DR. It is a fairly simple model, introducing the concept of turbulent polymer viscosity to account for the combined effects of turbulence and viscoelasticity on the polymer extra stress tensor term in the momentum equation. This turbulent polymer viscosity depends on the turbulent kinetic energy, the polymer relaxation time and the trace of the conformation tensor. Their closure of the nonlinear term in the conformation tensor equation relies on the turbulent dissipation rate.

An improved k-ε -$\overline{v^2}$ -f model for FENE-P fluids, developed later by Masoudian *et al.* (2013), is also valid up to the maximum DR and uses also the concept of turbulent polymer viscosity. It improved the prediction of the viscoelastic stress and the viscoelastic stress work, which are the main viscoelastic contributions in the momentum and the turbulent kinetic energy transport equations, respectively. Moreover, the model was tested and performed well over a wide range of rheological parameters and Reynolds numbers.

More recently, Tsukahara et al. (2013) also proposed a low-Reynolds-number k-ε model valid up to the maximum DR, but for viscoelastic fluids described by the Giesekus constitutive equation, which is used frequently to describe the rheology of surfactant solutions. In their model, an additional damping function was introduced into the closure of eddy viscosity, while the treatment of the turbulent kinetic energy (k) and its dissipation rate (ε) is an extension of the model for Newtonian fluids.

In the present study, a new turbulence model for FENE-P fluids has been developed for the full Reynolds stress model that relies on a small number of coefficients and is capable to predict the whole range of drag reduction. An important contribution is the development of new closures for the nonlinear fluctuating terms appearing in the FENE-P rheological constitutive equation, and for the polymer stress work terms in the Reynolds stress transport equations. The model is assessed against DNS data covering a wide range of flow conditions in terms of Weissenberg number, maximum polymer extensibility (L) and Reynolds number ($Re_{\tau 0}$), and is also compared with other closures developed previously for FENE-P fluids. It is worth mentioning that only two constant coefficients were added to the original Newtonian RSM model in order to account for the influence of polymer additives on the carrier flow.

The section is organized as follows: Section 5.2 introduces the instantaneous and time-averaged governing equations and identifies the viscoelastic terms requiring modeling. In Section 5.3, the turbulent closures are developed for the unknown terms introduced in the

previous section, then Section 5.4 presents results of predictions for fully developed turbulent channel flow over the whole range of DR and this is followed by the conclusions.

5.2. Governing equations

5.2.1 Continuity and momentum equations

The instantaneous equations for the conservation of mass and momentum transport, appropriate for incompressible flow of FENE-P fluids are:

$$\frac{\partial \hat{u}_i}{\partial x_i} = 0 \tag{5.1}$$

$$\rho \frac{\partial \hat{u}_i}{\partial t} + \rho \hat{u}_k \frac{\partial \hat{u}_i}{\partial x_k} = -\frac{\partial \hat{p}}{\partial x_i} + \frac{\partial \hat{\tau}_{ik}}{\partial x_k} \tag{5.2}$$

where $\hat{\tau}_{ik}$ is the instantaneous stress tensor, $\hat{u}_i$ is the instantaneous velocity vector, $\hat{p}$ is the instantaneous pressure, and ρ is the fluid density. The stress tensor $\hat{\tau}_{ik}$ describes the rheology of the fluid and is given in eq. (5.3) as the sum of a Newtonian solvent contribution of viscosity η_s with a polymeric contribution $\hat{\tau}_{ij,p}$ described by the FENE-P rheological constitutive model:

$$\hat{\tau}_{ij} = 2\eta_s \hat{s}_{ij} + \hat{\tau}_{ij,p} \tag{5.3}$$

where $\hat{s}_{ij}$ is the instantaneous rate of strain tensor defined as $\hat{s}_{ij} = \frac{1}{2}\left(\frac{\partial \hat{u}_i}{\partial x_j} + \frac{\partial \hat{u}_j}{\partial x_i} \right)$.

5.2.2 Constitutive equation

The instantaneous polymeric contribution to the instantaneous total extra stress is given as an explicit function of the instantaneous conformation tensor $\hat{c}_{ij}$:

$$\hat{\tau}_{ij,p} = \frac{\eta_p}{\lambda}\left[f(\hat{c}_{kk})\hat{c}_{ij} - f(L)\delta_{ij} \right] \tag{5.4}$$

$$\text{with } f(\hat{c}_{kk}) = \frac{L^2 - 3}{L^2 - \hat{c}_{kk}} \text{ and } f(L) = 1 \tag{5.5}$$

where $f(\hat{c}_{kk})$ is the Peterlin function, and η_p, λ and L are the rheological parameters. Specifically, they are the polymer viscosity, the relaxation time, and the maximum extension of the dumbbells, respectively. The required instantaneous conformation tensor obeys a hyperbolic differential equation of the form:

$$\left(\frac{\partial \hat{c}_{ij}}{\partial t} + \hat{u}_k \frac{\partial \hat{c}_{ij}}{\partial x_k} - \hat{c}_{jk} \frac{\partial \hat{u}_i}{\partial x_k} - \hat{c}_{ik} \frac{\partial \hat{u}_j}{\partial x_k} \right) = -\frac{\hat{\tau}_{ij,p}}{\eta_p} \tag{5.6}$$

The terms within the parenthesis in Eq. (5.6) define Oldroyd's upper convective derivative of the instantaneous conformation tensor. The first two terms represent the local and

advective derivatives, which together form the material derivative, and the remaining two terms account for the distortion of c_{ij} by the flow.

Table 5.1. Summary of the physical and computational parameters for the DNS cases used in this work.

case	$Re_{\tau 0}$	Domain size $L_x \times L_y \times L_z$	Grid n_x, n_y, n_z	L^2	$Wi_{\tau 0}$	Wi_h	β
DNS0	180	$6.283h \times 2h \times 3.141h$	$128 \times 129 \times 128$	0	0	0	0
DNS1	395	$14.136h \times 2h \times 4.5h$	$384 \times 257 \times 192$	0	0	0	0
DNS2	590	$14.136h \times 2h \times 4.5h$	$512 \times 257 \times 256$	0	0	0	0
DNS3	180	$6.944h \times 2h \times 4.19h$	$128 \times 129 \times 128$	900	25	0.139	0.9
DNS4	180	$6.944h \times 2h \times 4.19h$	$128 \times 129 \times 128$	3600	100	0.55	0.9
DNS5	395	$14.136h \times 2h \times 4.5h$	$512 \times 129 \times 192$	900	25	0.063	0.9
DNS6	395	$14.136h \times 2h \times 4.5h$	$384 \times 257 \times 192$	900	75	0.19	0.9
DNS7	395	$14.136h \times 2h \times 4.5h$	$384 \times 257 \times 192$	3600	75	0.19	0.9
DNS8	395	$14.136h \times 2h \times 4.5h$	$384 \times 257 \times 192$	14400	75	0.19	0.9
DNS9	395	$14.136h \times 2h \times 4.5h$	$384 \times 257 \times 192$	3600	100	0.25	0.9
DNS10	395	$14.136h \times 2h \times 4.5h$	$384 \times 257 \times 192$	3600	50	0.125	0.9
DNS11	590	$25.136h \times 2h \times 4.5h$	$512 \times 257 \times 256$	3600	50	0.085	0.9
DNS12	590	$25.136h \times 2h \times 4.5h$	$512 \times 257 \times 256$	10000	100	0.17	0.9

5.2.3. DNS cases

In this study we investigate fully developed channel flow of FENE-P fluids over a wide range of conditions as described in Table (5.1), which lists the DNS data sets. The Reynolds number is defined as $Re_{\tau 0} \equiv hU_\tau/\nu_0$ where U_τ is the friction velocity, h is the channel half-height and ν_0 is the zero shear-rate kinematic viscosity of the solution, i.e., the sum of the kinematic viscosities of the solvent and polymer $\nu_0 = \nu_p + \nu_s$. The Weissenberg number based on the wall friction velocity is defined as $Wi_{\tau 0} \equiv \lambda U_\tau{}^2/\upsilon_0$ and a second

Weissenberg number based on the channel half height (h) is $Wi_h \equiv \frac{Wi_{\tau 0}}{Re_{\tau 0}} = \lambda U_\tau / h$.Another relevant independent dimensionless quantity is β, the ratio between the solvent viscosity and the zero shear-rate kinematic viscosity of the solution, ($\beta \equiv \nu_s/\nu_0$). In this work, as in Sureshkumar et al. (1997), and Thais et al. (2013), a numerical diffusivity term $D\nabla^2 c$ was added to the FENE-P constitutive equation in order to perform stable numerical integration of the evolution equation for the conformation tensor, where D is a dimensionless number (equivalent to the inverse of a Schmidt number) defined as $D= \kappa/hU_\tau$, with κ denoting a constant isotropic artificial numerical diffusivity. The diffusivity is chosen in a way that it is large enough for the calculations to ensure the numerical stability of the calculations and the realizability of the conformation tensor values, while small enough that it does not affect the computational results. This follows on the steps of Sureshkumar et al. (1997) and the normalized artificial numerical diffusivity D was taken to be of $O(10^{-2})$ resulting in a numerical Schmidt number $Sc^+=1/Re_{\tau 0}D$ of the order $O(10^{-1})$.

Periodic boundary conditions were applied along the streamwise and spanwise directions. The channel size was chosen to adequately capture the streaky structures and the elongated vortical structures developed in the flow. In the two periodic directions, *x and z*, Fourier representations were used, whereas in the non-homogeneous shear direction a Chebyshev approximation was employed. As shown above, the flow and polymer stress fields can be fully characterized by dimensionless groups, namely, Re_τ, β, L^2 and Wi_h (or $Wi_{\tau 0}$). Further details of the numerical approaches used in this work can be found in Li et al. (2006). Table 5.1 summarizes the computational parameters for the simulations performed. For the sake of comparison profiles of the streamwise mean velocity and corresponding root mean square of the velocity fluctuations extracted from DNS are plotted in Figure 5.1 in wall coordinates for the low and high drag reduction cases, sets DNS3 and DNS4 in table 5.1,

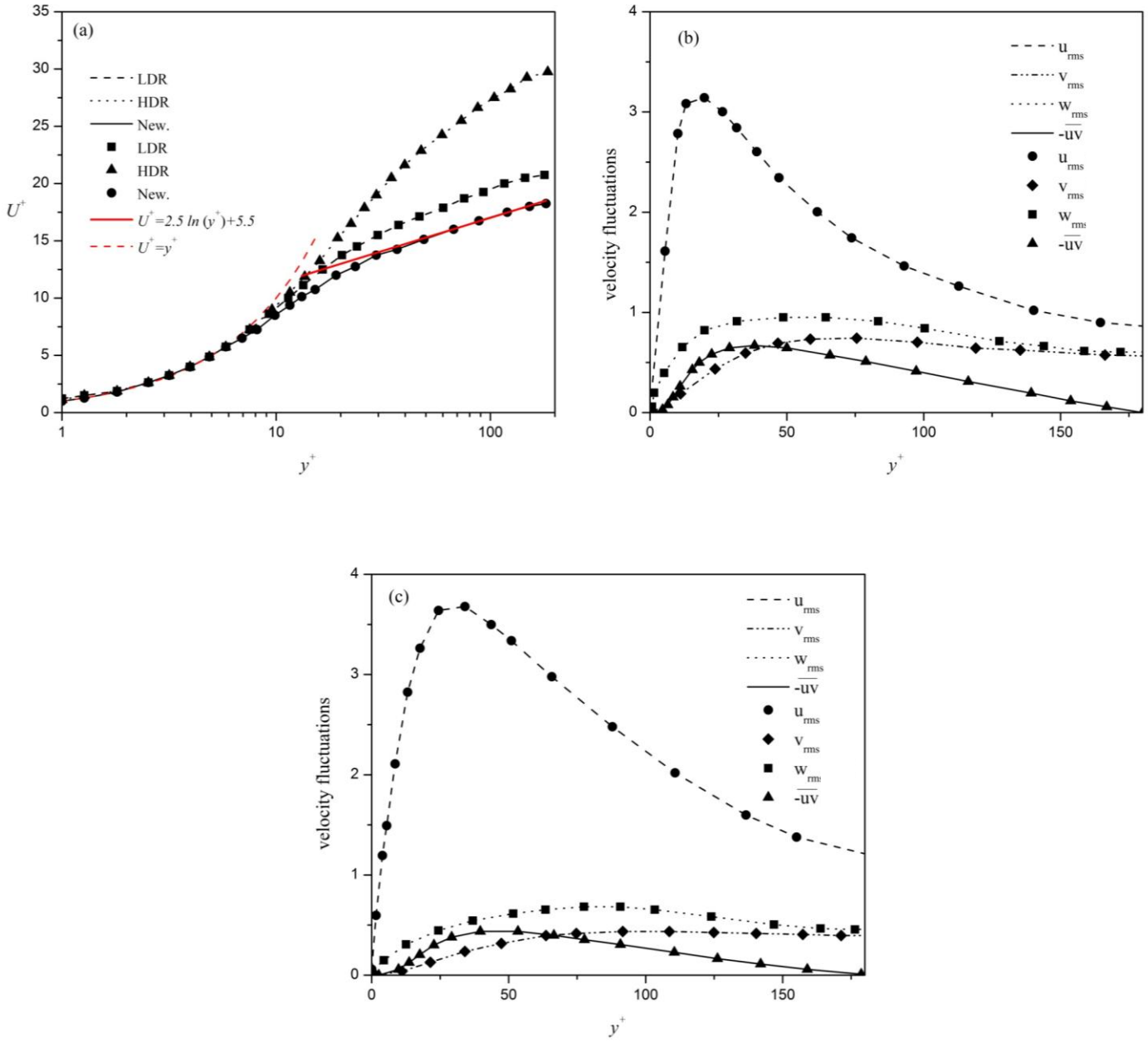

Figure 5.1. Comparison of current DNS results for LDR and HDR (cases DNS3, and DNS4 table 1) with DNS results of Li et al. (2006) (symbols), (a) Mean streamwise velocity profiles, (b) rms of velocity fluctuations and Reynolds stress for LDR case, (c) rms of velocity fluctuations and Reynolds stress for HDR case.

and compared with DNS data from Li et al. (2006) and, as it can be seen, there is excellent agreement. Note that, as demonstrated in Li et al. (2006), for low drag reduction the

temporal averaging is performed over 10-15 computational units (h/U_τ), whereas for high drag reduction to obtain good statistics averaging is over 30–50 h/U_τ due to the significant variations in *xz* plane. Although this approach ensures the time averaged statistics to remain stationary, an uncertainty analysis can be performed in future to assess the DNS data of turbulent polymer dilute solution as was carried out recently to analyze DNS of Newtonian channel flow by Olivier et al. (2014).

5.2.4 Reynolds-Averaged equations

In Reynolds-averaged methods the instantaneous quantities are decomposed into the sum of a mean value and a fluctuating value as in $\hat{u}_i = U_i + u_i$, $\hat{p} = P + p$, and $\hat{c}_{ij} = C_{ij} + c_{ij}$, where upper-case letters or overbars denote Reynolds-averaged quantities and lower-case letters or primes denote fluctuating quantities. A hat denotes an instantaneous quantity. The Reynolds-averaged equations appropriate for incompressible flow of FENE-P fluids are the continuity equation:

$$\frac{\partial U_i}{\partial x_i} = 0 \tag{5.7}$$

and the momentum equation

$$\rho \frac{\partial U_i}{\partial t} + \rho U_k \frac{\partial U_i}{\partial x_k} = -\frac{\partial \overline{P}}{\partial x_i} + \rho \frac{\partial}{\partial x_k}(-\overline{u_i u_k}) + \frac{\partial \bar{\tau}_{ik}}{\partial x_k} \tag{5.8}$$

where $\bar{\tau}_{ik}$ is the Reynolds-averaged stress tensor, U_i is the mean velocity, P is the mean pressure, $-\overline{u_i u_k}$ is the Reynolds stress tensor, and $\bar{\tau}_{ik}$ is the Reynolds averaged fluid extra stress tensor. In the Reynolds-averaged Navier-Stokes (RANS) equation (Eq. 5.8) the Reynolds stress tensor ($-\overline{u_i u_k}$) is unknown, and needs a closure. The full RSM turbulence model is used to determine the Reynolds stresses. An exact transport equation for the Reynolds stresses can be derived from the Navier-Stokes equation for FENE-P fluids. It is emphasized that this equation is exact or rather as exact as the Navier-Stokes equations. The Reynolds stress transport equation appropriate for FENE-P fluids can be written as:

$$\frac{\partial \overline{u_i u_j}}{\partial t} + U_k \frac{\partial \overline{u_i u_j}}{\partial x_k} = \underbrace{\left(-\overline{u_i u_k} \frac{\partial U_j}{\partial x_k} - \overline{u_j u_k} \frac{\partial U_i}{\partial x_k} \right)}_{P_{ij}} + \underbrace{\frac{\partial}{\partial x_k}\left(\nu \frac{\partial \overline{u_i u_j}}{\partial x_k} \right)}_{D_{ij,\nu}} \underbrace{- \frac{\partial}{\partial x_k}\left(\overline{u_i u_j u_k} + \overline{\frac{p}{\rho}\left(\delta_{jk} u_i + \delta_{ik} u_j \right)} \right)}_{D_{ij,t}}$$
$$\underbrace{-2\nu \overline{\frac{\partial u_i}{\partial x_k} \frac{\partial u_j}{\partial x_k}}}_{\varepsilon_{ij}} + \underbrace{\overline{\frac{p}{\rho}\left(\frac{\partial u_i}{\partial x_j} + \frac{\partial u_j}{\partial x_i} \right)}}_{\Pi_{ij}} + \underbrace{\frac{\partial}{\partial x_k}\left(\overline{u_i \tau_{jk,p} + u_j \tau_{ik,p}} \right)}_{D_{ij,p}} \underbrace{- \overline{\left(\tau_{ik,p} \frac{\partial u_j}{\partial x_k} + \tau_{jk,p} \frac{\partial u_i}{\partial x_k} \right)}}_{\varepsilon_{ij,p}} \tag{5.9}$$

Except for the last two terms on the right-hand-side, which involve the fluctuating polymer stresses, the other terms are classical terms appearing in the corresponding equation for Newtonian fluids and represent the turbulence production by the mean strain (P_{ij}), molecular diffusion ($D_{ij,\nu}$), turbulent transport ($D_{ij,t}$), viscous dissipation by the solvent (ε_{ij}) and the pressure–strain term ($\Pi_{ij,\nu}$). The last two terms on the right-hand-side are viscoelastic terms representing the viscoelastic turbulent transport ($D_{ij,p}$) and the viscoelastic stress work ($\varepsilon_{ij,p}$). In order to have an idea about the magnitude of the different terms in the Reynolds stress transport equation, the budgets of Eq. (5.9) for all components of the Reynolds stress tensor are plotted in Figure 5.2 for the data set DNS5. These data are presented in dimensionless form utilizing all turbulent scales and in order to normalize data the quantities υ / U_τ and υ / U_τ^2 are used as the length and time scales, respectively.

As it can be seen in Figure 5.2(a) the viscoelastic stress work is negative all across the channel meaning that it behaves as a sink in the transport of the streamwise Reynolds stress. Figure 5.2(a) also shows that although the viscoelastic stress work is small close to the wall, when compared with the other terms, far from the wall it has the same magnitude as the production and the solvent dissipation terms. Moreover, Figure 5.2(a) shows that the viscoelastic turbulent transport has a small magnitude near the wall, and it is almost zero away from the wall. Budgets of Reynolds stress terms in the wall-normal and spanwise directions are plotted in Figs. 5.2(b) and (c), respectively. As expected the pressure strain

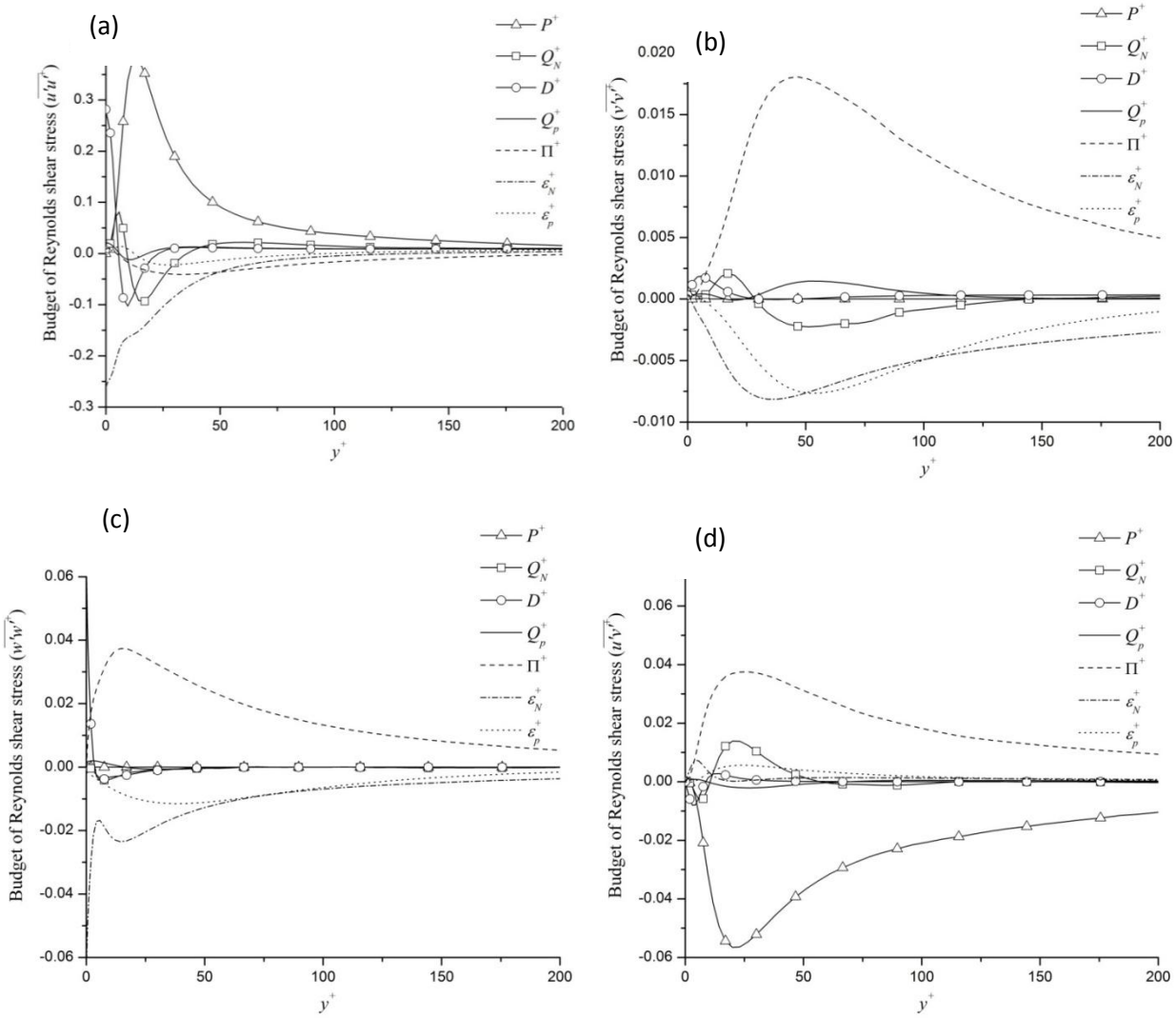

Figure 5.2. Budgets of components of Reynolds stress transport equation for the flow of FENE-P fluids for case DNS5 ($Re_{\tau 0}$= 395, $Wi_{\tau 0}$= 25 and L^2 = 900), a) $\overline{u'u'}$, b) $\overline{v'v'}$, c) $\overline{w'w'}$, d) $\overline{u'v'}$

term is the most important positive term in these directions, where it plays a pseudo-production role in its quantification of the transfer of energy from the streamwise direction. Viscoelastic stress work, on the other hand, is negative and behaves as a sink of energy, as in the streamwise direction. The figure also shows that for the $\overline{v'v'}$and $\overline{w'w'}$ components the viscoelastic stress work has the same magnitude as the pressure strain and the viscous dissipation terms all across the channel. Moreover, as in the streamwise direction, the viscoelastic turbulent transport is very small and active only close to the wall. Figure 5.2(d) shows the budget of the Reynolds shear stress (*xy* component) and, as expected, the viscoelastic stress work, the viscous dissipation by the solvent, and the pressure strain terms all have the same sign all across the channel. Moreover, the viscoelastic stress work has the

same intensity as the viscous dissipation by the solvent, whereas the viscoelastic turbulent transport is negligible as was the case previously for the normal components.

The Reynolds-averaged total extra stress tensor $\bar{\tau}_{ij}$ can be calculated by Reynolds averaging Eq. (5.3) leading to

$$\bar{\tau}_{ij} = 2\eta_s S_{ij} + \bar{\tau}_{ij,p} \tag{5.10}$$

where S_{ij} is the mean rate of strain tensor. Then, by Reynolds-averaging Eq. (5.4), the Reynolds-averaged polymer stress $\bar{\tau}_{ij,p}$ is given by:

$$\bar{\tau}_{ij,p} = \frac{\eta_p}{\lambda}\left[f(C_{kk})C_{ij} - f(L)\delta_{ij} \right] + \frac{\eta_p}{\lambda}\left[\overline{f(C_{kk}+c_{kk})(C_{ij}+c_{ij})} - f(C_{kk})C_{ij} \right] \tag{5.11}$$

Eq. (5.11) depends on the time-averaged form of the conformation tensor, which must be determined from the corresponding time averaged evolution equation, given as:

$$\overset{\nabla}{C}_{ij} + \overline{u_k \frac{\partial c_{ij}}{\partial x_k}} = \left(\overline{c_{jk}\frac{\partial u_i}{\partial x_k}} + \overline{c_{ik}\frac{\partial u_j}{\partial x_k}} \right) - \frac{\bar{\tau}_{ij,p}}{\eta_p} \tag{5.12}$$

After substitution of Eq. (5.11), and expanding $\overset{\nabla}{C}_{ij}$, Eq. (5.12) becomes:

$$\left(U_k \frac{\partial C_{ij}}{\partial x_k} - \underbrace{\left(C_{jk}\frac{\partial U_i}{\partial x_k} + C_{ik}\frac{\partial U_j}{\partial x_k} \right)}_{M_{ij}} \right) + \left(\underbrace{\left(\overline{u_k \frac{\partial c_{ij}}{\partial x_k}} \right)}_{CT_{ij}} - \underbrace{\left(\overline{c_{jk}\frac{\partial u_i}{\partial x_k}} + \overline{c_{ik}\frac{\partial u_j}{\partial x_k}} \right)}_{NLT_{ij}} \right) = \tag{5.13}$$

$$-\frac{1}{\lambda}\left[f(C_{kk})C_{ij} - f(L)\delta_{ij} \right] - \frac{1}{\lambda}\left[\overline{f(C_{kk}+c_{kk})(C_{ij}+c_{ij})} - f(C_{kk})C_{ij} \right]$$

On the left-hand-side of Eq. (5.13), the mean flow advective term vanishes for fully developed channel flow. The mean flow distortion term of $\overset{\nabla}{C}_{ij}$ is M_{ij} and the remaining two terms on the left-had-side of Eq. (5.13) correlate fluctuating velocities and conformation tensor components. Term CT_{ij} represents the contribution of the fluctuating velocity field to the advective transport of the mean conformation tensor. The interaction between the fluctuating components of the conformation tensor and of the velocity gradient tensor,

originating from the Oldroyd derivative, is denoted by NLT_{ij} and is the fluctuating counterpart of M_{ij}. In the Reynolds-averaged constitutive equation (Eq. 5.13) the mean flow distortion term (M_{ij}) needs no closure. The advective transport of the conformation tensor (CT_{ij}) and the fluctuating polymer stretching terms (NLT_{ij}), which account for the fluctuating counterpart of M_{ij} are both non-linear and developing closures for them will be one of the main tasks of this work. Finally, a closure is also needed for the last term on the right-hand-side of Eq. (5.13).

To ascertain the contributions of different terms in Eq. (5.13), the components of the M_{ij}, NLT_{ij}, and CT_{ij} tensors are plotted in Figure 5.3 in all directions. As expected, the mean flow distortion term of $\overset{\nabla}{C}_{ij}$, M_{ij}, is the most important term close to the wall in the evolution equation for the transport of C_{xx}, then it decays with wall distance, whereas NLT_{xx} increases from zero at the wall and becomes the main contributor in the buffer layer. It is clear from Figure 5.3(a) that in the log-law region both M_{xx} and NLT_{xx} have similar magnitudes. In contrast CT_{xx} is very small in comparison with both M_{xx}, and NLT_{xx} all across the channel. For the shear component shown in Figure 5.3(b), the shape of the curves is somewhat different, but again the main contributions come from NLT_{xy}, and M_{xy}. Likewise the streamwise direction, CT_{xy} is negligible. For the remaining two normal directions, as shown in Figs. 5.3(c) and (d) the mean flow distortion term is null, hence NLT_{yy}, and NLT_{zz} provide the main contribution for the y and z component equations, respectively. In contrast, both CT_{yy} and CT_{zz} are again small and negligible for each of the corresponding balances. The obvious conclusion is that a closure must be developed for NLT_{ij}, but CT_{ij} can simply be ignored. Note that, this simplification investigated for all the cases described in table (5.1) to ensure that CT_{ij} has negligible magnitude regardless of the flow and rheological parameters. It was found that for all DNS cases CT_{ij} is less than 5% of the main contributors i.e., NLT_{ij}, and M_{ij}. For the sake of comparison this term plotted along with NLT_{ij} and M_{ij} terms for the high drag reduction case (DNS9) in figure 5.4 confirming that this assumption is correct. it is worth mentioning that a similar conclusion had already been reached in Masoudian et al. (2013) in the context of k-ε-$\overline{v^2}$-f.

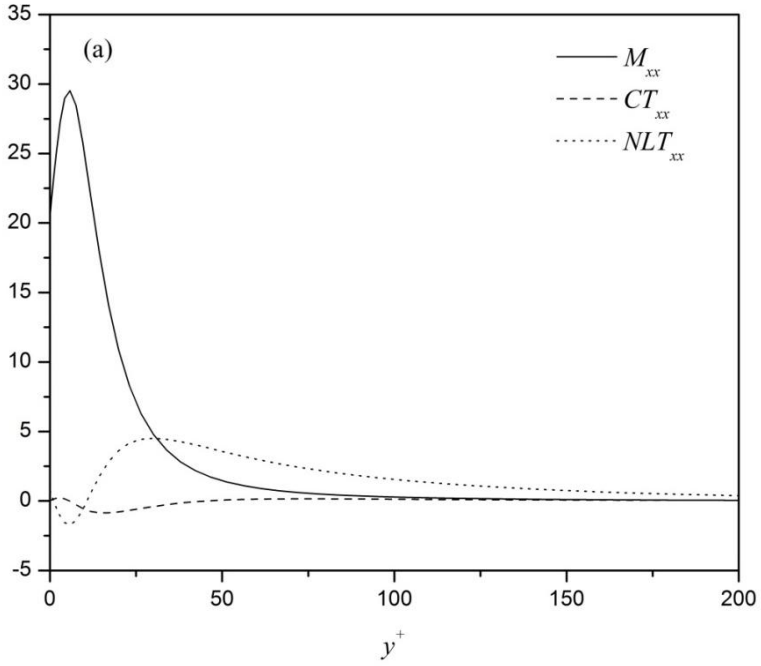
(a)
M_{xx}
CT_{xx}
NLT_{xx}
35
30
25
20
15
10
5
0
-5
0
50
100
150
200
y^+

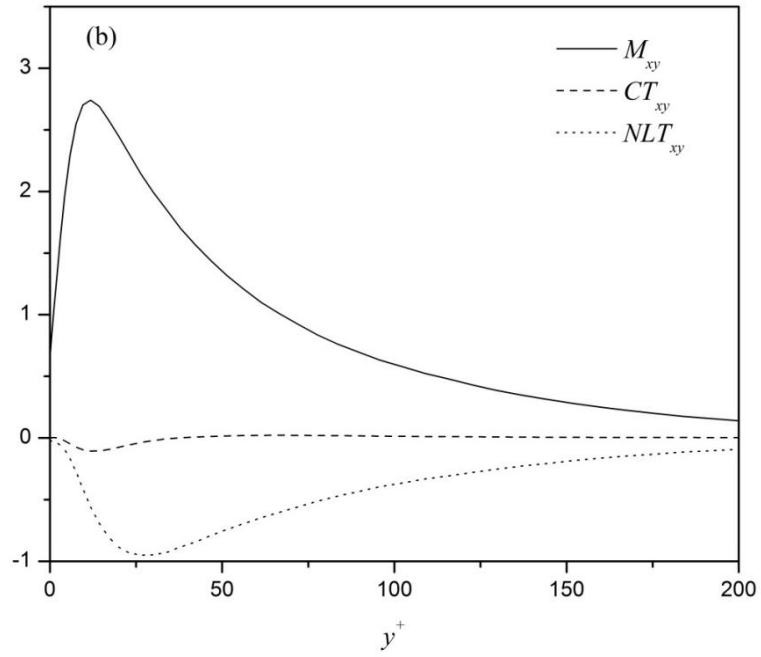
(b)
M_{xy}
CT_{xy}
NLT_{xy}
3
2
1
0
-1
0
50
100
150
200
y^+

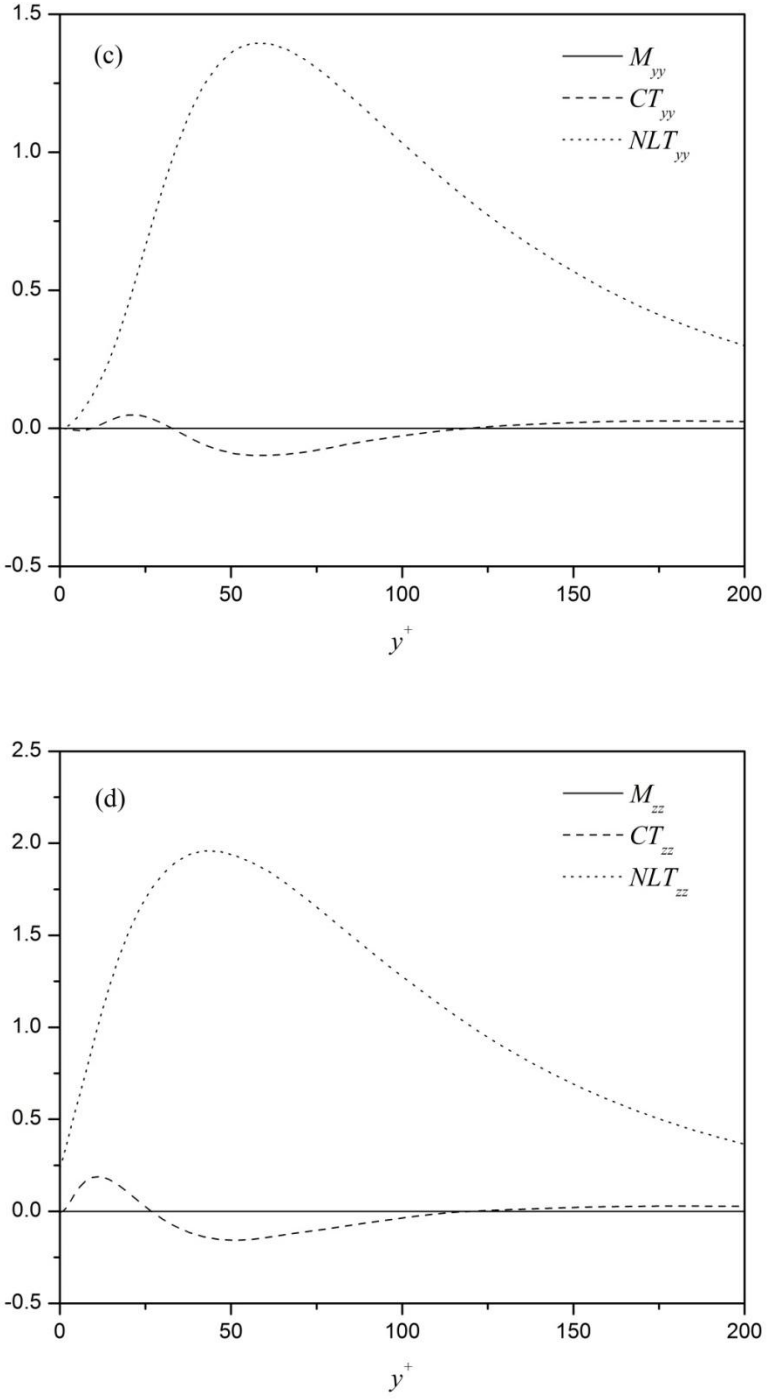

Figure 5.3. Variation across the channel of components M_{ij}, NLT_{ij}, and CT_{ij} for case DNS5, $Re_{\tau 0}$= 395, $Wi_{\tau 0}$= 25 and L^2 = 900 , a) *xx*-component, b) *xy*- component, c) *yy*- component, d) *zz*-component

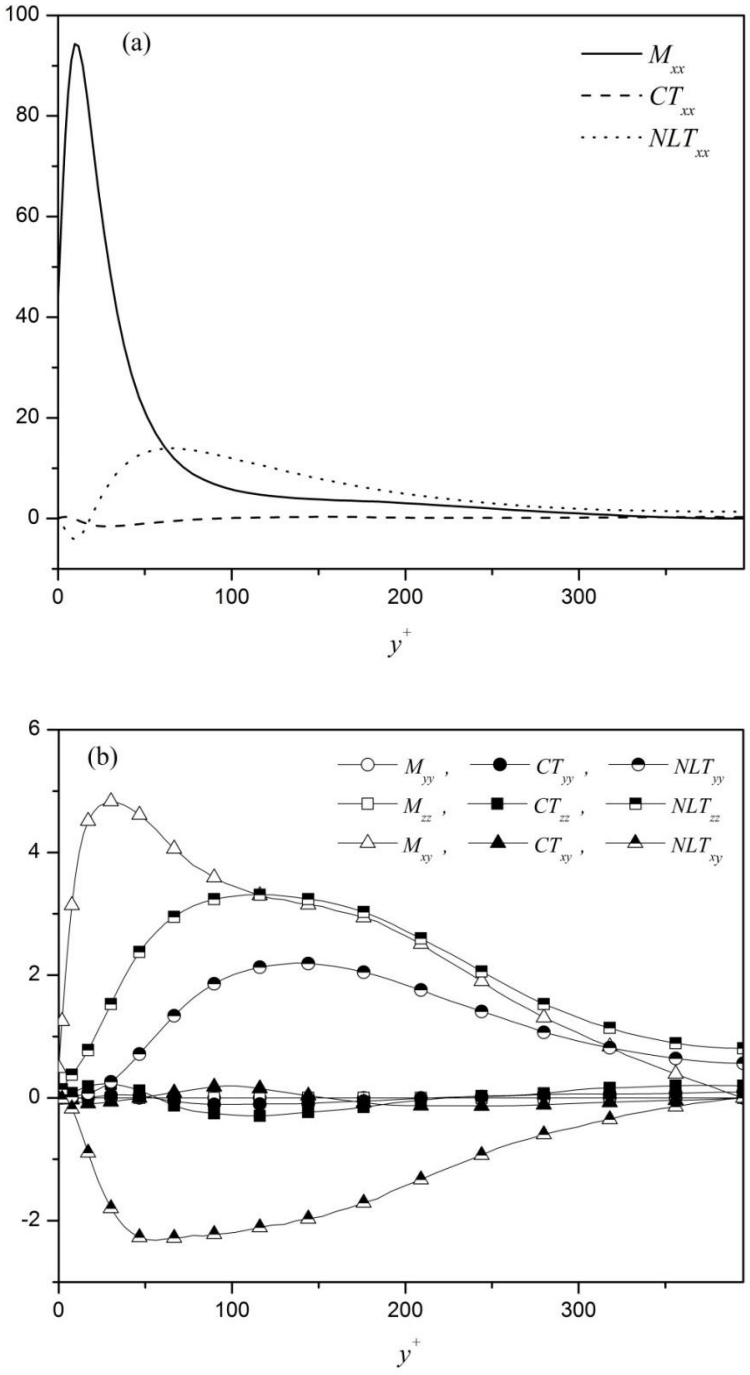

Figure 5.4. Variation across the channel of components M_{ij}, NLT_{ij}, and CT_{ij} for high drag reduction case DNS9, $Re_{\tau 0}$= 395, $Wi_{\tau 0}$= 100 and L^2 = 3600, a) *xx*-component, b) *xy*, *yy*, *zz*- components

5.3. Development of closures

In this section closures are developed for all non-negligible unknown turbulent cross-correlations in the various governing equations. The terms requiring closures in the time-averaged constitutive equation are the second term on the right-hand-side of the time-averaged polymer stress (Eq. 5.11), and the cross-correlation between the fluctuating components of the conformation tensor and of the velocity gradient tensor, $NLT_{ij} = \overline{c_{jk}\,\partial u_i/\partial x_k} + \overline{c_{ik}\,\partial u_j/\partial x_k}$. In addition, closures must be developed for the nonlinear viscoelastic terms appearing in the transport equation for the Reynolds-averaged stress tensor, the last two terms on the left hand side of Eq. (5.9), namely the viscoelastic turbulent transport ($D_{ij,p}$) and the viscoelastic stress work ($\varepsilon_{ij,p}$).

5.3.1 A model for the constitutive equation

As described in the previous section the first term that needs to be calculated is the time-averaged polymer stress, Eq. (5.11). In this work $\bar{\tau}_{ij,p}$ is approximated as the first term on the right hand side of Eq. (5.11), i.e., the second term is neglected, because both terms on the right-hand-side of Eq. (5.11) were compared in Masoudian et al. (2013), and Iaccarino et al. (2010) by using *a priori* DNS data at different values of $Wi_{\tau 0}$ and L^2, and it was shown that the first exact term is nearly 20 times larger than the second term regardless of the amount of drag reduction. Consequently by using this assumption the Reynolds-averaged polymer stress will be calculated by using only the first term as:

$$\bar{\tau}_{ij,p} = \frac{\eta_p}{\lambda}\left[f(C_{kk})C_{ij} - f(L)\delta_{ij} \right] \tag{5.14}$$

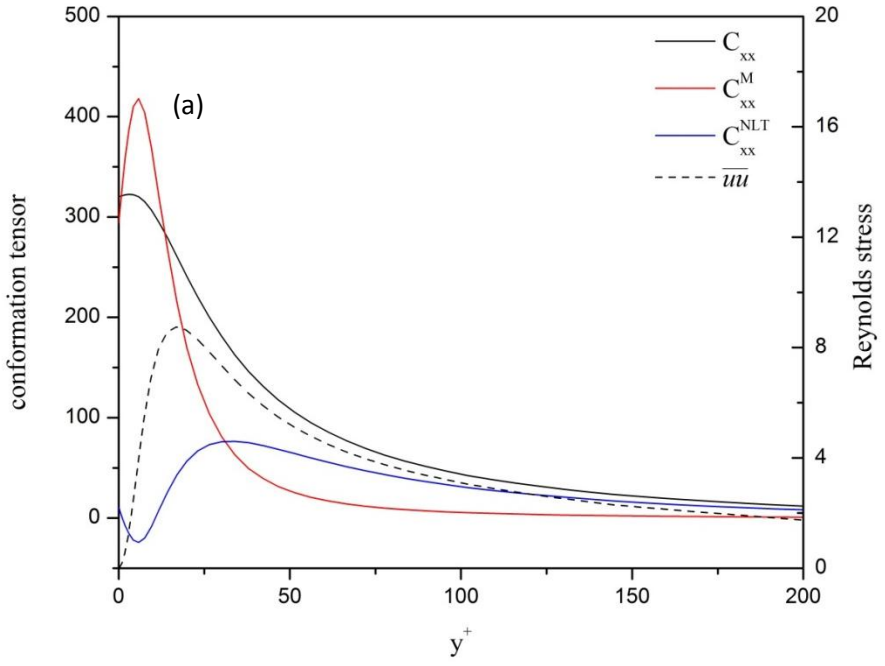
(a)
C_{xx}
C_{xx}^{M}
C_{xx}^{NLT}
$\overline{uu}$
conformation tensor
Reynolds stress
y^+
0
50
100
150
200
0
100
200
300
400
500
0
4
8
12
16
20

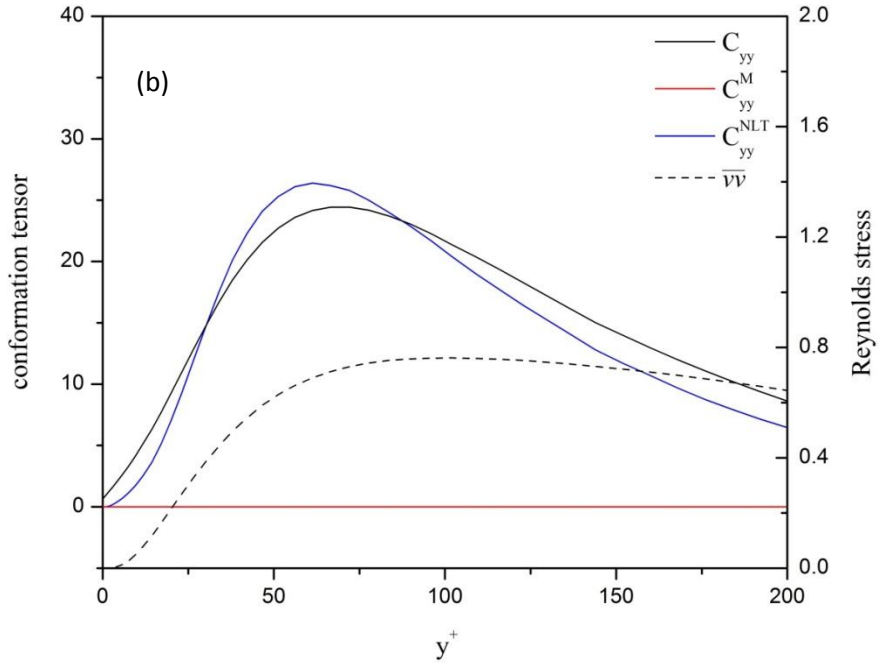
(b)
C_{yy}
C_{yy}^{M}
C_{yy}^{NLT}
$\overline{vv}$
conformation tensor
Reynolds stress
y^+
0
50
100
150
200
0
10
20
30
40
0.0
0.4
0.8
1.2
1.6
2.0

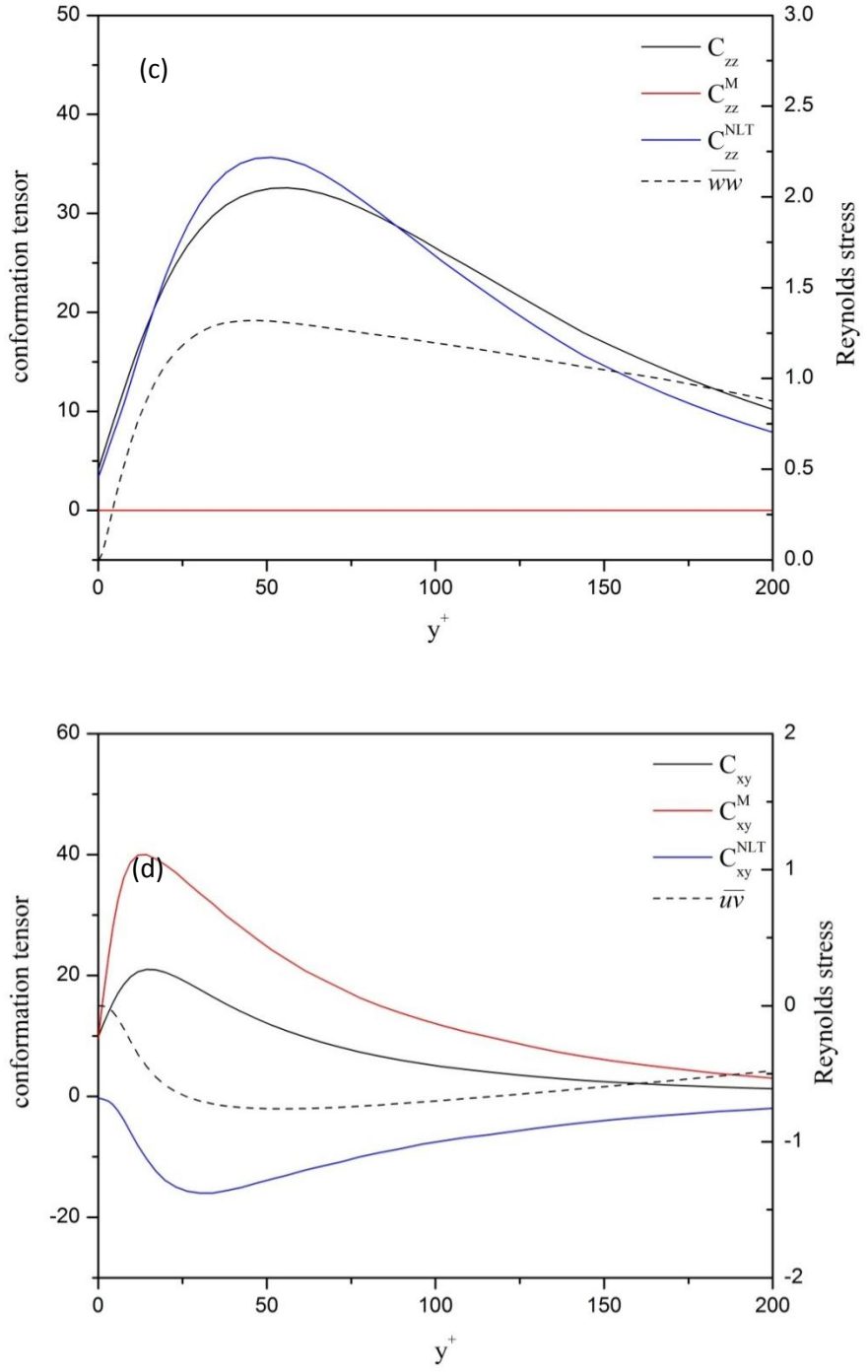

Figure 5.5. Profiles of C_{ij}, C_{ij}^{M}, C_{ij}^{NLT}, and $\overline{u'_i u'_j}$ for case DNS5, $Re_{\tau 0}$= 395, $Wi_{\tau 0}$= 25 and L^2 = 900, a) *xx* -component, b) *yy* - component, c) *zz*- component, d) *xy* - component

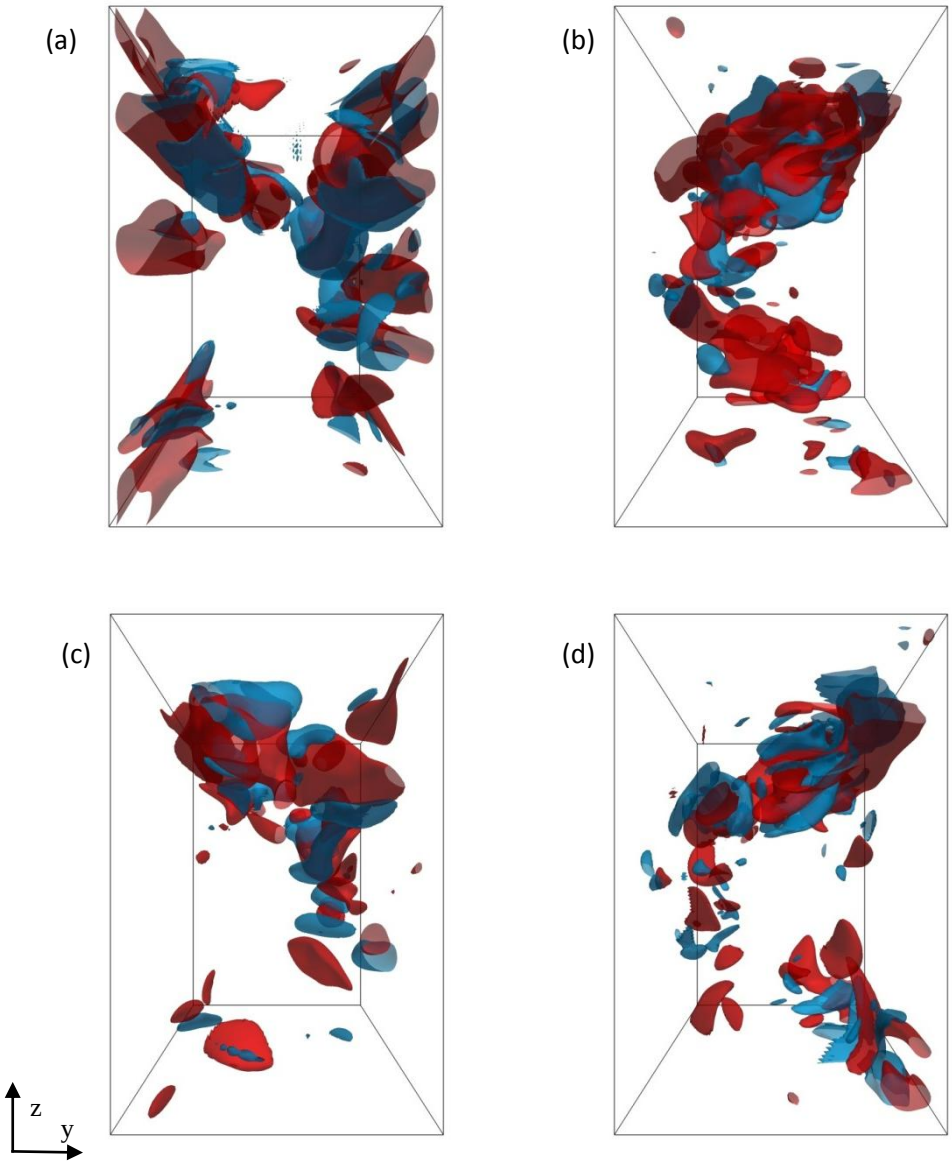

Figure 5.6. Visualizations of iso-surfaces of instantaneous fields of the "Reynolds stress" (u_iu_j) components (Red) and $N\hat{L}T_{ij}$ components (Blue) using DNS3 case. Figures show *y*-*z* plane, and iso-surfaces were made transparent (70% opacity) to help visualizations. The threshold for all quantities is 10% of the maximum value of each quantity. a) $N\hat{L}T_{xx}$, u_xu_x, b) $N\hat{L}T_{yy}$, u_yu_y, c) $N\hat{L}T_{zz}$, u_zu_z , d) $N\hat{L}T_{xy}$, u_xu_y

As described in the previous section, NLT_{ij} plays an important role in the Reynolds-averaged conformation tensor equation, and its closure constitutes a major task in this work. Apart from NLT_{ij}, the other main contribution to the Reynolds-averaged conformation tensor equation comes from the exact mean flow term (M_{ij}), especially close

to the wall. In the context of k-ε-$\overline{v^2}$-f models Iaccarino et al. (2010) and Masoudian et al. (2013) proposed closures for the trace of NLT_{ij}, but since in this work a full RSM model is being developed all components of NLT_{ij} need closure.

Using the DNS data all components of the mean polymer conformation tensor, C_{ij}, are plotted in the various parts of Figure 5.5. In addition, the polymer conformation that would result only from the mean flow distortion term (M_{ij}) is calculated and plotted in Figure 5.5 as C_{ij}^{M}. This is equivalent to considering Eq. 5.13 as if M_{ij} was the single existing term and NLT_{ij} was zero. Due to the elimination of CT_{ij} from Eq. 5.13, because of its negligible magnitude for all components, the difference between those two quantities, $C_{ij}^{NLT} = C_{ij} - C_{ij}^{M}$, corresponds to the effect of NLT_{ij} upon polymer elongation and orientation, which we refer to as the turbulent polymer conformation difference. Figure 5.5 shows that the turbulent polymer conformation difference exhibits qualitatively a very similar behavior to the time-averaged Reynolds stress components in terms of peak location, overall sign and shape (note the different ordinate axis). The correlation between NLT_{kk} term and the turbulent kinetic energy was introduced by Iaccarino et al. (2010) in the context of k-ε-$\overline{v^2}$-f, and here we are adapting and generalizing the same concept to the RS model by introducing a direct relation between NLT_{ij} and the Reynolds stress tensor.

In order to have an idea about instantaneous fields, iso-surfaces of instantaneous "Reynolds stress" components and instantaneous NLT_{ij} components are plotted for case DNS3 in Figure 5.6. It is interesting to note that instantaneous $\hat{NLT}_{ij}$ and $u_i u_j$ events usually occur in close proximity to each other, and as it can be seen the $\hat{NLT}_{ij}$ events being generally surrounded by a region of significant $u_i u_j$ events. In physical terms the polymer elongation and orientation due to the NLT_{ij} contribution represents the ability of the turbulent fluctuations to act on the polymer chains. In summary, the DNS data analysis of all cases described in Table 5.1 shows a direct relation between the components of the averaged Reynolds stress tensor and the NLT_{ij} tensor on a component to component basis, both near and far from the wall, i.e. $NLT_{ij} \propto \overline{u_i u_j}$. Moreover the stretching of the polymers can be effective only if the turbulent time scale is short enough with respect to the relaxation time, therefore the ratio of the polymer relaxation time, λ, to the turbulent time scale, $T_t = k/\varepsilon$, must be added to the closure.

Furthermore, analyzing the current DNS data sets together with the independent DNS results of Thais et al. (2013) at different Reynolds numbers shows that NLT_{ij} has a direct relation with the polymer maximum extension. Hence, the quantity $Wi_h \sqrt{L} \big/ \left(\upsilon_p f(C_{kk}) \right)$ and the coefficient a_1 were added to the closure of NLT_{ij} after running an optimization algorithm

to quantify the coefficient for optimum model performance. The final form of the closure for NLT_{ij} is:

$$NLT_{ij} = a_1 \frac{\lambda}{\upsilon_p} \frac{\varepsilon}{k} \frac{Wi_h \sqrt{L}}{f(C_{kk})} \overline{u_i u_j} \tag{5.15}$$

Note that the product $\lambda \overline{u_i u_j}$ in Eq. 5.15 has the dimensions of a diffusivity and can be interpreted as a turbulent viscoelastic viscosity, $\upsilon_{T,p}$. Conceptually, this is in agreement with the previous closures developed in Iaccarino et al. (2010), and Masoudian et al. (2013) for NLT_{kk} in the context of $k-\varepsilon-v^2-f$ turbulence models.

5.3.2 Closures required for the Reynolds stress transport equation

In this work we use the Reynolds stress (RS) model developed by Lai et al. (1990) for Newtonian fluids as the base model to develop the modified RS model for FENE-P fluids. The terms on the left-hand side of the exact Reynolds stress transport equation (Eq. 5.9) concern the time variation, and the advection of the Reynolds stress. These are exact terms that do not require modeling. The first two terms on the right-hand-side of Eq. (5.9), representing the production and the molecular diffusion of the Reynolds stress, are also exact are do not require a closure, whereas the remaining terms need to be modeled. Except for the last two terms, which are the viscoelastic contributions, all other terms in the Reynolds stress transport equation are identical to those in the corresponding equation for Newtonian fluids. The first term that needs closure is the turbulent transport ($D_{ij,t}$), consisting of the turbulent diffusion by velocity fluctuations and the turbulent diffusion by pressure fluctuations. Usually the turbulent diffusion by pressure is neglected at high Reynolds number flows or incorporated as part of the turbulent diffusion by velocity fluctuations Lai et al. (1990). In the budget of the Reynolds stress equation for FENE-P fluids the turbulent diffusion is small and behaves similarly to the corresponding term for Newtonian fluids, consequently in this work we use the Newtonian closure of Lai et al. (1990) to model turbulent diffusion for viscoelastic fluids as:

$$D_{ij,t} = \rho \frac{\partial}{\partial x_k} \left(C_s \frac{k}{\varepsilon} \left[\overline{u_i u_l} \frac{\partial \overline{u_j u_k}}{\partial x_l} + \overline{u_j u_l} \frac{\partial \overline{u_k u_i}}{\partial x_l} + \overline{u_k u_l} \frac{\partial \overline{u_i u_j}}{\partial x_l} \right] \right) \tag{5.16}$$

The second classical term that needs closure is the viscous dissipation by the solvent (ε_{ij}), here modeled as by Lai et al. (1990) in Eq. (5.17) (note that this closure was initially developed by Shima (1988)).

$$\varepsilon_{ij} = \frac{2}{3}\varepsilon\left(1-f_w\right)\delta_{ij} + \frac{f_w(\varepsilon/k)\left[\overline{u_i u_j} + \overline{u_i u_k} n_k n_j + \overline{u_j u_k} n_k n_i + n_i n_j \overline{u_k u_l} n_k n_l\right]}{1+3\overline{u_k u_l} n_l n_k / 2k} \tag{5.17}$$

In this equation n_i denotes the wall unit normal vector. The rate of dissipation tensor ε_{ij} relies on the isotropic scalar rate of dissipation of turbulent kinetic energy (ε), which is calculated by its own transport equation:

$$\frac{D\varepsilon}{Dt} = \frac{\partial}{\partial x_k}\left(\upsilon\frac{\partial\varepsilon}{\partial x_k}\right) + \frac{\partial}{\partial x_k}\left(C_s\frac{k}{\varepsilon}\overline{u_k u_i}\frac{\partial\varepsilon}{\partial x_i}\right) + C_{\varepsilon 1}\left(1+\sigma f_{w,2}\right)\frac{\varepsilon}{k}\tilde{P} - \tag{5.18}$$

$$C_{\varepsilon 2} f_\varepsilon \frac{\varepsilon\tilde{\varepsilon}}{k} + f_{w,2}\left[\left(\frac{7}{9}C_{\varepsilon 2} - 2\right)\frac{\varepsilon\tilde{\varepsilon}}{k} - \frac{1}{2k}\left(\varepsilon - \frac{2\upsilon k}{y^2}\right)^2\right] - E_p$$

where the pseudo-dissipation ($\tilde{\varepsilon}$) and $\tilde{P}$ appearing in Eq. (5.18) are given by:

$$\tilde{\varepsilon} = \varepsilon - 2\upsilon\left(\frac{\partial k^{0.5}}{\partial x_y}\right)^2$$

$$\tilde{P} = 0.5P_{ii}, \quad P_{ii} = \overline{u_i u_k}\frac{\partial U_j}{\partial x_k} + \overline{u_j u_k}\frac{\partial U_i}{\partial x_k}$$

In Eq. 5.18, all terms are conceptually identical to those for a Newtonian fluid except for the last term (E_p) representing the viscoelastic contribution to the transport equation of ε. In this work as in Masoudian et al. (2013) E_p is assumed to be a destruction term of ε, and we use the closure given by Masoudian et al. (2013) as:

$$E_p = a_2\,\varepsilon_{ii,p}\frac{\varepsilon}{k} \tag{5.19}$$

The prediction of the dissipation rate using the above model equation together with the DNS data for the independent quantities is compared in Figure 5.7 with the dissipation rate directly computed from the DNS data using its definition. As it can be observed the prediction of ε^+ using the closure of Eq. 5.19 for E_p is in good agreement with DNS data, i.e., the model of Masoudian et al. (2013) is capable of predicting the scalar rate of turbulent dissipation both close and far from the wall.

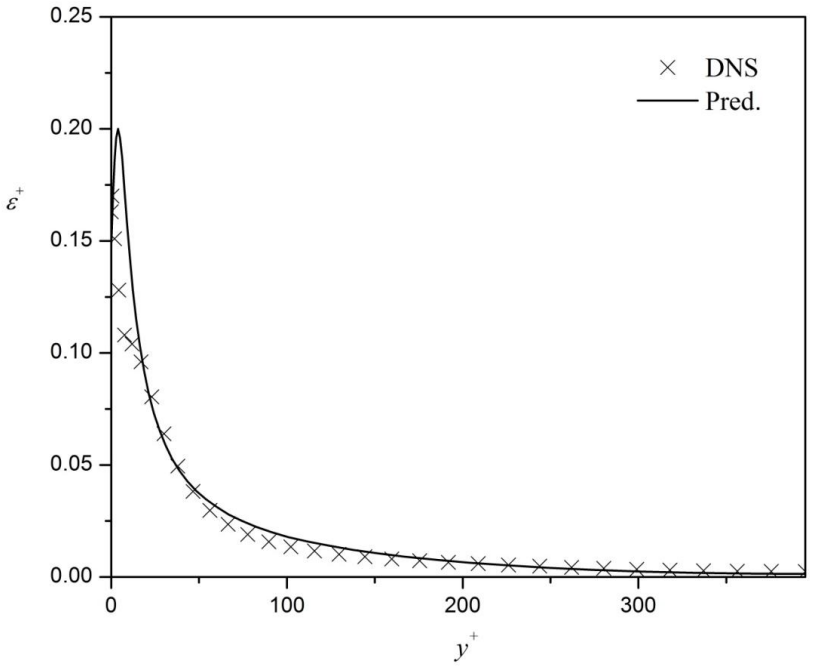

Figure 5.7) Prediction of dissipation of turbulent kinetic energy using Eq. (19). Re_τ= 395, Wi_τ= 25 and L^2 = 900

The pressure–strain term is important in the budgets of the normal components of the Reynolds stress tensor, especially in the wall-normal and spanwise directions. It distributes the turbulent kinetic energy across the components, namely extracting the energy from the streamwise component to inject it into the two cross-stream components. As for the Newtonian case the pressure strain for the streamwise component is negative (sink) and by adding polymer, based on the numerical and experimental findings of Ptasinski et al. (2003), and Li et al. (2006), its peak value decreases and moves away from the wall. Similar variations are observed for the pressure strain terms in the wall-normal and spanwise components, except that the quantities are now positive (source). This is consistent with the lower levels of v_{rms} and w_{rms} observed experimentally and numerically in drag-reduced flows by polymer additives in comparison to the corresponding values for Newtonian flows. Due to the importance of the pressure strain especially in the wall-normal and spanwise directions, predicted pressure strain terms for all components are plotted in Figure 5.8 using the original closure developed for Newtonian fluids by Lai et al. (1990). As it can be seen the Newtonian closure is capable of predicting the suppression of pressure strain term typically observed with polymer solutions without need for any closure modification. And as we will see in the results section the predictions of the wall normal and spanwise turbulent intensities, in which the pressure strain term is the most important source term, are in perfect agreement with DNS data using the Newtonian pressure strain closure. It is worth mentioning that Masoudian et al. (2013), and Iaccarino et al. (2010) examined different closures to account for the reduction of the pressure strain term of the wall-normal component of Reynolds stress in the context of k-ε-$\overline{v^2}$-f and they found that

incorporation of corrections to the pressure strain term caused complete flow laminarization and numerical divergence at high drag reduction, very much as we found here in the context of the full second order Reynolds stress model. As a result the pressure strain term for viscoelastic fluid flows is here calculated by the Newtonian closure of Lai et al. (1990) as:

$$\Pi_{ij} = \Pi_{ij,1} + \Pi_{ij,w} f_{w1} \tag{5.20}$$

$$\Pi_{ij,1} = -C_1 \frac{\varepsilon}{k}\left(\overline{u_i u_j} - \frac{2}{3}k\delta_{ij}\right) - \alpha\left(P_{ij} - \frac{2}{3}\tilde{P}\delta_{ij}\right) - \beta\left(D_{ij} - \frac{2}{3}\tilde{P}\delta_{ij}\right) - \gamma k\left(\frac{\partial U_i}{\partial x_j} + \frac{\partial U_j}{\partial x_i}\right)$$

$$\Pi_{ij,w} = C_1 \frac{\varepsilon}{k}\left(\overline{u_i u_j} - \frac{2}{3}k\delta_{ij}\right) - \frac{\varepsilon}{k}\left(\overline{u_i u_k}\, n_k n_j + \overline{u_j u_k}\, n_k n_i\right) - \alpha^*\left(P_{ij} - \frac{2}{3}\tilde{P}\delta_{ij}\right)$$

where D_{ij} in equation (5.20) is defined by:

$$D_{ij} = \overline{u_i u_k}\frac{\partial U_k}{\partial x_j} + \overline{u_j u_k}\frac{\partial U_k}{\partial x_i}$$

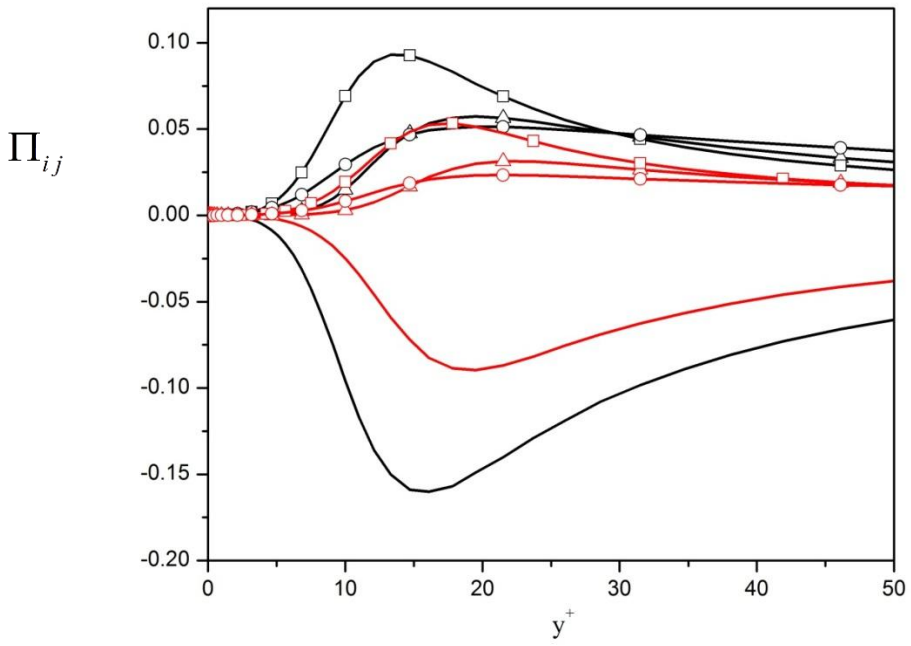

Figure 5.8 Prediction of pressure strain term using Eq. (20). Black line: Newtonian, Red line: Viscoelastic case. Solid line: streamwise, □: spanwise, ∆: wall normal, and ○: shear components of pressure strain term. Re_τ= 395, Wi_τ= 25 and L^2 = 900

Closures are required for the two viscoelastic contributions on the right hand side of the Reynolds stress transport equation (Eq. 5.9), namely for the viscoelastic turbulent transport ($D_{ij,p}$) and the viscoelastic stress work ($\varepsilon_{ij,p}$). The DNS data of Masoudian et al. (2013), and Iaccarino et al. (2010) show that for the whole ranges of tested rheological parameters and Reynolds number, the viscoelastic turbulent transport is negligible in comparison to other terms appearing in the Reynolds stress transport equation and consequently this contribution is neglected in the turbulence model. In contrast, we observed in Section 2 that the viscoelastic stress work is comparable to other contributions, especially far from the wall. It has a similar magnitude to the viscous dissipation and the turbulence production, and it is the main responsible term accounting for the energy transfer with the polymers, consequently developing a closure for this term is required. The viscoelastic stress work appearing in the transport equation of $\overline{u_i u_j}$ is defined as:

$$\varepsilon_{ij,p} = \frac{1}{\rho}\left(\overline{\tau_{ik,p}\frac{\partial u_j}{\partial x_k}} + \overline{\tau_{jk,p}\frac{\partial u_i}{\partial x_k}}\right) =$$

$$\frac{\eta_p}{\rho\lambda}\Bigg[\underbrace{C_{ik}\,\overline{f(C_{mm}+c_{mm})\frac{\partial u_j}{\partial x_k}} + C_{jk}\,\overline{f(C_{mm}+c_{mm})\frac{\partial u_i}{\partial x_k}}}_{term\ 1} + \underbrace{\overline{c_{ik}\,f(C_{mm}+c_{mm})\frac{\partial u_j}{\partial x_k}} + \overline{c_{jk}\,f(C_{mm}+c_{mm})\frac{\partial u_i}{\partial x_k}}}_{term\ 2}\Bigg] \tag{5.21}$$

In order to develop a closure for $\varepsilon_{ij,p}$ we start from its exact definition, eq. (5.21). Pinho et al. (2008) and Masoudian et al. (2013) showed that the first two terms on the right hand side of Eq. (5.21) are negligible in comparison to the remaining triple correlations regardless of the rheological and flow parameters. To model them these triple correlation (last two terms on the right hand side of Eq. (5.21)) can be decoupled, with good accuracy, into the product of function $f(C_{kk})$ by the remaining double correlation, which is NLT_{ij}. Therefore, the viscoelastic stress work can be calculated by:

$$\varepsilon_{ij,p} \approx \frac{\eta_p}{\rho\lambda} f(C_{mm})\left[\overline{c_{ik}\frac{\partial u_j}{\partial x_k}} + \overline{c_{jk}\frac{\partial u_i}{\partial x_k}}\right] = \frac{\eta_p}{\rho\lambda} f(C_{mm}) NLT_{ij} \tag{5.22}$$

Figure 5.9 compares the predictions of $\varepsilon_{ij,p}$ using Eq. (5.22) with the corresponding DNS data. Note that neglecting term 1 on the right hand side of Eq. (5.21) and decoupling the remaining triple correlations, term 2, into the product of function $f(C_{kk})$ by the remaining double correlation are exact assumptions if the Oldroyd-B constitutive equation is considered which is a limiting case of the FENE-P model for which $f(C_{kk})=1$, in other words, the closure developed here for the polymer stress work can also be applied for fluids

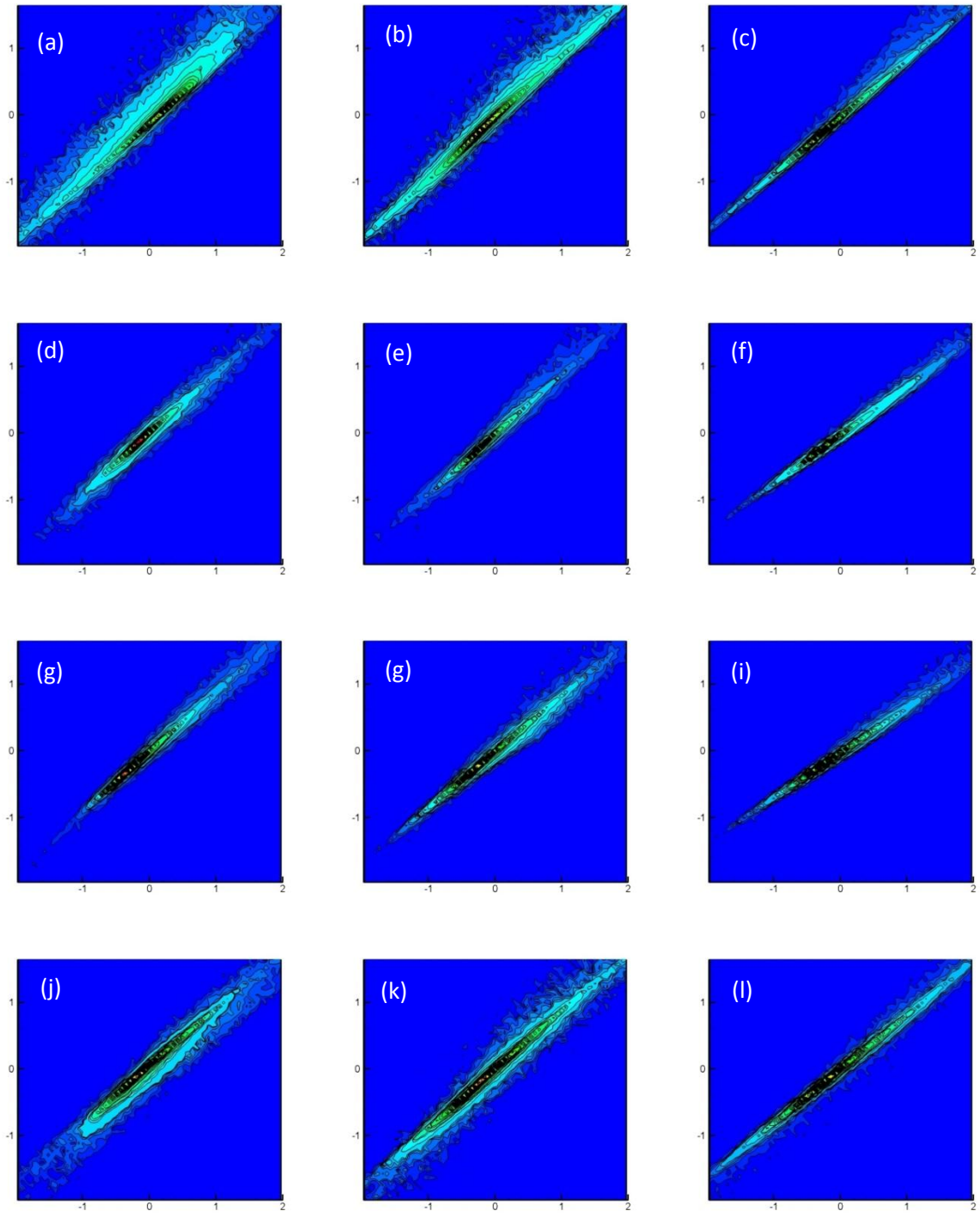

Figure 5.10. Joint PDF of a) NLT_{xx} , $\varepsilon_{xx,p}$ at y^+=5, b) NLT_{xx} , $\varepsilon_{xx,p}$ at y^+=15, c) NLT_{xx} , $\varepsilon_{xx,p}$ at y^+=75, d) NLT_{yy} , $\varepsilon_{yy,p}$ at y^+=5, e) NLT_{yy} , $\varepsilon_{yy,p}$ at y^+=15, f) NLT_{yy} , $\varepsilon_{yy,p}$ at y^+=75, g) NLT_{zz} , $\varepsilon_{zz,p}$ at y^+=5, h) NLT_{zz} , $\varepsilon_{zz,p}$ at y^+=15,i) NLT_{zz} , $\varepsilon_{zz,p}$ at y^+=75, j) NLT_{xy} , $\varepsilon_{xy,p}$ at y^+=5, k) NLT_{xy} , $\varepsilon_{xy,p}$ at y^+=15, l) NLT_{xy} , $\varepsilon_{xy,p}$ at y^+=75, for DNS data described as: Re_τ= 395, Wi_τ= 25 and L^2 = 900

governed by the Oldroyd-B model. For FENE-P fluids those assumptions remain valid with a maximum uncertainty of 5%, as depicted in Figure 5.9. In Figure 5.10 the joint probability density function of the instantaneous *NLT* and viscoelastic stress work are plotted for all components at different distances from the wall using DNS data. These quantities are highly correlated for all events, and everywhere across the channel, thus confirming the accuracy of the closure of equation 5.22.

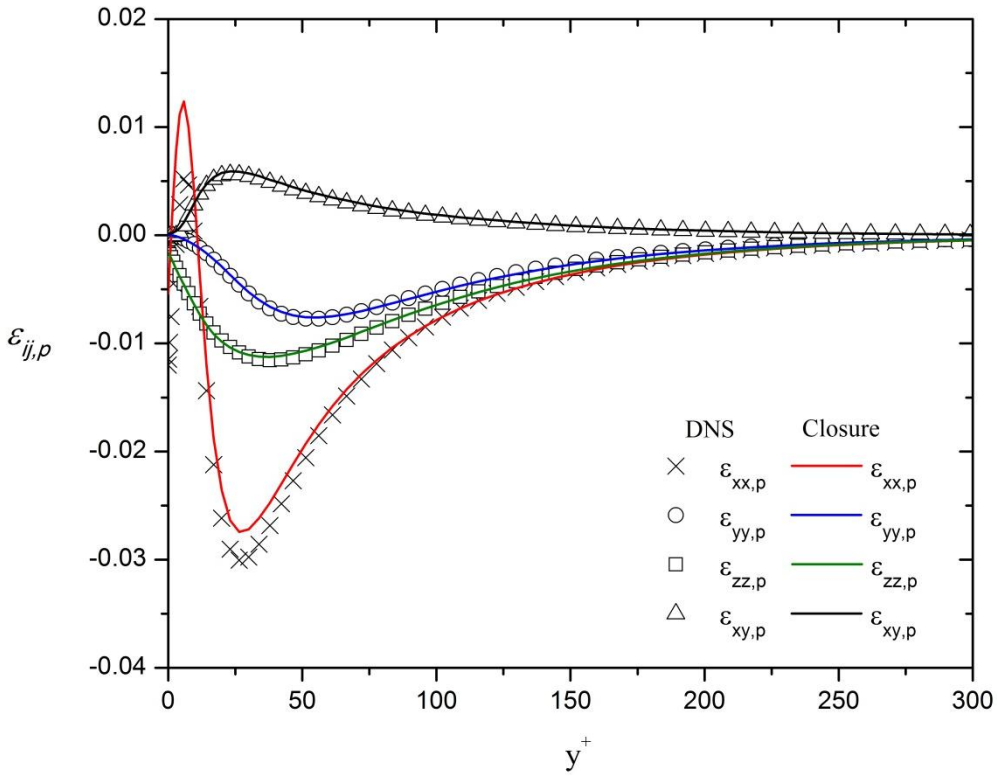

Figure 5.9. Comparison between the predictions of $\varepsilon_{ij,p}$ by using the closure developed in Eq. (22), and DNS data for Re_τ= 395, Wi_τ= 25 and L^2 = 900

Using the closure developed for $\varepsilon_{ij,p}$ term and substituting it in Eq. (5.9) the extension of the model of Lai et al. (1990) is complete to deal with FENE-P fluids. It is important to emphasize that to capture drag reduction and the influence of polymer additives on the Reynolds-averaged equations only two constant coefficients are added to the original model of Lai et al. (1990), namely a_1=0.135 and a_2=0.1 for the NLT_{ij} and E_p closures, respectively. A computer optimization algorithm was used to quantify these two constant coefficients.
The remaining constant coefficients and damping functions are those of the original model of Lai et al. (1990): C_1 = 1.5, C_2 = 0.4, α^* = 0.45, $C_{\varepsilon 1}$ = 1.35, $C_{\varepsilon 2}$ = 1.8, C_s = 0.11, α =

$(8+C_2)/11$, $\beta = (8C_2\text{-}2)/11$, $\gamma = (30C_2\text{-}2)/55$, $f_{w1} = \exp\left[-\left(\frac{R_T}{150}\right)^2\right]$, $f_{w2} = \exp\left[-\left(\frac{R_T}{64}\right)^2\right]$,

$f_\varepsilon = 1 - \frac{2}{9}\exp\left[-\left(\frac{R_T}{6}\right)^2\right]$

Note also that a Van-Driest type damping function equal to $(1-f_{w1})$ was added to the NLT_{ij} closure in order to improve predictions near the wall.

5.3.3 Summary of the model

Using the closures developed in the previous subsections, the governing and model equations are summarized below.

$$\rho\frac{\partial U_i}{\partial t} + \rho U_k\frac{\partial U_i}{\partial x_k} = -\frac{\partial \bar{P}}{\partial x_i} - \rho\frac{\partial}{\partial x_k}(\overline{u_i u_k}) + \frac{\partial \bar{\tau}_{ik}}{\partial x_k}$$

$$\bar{\tau}_{ij} = 2\eta_s S_{ij} + \bar{\tau}_{ij,p}$$

$$\bar{\tau}_{ij,p} = \frac{\eta_p}{\lambda}\left[\, f(C_{kk})C_{ij} - f(L)\delta_{ij}\,\right]$$

$$\lambda\left(\left(C_{jk}\frac{\partial U_i}{\partial x_k} + C_{ik}\frac{\partial U_j}{\partial x_k}\right) + NLT_{ij}\right) = \left[\, f(C_{kk})C_{ij} - f(L)\delta_{ij}\,\right]$$

$$\frac{\partial \overline{u_i u_j}}{\partial t} + U_k\frac{\partial \overline{u_i u}}{\partial x_k} = \left(-\overline{u_i u_k}\frac{\partial U_j}{\partial x_k} - \overline{u_j u_k}\frac{\partial U_i}{\partial x_k}\right) + D_{ij,v} + D_{ij,t} + \varepsilon_{ij} + \Pi_{ij} - \varepsilon_{ij,p}$$

$$\frac{D\varepsilon}{Dt} = \frac{\partial}{\partial x_k}\left(\upsilon\frac{\partial \varepsilon}{\partial x_k}\right) + \frac{\partial}{\partial x_k}\left(C_s\frac{k}{\varepsilon}\overline{u_k u_i}\frac{\partial \varepsilon}{\partial x_i}\right) + C_{\varepsilon 1}\left(1+\sigma f_{w,2}\right)\frac{\varepsilon}{k}\tilde{P} -$$
$$C_{\varepsilon 2} f_\varepsilon\frac{\tilde{\varepsilon}\tilde{\varepsilon}}{k} + f_{w,2}\left[\left(\frac{7}{9}C_{\varepsilon 2} - 2\right)\frac{\tilde{\varepsilon}\tilde{\varepsilon}}{k} - \frac{1}{2k}\left(\varepsilon - \frac{2\upsilon k}{y^2}\right)^2\right] - E_p$$

where the specific terms and closures associated with the FENE-P fluid are:

$$NLT_{ij} = a_1(1-f_{w1})\frac{\lambda}{\upsilon_p}\frac{\varepsilon}{k}\frac{Wi_h\sqrt{L}}{f(C_{kk})}\overline{u_i u_j}, \qquad a_1 = 0.135$$

$$\varepsilon_{ij,p} = \frac{\eta_p}{\rho\lambda} f(C_{mm}) NLT_{ij}$$

$$E_p = a_2\varepsilon_{ii,p}\frac{\varepsilon}{k}, \quad a_2 = 0.1$$

Table 5.2. Mesh independency analyses.

Grid points across the channel	Predicted drag reduction	DNS
59	Diverged	18%
79	14.1	18%
99	16.2	18%
199	16.2	18%

5.4. Results and discussion

In this section, predictions using the developed closures are presented for fully-developed turbulent channel flow of FENE-P fluids. The closures are assessed against the DNS data for FENE-P fluids. All viscoelastic flow calculations were carried out using the same flow conditions as for the DNS.

The computer code used to carry out the numerical simulations for fully developed channel flow is based on a finite-volume discretisation of the governing and turbulence model equations using staggered meshes and second-order central differences. The Tri-Diagonal Matrix Algorithm (TDMA) solver is used to calculate the solution of the discretised algebraic governing equations. The mesh is non-uniform with 99 cells across the channel, giving mesh independent results for the low drag reduction case with 0.1% uncertainty in drag reduction prediction, cf. table (5.2). The full domain is mapped exclusively in the transverse direction, hence only the following wall boundary condition needs to be imposed on both walls:

$$U_i = 0,\ \overline{u_i u_j} = 0,\ \textit{and}\ \ \varepsilon = 2\upsilon\left(\frac{\partial\sqrt{k}}{\partial y}\right)^2$$

5.4.1. Channel flow prediction for low and high drag reduction cases

Predicted transverse profiles of the mean streamwise velocity are plotted in Figure 5.11, along with the corresponding DNS predictions. In the viscous sublayer the velocity profiles collapse on the linear distribution $U^+ = y^+$ as they should. Further away from the wall, as expected, the mean velocity of the drag reduced flows increases, and the logarithmic profile shifts upwards but remains parallel to that of the Newtonian flow as is also found in the DNS results. The upward shift of the logarithmic profile can be interpreted as a thickening of the buffer layer in agreement with the experimental and numerical findings of Ptasinski et al. (2003), and Li et al. (2006).

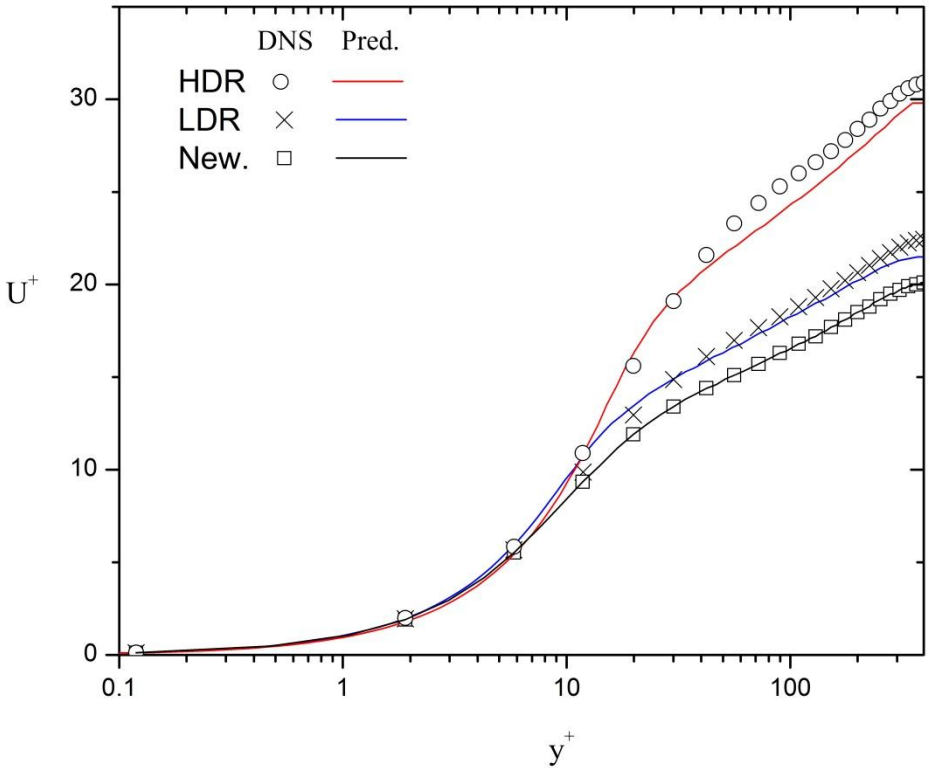

Figure 5.11. Transverse profiles of the mean streamwise velocity in wall coordinates, LDR: case DNS5, HDR: case DNS9

The corresponding predictions of the dimensionless u_{rms}, v_{rms}, w_{rms}, and $\overline{uv}$ profiles are shown in Figure 5.12, and compared with the corresponding DNS profiles for low DR (LDR) and high DR (HDR) in Figs. 5.12(a) and 5.12(b), respectively. It is well known Ptasinski et al. (2003), and Li et al. (2006) that streamwise velocity fluctuations u_{rms} increase slightly with DR, while the wall-normal and spanwise components monotonically decrease. Moreover the peak location of u_{rms} shifts away from the wall as DR increases, which is consistent with the upward shift of the logarithmic region in the mean velocity profile. Figure 5.12(a) compares the DNS and predictions of u_{rms},v_{rms},w_{rms} and $\overline{uv}$ profiles

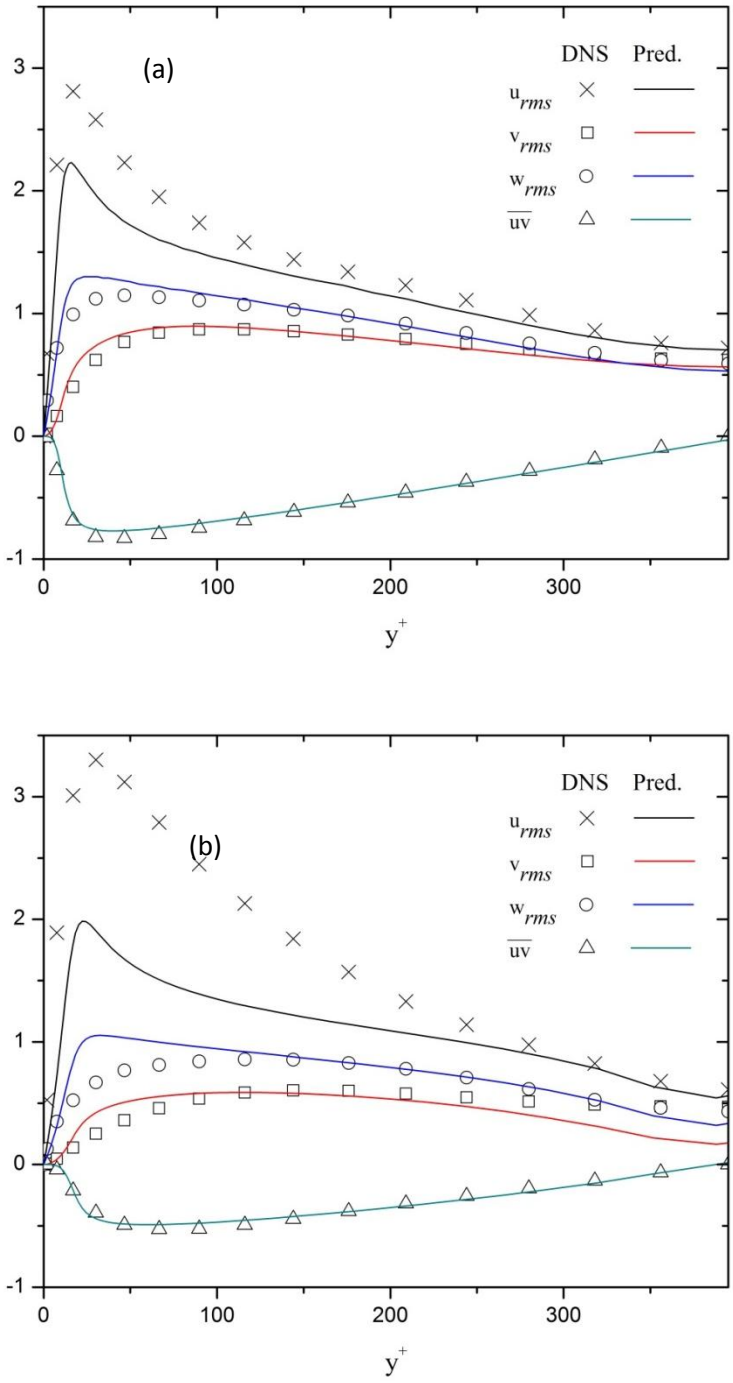

Figure 5.12. Transvers profiles of the of u_{rms},v_{rms},w_{rms} and $\overline{uv}$, (a) LDR (case DNS5), (b) HDR (case DNS9).

for LDR and as it can be seen, except for u_{rms} the predictions are in good agreement with DNS results, with the model being capable of capturing the suppression of wall-normal and

spanwise turbulent intensities which is inherent to turbulent DR with dilute polymer solutions. Moreover $\overline{uv}$ is in good agreement with DNS results, and the proposed model predicts very well both the reduction in magnitude of the stress and the shift of the location of its peak value. The predictions of $u_{rms}, v_{rms}, w_{rms}, and\ \overline{uv}$ along with DNS results for HDR regimes, DNS9, are plotted in Figure 5.12(b). It is well known that for the HDR cases v_{rms}, w_{rms} and $\overline{uv}$ decrease until around 30% of the corresponding Newtonian values. As it can be seen in Figure 5.12(b) the predictions of these suppressions of v_{rms},w_{rms} and $\overline{uv}$ are well captured by the present model, also confirming that the Newtonian closure developed by Lai and So for the pressure strain term is also capable of predicting well in viscoelastic fluids. However, in both cases the model under-predicts u_{rms}, but it should be noted that this under prediction of u_{rms} is arguably somewhat fictitious: in the experiments of Ptasinski et al. (2003) the streamwise turbulence (u_{rms}) increases slightly by increasing DR. On the other hand their corresponding DNS results over-predict those peak values i.e., DNS with the FENE-P constitutive equation predicts higher values of u_{rms} than is usually measured with real fluids. They extensively discuss this difference and state that this might be due to shortcomings in the FENE-P model. An extensive discussion can be found in Ptasinski et al. (2003).

The overall shear stress balances for the low and high DR cases are plotted in Figure 5.13 using wall coordinates. It includes the Reynolds stress, the solvent stress, and the polymer stress. In a fully developed flow condition, the total shear stress, the sum of the Reynolds, solvent, and polymer stresses, must follow a straight line across the channel varying from zero at the centerline to the wall shear stress at the wall. Here, the total shear stress is the sum of three contributions, namely, the Reynolds stress, the solvent viscous stress and the polymer stress. All stresses are normalized by the wall shear stress for low and high DR and compared with the corresponding DNS. For both LDR and HDR the total shear stress follows the expected linear profiles over the channel height, indicating that a stationary fully developed state has been reached. In the low drag reduction case the polymer stress contribution is relatively small, and it occurs mainly in the near wall region. However, as DR increases, the Reynolds stress is significantly reduced, and correspondingly the polymer stress increases to ensure the balance, thus becoming comparable to the Reynolds stress, specifically at HDR. In both cases the proposed model predicts the peak and the general trend of the Reynolds stresses, the solvent stresses, and the polymer stresses very well. These observations are also consistent with the numerical findings of Li et al. (2006) and the experimental results of Ptasinski et al. (2003).

Predictions of the Peterlin function and of the trace of the polymer length, normalized by its possible maximum extension length (L^2) are compared with DNS data for the low and high DR cases in Figure 5.14. In both cases the predictions are in good agreement with the DNS data. In agreement with findings of Li et al. (2006), the region of high chain dumbbell extension is limited to the near wall region ($y^+ < 50$) and the developed model is predicting well these quantities near and far from the wall.

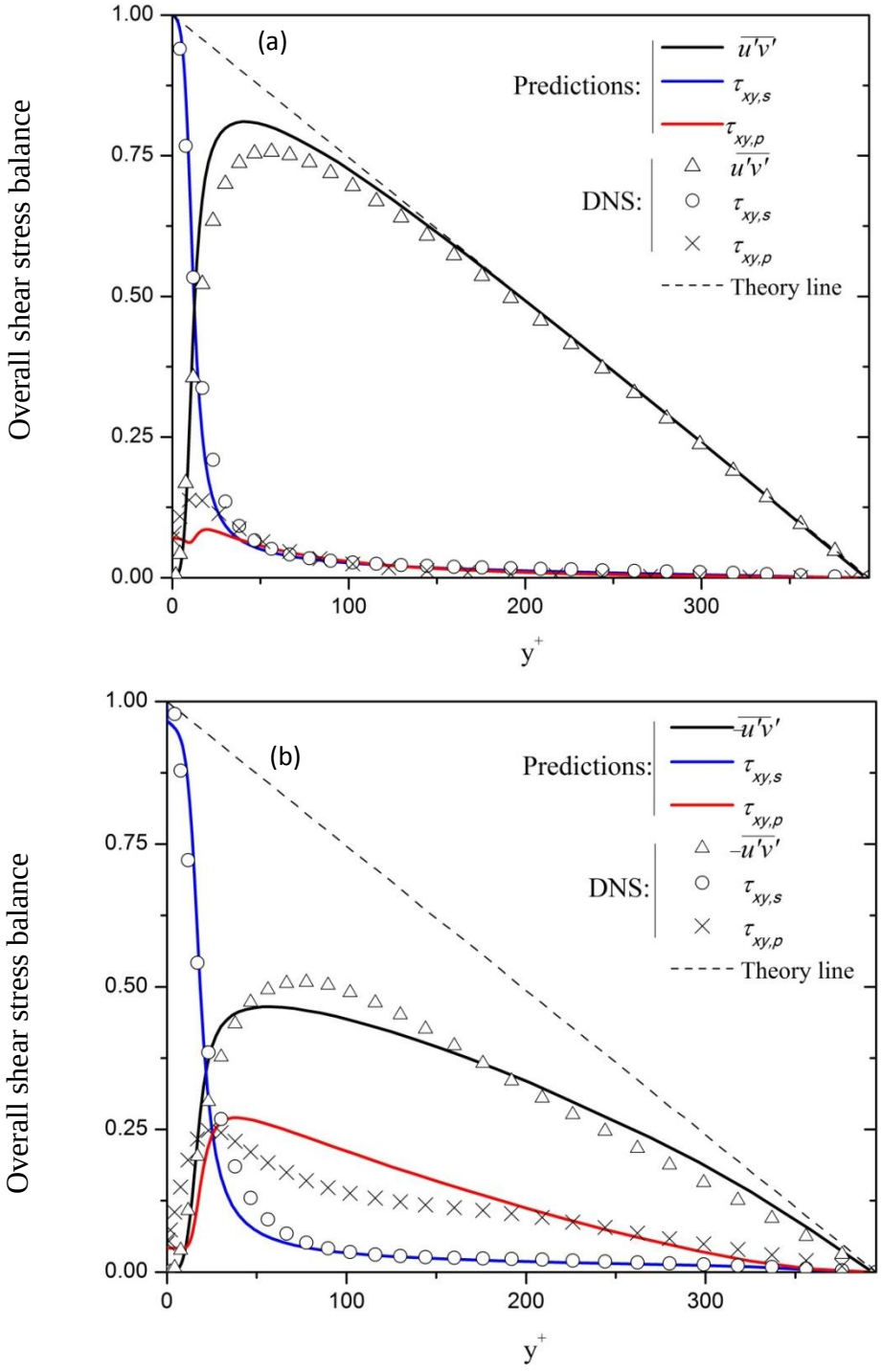

Figure 5.13. Predictions of overall stress balance, (a) LDR (case DNS5), (b) HDR (case DNS9)

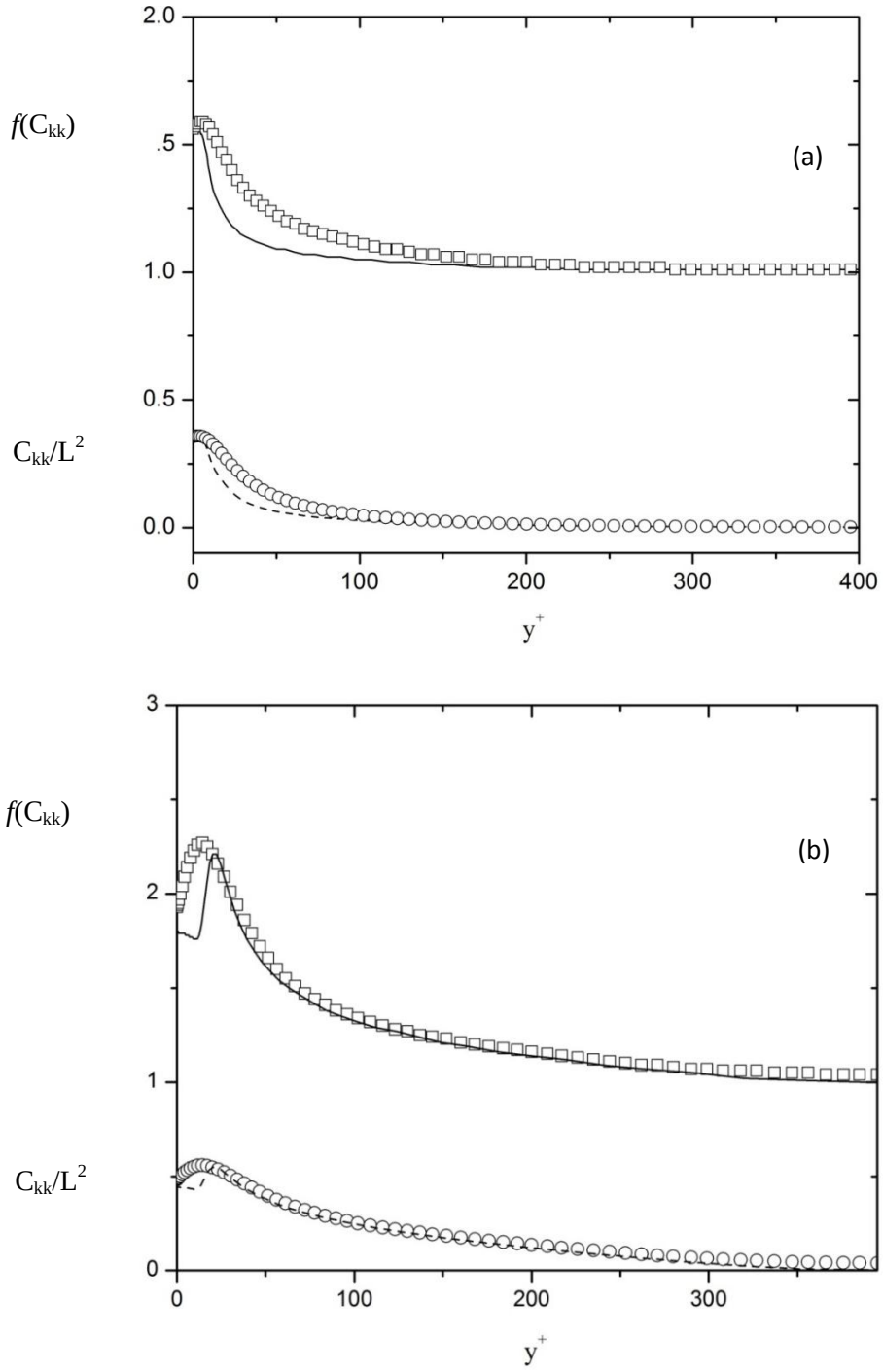

Figure 5.14. Transverse profiles of the $f(C_{kk})$, and C_{kk}/L^2. □: DNS of $f(C_{kk})$, ○: DNS of C_{kk}/L^2 dash line: predictions of C_{kk}/L^2, solid line: predictions of $f(C_{kk})$. (a) LDR (case DNS5), (b) HDR (case DNS9)

The performance of this new model is evaluated next against existing turbulence for FENE-P fluids. As reviewed in the Introduction, the first k-ε based turbulence model for FENE-P fluids was developed by Pinho et al. (2008). This early model is only capable of predicting LDR flows, and contains three new damping functions and five constant coefficients. Subsequent development by Resende et al. (2011) resulted in a very complex model, with circa twenty new tunable parameters among coefficients and damping functions, and was only valid for low and intermediate DRs. The best of those earliest models for FENE-P fluids were developed in the context of the k-ε -$\overline{v^2}$ -f first by Iaccarino et al. (2010) and then by Masoudian et al. (2013). Both models are valid up to the maximum DR, containing only three new constant coefficients.

In Figure 5.15, the normalized mean velocity and turbulent kinetic energy predicted by the current model are compared with the corresponding predictions by the earlier models of Pinho et al. (2008), Resende et al. (2011), and Masoudian et al. (2013). Note that the present model only has two additional constant coefficients compared with the base Newtonian RSM model, whereas the earlier models have more new terms coefficients than their base Newtonian models. The second-order Reynolds stress model developed here predicts better the mean velocity profile all across the channel, whereas for the turbulent kinetic energy it predicts better than the models of Pinho et al. (2008), Resende et al. (2011), but it is outperformed by the model of Masoudian et al. (2013). However, note the worse prediction of Masoudian et al. (2013) in terms of the mean velocity profile so that overall the current model is judged as a better turbulence model. Nevertheless, as discussed above, the higher peak of k calculated by DNS comes from the over prediction of the streamwise Reynolds stress, which is likely to be due to drawbacks of the FENE-P model. In addition, the current second order RS model is theoretically capable of better performance in other more complex flows especially involving secondary flows, flow separation or 3D flow, where all components of the Reynolds stress tensor play a role. This is the topic of future research as it needs also the availability of the corresponding DNS data for assessment.

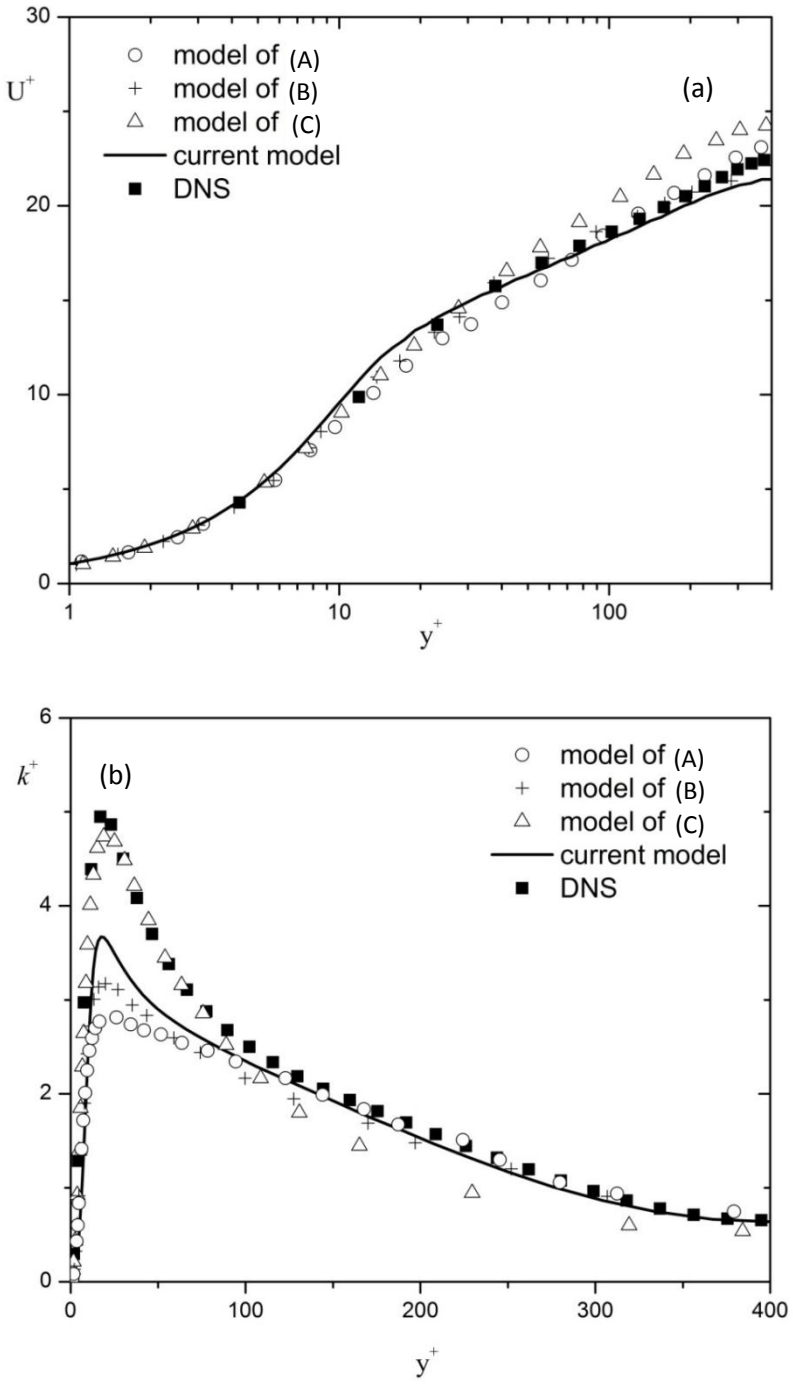

Figure 5.15. Comparison of current RS model with previous models developed for FENE-P fluids, (a) Mean velocity profile, (b) Turbulent kinetic energy (case DNS5) (A:Pinho et al (2008, B: Resende et al. (2011), and C: Masoudian et al. (2013))

Table 5.3. Overall drag reduction prediction and comparison with independent DNS results.

Reference DNS	$Re_{\tau 0}$	Rheological parameters		Drag reduction	
		$Wi_{\tau 0}$	L^2	DNS	Current model
Li et al. (2006)	125	25	900	18%	19%
Iaccarino et al. (2010)	300	36	10000	35%	34%
Iaccarino et al. (2010)	300	60	3600	47%	44%
Iaccarino et al. (2010)	300	36	19600	32%	32%
Iaccarino et al. (2010)	300	36	3600	33%	33%
Iaccarino et al. (2010)	300	60	19600	42%	41%
Li et al. (2006)	395	25	3600	19%	20%
Li et al. (2006)	395	50	3600	38%	36%
Li et al. (2006)	395	75	3600	44%	44%
Li et al. (2006)	395	100	14400	61%	60%
Li et al. (2006)	395	75	900	34%	31%
Thais et al. (2013)	1000	50	900	30%	31%

The present model compares well with the DNS data in terms of overall drag reduction; a collection of representative calculations is reported in Table (5.3). In total twelve cases of independent DNS results Li et al. (2006), Iaccarino et al. (2010), and Thais et al. (2013) are gathered and the performance of the model investigated in terms of DR intensity. The data cover a wide range of Reynolds number (125 <Re< 1000) with different amounts of drag reduction and the good comparison shows the robustness of the model.

In order to investigate the sensitivity of the predictions to changes in the *NLT* closure via its constant coefficient (a_1), and wall damping function $(1-f_{w1})$ several different values/ expressions for these quantities were tested independently, as listed in tables 5.4 and 5.5 for f_{w1} and a_1, respectively, and the corresponding predictions assessed through transverse profiles of the mean polymer extension (C_{kk}) and mean velocity profiles, the objective functions in the optimization process. These results are shown in Figures 5.16 and 5.17, for the effects of f_{w1} and a_1, respectively and it is clear that the best predictions are obtained with the optimum expression and value of the damping function and coefficient introduced above.

Table 5.4. Different values of damping function (f_{w1}) in closure of *NLT*.

run	Dapping function
Optimized model	$f_{w1} = \exp\left[-\left(\frac{R_T}{150}\right)^2\right]$
(a)	Without damping
(b)	$f_{w1} = \exp\left[-\left(\frac{R_T}{100}\right)^2\right]$
(c)	$f_{w1} = \exp\left[-\left(\frac{R_T}{200}\right)^2\right]$

Table 5.5. Different values of constant coefficient (a_1) in closure of *NLT*.

run	a_1
Optimized model	0.135
(d)	0.15
(e)	0.17
(f)	0.1
(g)	0.115

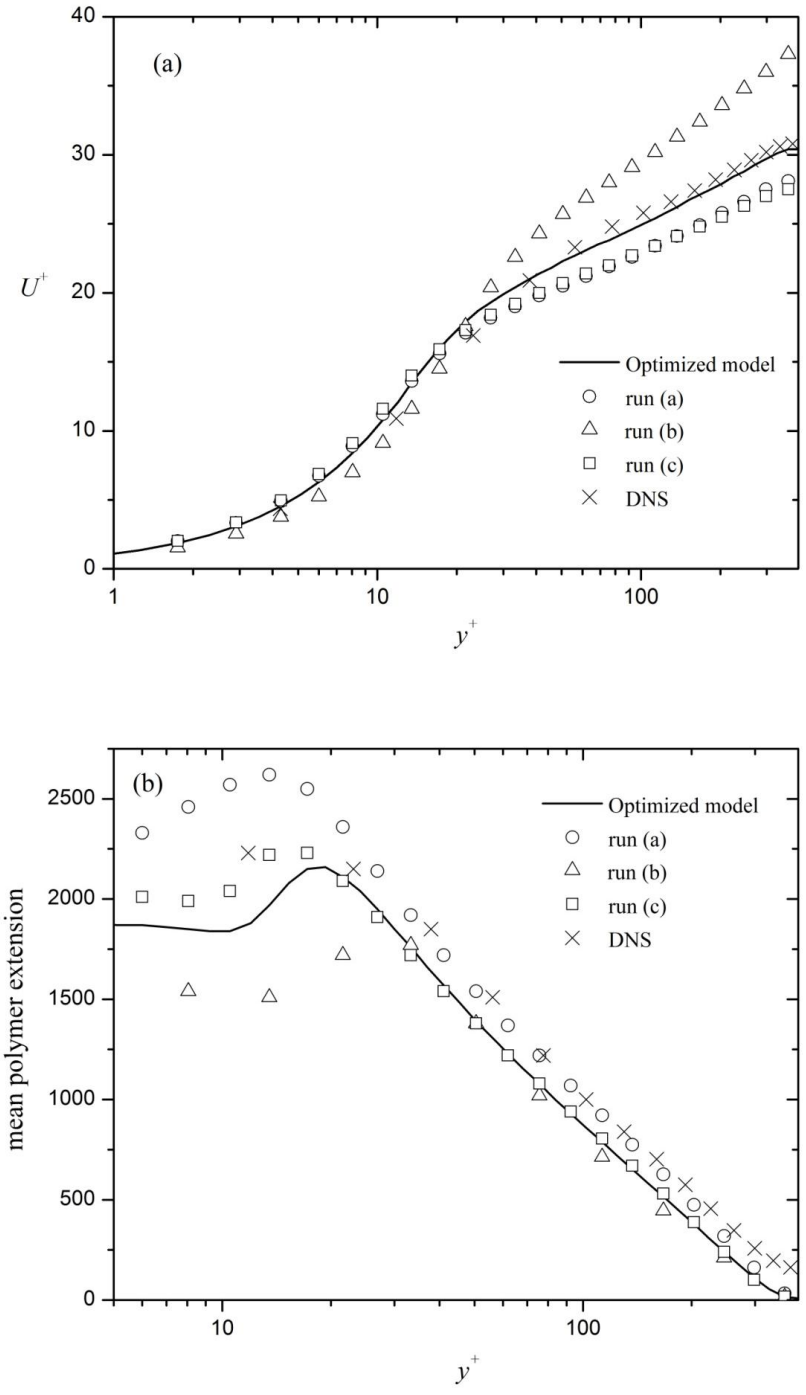

Figure 5.16. Influence of the utilized damping function in *NLT* closure on (a) mean velocity profile (b) mean polymer length (C_{kk}) for HDR case (case DNS9). See table 4 for detail about runs (a), (b), (c), and optimized model.

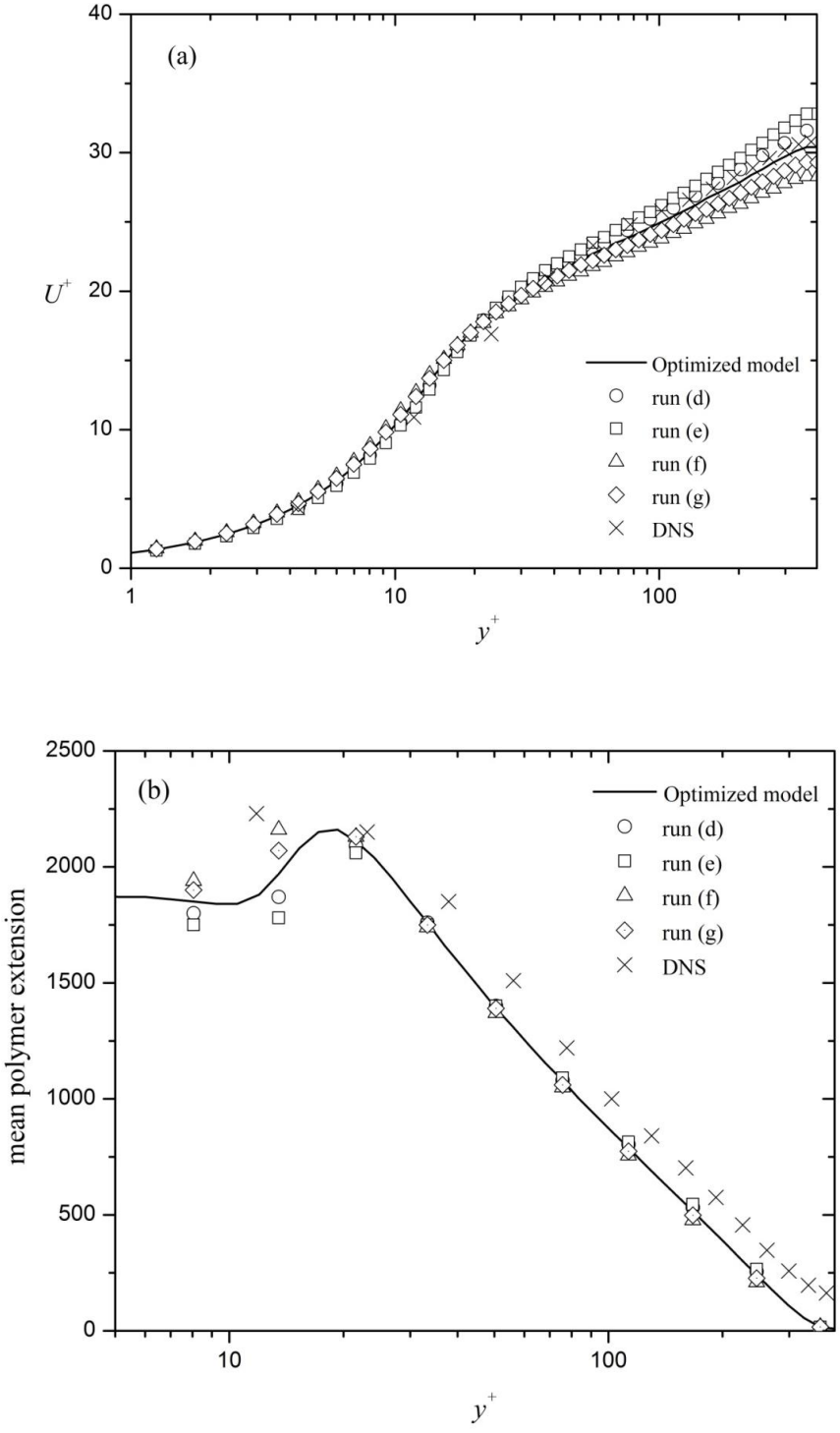

Figure 5.17. Influence of the utilized constant coefficient, a_1, in *NLT* closure on (a) mean velocity profile (b) mean polymer length (C_{kk}) for HDR case (case DNS9). See table 5 for detail about runs (d), (e), (f), (g), and optimized model.

Although the closures for the non-linear term in the constitutive equation and for the polymer stress work in the transport equation for the Reynolds stress were developed in the context of the RSM model of Lai et al. (1990), they were inspired and are extensions of earlier closures developed in the context of earlier models. These and their good near wall predicting capabilities of turbulent statistics suggest that their use with a different Reynolds stress base model, such as the model of Speziale et al. (1991), only require minor changes in the closures to account for the correct influence of polymer additives on the flow.

5.5. Conclusion

A low-Reynolds-number second-order Reynolds stress model was developed to predict turbulent flow of homogeneous polymer solutions described by the FENE-P constitutive equation. The model is an adaptation of the Reynolds stress model of Lai et al. (1990) for Newtonian fluids, it is here used for predictions of turbulent channel flow and represents a significant improvement over the previous second-order RS model of Leighton et al. (2003), which was limited to low drag reduction in spite of a large number of coefficient. The assessment of its performance in other canonical turbulent flows is the subject of future research as it requires DNS and/or experimental data in such flows as wall free jets or recirculating flows.

In order to develop this model, thirteen sets of DNS data were analyzed to investigate budgets of the Reynolds stress transport equation and of the time-averaged FENE-P constitutive equation. The developed closure for the turbulent nonlinear distortion term of the conformation tensor (*NLT*) is based on the rheological and turbulent flow parameters. In addition, closures are also developed for the viscoelastic stress work, which shows its robustness through a series of comparisons of its instantaneous and mean values. It was not necessary to develop a specific closure for the pressure strain, so its computation relies on the closure of Lai et al. (1990).

The performance of the present model is assessed against a large number of DNS data, including independent sets from the literature and covers a wide range of flow and rheological conditions ($125< Re_{\tau 0}<1000$, $25 <Wi_{\tau 0}<100$, $900<L^2<19600$). This assessment also includes predictions by earlier turbulence models for fully developed viscoelastic channel flow.

The predictions in fully-developed channel flow compare very well with DNS data in terms of mean velocity, turbulent kinetic energy and viscoelastic stresses at all ranges of drag reduction. The turbulence model developed here uses the same wall damping functions as the original model of Lai et al. (1990) and the new closures required to account for viscoelastic fluid behavior are simple, numerically inexpensive and stable with the model showing effectively a good predictive capability for FENE-P fluids.

6

Chapter 6:
A viscoelastic model for passive scalar transport

M. Masoudian, F. T. Pinho, K. Kim, and R. Sureshkumar, International Journal of Heat and Mass Transfer (Under review-2015)

"Time is a drug. Too much of it kills you."
—Terry Pratchett

Abstract

Direct numerical simulations (DNS) were carried out to investigate the passive scalar transport in a channel flow of homogenous polymer solutions described by the Finitely Extensible Nonlinear Elastic-Peterlin (FENE-P) constitutive model at intermediate and high Prandtl numbers (Pr=1.25 and 5). Time averaged statistics such as temperature fluctuations, turbulent heat fluxes, thermal turbulent diffusivity, and budget terms of the transport equation of the temperature variance were reported and compared with those of the Newtonian fluid cases at same Prandtl and Reynolds numbers. Moreover, twenty one sets of DNS of fluid flow are utilized to improve previous attempts on k-ε-$\overline{v^2}$-f models for FENE-P fluids to deal with turbulent flow of dilute polymer solutions up to the high drag reduction regime, particularly the dependency on the wall friction velocity is removed. Furthermore, five sets of recent DNS data of fluid flow and heat transfer of FENE-P fluids were used to devise the first RANS model capable of predicting the heat transfer in turbulent viscoelastic fluids. The closure for calculating turbulent Prandtl number for Newtonian fluids is extended to deal with heat transfer in turbulent viscoelastic fluids. Predicted polymer stresses, velocity profiles, mean temperature profiles, and turbulent flow characteristics are all in good agreement with the DNS data, and show improvement over previous models in the context of RANS models.

6.1. Introduction

Drag reduction by addition of polymer molecules to the turbulent flow has been extensively investigated both experimentally and numerically over the last decades; comprehensive early reviews on the subject are those of Hoyt (1972), Lumley (1969) and Virk (1975). From the outset it was observed that the addition of small amounts of high molecular weight linear polymers, such as polyethylene oxide (PEO) or polyacrylamide among others, to low viscosity Newtonian solvents flowing in turbulent pipe or channel flow would reduce drag by up to 80%.

Recent comprehensive theories on the mechanisms of drag reduction induced by polymer additives have been put forward in the literature White et al. (2008) and Procaccia et al. (2008). One mechanism is based on the fact that polymer molecules undergo a coil-to-stretch transition, causing an increase in the extensional viscosity of the solution that helps suppress Reynolds stress-producing events. A second mechanism assumes that coil-to-stretch transition is not possible in channel or pipe flows and that drag reduction is associated with the storage of elastic energy by the polymer molecules in a polymer-induced energy cascade with the consequent depletion of the classical energy cascade.

Over the last two decades, the development of accurate and efficient numerical and experimental methods for viscoelastic fluids has made it possible to investigate in detail turbulent DR in dilute polymer solutions (Kawaguchi et al. (2002), Ptasinski et al.(2003), Dubief et al. (2004), Dimitropoulos et al. (2005), Thais et al. (2013), and Li et al. (2006)).

Most of the numerical simulations used constitutive equations based on the FENE-P (finitely extensible nonlinear elastic-Peterlin) rheological constitutive equation which allows one to probe the effects on the flow of the polymer relaxation time, chain extensibility and of the ratio of polymer to solution viscosities. In this constitutive equation, a polymer chain is represented by a single dumbbell consisting of two beads, representing the hydrodynamic resistance, connected by a finitely extensible entropic spring.

Direct numerical simulations (DNS) of polymer induced drag reduction in turbulent channel flows up to the maximum drag reduction (MDR) limit were carried out using a fully spectral method by Ptasinski et al.(2003), Dubief et al. (2004), Dimitropoulos et al. (2005), Thais et al. (2013), and Li et al. (2006). They showed that to obtain significant levels of drag reduction large polymer chain extensibilities and high Weissenberg numbers are required. In addition, they studied the influence of rheological parameters of the FENE-P model on the amount of polymer-induced drag reduction.

Passive scalar transport in turbulent channel flow of viscoelastic dilute polymer solutions has been much less studied using direct numerical simulations, but nevertheless an investigation for DR of up to 74.0% was carried out by Gupta et al. (2005). They showed that DR is accompanied by increased coherence of the low-speed streaks in the buffer layer and that they are responsible for the streamwise heat transport, which is actually enhanced relative to the corresponding Newtonian flow. Simultaneously the wall-normal and spanwise heat fluxes decrease with DR very much as happens with the Reynolds shear stress and the root mean square fluctuations in the wall-normal and spanwise directions. The enhanced anisotropy of the scalar heat fluxes, and in particular the enhancement of the streamwise heat flux, is a rather unexpected result, whereas the reduced flow-normal heat flux was somewhat expected.

Yu et al. (2004) carried out DNS of fully developed turbulent heat transfer of a viscoelastic drag-reducing flow described by Giesekus model at low Prandtl number (Pr=0.71) and reported turbulent thermal statistics such as temperature fluctuations, turbulent heat fluxes and budget terms of the temperature variance and compared with those of a Newtonian fluid flow.

DNS simulation of turbulent viscoelastic flow is significantly more expensive than Newtonian DNS, Li et al. (2006). Hence, Reynolds-Averaged Navier–Stokes (RANS), and Large Eddy Simulation (LES) models must be developed.

In the context of k-ε turbulence models for viscoelastic fluids Pinho et al. (2008), followed by on Resende *et* al. (2011) proposed closures for Reynolds stresses of viscoelastic fluids described by the FENE-P model that relied on *a priori* analyses of DNS data. In these works Reynolds averaged flow and conformation quantities were predicted well, but both models were limited to applications in the low DR regime (DR<34%). In addition both models rely on overly complex viscoelastic closures, do not cover the whole range of drag reduction and are not capable to deal with simulations in complex geometries.

More recently, Tsukahara et al. (2013) proposed a low Reynolds number k-ε model for viscoelastic fluids described by the Giesekus constitutive equation. Their closure is valid up to the maximum DR. In their proposal, an extra damping function was added to the closure of eddy viscosity, while the treatment of the turbulent kinetic energy (k) and its dissipation rate (ε) is an extension of the model for Newtonian fluids.

The first turbulence model of first order to be capable of predicting turbulent viscoelastic flows in the high drag reduction regime was developed by Iaccarino et al. (2010) in the context of k-ε -$\overline{v^2}$ -f model. They used the concept of turbulent polymer viscosity to account for the combined effects of turbulence and viscoelasticity on the momentum and conformation equations. Their closure for turbulent polymer viscosity depends on the turbulent kinetic energy, the polymer relaxation time and the trace of conformation tensor and the model of the nonlinear terms in the conformation tensor equation relied on the turbulent dissipation rate. However, although their model predicts accurately the amount of drag reduction, their predictions of the polymer shear stress, of the budget of the turbulent kinetic energy and of the various contributions to the evolution equation for the conformation tensor are not in agreement with DNS results.

Later on, Masoudian *et al.* (2013) using *a priori* analyses of the DNS data proposed a new model for FENE-P fluids in the context of k-ε -$\overline{v^2}$ -f, which was also valid up to the maximum amount of DR, and relying also on the concept of turbulent polymer viscosity previously introduced by Iaccarino et al. (2010). Relative to Iaccarino's model they improved the predictions of the viscoelastic stress and of the viscoelastic stress work, which is the main viscoelastic contribution in the turbulent kinetic energy transport equation. Instead of using the turbulent dissipation rate to model the non-linear term in the conformation equation, as previously done by Iaccarino et al. (2010), by analyzing DNS data Masoudian et al. (2013) introduced a Boussinesq-like relation to model the non-linear contribution (*NLT*) in the conformation equation, and their model was validated over a wide range of rheological and flow parameters.

These models of Iaccarino et al. (2010), and Masoudian et al. (2013), which are the only first-order models valid for the whole range of drag reduction, use two separate closures to model quantities associated with the non-linear term of the conformation tensor, which represents a loss of consistency in the model: one closure for the trace, NLT_{kk}, and one closure for the NLT_{xy}. In addition to the inconsistency of this approach the inherent dependency of these terms on each other, make the model numerically unstable. Finally, the dependency of the previous model on the wall friction velocity hinders the use of the model in complex geometries.

The single-point turbulence model developed here is based on the time-averaged governing equations for viscoelastic fluids presented originally by Iaccarino et al. (2010), and Masoudian et al. (2013). An important contribution of the present work is the development of a single closure for the nonlinear fluctuating terms appearing in the FENE-P rheological

constitutive equation by using a Boussinesq like relation to model the non-linear term (*NLT*). In addition, the dependency of the previously developed closure to the wall friction velocity is eliminated, i.e., all closures are based on the local quantities, which give the model the capacity to be used in complex geometries. Furthermore, as far as we are aware of, there is no RANS model to deal with heat transfer in turbulent flows of viscoelastic fluids, so in this work the closure of Kays (1994) is extended for the first time to cope with viscoelastic fluids. Five sets of recent DNS data for channel flow of viscoelastic fluids pertaining to low, intermediate and high drag reductions are used to quantify the heat transfer in viscoelastic turbulent flows.

The section is organized as follows: section 6.2 introduces the governing equations and identifies the viscoelastic terms requiring modeling, section 6.3 introduces the numerical methods applied in DNS and reports time averaged statistics, in Section 6.4 the turbulent closures are developed and section 6.5 presents model predictions. Conclusions are offered in section 6.6.

6.2. Governing equations

In what follows, upper-case letters or overbars denote Reynolds-averaged quantities and lower-case letters or primes denote fluctuating quantities. Since the work makes significant improvements on an existing k-ε-$\overline{v^2}$-f model, prior to presenting the new closure for the Reynolds scalar fluxes the governing equations are presented first for isothermal flows and subsequently the thermal energy equation and the required closure are presented. Details on the Reynolds averaging procedure can be found elsewhere (Iaccarino et al. (2010), and Masoudian et al. (2013)).

6.2.1. Momentum equation

The instantaneous momentum equation appropriate for the FENE-P fluids can be expressed as,

$$\rho\frac{\partial u_i}{\partial t}+\rho u_k\frac{\partial u_i}{\partial x_k}=-\frac{\partial p}{\partial x_i}+\frac{\partial \tau_{ik}}{\partial x_k} \tag{6.1}$$

where τ_{ik} is the fluid stress tensor, u_i is the velocity, p is the pressure, and ρ is the fluid density. The fluid extra stress tensor in Eq. (6.1) is given in Eq. (6.2) as the sum of a Newtonian solvent contribution of viscosity η_s with a polymeric contribution $\tau_{ij,p}$ described by the FENE-P rheological constitutive model.

$$\tau_{ij}=2\eta_s S_{ij}+\tau_{ij,p} \tag{6.2}$$

S_{ij} is the rate of strain tensor defined as

$$S_{ij}=\frac{1}{2}\left(\frac{\partial u_i}{\partial x_j}+\frac{\partial u_j}{\partial x_i}\right) \tag{6.3}$$

In the context of RANS, the instantaneous quantities are decomposed into mean and fluctuating components (Reynolds decomposition). Using this process in the momentum equation and subsequently averaging, the Reynolds averaged momentum equation is described by,

$$\rho\frac{\partial U_i}{\partial t}+\rho U_k\frac{\partial U_i}{\partial x_k}=-\frac{\partial P}{\partial x_i}-\frac{\partial}{\partial x_k}(\overline{\rho u_i u_k})+\frac{\partial \bar{\tau}_{ik}}{\partial x_k} \tag{6.4}$$

where $\overline{\rho u_i u_k}$ is the Reynolds stress tensor. Note that over bar or uppercase letters denote Reynolds averaged quantities.

6.2.2. Constitutive equation

The polymeric contribution to the total extra stress, Eq. (6.2), is given as an explicit function of the conformation tensor c_{ij}

$$\tau_{ij,p}=\frac{\eta_p}{\lambda}\left[\, f(c_{kk})c_{ij}-f(L)\delta_{ij}\,\right] \tag{6.5}$$

where λ is the polymer relaxation time, η_p is the polymer viscosity, and $f(c_{kk})$ is the Peterlin function, which takes here the form used by Li et al. (2006) and given by,

$$f(c_{kk})=\frac{L^2-3}{L^2-c_{kk}} \quad \text{together with} \quad f(L)=1 \tag{6.6}$$

In this equation L^2 is the dimensionless polymer dumbbell maximum extension length.
In Eq. (6.5) the conformation tensor components must be calculated using FENE-P constitutive equation,

$$\frac{\partial c_{ij}}{\partial t}+u_k\frac{\partial c_{ij}}{\partial x_k}-\left(c_{jk}\frac{\partial u_i}{\partial x_k}+c_{ik}\frac{\partial u_j}{\partial x_k}\right)=-\frac{\tau_{ij,p}}{\eta_p} \tag{6.7}$$

By Reynolds averaging the instantaneous FENE-P constitutive equation the Reynolds-averaged conformation tensor is obtained by,

$$\begin{aligned} U_k\frac{\partial C_{ij}}{\partial x_k}+\underbrace{\overline{u_k\frac{\partial c_{ij}}{\partial x_k}}}_{CT_{ij}}-\underbrace{\left(C_{jk}\frac{\partial U_i}{\partial x_k}+C_{ik}\frac{\partial U_j}{\partial x_k}\right)}_{M_{ij}}-\underbrace{\left(\overline{c_{jk}\frac{\partial u_i}{\partial x_k}}+\overline{c_{ik}\frac{\partial u_j}{\partial x_k}}\right)}_{NLT_{ij}}= \\ \underbrace{-\frac{1}{\lambda}\left[\overline{f(C_{kk}+c_{kk})(C_{kk}+c_{kk})}-f(L)\delta_{ij}\right]}_{\bar{\tau}_{ij,p}/\eta_p} \end{aligned} \tag{6.8}$$

In this equation the first term on the left hand side is the mean flow advective of C_{ij} which vanishes for fully developed channel flow, CT_{ij} is the contribution to the advective transport of the conformation tensor by the fluctuating velocity and conformation fields, M_{ij} is the

mean flow distortion term of Oldroyd derivative of C_{ij}, and NLT_{ij} accounts for the interactions between the fluctuating components of the conformation tensor and of the velocity gradient tensor. This term also originates from the distortion term of the Oldroyd derivative and is the fluctuating counterpart of M_{ij}.

6.2.3. Reynolds stresses

To calculate the Reynolds stress tensor in eq. (6.4) Boussinesq's turbulent stress–strain relationship was adopted:

$$-\rho\overline{u_i u_j} = 2\rho\nu_T S_{ij} - \frac{2}{3}\rho k\delta_{ij} \tag{6.9}$$

where υ_T is the eddy viscosity and k is the turbulent kinetic energy, $\overline{u_i u_i}/2$. In this work as in Masoudian et al. (2013) the eddy viscosity is modeled according to the $k-\varepsilon-\overline{v^2}-f$ model of Durbin et al. (1991, 1996). This particular choice is because of the capability of this turbulence model in calculating accurately the turbulence statistics in wall bounded flows without introducing the wall-distance or low-Reynolds number damping functions. In this model the eddy viscosity is calculated as:

$$\nu_T = C_\mu \overline{v^2} T_t \tag{6.10}$$

where C_μ is the constant coefficient, $\overline{v^2}$ is the wall normal Reynolds stress, and T_t is turbulent time scale defined as:

$$T_t = \max\left\{\frac{k}{\varepsilon^2}, 6\sqrt{\frac{\upsilon}{\varepsilon}}\right\} \tag{6.11}$$

This model is an extension of the k-ε model, and requires solving two extra equations for $\overline{v^2}$, and f along with the k and ε equations. The extended transport equations for the turbulent kinetic energy and its dissipation rate appropriate to deal with the FENE-P fluids in the context of the $k-\varepsilon-\overline{v^2}-f$ model were presented in Masoudian et al. (2013) and are given by Eqs. (6.12) and (6.13), note that both of the k and ε equations contain additional terms in order to account for viscoelasticity,

$$U_j\frac{\partial k}{\partial x_j} = P_k - \varepsilon + \frac{\partial}{\partial x_j}\left(\left(\nu + \frac{\nu_T}{\sigma_k}\right)\frac{\partial k}{\partial x_j}\right) - \left(\overline{\tau_{ij}^p \frac{\partial u_i}{\partial x_j}}\right) + \frac{\partial}{\partial x_j}\left(\overline{\tau_{ij}^p u_i}\right) \tag{6.12}$$

$$U_j\frac{\partial \varepsilon}{\partial x_j} = \frac{C_{\varepsilon 1}P_k - C_{\varepsilon 2}\varepsilon}{T_t} + \frac{\partial}{\partial x_j}\left(\left(\nu + \frac{\nu_T}{\sigma_\varepsilon}\right)\frac{\partial \varepsilon}{\partial x_j}\right) - E_p \tag{6.13}$$

Here, all terms are conceptually identical to those for a Newtonian fluid except for the last two terms in the turbulent kinetic energy equation, Eq. 6.12, and the term E_p in the dissipation equation. In the former equation they represent the viscoelastic turbulent

transport ($Q_p \equiv \partial\left(\overline{\tau_{ij}^p u_i}\right)/\partial x_j$), and the viscoelastic stress work ($\varepsilon_p \equiv \overline{\tau_{ij}^p \partial u_i/\partial x_j}$), whereas in the latter equation the new term accounts for the viscoelastic contribution to the transport equation of ε.

The other two equations required to compute the eddy viscosity are the transport equation for the scalar $\overline{v^2}$, which is derived from the transport equation for the wall normal turbulent fluctuations according to Masoudian et al. (2013), and the equation for the turbulence energy redistribution process, *f*. As discussed in Masoudian et al. (2013) the equations for $\overline{v^2}$ and *f* appropriate for the FENE-P fluids are given by:

$$U_j \frac{\partial \overline{v^2}}{\partial x_j} = kf + \frac{\partial}{\partial x_j}\left(\left(\nu + \frac{\nu_T}{\sigma_k}\right)\frac{\partial \overline{v^2}}{\partial x_j}\right) - 6\frac{\varepsilon}{k}\overline{v^2} - \varepsilon_{p,v2} + Q_{p,v2} \tag{6.14}$$

$$f - L_t^2 \frac{\partial^2 f}{\partial x_j \partial x_j} = C_1 \frac{\left(\frac{2}{3} - \frac{\overline{v^2}}{k}\right)}{T_t} + C_2 \frac{P_k}{k} - 5\varepsilon\frac{\overline{v^2}}{k} \tag{6.15}$$

where L_t is a length scale accounting for turbulence and wall proximity defined as:

$$L_t^2 = C_L \max\left\{\frac{k^3}{\varepsilon^2}, C_\eta^2\sqrt{\frac{\nu^3}{\varepsilon}}\right\} \tag{6.16}$$

As reported in Durbin et al. (1996) the coefficients appearing in the above equations are : $C_\mu = 0.19$, $\sigma_k = 1$, $\sigma_\varepsilon = 1.3$, $C_{\varepsilon 1} = 1.4\left[1 + 0.05\sqrt{k/\overline{v^2}}\right]$, $C_{\varepsilon 2} = 1.9$, $C_1 = 1.4$, $C_2 = 0.3$, $C_L = 0.23$, $C_\eta = 70$.

6.2.4. Energy equation

The instantaneous thermal energy equation for incompressible flow can be written as,

$$\frac{\partial T}{\partial t} + u_j \frac{\partial T}{\partial x_j} = \frac{k}{\rho C_p}\frac{\partial^2 T}{\partial x_j^2} \tag{6.17}$$

The thermal boundary condition of uniform heat flux at the both walls is considered in this study to which corresponds a linear variation of the wall temperature in thermally fully-developed flow, Kays et al. (1980). To impose the periodic boundary condition for temperature, the temperature is made dimensionless as following,

$$\theta = \frac{\langle T_w \rangle - T}{T^*},\ T^* = \frac{q''}{\rho C_p U_m} \tag{6.18}$$

Using the normalized temperature, the non-dimensional governing equation becomes with velocity scale of the friction velocity and length scale of the channel half height. If the temperature is normalized by the friction temperature the governing equation becomes the

same as in Kasagi et al. (1992).

$$\frac{\partial \theta^+}{\partial t} + u_j \frac{\partial \theta^+}{\partial x_j} - \frac{u_1}{U_m} = \frac{1}{\mathrm{Re}_\tau \, \mathrm{Pr}} \frac{\partial^2 \theta^+}{\partial x_j^2} \tag{6.19}$$

In eq. (6.19) θ^+ represents the instantaneous temperature; *Pr* denotes the molecular Prandtl number, defined as the ratio of kinematic viscosity to thermal diffusivity. By Reynolds averaging the Eq. (6.19) the thermal field is obtained by,

$$\frac{D\Theta^+}{Dt} - \frac{\overline{u_1}}{U_m} = \frac{1}{\mathrm{Re}_\tau \, \mathrm{Pr}} \frac{\partial^2 \Theta^+}{\partial x_j^2} - \frac{\partial \overline{u_j \theta'^+}}{\partial x_j} \tag{6.20}$$

In this equation $\overline{u_j \theta'^+}$ is the thermal flux, which is non-linear and requires a closure.

Table 6.1. Summary of the physical and computational parameters for the DNS of fluid flow

case	$Re_{\tau 0}$	Domain size $L_x \times L_y \times L_z$	Nodes $N_x \times N_y \times N_z$	L^2	$Wi_{\tau 0}$	β
(1)	125	6.283h x 2h x 3.141h	96 x 97 x 96	0	0	0
(2)	180	6.283h x 2h x 3.141h	128 x 129 x 128	0	0	0
(3)	395	14.136h x 2h x 4.5h	384 x 257 x 192	0	0	0
(4)	590	14.136h x 2h x 4.5h	512 x 257 x 256	0	0	0
(5)	125	6.944h x 2h x 4.19h	96 x 97 x 96	900	25	0.9
(6)	125	6.944h x 2h x 4.19h	96 x 97 x 96	900	50	0.9
(7)	125	6.944h x 2h x 4.19h	96 x 97 x 96	900	100	0.9
(8)	125	6.944h x 2h x 4.19h	96 x 97 x 96	3600	25	0.9
(9)	125	6.944h x 2h x 4.19h	96 x 97 x 96	3600	50	0.9
(10)	125	6.944h x 2h x 4.19h	96 x 97 x 96	3600	100	0.9
(11)	125	6.944h x 2h x 4.19h	96 x 97 x 96	14400	25	0.9
(12)	125	6.944h x 2h x 4.19h	96 x 97 x 96	14400	50	0.9
(13)	180	6.944h x 2h x 4.19h	128 x 129 x 128	900	25	0.9
(14)	180	13.888h x 2h x 4.19h	128 x 129 x 128	900	50	0.9
(15)	180	13.888h x 2h x 4.19h	128 x 129 x 128	900	100	0.9
(16)	180	13.888h x 2h x 4.19h	128 x 129 x 128	3600	50	0.9
(17)	180	13.888h x 2h x 4.19h	128 x 129 x 128	3600	100	0.9
(18)	395	14.136h x 2h x 4.5h	384 x 129 x 128	900	25	0.9
(19)	395	14.136h x 2h x 4.5h	384 x 257 x 192	900	100	0.9
(20)	395	14.136h x 2h x 4.5h	384 x 257 x 192	3600	75	0.9
(21)	395	14.136h x 2h x 4.5h	384 x 257 x 192	14400	75	0.9
(22)	395	14.136h x 2h x 4.5h	384 x 257 x 192	3600	100	0.9
(23)	395	14.136h x 2h x 4.5h	384 x 257 x 192	3600	50	0.9
(24)	590	25.136h x 2h x 4.5h	512 x 257 x 256	3600	50	0.9
(25)	590	25.136h x 2h x 4.5h	512 x 257 x 256	10000	100	0.9

6.3. DNS of heat transfer of viscoelastic dilute polymer solutions

6.3.1. Computational and physical parameters

The fully developed channel flow of FENE-P fluids over a wide range of rheological and flow properties is investigated and the DNS cases studied are summarized in Table (6.1). A semi-implicit method is used for time-integration of the governing equations. In space, a spectral method is used with Fourier representations in the streamwise and spanwise directions, and Chebyshev expansion in the wall-normal direction. To achieve stable numerical integration a stress diffusion term is introduced. As in earlier studies Lai et al. (2006) and Masoudian et al. (2013), the dimensionless artificial numerical diffusivity is taken to be $O(10^{-2})$. Periodic boundary conditions are applied in the streamwise (x) and spanwise (z) directions, and the no-slip boundary condition is imposed on velocity at the solid walls. Details of the numerical approaches used in this work can be found in Lai et al. (2006).

Table 6.2. Summary of the physical and computational parameters for the DNS of fluid flow with heat transfer

case	$Re_{\tau 0}$	Domain size $L_x \times L_y \times L_z$	Nodes $N_x \times N_y \times N_z$	L^2	$Wi_{\tau 0}$	β	Pr
(H0)	125	10h x 2h x 5h	128 x 97 x 257	0	0	0	5.0
(H1)	180	10h x 2h x 5h	128 x 129 x 128	0	0	0	1.25
(H2)	180	10h x 2h x 5h	128 x 129 x 128	900	25	0.9	1.25
(H3)	180	10h x 2h x 5h	128 x 129 x 128	3600	75	0.9	1.25
(H4)	125	10h x 2h x 5h	128 x 97 x 257	900	25	0.9	5.0
(H5)	125	10h x 2h x 5h	128 x 97 x 257	900	100	0.9	5.0
(H6)	125	10h x 2h x 5h	128 x 97 x 257	3600	100	0.9	5.0

It is known that the smallest scales of the instantaneous temperature field decrease with the Prandtl number, in inverse proportion to $Pr^{1/2}$, Kasagi et al. (1992). Therefore, for the simulation of the thermal field with high Prandtl number, the mesh should be finer than the requirement for the velocity field only. To solve the energy equation, Eq. (6.19) is discretized in time with second-order temporal accuracy. Details of the numerical methods for solving thermal field in this work can be found in Gupta et al. (2005). Table 6.2 lists the simulations of heat transfer of FENE-P fluid flows for all cases studied in this work.

6.3.2. Time averaged statistics

The mean temperature profiles for the viscoelastic and Newtonian cases corresponding to Re_τ=180, Pr=1.25 and Re_τ =125, Pr=5 are plotted in Figures 6.1 and 6.2, respectively. As expected, the Figures clearly show that near the wall all the mean temperature profiles,

(regardless of the amount of Re_τ, Pr, L^2, *and* Wi_τ) collapse on the linear distribution: $y^+=Pr\Theta^+$. Further away from the wall the mean temperature profiles of the drag reduced flows (regardless of the amount of Re_τ, Pr) increases as compared to that of Newtonian flows. These Figures further indicate that the conduction region penetrates more deeply into the core region with decrease of amount of drag reduction.

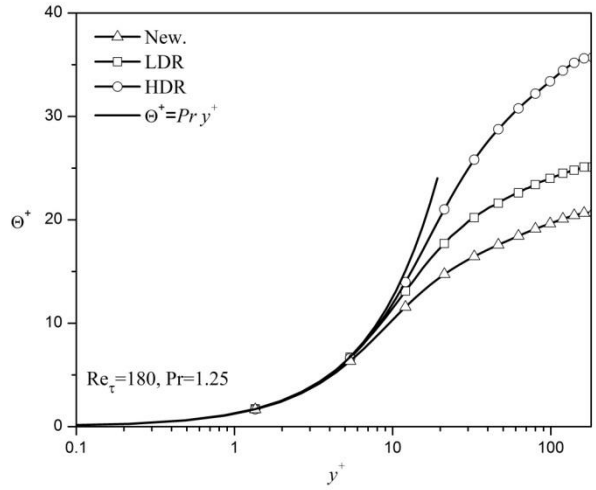

Figure 6.1. DNS data of mean temperature profile for Newtonian (New: H1) and viscoelastic (LDR: H2, HDR: H3) cases. Flow and rheological parameters are described in Table (6.2).

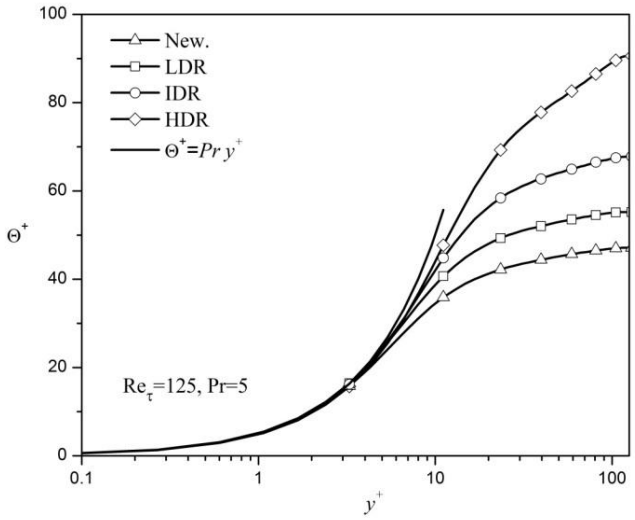

Figure 6.2. DNS data of mean temperature profile for Newtonian (New: H0) and viscoelastic (LDR: H4, IDR: H5, HDR: H6) cases. Flow and rheological parameters are described in Table (6.2).

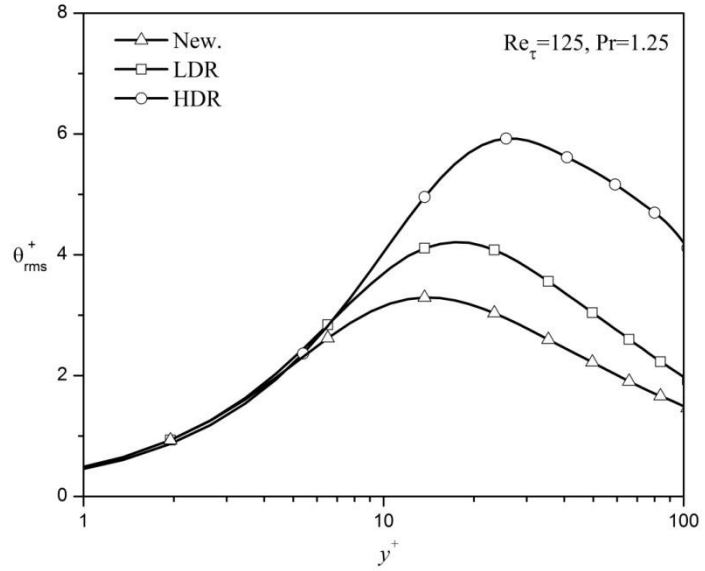

Figure 6.3. Root mean square of temperature fluctuation for Newtonian (New: H1) and viscoelastic (LDR: H2, HDR: H3) cases. Flow and rheological parameters are described in Table (6.2).

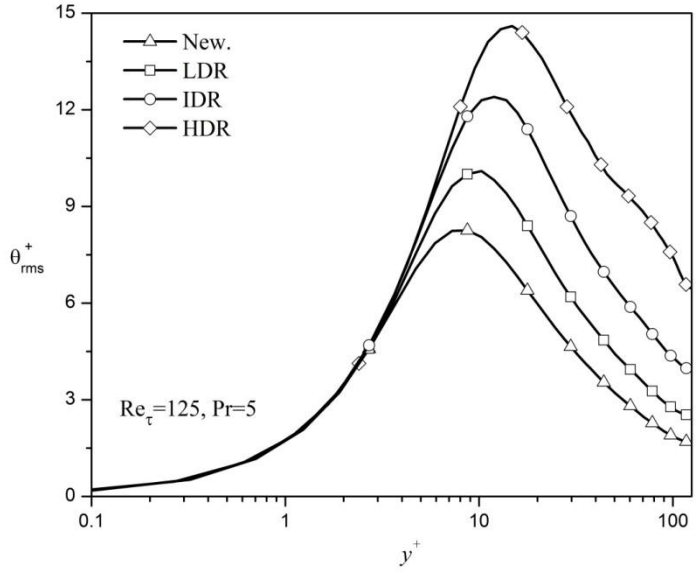

Figure 6.4. Root mean square of temperature fluctuation for Newtonian (New: H0) and viscoelastic (LDR: H4, IDR: H5, HDR: H6) cases. Flow and rheological parameters are described in Table (6.2).

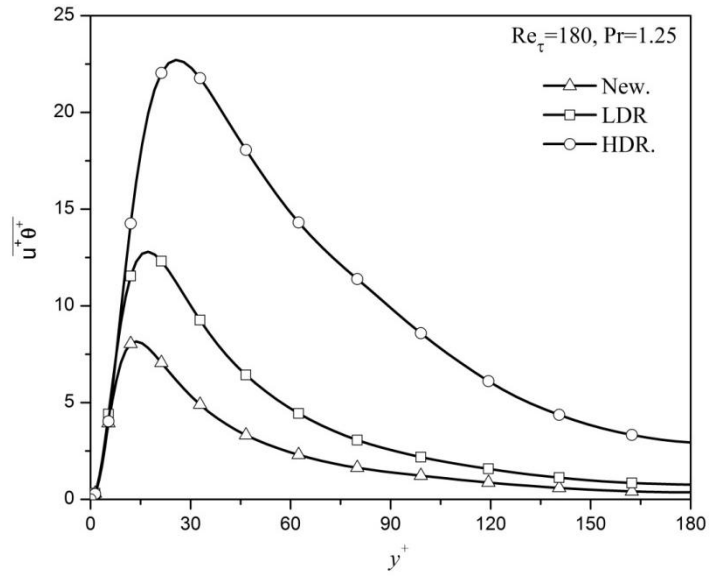

Figure 6.5. Streamwise turbulent heat flux for Newtonian (New: H1) and viscoelastic (LDR: H2, HDR: H3) cases. Flow and rheological parameters are described in Table (6.2).

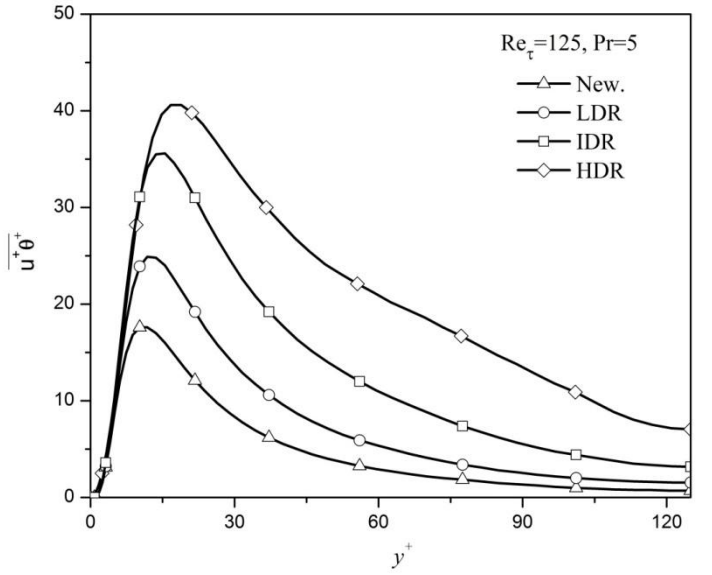

Figure 6.6. Streamwise turbulent heat flux for Newtonian (New: H0) and viscoelastic (LDR: H4, IDR: H5, HDR: H6) cases. Flow and rheological parameters are described in Table (6.2).

Figures 6.3 and 6.4 show that although the overall shape of temperature fluctuation intensity for the viscoelastic cases remains same as Newtonian case, the maximum temperature fluctuation intensity increases and shifts toward bulk flow region by increasing the amount of DR. For instance, the maximum temperature fluctuation intensity of the high

drag reduction case corresponding to Re_τ =125, *Pr*=5, is around 14.6, same quantity for the Newtonian case is around 8.2. The streamwise turbulent heat flux for all cases are plotted in Figures 6.5 and 6.6, as can be seen by increasing the *Pr* number this quantity is enhanced for both Newtonian and viscoelastic cases. The Figures also indicate that the streamwise turbulent heat flux monotonically increases by increasing DR, in agreement with Gupta et al. (2005) and Yu et al. (2005).

The wall normal turbulent heat flux and the conductive heat flux for the Newtonian and high drag reduction cases are plotted in Figure 6.7. As can be observed, unlike the streamwise turbulent heat flux, the wall normal heat flux for viscoelastic fluids is decreasing, comparing with Newtonian case. For the viscoelastic case a shift in the peak location toward the bulk flow can also be observed. Moreover, the Figure shows that the conductive heat flux compensate for the decrease of wall-normal heat flux, meaning the importance of conduction in viscoelastic fluids, particularly at high drag reduction regimes.

It is well known that the thermal structures closely resemble the velocity field structures, i.e. high and low temperature structures are associated with high and low velocity regions, respectively. In Figure 6.8 the iso-surfaces of the instantaneous temperature filed for Newtonian, low and high drag reduction cases are depicted. As can be observed from the Figure the thermal structures become elongated and highly organized by increasing the amount of drag reduction, typical characteristics of polymer dilute solutions. Note that for all cases in Figure 6.8 the threshold of iso-surfaces is 75% of the mean centerline temperature.

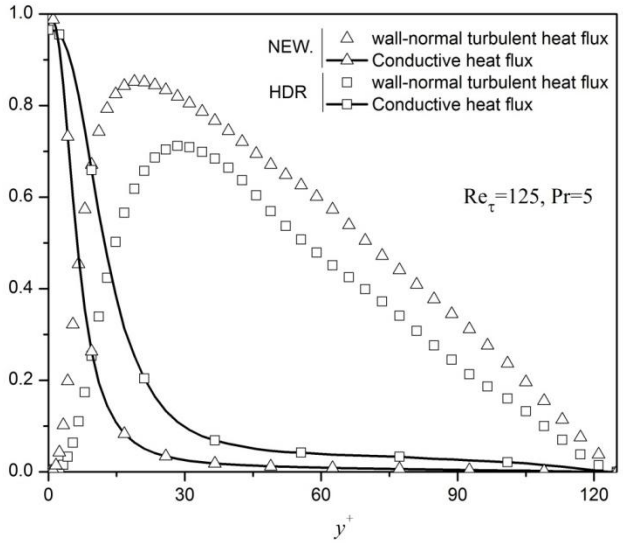

Figure 6.7. Budget of heat flux for Newtonian (New: H0) and viscoelastic (HDR: H6) cases. Flow and rheological parameters are described in Table (6.2).

The budget terms of the transport equation of the temperature variance for Newtonian, low and high drag reduction cases are plotted in Figure 6.9. It is seen that by addition of polymer to the flow although the overall shape and behavior of different terms remain same as Newtonian case, the magnitude and location of the peak location for these terms dramatically are influenced by additives. The Figures further illustrate that by increasing the amount of drag reduction the peak location of all terms shifts toward bulk flow region this shift of the peak location can be interpreted as a thickening of the buffer layer.

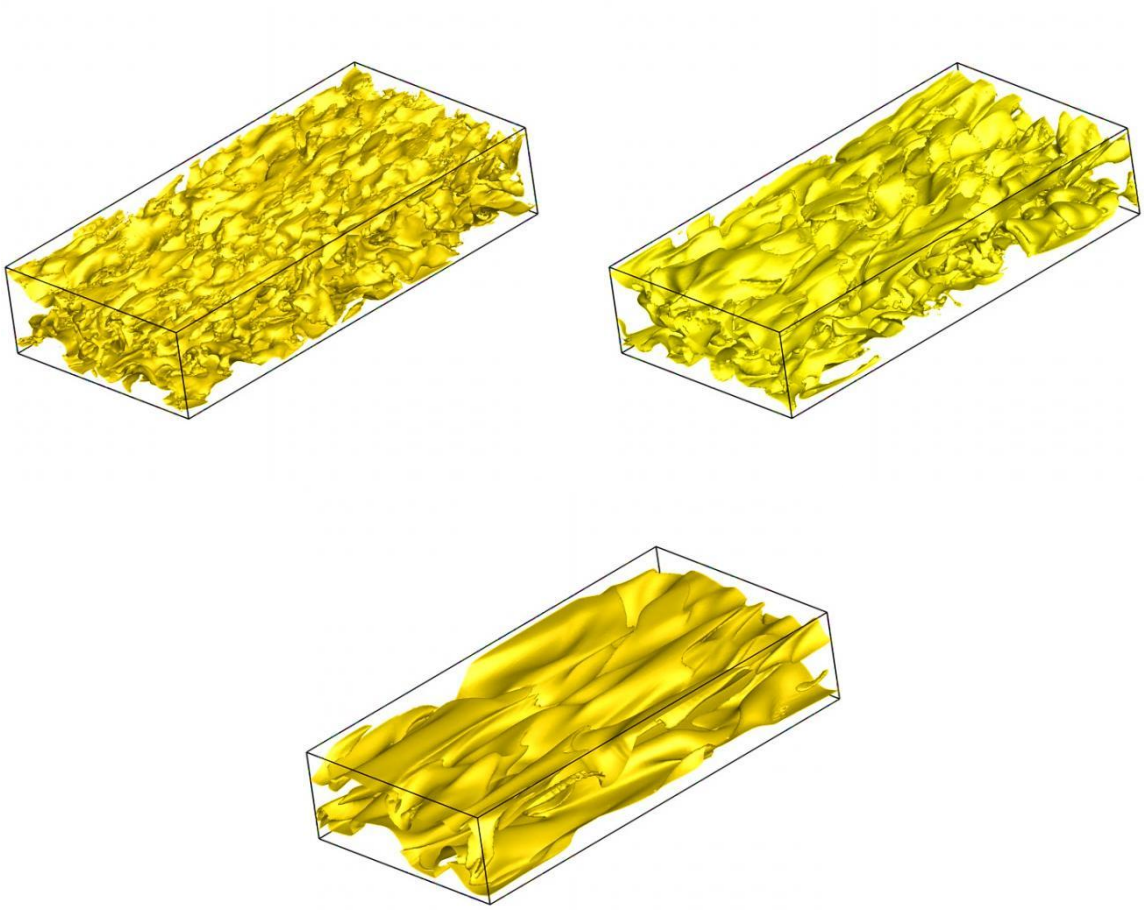

Figure 6.8. Iso-surfaces of the instantaneous temperature filed for Newtonian (H1), low (H2) and high (H3) drag reduction cases.

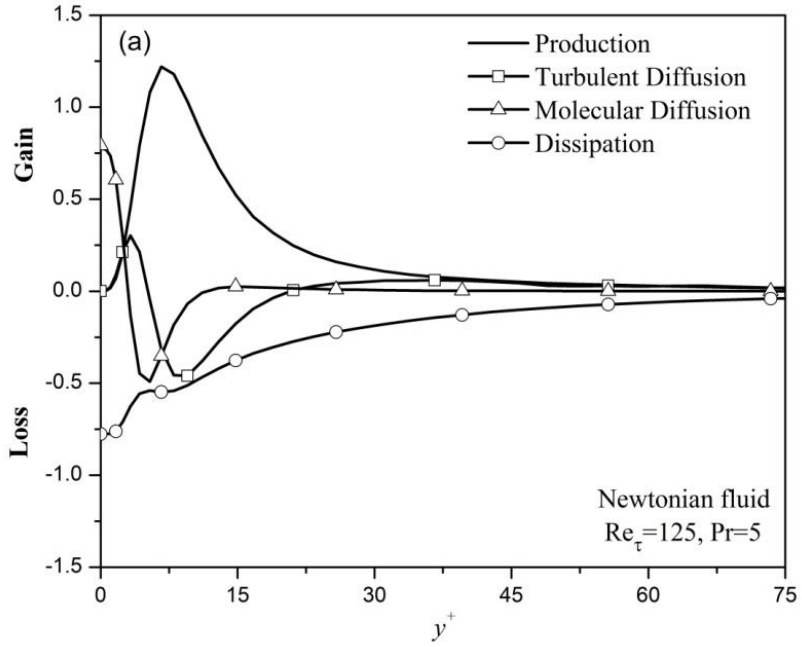
(a)
Production
Turbulent Diffusion
Molecular Diffusion
Dissipation
Gain
Loss
Newtonian fluid
Re$_\tau$=125, Pr=5
y^+

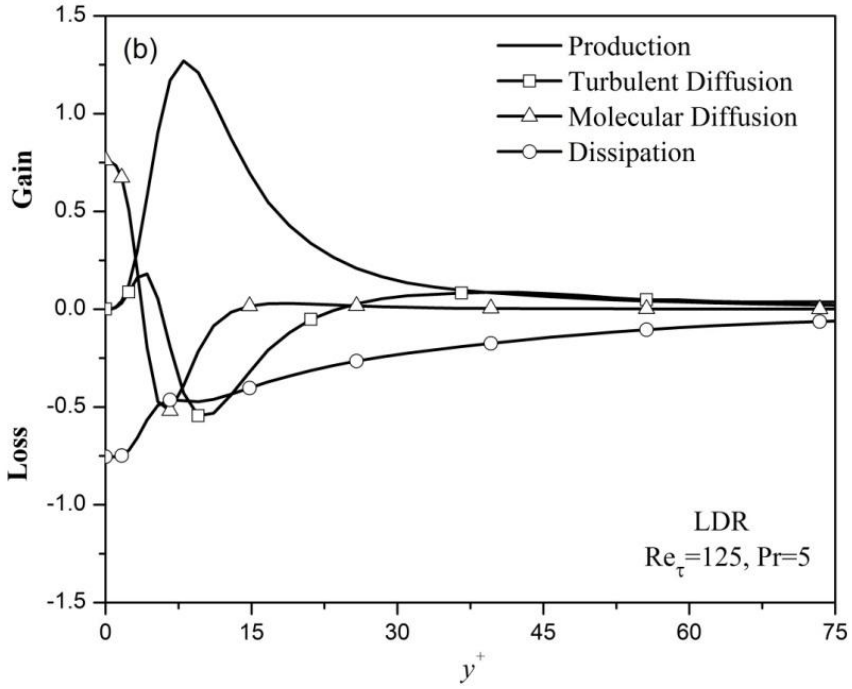
(b)
Production
Turbulent Diffusion
Molecular Diffusion
Dissipation
Gain
Loss
LDR
Re$_\tau$=125, Pr=5
y^+

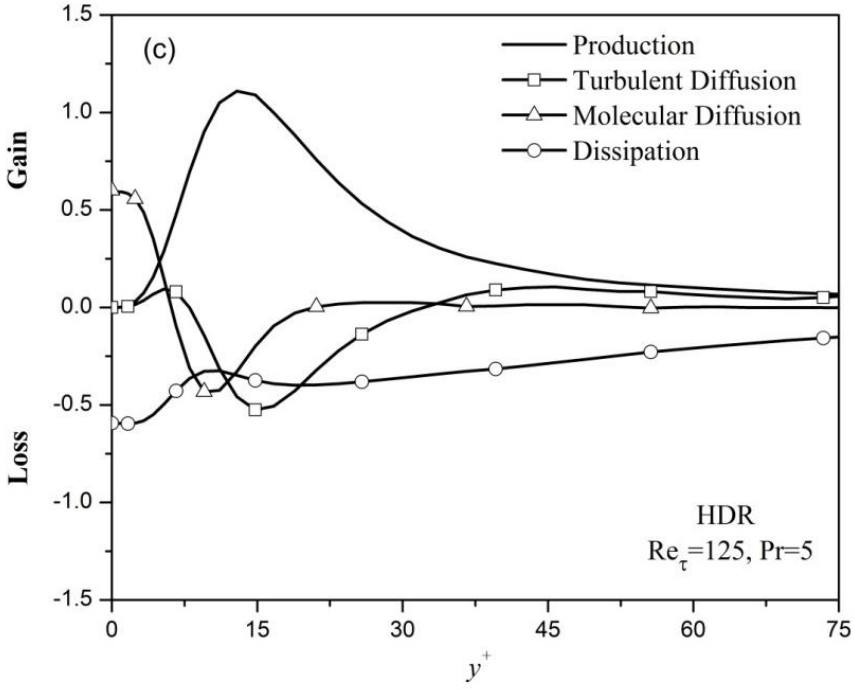

Figure 6.9. Budget terms of temperature variance. (a) Newtonian fluid (H0), (b) low drag reduction case (H4) (c) high drag reduction case (H6).

6.4. Development of the closures

First, we discuss the improvements in the model for predicting the isothermal flow and subsequently, in section 4.3 we discuss the closures required for the heat transfer Reynolds flux.

6.4.1. Improvements of closures needed by constitutive equation

The first term that needs closure is the time-averaged polymer stress, Eq. (6.4). The expanded form of the time-averaged polymer stress is given by,

$$\bar{\tau}_{ij,p} = \frac{\eta_p}{\lambda}\underbrace{\left[f(C_{kk})C_{ij} - f(L)\delta_{ij} \right]}_{term1} + \frac{\eta_p}{\lambda}\underbrace{\left[\overline{f(C_{kk}+c_{kk})(C_{ij}+c_{ij})} - f(C_{kk})C_{ij} \right]}_{term2} \tag{6.21}$$

Both terms on the right-hand-side of Eq. (6.21) were evaluated in Masoudian et al. (2013) and Iaccarino et al. (2010) by using *a priori* DNS data at different values of $Wi_{\tau 0}$ and L^2, and it was shown that the first term, which is exact, is nearly 20 times larger than the second term regardless of the rheological parameters. Consequently, here as in Masoudian et al. (2013) and Iaccarino et al. (2010), $\bar{\tau}_{ij,p}$ is approximated as the first term on the right hand side of Eq. (6.21), and the second term is neglected, hence the Reynolds-averaged polymer stress will be calculated by:

$$\bar{\tau}_{ij,p} = \frac{\eta_p}{\lambda}\left[f(C_{kk})C_{ij} - f(L)\delta_{ij} \right] \tag{6.22}$$

To compute the polymer stress using eq. (6.22) we need the components of the conformation tensor, C_{ij}, and these can be computed directly via the corresponding Reynolds-averaged equation, eq. (6.8). In equation (6.8) all terms are exact except for NLT_{ij}, which is the fluctuating counterpart of M_{ij}, and CT_{ij}, which is discarded for being negligible as Masoudian et al. (2015).

Previous attempts at developing closures for NLT_{ij} in the context of $k-\varepsilon-\overline{v^2}-f$ Masoudian et al. (2013) were based on a simplified representation of the polymer conformation tensor. In particular, they only considered the extension of the chains as characterized by the trace of the C_{ij} tensor, and a separate closure was proposed for the shear component of NLT_{ij} based on the concept of viscoelastic turbulent viscosity to account for the polymer shear stress, the only stress component relevant in turbulent fully-developed channel flow. The complete form of the Reynolds average FENE-P constitutive equation and its exact solution appears in the Appendix A of Pinho et al. (2008).

Since NLT_{kk} accounts for the interactions between the fluctuating components of the conformation tensor and of the velocity gradient tensor, and it is the fluctuating counterpart of M_{ij}, Masoudian et. al (2013) developed a model for the trace of NLT_{ij} as a function of its mean value (M_{kk}) and the eddy viscosity given by:

$$NLT_{kk} = a_{NLT} M_{kk} \frac{\nu_T}{\nu_o}, \quad a_{NLT} = 0.16 \tag{6.23}$$

In this work a general form of closure developed in Masoudian et al. (2013) is proposed by using a Boussinesq like relationship to account influence of NLT_{ij} upon polymer chain extension and orientation via:

$$NLT_{ij} = a_{NLT} \sqrt{L^2} M_{ij} \frac{\nu_T}{\nu_o}, \quad a_{NLT} = 0.04 \tag{6.24}$$

As it can be seen only the square root of the dimensionless polymer maximum extension coefficient is added to the closure of Masoudian et al. (2013). This particular change in the closure for NLT_{ij} was based on a numerical optimization using our DNS database summarized in table (6.1) with the objective function defined as a minimum error in the prediction of drag reduction. In Figure (6.10) this optimized closure is evaluated and compared with the DNS results and with the predictions by the previous closure of Masoudian et al. (2013). As it can be observed from Figure (6.10) the new closure is in good agreement with the DNS results and performs better than the previous closure.

The prediction of the mean polymer extension using the new closure is assessed against DNS data in Figure (6.11), showing again a good agreement with DNS results. It is worth mentioning that, since the polymer stress work in the turbulent kinetic energy equation, as described in Masoudian et al. (2013), is a direct function of NLT_{kk} , the current

improvement in the prediction of NLT_{kk} will benefit the prediction of turbulent kinetic energy.

The Extensive analysis of the performance of the closure will be presented in the result section, and comparison with the DNS data for a wide range of the rheological and flow parameters will be shown. It is worth mentioning that using this model the Reynolds averaged conformation tensor can be calculated now only by using one single constant coefficient which shows the robustness of the present model compared to the previous attempts in this context, all of which need more than one constant coefficient and *ad-hoc* damping functions.

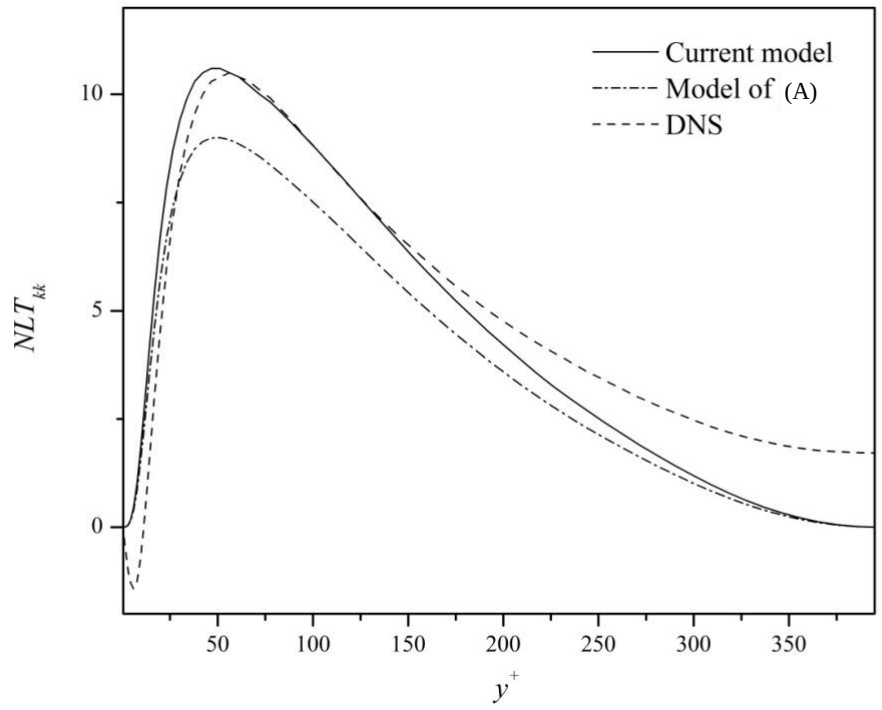

Figure 6.10. Comparison between predicted NLT_{kk} and DNS data for case (19). A: Masoudian et al. (2013)

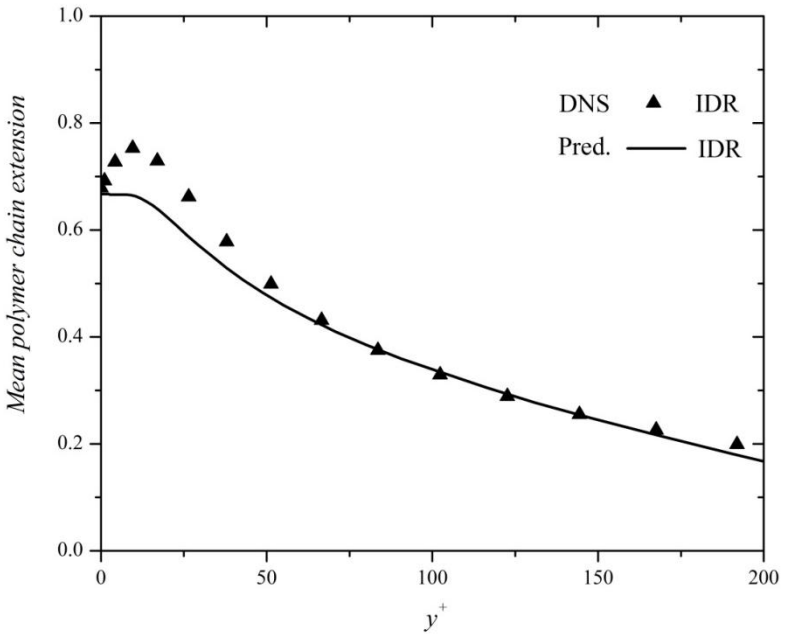

Figure 6.11. Comparison between mean polymer extension and DNS data for case (19).

6.4.2. Improvements of closures needed by the v^2f model

As emphasized, the turbulent kinetic energy and dissipation transport equations contain viscoelastic nonlinear terms, which require modeling. The viscoelastic terms appearing in the turbulent kinetic energy and dissipation equations were modeled using their exact definitions in Masoudian et al. (2013) and the closures tested for a wide range of rheological and flow parameters. There, it was demonstrated that those closures are robust enough to accurately account for the influence of viscoelasticity upon kinetic energy and its dissipation rate, hence they are used here unmodified.

However, the closure of the term accounting for the polymer influence in the transport equation of $\overline{v^2}$, is optimized to improve predictions of the wall normal Reynolds stress. Comparing with the corresponding closure developed in Masoudian et al. (2013) only the constant coefficient and the power exponent of the Peterlin function, which accounts for the influence of the polymer chain extension, are changed. The updated closure is given by,

$$\varepsilon_{p,v2} = a_{v2} L\left[f(C_{kk}) \right]^2 kf, \quad with \;\; a_{v2} = 0.002 \tag{6.25}$$

The predictions of k and $\overline{v^2}$ are plotted and compared with DNS and with the previous closures in Figure 6.12 for the intermediate drag reduction case (IDR). The new predictions of k and $\overline{v^2}$ are in good agreement with DNS data and compare better than those of the previous model of Masoudian et al. (2013). The predictions of Reynolds shear stress and mean streamwise velocity for same IDR case are assessed in Figures 6.13 and 6.14,

respectively. Both Figures show that the model is capable of predicting well both the Reynolds shear stress and the mean velocity. This particular modification in the closure of the viscoelastic term in the $\overline{v^2}$ equation, was performed because of the failure of the previously developed closure Masoudian et al. (2013) in predicting high drag reduction regime at very low Reynolds number flows, namely at $Re_{\tau 0} = 125$, for which the wall normal Reynolds stress is very small. In fact the calculation of high drag reduction flows at low Reynolds numbers using closure of Masoudian et al. (2013) lead to a complete laminarization of the flow. Extensive analyses of the performance of the closure will be presented in the result section.

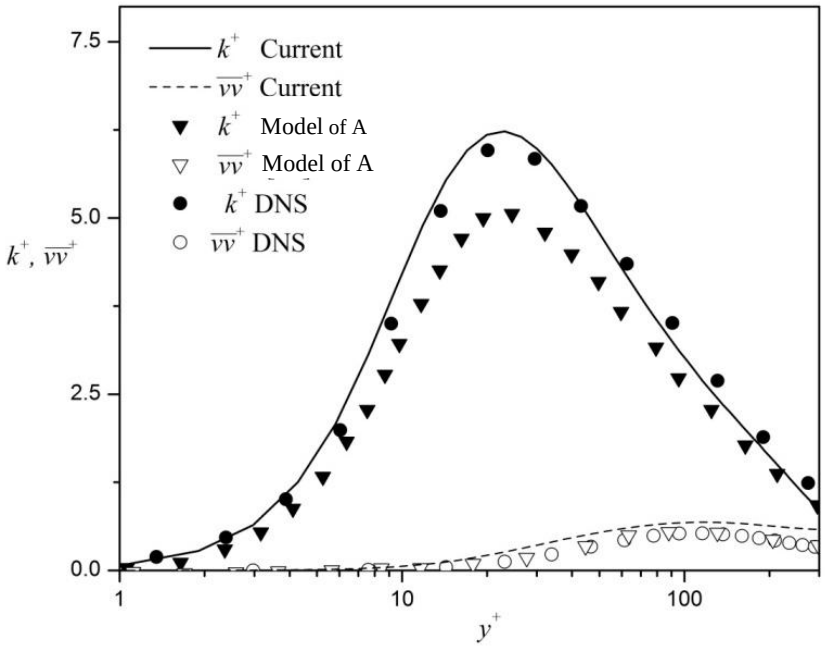

Figure 6.12. Comparison between predicted and DNS data of k^+, $\overline{v^2}$ for case (19). A: Masoudian et al. (2013)

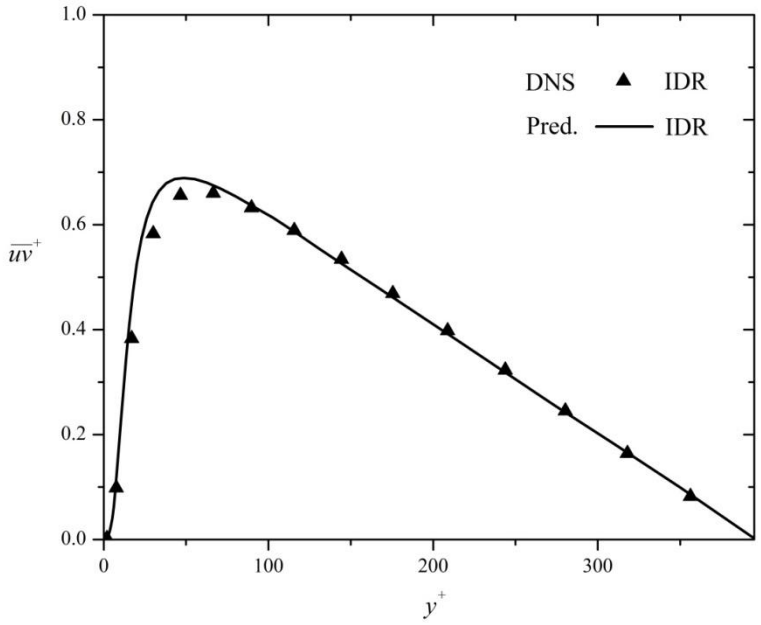

Figure 6.13. Comparison between predicted and DNS data of Reynolds shear stress for case (19).

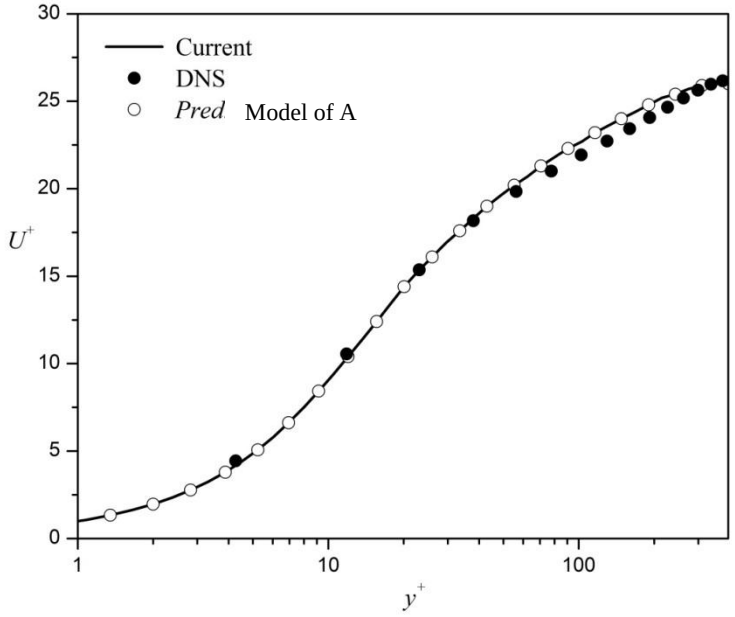

Figure 6.14. Comparison between predicted and DNS data of mean streamwise velocity profile for case (19). A: Masoudian et al. (2013).

6.4.3. Model for the Reynolds scalar flux of viscoelastic fluids

The turbulent thermal energy flux term, $\overline{u_j\theta'^{+}}$, appearing in the time averaged energy equation is non-linear and requires a closure to allow computations of heat transfer. A common and simple way to model thermal flux within the RANS approach is by using the concept of turbulent thermal diffusivity leading to,

$$\overline{u_j\theta'} = \alpha_t \frac{d\Theta}{dx_j} \tag{6.26}$$

where the turbulent thermal diffusivity, α_t, is expressed as a function of the eddy viscosity and a turbulent Prandtl number,

$$\alpha_t = \frac{\nu_t}{\mathrm{Pr}_t} \tag{6.27}$$

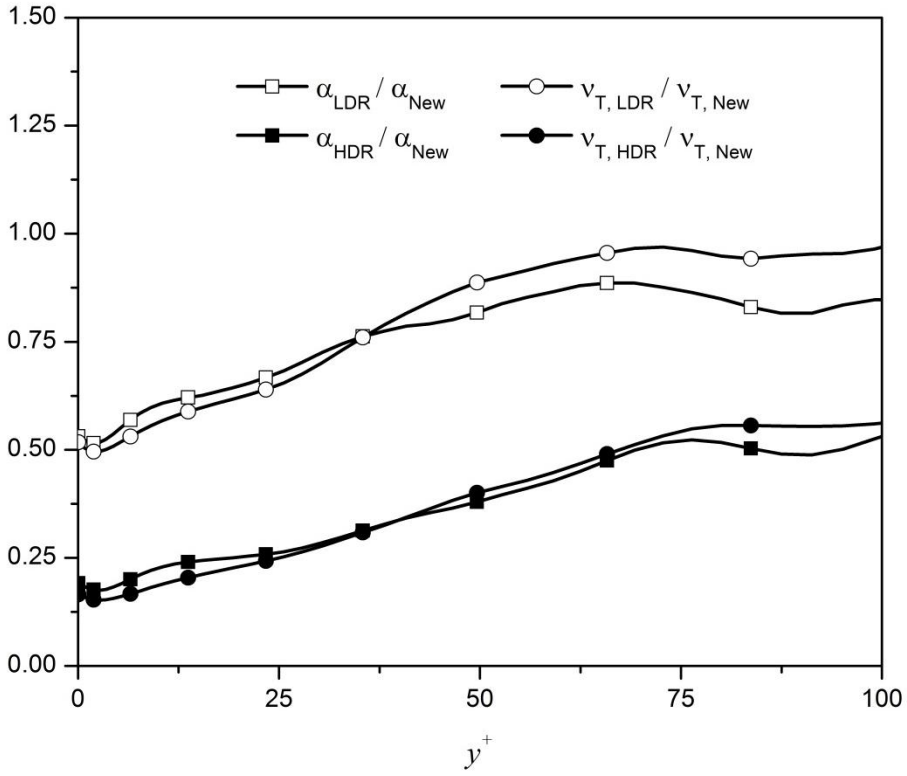

Figure 6.15. Influence of viscoelasticity on turbulent thermal diffusivity.
(LDR: H2, HDR: H3)

In this relation the eddy viscosity is available from the flow turbulence model, so the only unknown term is the turbulent Prandtl number. In order to have an idea about how α_t is influenced in presence of polymer additives, in Figure 6.15 the $\alpha_{viscoelastic} / \alpha_{Newtonian}$ and

$\nu_{T,viscoelastic}/\nu_{T,Newtonian}$ for low and high drag reduction cases are plotted using DNS data. The Figure shows that, as expected, the turbulent thermal diffusivity and turbulent viscosity are decreased by addition of polymers to the flow. Moreover, it is interesting to note that the ratio of turbulent thermal diffusivity almost collapse on the ratio turbulent viscosity, regardless of the amount of drag reduction, indicating that the closures developed for turbulent Prandtl number in the context of Newtonian fluids can be extended to be used in viscoelastic fluids. In this work we adapted one of the commonest closures for the turbulent Prandtl number that was introduced by Kays (1994), which only is based on the local quantities as a function of the turbulent Peclet number,

$$\mathrm{Pr}_t = 0.85 + \frac{0.7}{Pe_t}, \quad where\ Pe_t = \frac{\nu_T}{\nu}\mathrm{Pr} \tag{6.28}$$

Using this closure the energy equation was solved and the mean temperature profiles are plotted in Figure (16) for case H2 and H3, table (6.2). As it can be observed the original proposal of Kays (1994) under predicts the mean temperature for the FENE-P fluids, and shows that the approximation of Eq. (6.28) is no longer valid. As discussed above the turbulent thermal diffusivity, α_t, decreases by increasing DR, to capture this reduction of α_t in viscoelastic fluids in this work using the *a priori* DNS data analyses the extend Kays (1994) proposal has the form of equation (6.29).

$$\mathrm{Pr}_{t,extended} = \mathrm{Pr}_{t,Kays}\left(1 + \frac{a_p \nu_{T,viscoelastic}}{\nu_T}\right) \tag{6.29}$$

In this equation the $\nu_{T,viscoelastic}$ is the viscoelastic turbulent viscosity defined as: $\nu_{T,viscoelastic} = \frac{\tau_{xy,p}}{2\rho S_{xy}}$, and the constant a_p is equal to 2.6 which was quantified based on an iterative numerical optimization in order to achieve minimum error in prediction of mean temperature comparing with DNS data. The predictions of the mean temperature profiles using the extended closure are plotted in Figure 6.16, and compared with DNS and predictions using Kays (1994) original closure for low and high drag reduction cases at Pr=1.25. The Figure illustrates that the predictions using extended closure is in good agreement with DNS results. Note that changes in Kays's turbulent Prandtl number closure were made based on the analyses of the low drag reduction and low Prandtl number case, case H2 table (6.2), and its robustness examined in results section against DNS data for high Prandtl number cases from low to high drag reduction regimes.

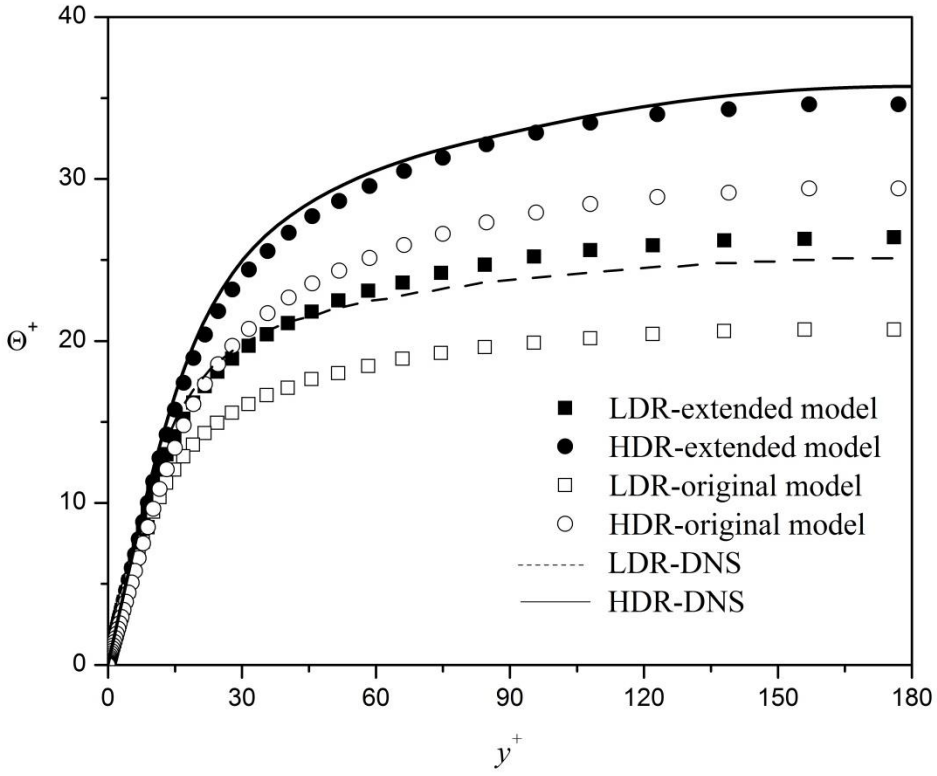

Figure 6.16. Comparison between predicted and DNS data of mean temperature profile using the original and extended closure of Kays (1994) for case (LDR: H2, HDR: H3).

6.4.4. Summary of the model and numerical method

Utilizing the closures developed in the previous section, the model equations are given below.

$$\rho\frac{\partial U_i}{\partial t}+\rho U_k\frac{\partial U_i}{\partial x_k}=-\frac{\partial \bar{P}}{\partial x_i}-\frac{\partial}{\partial x_k}(\overline{\rho u_i u_k})+\frac{\partial \bar{\tau}_{ik}}{\partial x_k} \tag{6.30}$$

$$\frac{D\Theta^+}{Dt}-\frac{\overline{u_1}}{U_m}=\frac{1}{\mathrm{Re}_\tau \,\mathrm{Pr}}\frac{\partial^2\Theta^+}{\partial x_j^2}-\frac{\partial\overline{u_j\theta'^+}}{\partial x_j} \tag{6.31}$$

$$U_j\frac{\partial k}{\partial x_j}=P_{kk}-\varepsilon+\frac{\partial}{\partial x_j}\left(\left(\nu_s+\frac{\nu_T}{\sigma_k}\right)\frac{\partial k}{\partial x_j}\right)-\frac{\eta_p}{2\rho\lambda}f(C_{mm})NLT_{kk} \tag{6.32}$$

$$U_j \frac{\partial \varepsilon}{\partial x_j} = \frac{C_{\varepsilon 1} P_k - C_{\varepsilon 2} \varepsilon}{T_t} + \frac{\partial}{\partial x_j}\left(\left(\nu_s + \frac{\nu_T}{\sigma_\varepsilon}\right)\frac{\partial \varepsilon}{\partial x_j}\right) - \frac{C_{\varepsilon 1}\eta_p}{2\rho\lambda T_t} f(C_{mm}) NLT_{kk} \tag{6.33}$$

$$U_j \frac{\partial \overline{v^2}}{\partial x_j} = kf + \frac{\partial}{\partial x_j}\left(\left(\nu_s + \frac{\nu_T}{\sigma_k}\right)\frac{\partial \overline{v^2}}{\partial x_j}\right) - 6\frac{\varepsilon}{k}\overline{v^2} - a_{v2} L\left[f(C_{kk})\right]^2 kf \tag{6.34}$$

$$f - L_t^2 \frac{\partial^2 f}{\partial x_j \partial x_j} = C_1 \frac{\left(\frac{2}{3} - \frac{\overline{v^2}}{k}\right)}{T_t} + C_2 \frac{P_k}{k} - 5\varepsilon \frac{\overline{v^2}}{k} \tag{6.35}$$

$$U_k \frac{\partial C_{ij}}{\partial x_k} - M_{ij} - NLT_{ij} = -\frac{\bar{\tau}_{ij,p}}{\eta_p} \tag{6.36}$$

Coefficients arising from the Newtonian part of the model take on the same numerical values as reported in Durbin et al. (1996) and listed in Table 6.3.

The computer code used for the present model calculations is based on a finite-volume method using a second-order central difference scheme on a staggered mesh. The Tri-Diagonal Matrix Algorithm (TDMA) solver is used to calculate the solution of the discretised algebraic governing equations. The non-uniform mesh consists of 99 cells across the channel, giving mesh independent results for the low drag reduction case. As mentioned before, in channel flow simulations we only need the trace and shear component of the conformation tensor, so only these components are solved. In order to stabilize the numerical simulation of the conformation tensor the quantity M_{kk} is calculated using the model of Iaccarino *et al.* (2010). The boundary conditions are those of no slip for velocities, k and v^2, whereas for the dissipation by the solvent and f we used the standard conditions for Newtonian fluids as described in Durbin et al. (1996).

6.5. Results and discussion

In this section, predictions of fully-developed channel flow using this model are presented and assessed against DNS data for FENE-P fluids. All viscoelastic flow calculations were carried out using the same flow dimensionless numbers as for the DNS.

The predicted transverse profiles of the mean streamwise velocity for cases corresponding to low and high drag reductions (LDR, and HDR) are plotted in Figure 6.17. The wall Reynolds number for all cases is 395, and the rheological parameters are listed in Table 6.1.

All profiles in the viscous sublayer collapse on the linear distribution $U^+ = y^+$. Further away from the wall the mean velocity of the drag reduced flows increases as compared to that in Newtonian flows. Specifically in the LDR regime, the logarithmic profile is shifted upwards but remains parallel to that of the Newtonian flow as is also found in the DNS results. The upward shift of the logarithmic profile can be interpreted as a thickening of the buffer layer. As it can be observed the predictions and DNS are consistent regardless of the amount of drag reduction. Predictions by the previous closure of Masoudian et al. (2013) are also included in Figure 6.17, and as it can be seen the current model performs better.

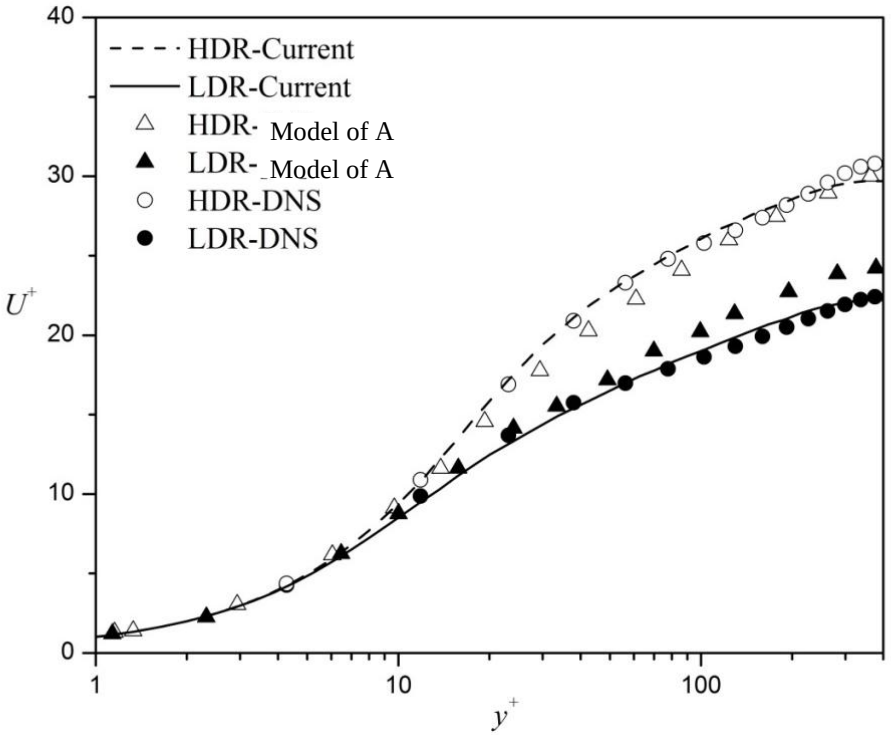

Figure 6.17. Comparison between predicted and DNS data of mean streamwise velocity profile for low and high drag reduction cases, LDR (case 14) and HDR (case 18) respectively. Flow and rheological parameters are described in Table (1). A: Masoudian et al. (2013).

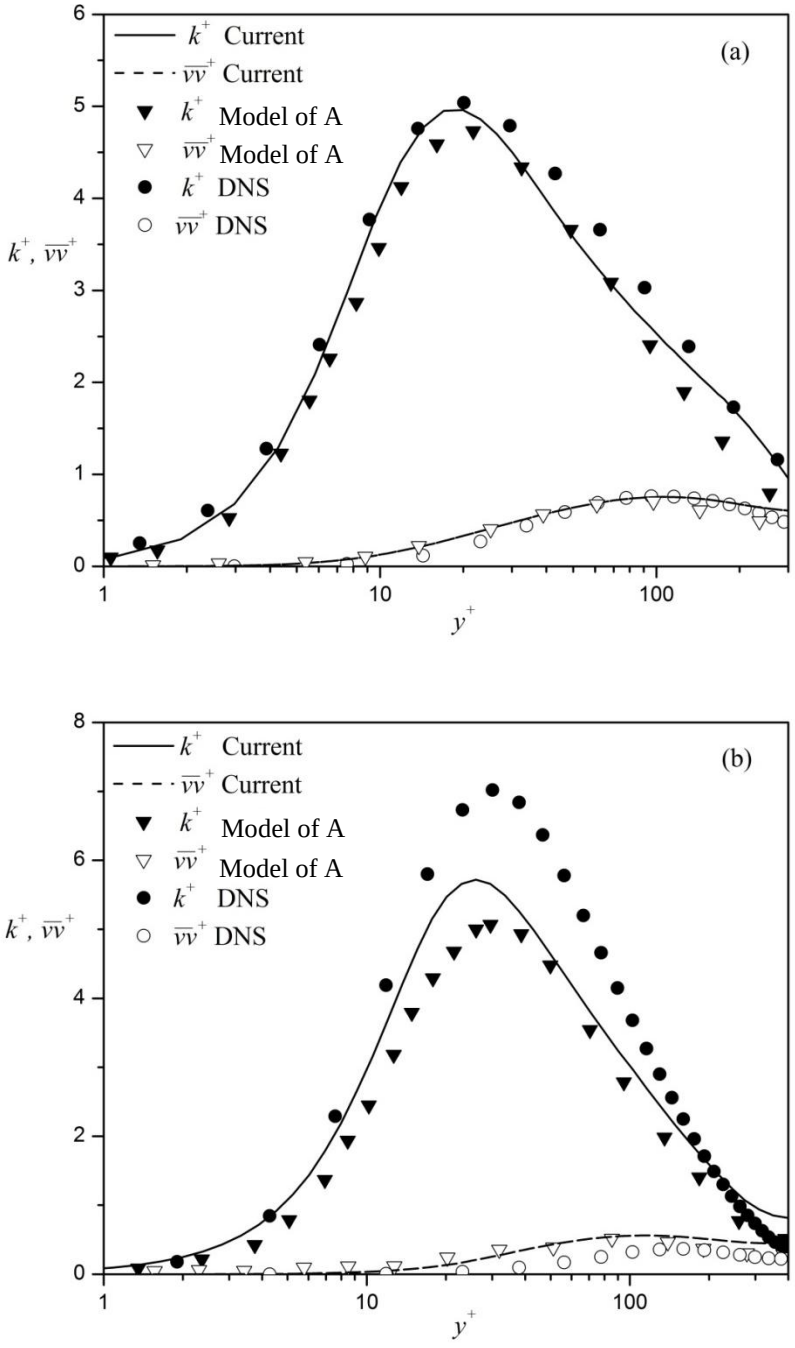

Figure 6.18. Comparison between predicted and DNS data of k^+, $\overline{v^2}$
for (a) LDR: case 14, (b) HDR: case 18. Flow and rheological parameters are described in Table (6.1). A: Masoudian et al. (2013).

Table 6.3. Coefficients needed by the model

Coefficient	Value
C_μ	0.19
σ_k	1.0
σ_ε	1.3
$C_{\varepsilon 1}$	$1.4\left[1+0.05\sqrt{k/\overline{v^2}}\right]$
$C_{\varepsilon 2}$	1.9
C_1	1.4
C_2	0.3
C_L	0.23
C_η	70.0

The predicted profiles of k and $\overline{v^2}$ are compared with the DNS data and with the predictions of the previous model of Masoudian et al. (2013) for LDR and HDR flows in Figure 6.18 (a,b), respectively. It is well known Li et al. (2006) that the turbulent kinetic energy monotonically increases with drag reduction and its peak location moves away from the wall as drag reduction increases, which is consistent with the upward shift of the logarithmic region in the mean velocity profile. This is observed when comparing Figures 6.18 (a-b) and the current predictions improve significantly on the previous predictions approaching the DNS data, with the current model capturing both physical characteristics of turbulent channel flow of dilute polymer solutions in terms of an increase in k and the upward shift of its peak location with drag reduction. Nevertheless and in spite of the noticeable improvement on the prediction of k at high drag reduction, the current model still under-predicts its peak intensity.

In contrast, by increasing drag reduction the Reynolds shear stress is significantly reduced in turbulent polymer dilute solution flows. The predicted Reynolds shear stress profiles are plotted in Figure 6.19, normalized by the wall shear stress for low and high drag reductions and are in good agreement with the corresponding DNS data regardless of the amount of DR. The corresponding predictions of the mean polymer extension (C_{kk}/L^2) are compared with DNS data in Figure 6.20 for LDR and HDR and again the agreement is good.

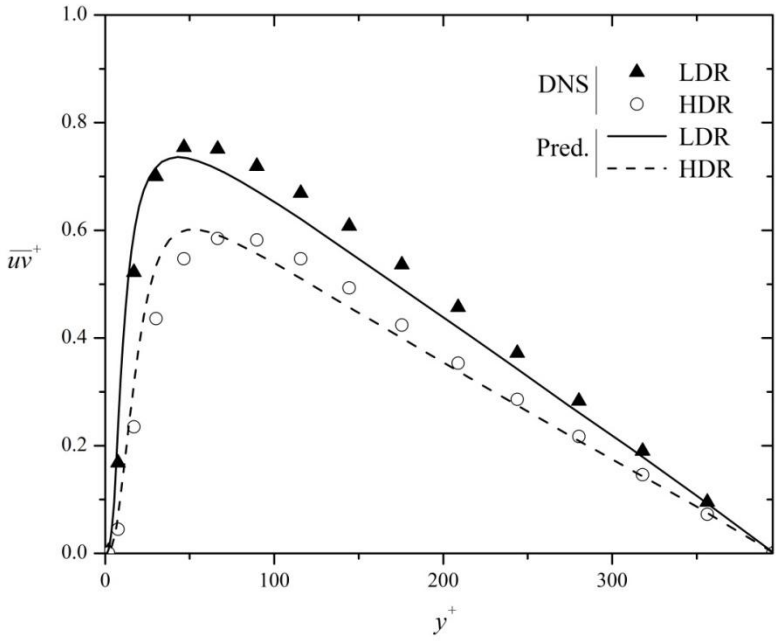

Figure 6.19. Comparison between predicted and DNS data of Reynolds shear stresses for low (LDR: case 14) and high (HDR: case 18) drag reductions cases. Flow and rheological parameters are described in Table (6.1).

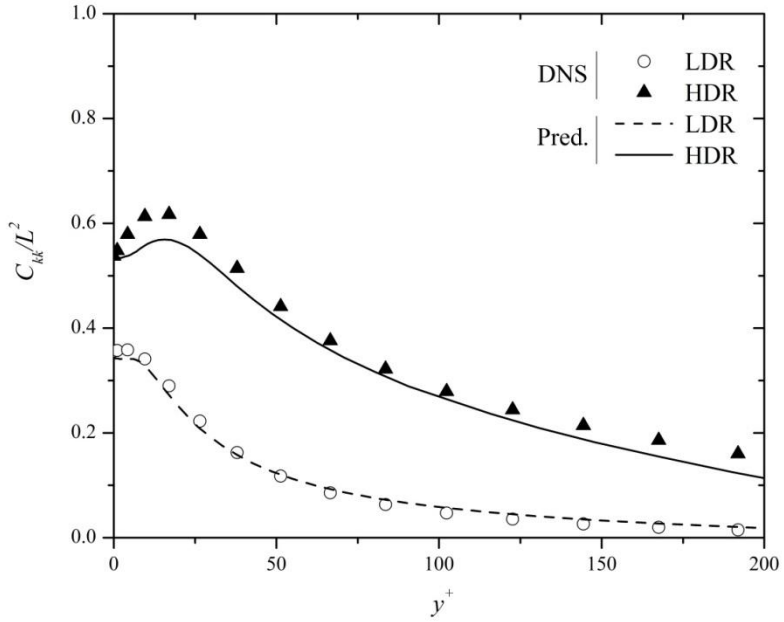

Figure 6.20. Comparison between mean polymer extension and DNS data for low (LDR) and high (HDR) drag reduction cases. Flow and rheological parameters are described in Table (6.1).

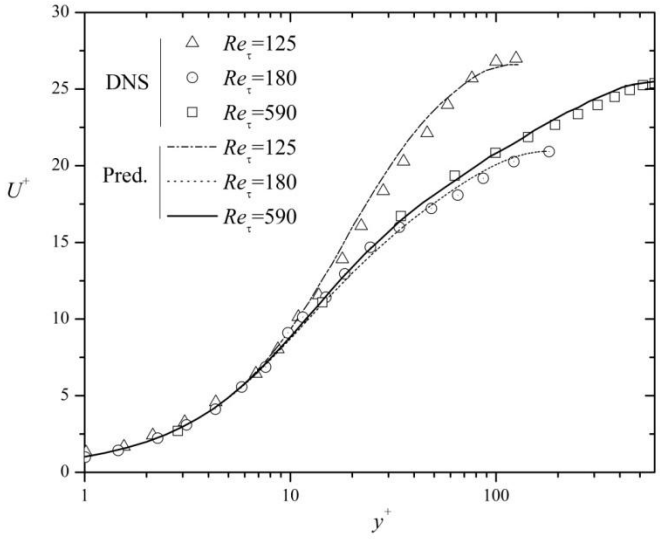

Figure 6.21. Prediction of mean streamwise velocity profile for cases 8, 9, and 20. Flow and rheological parameters are described in Table (6.4).

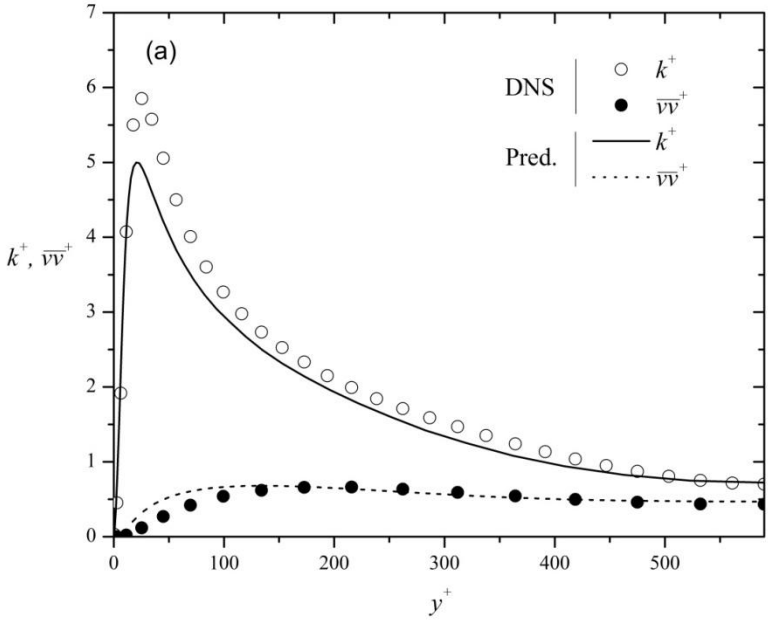

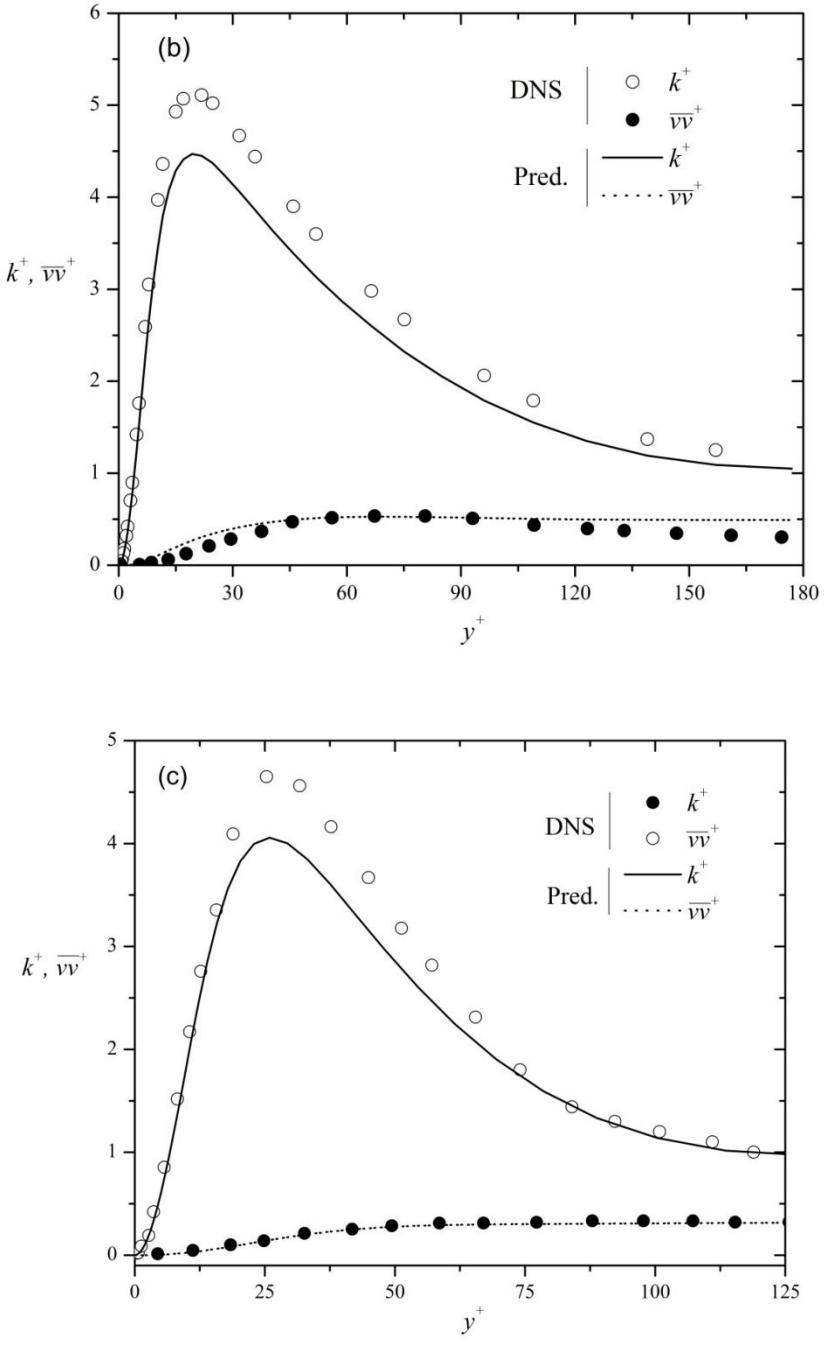

Figure 6.22. Predictions of k^+ and $\overline{v^2}$ a) case (20), b) case (9), and c) case (8). Flow and rheological parameters are described in Table (6.4).

Table 6.4. Comparison of drag reduction prediction levels using the model.

Case	Reference	*Flow and Rheological Properties*			Drag Reduction Predictions	
		$\mathrm{Re}_\tau = \frac{U_\tau h}{\nu_0}$	$Wi_\tau = \frac{U_\tau^2 \lambda}{\nu_0}$	L^2	DNS	Model
(1)	Li et. al (2006)	125	25	900	20 %	19 %
(2)	Li et. al (2006)	125	25	3600	22 %	22 %
(3)	Li et. al (2006)	125	25	14400	24 %	26 %
(4)	Li et. al (2006)	125	50	900	31 %	31 %
(5)	Li et. al (2006)	125	50	3600	43 %	39 %
(6)	Li et. al (2006)	125	50	14400	51 %	46 %
(7)	Li et. al (2006)	125	100	900	37 %	37 %
(8)	Li et. al (2006)	125	100	3600	56 %	51%
(9)	Li et. al (2006)	180	25	900	19 %	19 %
(10)	Li et. al (2006)	180	50	900	31 %	30 %
(11)	Li et. al (2006)	180	100	900	39 %	39 %
(12)	Li et. al (2006)	180	100	3600	54 %	50 %
(13)	Iaccarino et. al (2010)	300	36	10000	35 %	34 %
(14)	Current DNS data	395	25	900	19 %	20 %
(15)	Current DNS data	395	50	900	30 %	29 %
(16)	Current DNS data	395	50	3600	38 %	38 %
(17)	Current DNS data	395	100	900	37 %	36 %
(18)	Current DNS data	395	100	3600	48 %	46 %
(19)	Current DNS data	395	100	14400	61 %	58 %
(20)	Current DNS data	590	50	3600	39 %	38 %
(21)	Thais et. al (2013)	1000	50	900	30 %	30 %

The present turbulence model compares well with DNS data in terms of overall drag reduction; a collection of representative calculations is reported in Table 6.4. In total 21 cases including current DNS data and independent DNS data are gathered and the performance of the model investigated. As it can be seen the wide range of Reynolds number (125 <Re< 1000) with different amount of drag reduction are tested to examine the robustness of the model. For the sake of comparison for three cases at different Reynolds numbers (cases 8, 9, 20) the predictions of the U^+, k^+ and $\overline{v^2}$ profiles are plotted in Figure 6.21 and 6.22, respectively, and compare well with the corresponding DNS data.

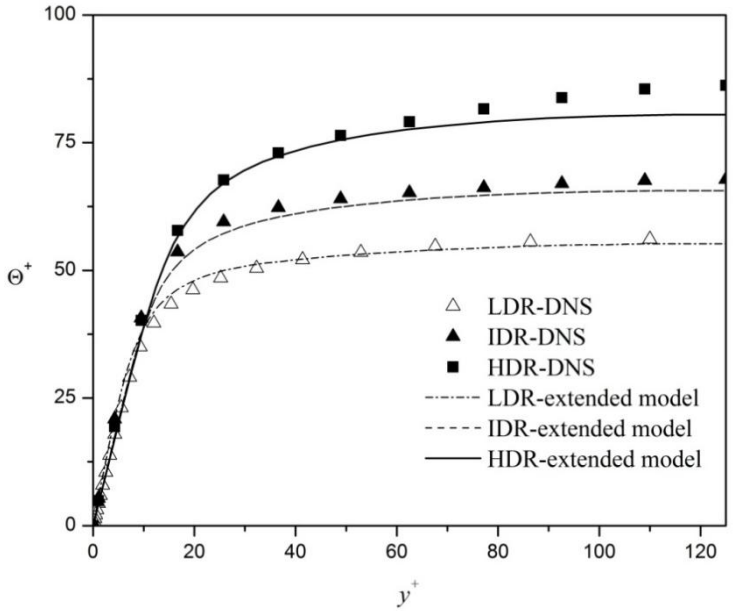

Figure 6.23. Comparison between predicted and DNS data of mean temperature profile using extended closure of Kays (1994) for cases, LDR (H4) IDR (H5), and HDR (H6). Flow and rheological parameters are described in Table (6.2).

The predicted profiles of the mean temperature using the extended model of the Kays (1994) for cases H4, H5, and H6, corresponding to low, intermediate and high drag reductions (LDR, IDR, and HDR), are plotted in Figure 6.23. The wall Reynolds number for all cases is 125, molecular Prandtl number is 5, and the rheological parameters are listed in Table 6.2. For all cases the fully-developed temperature profiles are in good agreement with the DNS data both close and far from the wall.

6.6. Conclusions

In this work, the *k*-ε -$\overline{v^2}$ -*f* model developed by Masoudian *et al.* (2013), for turbulent flow of homogenous polymer solutions described by the FENE-P constitutive model, was improved. In addition, an appropriate closure was developed to compute the scalar Reynolds flux required by the thermal energy equation for the same fluids.

All previous attempts of RANS modeling of turbulent FENE-P fluid flows in a channel, which are valid up to the maximum drag reduction limit Masoudian et al. (2013) and Iaccarino et al. (2010), contain two separate closures for the nonlinear term (NLT_{ij}) in the conformation tensor evolution equation: one closure for the NLT_{kk} and another for NLT_{xy}, which makes the model unattractive to be used in complex geometries. Instead, in this work a single Boussinesq like relation is proposed for modeling the NLT_{ij} term, from which its trace can also be obtained thus making the model fully consistent.

Furthermore, since the closures are based on the *a priori* analysis of DNS data, a more extensive set of direct numerical simulations with different rheological parameters and at different Reynolds numbers was used to optimize the closures initially developed in Masoudian et al. (2013)**.** As a consequence of this optimization process the closure for the wall normal polymer stress work was updated, which gives the current version of the model the capability of good prediction at very low Reynolds number flows. Moreover, the dependency of the previous model of Masoudian et al. (2013) on the wall friction velocity was removed to make the model more suitable to deal with complex geometries.

The performance of the proposed model is here assessed against 21 sets of DNS data for $Re_{\tau 0} = 128, 180, 300, 395, 590,$ and 1000 over a wide range of Weissenberg numbers for different values of L^2 as summarized in Table 6.4, thus confirming the robustness of the current model.

Regarding the Reynolds scalar fluxes, to the best of our knowledge this is the first ever closure used to deal with the heat transfer of FENE-P fluids under turbulent flow conditions. The commonly used turbulent Prandtl number closure originally developed by Kays (1994) for Newtonian fluids was extended to deal with viscoelastic turbulent flows after an extensive a priori analysis of DNS data. The model for the turbulent Prandtl number of FENE-P fluids was developed here for low drag reduction case at $Re_{\tau 0} = 180$, but its performance was assessed against sets of DNS data from low to high drag reduction and higher Prandtl numbers (Pr=5), a value closer to that of polymer solutions. In this assessment, the Reynolds scalar flux model compared well with DNS.

7

Chapter 7:
Conclusions and future work

"Nothing in life is to be feared, it is only to be understood. Now is the time to understand more, so that we may fear less."
—Marie Curie

This thesis is aimed at increasing the current knowledge on wall turbulence of homogeneous viscoelastic fluids, here described by the FENE-P rheological constitutive model, and to develop turbulence models for the prediction of their flows. Over the next pages these contributions are summarized in more detail.

I. DNS database

A large number of DNS cases (as far as we are aware of, one of the most complete DNS sets in the field) of isothermal turbulent flow and turbulent flow with heat transfer of viscoelastic fluids in a channel were performed in this work to analyze the main characteristics of turbulent flow and heat transfer of polymer dilute solutions. These DNS cases cover the whole range of drag reduction from low (12%) to the high drag reduction (75%) and from low to high Reynolds numbers (Re_τ=590). This DNS database was generated to be used to help understand the turbulent flow characteristics through *a-priori* analyses, and to help develop and validate new and better turbulence models in the context of RANS. The *a-priori* analyses focused on the behavior of non-linear terms in the instantaneous and averaged/ filtered governing equations which is the key for development of reliable turbulent viscoelastic models in the context of RANS or LES. The diagram of Figure 7.1 briefly shows how this DNS database sheds light on the path of pursuing current and future research work in developing RANS or LES models.

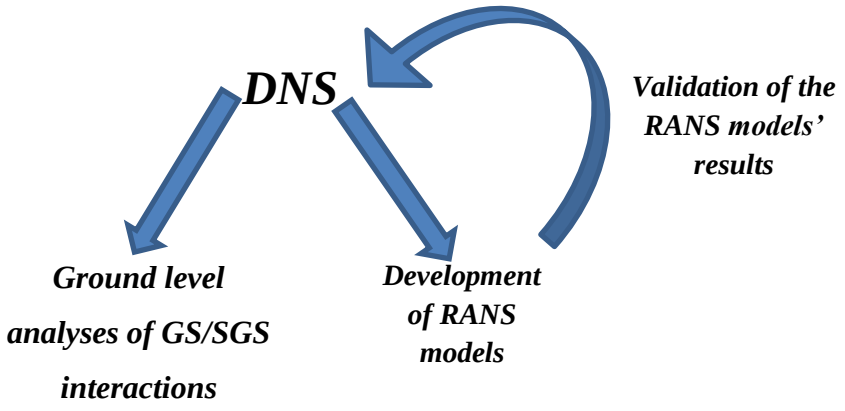

Figure 7.1. Brief explanation of usefulness of DNS data base.

II. Ground level analyses of GS/SGS interactions

As mentioned earlier there is as yet no SGS model to account for the influence of viscoelasticity on fluid flow, hence *a-priori* analyzes of the filtered momentum and FENE-P constitutive equations were performed for the first time to establish ground level analyses for future attempts in the context of LES. The influence of the polymer additives on the subgrid-scale (SGS) energy is evaluated by comparing the Newtonian and the viscoelastic

flows. All the terms of the transport equation of the SGS kinetic energy for FENE-P fluids were analyzed and suggestions for modeling purposes were proposed. In short this part of the work provided background knowledge, but at the same time it open a window for development of the SGS models for viscoelastic non-Newtonian fluids in the near future.

III. RANS models for FENE-P fluids

In this work RANS turbulence models were developed for turbulent viscoelastic fluids described by FENE-P constitutive equation. More specifically, the k-ε-$\overline{v^2}$-f turbulence model introduced by Durbin (1993) and Reynolds stress model of Lai and So (1990) are extended to account for the influence of polymer additives. Furthermore, recent DNS of fluid flow and heat transfer of FENE-P fluids were used to devise the first RANS closure for the Reynolds scalar fluxes for heat transfer in turbulent viscoelastic fluids.

Comparing the viscoelastic k-ε-$\overline{v^2}$-f model developed in this work with the previous attempts in development of viscoelastic RANS models (Pinho et al. (2008), Resende et al. (2011), and Iaccarino et al. (2010)) the model developed here shows significant improvement in the prediction of mean flow statistics. More specifically, the previous models of Pinho et al. (2008), and Resende et al. (2011) are valid only in the low and intermediate drag reductions (up to about 35%), whereas the model developed in this thesis is valid up to the maximum drag reduction limit, and additionally the closures developed for non-linear terms are robust and numerically stable. Comparing with the model of Iaccarino et al. (2010) the model developed in this work uses a Boussinesq like relation (for the first time) to model the non-linear term in FENE-P constitutive equation, which leads to a significant improvement in prediction of mean polymer stresses, while maintaining model simplicity.

A robust second order Reynolds-Stress Model (RSM), valid up to the high drag reduction limit, was developed for the first time for turbulent viscoelastic flows described by FENE-P model. An important contribution of this model is the development of a single closure for the nonlinear fluctuating terms appearing in the FENE-P constitutive equation. All the closures developed in this work are based on the mean and instantaneous analyses of the DNS data, hence the developed closures are reliable. The polymer stresses, velocity profiles, turbulent flow statistics and drag reduction intensity predicted by the RSM model are in good agreement with present DNS data and independent DNS data from the literature over a wide range of rheological and flow parameters.

Furthermore, as far as we are aware of, there is no RANS model to deal with heat transfer in turbulent flows of viscoelastic fluids, so in this work such a model was developed for the first time. Here, the Newtonian closure of Kays (1993, 1994) was extended to cope with viscoelastic fluids. The DNS data base for channel flow of viscoelastic fluids pertaining to low, intermediate and high drag reductions was extended to

include the DNS solution of the instantaneous energy equation and its results then used to develop a model, as it allowed the detailed quantification of terms in the relevant transport equations for heat transfer in viscoelastic turbulent flows. All predictions by this new turbulent heat transfer model are in good agreement with DNS data over a wide range of Prandtl numbers.

Currently, the vast majority of DNS investigations of turbulent viscoelastic flows concern fully developed channel flow and homogeneous turbulence, both forced and decaying. DNS of turbulent FENE-P fluid flows in other geometries involving wall-free turbulence, such as turbulent jet flow (see fig. 7.2), recirculating flow such as flow over a backward-facing step, or flows with rotation or acceleration of the mean flow are scarce or unknown. Knowledge on these flows are fundamental both to increase our understanding of turbulence of polymer solutions and to help developed and test the performance of closures required to make the turbulence models as general as possible to deal with real turbulent flows that combine those fundamental features as wall-dominated and wall-free turbulence.

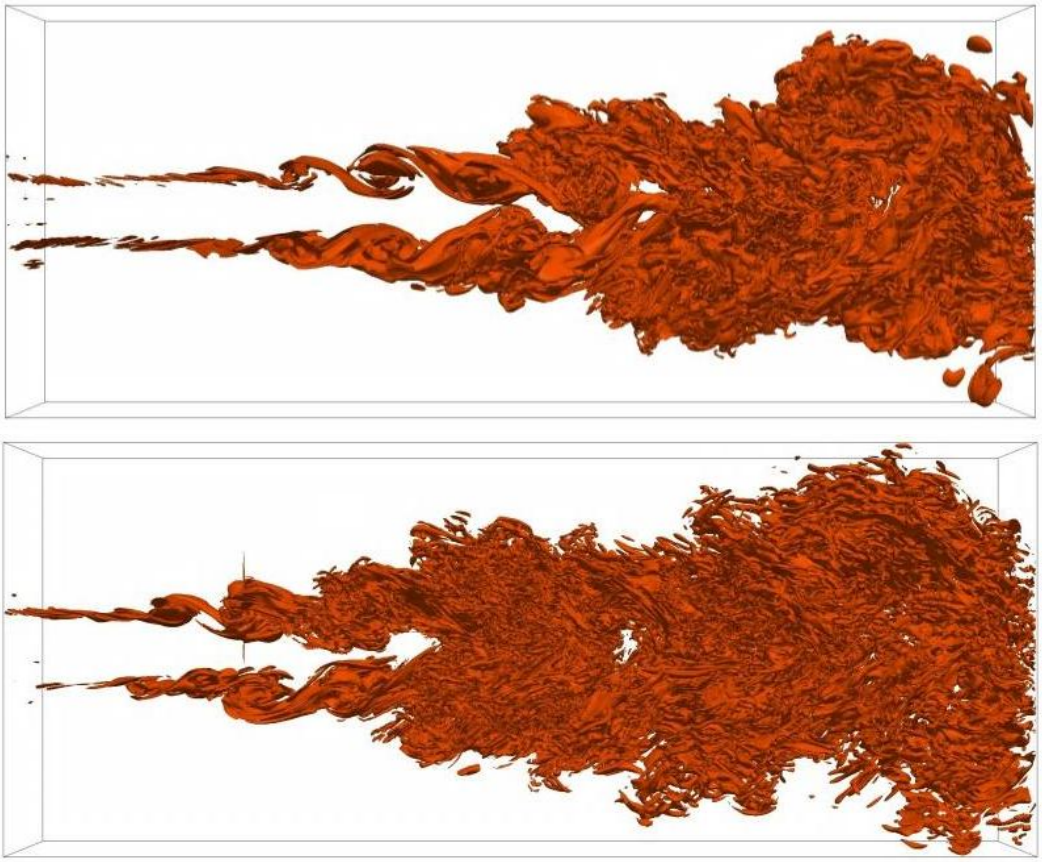

Figure 7.2. DNS of turbulent jet flow (vorticity field above: Newtonian, below Non-Newtonian). Simulation performed during the last year in collaboration with LASEF center in IST.

DNS of such a variety of flows will allow a better understanding of turbulence of polymer solutions, but also the improvement of closures, some of which respond specifically to certain types of flow forcing.

In terms of turbulence modeling for viscoelastic fluids, most effort has also been put forward on the development of closures for Reynolds-averaged equations, but nowadays,

large eddy simulation stands as a major method of computing engineering flows and consequently the development of adequate closures for LES is needed. The number of existing SGS models to account for the influence of viscoelasticity upon turbulent flows is very limited and usually they have been developed on an ad-hoc basis. The development of SGS models for viscoelastic fluids is a major research direction compounded with the previously identified need to investigate the behavior of turbulence of polymer solutions in flows other than the fully-develop channel/ pipe flow. This merely follows the path previously taken for the understanding of turbulence and the development of the corresponding models for Newtonian fluids. An important first step was given here through the analysis of the interaction between large and small scales via filtered governing equations and suggestions for the development of reliable SGS models.

The rheological description of dilute and semi-dilute of polymer solutions is in itself a topic of research. Most of the numerical and theoretical investigation of turbulence with polymer solutions relies on simplified representations of the fluid rheology. A constitutive model such as the FENE-P is a very simplified version of the more accurate, but still simple mesoscopic FENE equation based on the representation of ensembles of molecules as dumbbells. The experiments of Ptasinski et al. (2002) have shown the streamwise turbulence (u_{rms}) to increase slightly with DR, whereas DNS results using the FENE-P model over-predict those peak values significantly. Investigations on the performance of the FENE-P closure of the FENE dumbbell have shown the shortcomings of the Peterlin approximation, such as the removal of the hysteresis and the differences in extensional rheology, features that certainly affect the vortex dynamics, and consequently the turbulent flow characteristics. Consequently, it is necessary to investigate through DNS both wall and wall-free turbulence using a more exact description of polymer rheology such as with the FENE model or even better bead-spring and/ or bead-rod models. Then, based on such expensive DNS simulations, turbulence closures need to be developed to be inserted in the governing equations of the simplified averaged FENE constitutive equation, like the FENE-P equation, to allow for speedy engineering calculations.

Finally, experimental data shows that polymer solutions are easily degradable and this limits their application in some engineering processes, such as district heating and cooling systems. Alternatively, similar drag and heat transfer reductions can be obtained with solutions of worm-like micelles, but again experimental data for pipe/ channel flows have shown differences relative to what is observed with polymer solutions (for instance, the maximum drag and heat transfer reductions is higher for surfactants than for polymer solutions). This will necessarily imply differences in rheology and in its description, as have been under development by several research groups, so the turbulent flow characteristics need to be investigated with these other constitutive equations that better describe the rheology of solutions of worm-like micelles.

Needless to say, the numerical investigations of the flow characteristics of polymer solutions and surfactant solutions in the new flows referred to above (backward-facing step, jets, rotating flows, accelerating flows) requires also experimental data for validation.

Bibliography

- ✓ Baldwin, B. S., & Lomax, H. (1978). Thin layer approximation and algebraic model for separated turbulent flows, AIAA Paper 02/1978; 78.
- ✓ Berger, T. W., Kim, J., Lee, C., & Lim, J. (2000). Turbulent boundary layer control utilizing the Lorentz force. Physics of Fluids (1994-present), 12(3), 631-649.
- ✓ Bewersdorff, D. I. H. (1982). Effect of a centrally injected polymer thread on drag in pipe flow. In Progress and Trends in Rheology (pp. 233-235). Steinkopff.
- ✓ Bewersdorff, H. W. (1984). Heterogene Widerstandsverminderung bei turbulenten Rohrströmungen. Rheologica acta, 23(5), 522-543.
- ✓ Bird, R. B., Armstrong, R. C., Hassager, O., & Curtiss, C. F. (1977). Dynamics of polymeric liquids (Vol. 1, p. 210). New York: Wiley.
- ✓ Bird, R. B., Dotson, P. J., & Johnson, N. L. (1980). Polymer solution rheology based on a finitely extensible bead—spring chain model. Journal of Non-Newtonian Fluid Mechanics, 7(2), 213-235.
- ✓ Beris, A. N., & Edwards, B. J. (2013). Thermodynamics of flowing systems: with internal microstructure, University Press, Oxford.
- ✓ Cai, W. H., Li, F. C., & Zhang, H. N. (2010). DNS study of decaying homogeneous isotropic turbulence with polymer additives. Journal of Fluid Mechanics, 665, 334-356.
- ✓ Cardy, J., Falkovich, G., Gawedzki, K., Nazarenko, S., & Zaboronski, O. V. (2008). Non-equilibrium statistical mechanics and turbulence (Vol. 355). Cambridge University Press.
- ✓ Casciola, C. M., & De Angelis, E. (2007). Energy transfer in turbulent polymer solutions. Journal of Fluid Mechanics, 581, 419-436.
- ✓ Castro, W., & Squire, W. (1968). The effect of polymer additives on transition in pipe flow. Applied Scientific Research, 18(1), 81-96.
- ✓ Davidson, L. (2006). Transport equations in incompressible URANS and LES, University Press, Chalmers.
- ✓ Davidson, L. (1997, September). Large eddy simulation: a dynamic one-equation subgrid model for three-dimensional recirculating flow. In 11th International Symposium on Turbulent Shear Flow, Grenoble, France (Vol. 3, pp. 26-1).
- ✓ da Silva, C. B., & Métais, O. (2002). On the influence of coherent structures upon interscale interactions in turbulent plane jets. Journal of Fluid Mechanics,473, 103-145.
- ✓ De Gennes, P. G. (1990). Introduction to polymer dynamics. CUP Archive.
- ✓ De Angelis, E., Casciola, C. M., L'vov, V. S., Piva, R., & Procaccia, I. (2003). Drag reduction by polymers in turbulent channel flows: Energy redistribution between invariant empirical modes. Physical Review E, 67(5), 056312.
- ✓ De Angelis, E., Casciola, C. M., Benzi, R., & Piva, R. (2005). Homogeneous isotropic turbulence in dilute polymers. Journal of Fluid Mechanics, 531, 1-10.

- ✓ Dimitropoulos, C. D., Dubief, Y., Shaqfeh, E. S., Moin, P., & Lele, S. K. (2005). Direct numerical simulation of polymer-induced drag reduction in turbulent boundary layer flow. Physics of Fluids (1994-present), 17(1), 011705.
- ✓ Dimitropoulos, C. D., Sureshkumar, R., & Beris, A. N. (1998). Direct numerical simulation of viscoelastic turbulent channel flow exhibiting drag reduction: effect of the variation of rheological parameters. Journal of Non-Newtonian Fluid Mechanics, 79(2), 433-468.
- ✓ Dimitropoulos, C. D., Sureshkumar, R., Beris, A. N., & Handler, R. A. (2001). Budgets of Reynolds stress, kinetic energy and streamwise enstrophy in viscoelastic turbulent channel flow. Physics of Fluids (1994-present), 13(4), 1016-1027.
- ✓ Dubief, Y., White, C. M., Terrapon, V. E., Shaqfeh, E. S., Moin, P., & Lele, S. K. (2004). On the coherent drag-reducing and turbulence-enhancing behaviour of polymers in wall flows. Journal of Fluid Mechanics, 514, 271-280.
- ✓ Durbin, P. A. (1991). Near-wall turbulence closure modeling without "damping functions". Theoretical and Computational Fluid Dynamics, 3(1), 1-13.
- ✓ Frohnapfel, B., Jovanović, J., & Delgado, A. (2007). Experimental investigations of turbulent drag reduction by surface-embedded grooves.Journal of Fluid Mechanics, 590, 107-116.
- ✓ Fureby, C., Tabor, G., Weller, H. G., & Gosman, A. D. (1997). Differential subgrid stress models in large eddy simulations. Physics of Fluids (1994-present), 9(11), 3578-3580.
- ✓ Deardorff, J. W. (1972). Numerical investigation of neutral and unstable planetary boundary layers. Journal of the Atmospheric Sciences, 29(1), 91-115.
- ✓ Deardorff, J. W. (1974). Three-dimensional numerical study of turbulence in an entraining mixed layer. Boundary-Layer Meteorology, 7(2), 199-226.
- ✓ Du, Y., Symeonidis, V., & Karniadakis, G. E. (2002). Drag reduction in wall-bounded turbulence via a transverse travelling wave. Journal of Fluid Mechanics, 457, 1-34.
- ✓ Frisch, U. (1995). Turbulence: the legacy of AN Kolmogorov, University press, Cambridge.
- ✓ Gampert, B., & Yong, C. K. (1990). The influence of polymer additives on the coherent structure of turbulent channel flow. In Structure of turbulence and drag reduction (pp. 223-232). Springer Berlin Heidelberg.
- ✓ Germano, M., Piomelli, U., Moin, P., & Cabot, W. H. (1991). A dynamic subgrid-scale eddy viscosity model. Physics of Fluids A: Fluid Dynamics (1989-1993), 3(7), 1760-1765.
- ✓ Giles, W. B., & Pettit, W. T., Stability of dilute viscoelastic flows, Nature 216, 470 - 472.

- ✓ Gupta, V. K., Sureshkumar, R., & Khomami, B. (2005). Passive scalar transport in polymer drag-reduced turbulent channel flow. AIChE Journal, 51(7), 1938-1950.
- ✓ Gyr, A., & Bewersdorff, H. W. (1990). Change of structures close to the wall of a turbulent flow in drag reducing fluids. In Structure of Turbulence and Drag Reduction (pp. 215-222). Springer Berlin Heidelberg.
- ✓ Hinch, E. J. (1977). Mechanical models of dilute polymer solutions in strong flows. Physics of Fluids (1958-1988), 20(10), S22-S30.
- ✓ Housiadas, K. D., Beris, A. N., & Handler, R. A. (2005). Viscoelastic effects on higher order statistics and on coherent structures in turbulent channel flow.Physics of Fluids (1994-present), 17(3), 035106.
- ✓ Housiadas, K. D., & Beris, A. N. (2003). Polymer-induced drag reduction: Effects of the variations in elasticity and inertia in turbulent viscoelastic channel flow. Physics of Fluids (1994-present), 15(8), 2369-2384.
- ✓ Hoyt, J. W. (1972). A Freeman Scholar Lecture: The Effect of Additives on Fluid Friction. Journal of Fluids Engineering, 94(2), 258-285.
- ✓ Iaccarino, G., Shaqfeh, E. S., & Dubief, Y. (2010). Reynolds-averaged modeling of polymer drag reduction in turbulent flows. Journal of Non-Newtonian Fluid Mechanics, 165(7), 376-384.
- ✓ Itoh, M., Tamano, S., Yokota, K., & Taniguchi, S. (2006). Drag reduction in a turbulent boundary layer on a flexible sheet undergoing a spanwise traveling wave motion. Journal of Turbulence, (7), N27.
- ✓ Jung, W. J., Mangiavacchi, N., & Akhavan, R. (1992). Suppression of turbulence in wall-bounded flows by high-frequency spanwise oscillations.Physics of Fluids A: Fluid Dynamics (1989-1993), 4(8), 1605-1607.
- ✓ Kays, W. M. (1994). Turbulent Prandtl number—where are we?. Journal of Heat Transfer, 116(2), 284-295.
- ✓ Oertel, H. (2010). Convective Heat and Mass Transfer (pp. 409-453). Springer New York.
- ✓ Kasagi, N., Tomita, Y., & Kuroda, A. (1992). Direct numerical simulation of passive scalar field in a turbulent channel flow. Journal of heat transfer, 114(3), 598-606.
- ✓ Kawaguchi, Y., Segawa, T., Feng, Z., & Li, P. (2002). Experimental study on drag-reducing channel flow with surfactant additives—spatial structure of turbulence investigated by PIV system. International Journal of Heat and Fluid Flow, 23(5), 700-709.
- ✓ Kawaguchi, Y., Wei, J., Yu, B., & Feng, Z. (2003, January). Rheological Characterization of Drag-Reducing Cationic Surfactant Solution: Shear and Elongational Viscosities of Dilute Solutions. In ASME/JSME 2003 4th Joint

Fluids Summer Engineering Conference (pp. 721-728). American Society of Mechanical Engineers.

- ✓ Kim, K., Adrian, R. J., Balachandar, S., & Sureshkumar, R. (2008). Dynamics of hairpin vortices and polymer-induced turbulent drag reduction. Physical review letters, 100(13), 134504.
- ✓ Kim, K., Li, C. F., Sureshkumar, R., Balachandar, S., & Adrian, R. J. (2007). Effects of polymer stresses on eddy structures in drag-reduced turbulent channel flow. Journal of Fluid Mechanics, 584, 281-299.
- ✓ Launder, B. E., Reece, G. J., & Rodi, W. (1975). Progress in the development of a Reynolds-stress turbulence closure. Journal of fluid mechanics, 68(03), 537-566.
- ✓ Laadhari, F. (2007). Reynolds number effect on the dissipation function in wall-bounded flows. Physics of Fluids (1994-present), 19(3), 038101.
- ✓ Leighton, R., Walker, D. T., Stephens, T., & Garwood, G. (2003, January). Reynolds stress modeling for drag reducing viscoelastic flows. In ASME/JSME 2003 4th Joint Fluids Summer Engineering Conference (pp. 735-744). American Society of Mechanical Engineers.
- ✓ Lesieur, M., Métais, O., & Comte, P. (2005). Large-eddy simulations of turbulence, Journal of fluid mechanics, 555, 474.
- ✓ Lien, F. S., & Durbin, P. A. (1996). Non-linear k–v2f modelling with application to high-lift. Proceedings of the Summer Program Centre for Turbulence Research. Stanford University, 5-22.
- ✓ Lai, Y. G., & So, R. M. C. (1990). Near-wall modeling of turbulent heat fluxes. International Journal of Heat and Mass Transfer, 33(7), 1429-1440.
- ✓ Li, C. F., Sureshkumar, R., & Khomami, B. (2006). Influence of rheological parameters on polymer induced turbulent drag reduction. Journal of Non-Newtonian Fluid Mechanics, 140(1), 23-40.
- ✓ Li, C. F., Gupta, V. K., Sureshkumar, R., & Khomami, B. (2006). Turbulent channel flow of dilute polymeric solutions: drag reduction scaling and an eddy viscosity model. Journal of Non-Newtonian Fluid Mechanics, 139(3), 177-189.
- ✓ Lilly, D. K. (1962). On the numerical simulation of buoyant convection. Tellus A, Volume 14, Issue 2, pages 148–172.
- ✓ Lu, W., Wei-Hua, C., & Feng-Chen, L. (2014). Large-eddy simulations of a forced homogeneous isotropic turbulence with polymer additives. Chinese Physics B, 23(3), 034701.
- ✓ Lumley, J. L. (1969). Drag reduction by additives. Annual Review of Fluid Mechanics, 1(1), 367-384.
- ✓ Lumley, J. L. Drag reduction in turbulent flow by polymer additives, Journal of Polymer Science 7 (1973) 263–290.
- ✓ Malin, M. R. (1998). Turbulent pipe flow of Herschel-Bulkley fluids. International Communications in Heat and Mass Transfer, 25(3), 321-330.

- ✓ Malin, M. R. (1997). Turbulent pipe flow of power-law fluids. International Communications in Heat and Mass Transfer, 24(7), 977-988.
- ✓ Masoudian, M., Kim, K., Pinho, F. T., & Sureshkumar, R. (2013). A viscoelastic turbulent flow model valid up to the maximum drag reduction limit. Journal of Non-Newtonian Fluid Mechanics, 202, 99-111.
- ✓ Masoudian, M., Kim, K., Pinho, F. T., & Sureshkumar, R. (2015). A Reynolds stress model for turbulent flow of homogeneous polymer solutions. International Journal of Heat and Fluid Flow, 54, 220-235.
- ✓ McComb, W. D., & Rabie, L. H. (1982). Local drag reduction due to injection of polymer solutions into turbulent flow in a pipe. Part I: Dependence on local polymer concentration. AIChE Journal, 28(4), 547-557.
- ✓ McComb, W. D., & Rabie, L. H. (1979). Development of local turbulent drag reduction due to nonuniform polymer concentration. Physics of Fluids (1958-1988), 22(1), 183-185.
- ✓ Min, T., Yul Yoo, J., Choi, H., & Joseph, D. D. (2003). Drag reduction by polymer additives in a turbulent channel flow. Journal of Fluid Mechanics, 486, 213-238.
- ✓ Mito, Y., & Kasagi, N. (1998). DNS study of turbulence modification with streamwise-uniform sinusoidal wall-oscillation. International Journal of Heat and Fluid Flow, 19(5), 470-481.
- ✓ Monin, A. S., ÎAglom, A. M., & Lumley, J. L. (2007). Statistical fluid mechanics: mechanics of turbulence (Vol. 1). Courier Corporation.
- ✓ Ohta, T., & Miyashita, M. (2014). DNS and LES with an extended Smagorinsky model for wall turbulence in non-Newtonian viscous fluids. Journal of Non-Newtonian Fluid Mechanics, 206, 29-39.
- ✓ Oliver, T. A., Malaya, N., Ulerich, R., & Moser, R. D. (2014). Estimating uncertainties in statistics computed from direct numerical simulation. Physics of Fluids (1994-present), 26(3), 035101.
- ✓ Oldaker, D. K., & Tiederman, W. G. (1977). Spatial structure of the viscous sublayer in drag-reducing channel flows. Physics of Fluids (1958-1988), 20(10), S133-S144.
- ✓ Orszag, S. A. (1970). Analytical theories of turbulence. Journal of Fluid Mechanics, 41(02), 363-386.
- ✓ Pang, J., & Choi, K. S. (2004). Turbulent drag reduction by Lorentz force oscillation. Physics of Fluids (1994-present), 16(5), L35-L38.
- ✓ Pinho, F. T., Li, C. F., Younis, B. A., & Sureshkumar, R. (2008). A low Reynolds number turbulence closure for viscoelastic fluids. Journal of Non-Newtonian Fluid Mechanics, 154(2), 89-108.

- ✓ Pinho, F. T. (2003). A GNF framework for turbulent flow models of drag reducing fluids and proposal for a k–ε type closure. Journal of Non-Newtonian Fluid Mechanics, 114(2), 149-184.
- ✓ Pinho, F. T., Li, C. F., Younis, B. A., & Sureshkumar, R. (2008). A low Reynolds number turbulence closure for viscoelastic fluids. Journal of Non-Newtonian Fluid Mechanics, 154(2), 89-108.
- ✓ Piomelli, U., Cabot, W. H., Moin, P., & Lee, S. (1991). Subgrid-scale backscatter in turbulent and transitional flows. Physics of Fluids A: Fluid Dynamics (1989-1993), 3(7), 1766-1771.
- ✓ Piomelli, U., Yu, Y., & Adrian, R. J. (1996). Subgrid-scale energy transfer and near-wall turbulence structure. Physics of Fluids (1994-present), 8(1), 215-224.
- ✓ Poole, R. J., & Escudier, M. P. (2003). Turbulent flow of non-Newtonian liquids over a backward-facing step: Part II. Viscoelastic and shear-thinning liquids. Journal of Non-Newtonian Fluid Mechanics, 109(2), 193-230.
- ✓ Hassid, S., & Poreh, M. (1978). A turbulent energy dissipation model for flows with drag reduction. Journal of Fluids Engineering, 100(1), 107-112.
- ✓ Ptasinski, P. K., Boersma, B. J., Nieuwstadt, F. T. M., Hulsen, M. A., Van den Brule, B. H. A. A., & Hunt, J. C. R. (2003). Turbulent channel flow near maximum drag reduction: simulations, experiments and mechanisms. Journal of Fluid Mechanics, 490, 251-291.
- ✓ Procaccia, I., L'vov, V. S., & Benzi, R. (2008). Colloquium: Theory of drag reduction by polymers in wall-bounded turbulence. Reviews of Modern Physics,80(1), 225.
- ✓ Pope, S. B. (2000). Turbulent flows. University press, Cambridge.
- ✓ Quadrio, M., Ricco, P., & Viotti, C. (2009). Streamwise-travelling waves of spanwise wall velocity for turbulent drag reduction. Journal of Fluid Mechanics,627, 161-178.
- ✓ Resende, P. R., Kim, K., Younis, B. A., Sureshkumar, R., & Pinho, F. T. (2011). A FENE-P k–ε turbulence model for low and intermediate regimes of polymer-induced drag reduction. Journal of Non-Newtonian Fluid Mechanics,166(12), 639-660.
- ✓ Resende, P. R., Pinho, F. T., & Cruz, D. O. (2013). A Reynolds stress model for turbulent flows of viscoelastic fluids. Journal of Turbulence, 14(12), 1-36.
- ✓ Resende, P. R., Escudier, M. P., Presti, F., Pinho, F. T., & Cruz, D. O. A. (2006). Numerical predictions and measurements of Reynolds normal stresses in turbulent pipe flow of polymers. International Journal of Heat and Fluid Flow,27(2), 204-219.
- ✓ Roiter, Y., & Minko, S. (2005). AFM single molecule experiments at the solid-liquid interface: in situ conformation of adsorbed flexible polyelectrolyte chains. Journal of the American Chemical Society, 127(45), 15688-15689.

- ✓ Ryskin, G. (1987). Turbulent drag reduction by polymers: a quantitative theory. Physical Review Letters, 59(18), 2059.
- ✓ SAIF, M. T. A., JOSEPH, D., Riccius, O., & Christodoulou, C. (1990). Drag reduction in pipes lined with riblets. AIAA Journal, 28(10), 1697-1698.
- ✓ Segawa, T., Mizunuma, H., Murakami, K., Li, F. C., & Yoshida, H. (2007). Turbulent drag reduction by means of alternating suction and blowing jets. Fluid Dynamics Research, 39(7), 552-568.
- ✓ Seyer, F. A., & Metzner, A. B. (1969). Turbulence phenomena in drag reducing systems. AIChE Journal, 15(3), 426-434.
- ✓ Shima, N. (1988). A Reynolds-stress model for near-wall and low-Reynolds-number regions. Journal of Fluids Engineering, 110(1), 38-44.
- ✓ Smagorinsky, J. (1963). General circulation experiments with the primitive equations: I. the basic experiment. Monthly Weather Review, 91(3), 99-164.
- ✓ Smith, A., & Cebeci, T. (1967). Numerical Solution of the Turbulent-boundary-layer Equations (No. DAC-33735). Douglas Aircraft Co Inc Long Beach Calif Aircraft Div.
- ✓ Spalart, P. R., & Allmaras, S. R., A one-equation turbulence model for aerodynamic flows, AIAA 01/1992; 439(1).
- ✓ Speziale, C. G., Sarkar, S., & Gatski, T. B. (1991). Modeling the pressure–strain correlation of turbulence: an invariant dynamical systems approach. Journal of Fluid Mechanics, 227, 245-272.
- ✓ Sreenivasan, K. R., & White, C. M. (2000). The onset of drag reduction by dilute polymer additives, and the maximum drag reduction asymptote. Journal of Fluid Mechanics, 409, 149-164.
- ✓ Sureshkumar, R., Beris, A. N., & Handler, R. A. (1997). Direct numerical simulation of the turbulent channel flow of a polymer solution. Physics of Fluids (1994-present), 9(3), 743-755.
- ✓ Tabor, M., & De Gennes, P. G. (1986). A cascade theory of drag reduction. EPL (Europhysics Letters), 2(7), 519.
- ✓ Tennekes, H., & Lumley, J. L. (1972). A first course in turbulence. MIT Press, Massachusett.
- ✓ Tiederman, W. G., Luchik, T. S., & Bogard, D. G. (1985). Wall-layer structure and drag reduction. Journal of Fluid Mechanics, 156, 419-437.
- ✓ Toms, B. A. (1948, September). Some observations on the flow of linear polymer solutions through straight tubes at large Reynolds numbers. In Proceedings of the 1st International Congress on Rheology (Vol. 2, pp. 135-141).
- ✓ Tsukahara, T., & Kawaguchi, Y. (2013). Proposal of Damping Function for Low-Reynolds-Number-Model Applicable in Prediction of Turbulent Viscoelastic-Fluid Flow. Journal of Applied Mathematics, 2013.

- ✓ Thais, L., Tejada-Martinez, A. E., Gatski, T. B., & Mompean, G. (2010). Temporal large eddy simulations of turbulent viscoelastic drag reduction flows. Physics of Fluids (1994-present), 22(1), 013103.
- ✓ Thais, L., Gatski, T. B., & Mompean, G. (2013). Analysis of polymer drag reduction mechanisms from energy budgets. International Journal of Heat and Fluid Flow, 43, 52-61.
- ✓ Thais, L., Gatski, T. B., & Mompean, G. (2012). Some dynamical features of the turbulent flow of a viscoelastic fluid for reduced drag. Journal of Turbulence, (13), N19.
- ✓ Vaithianathan, T., & Collins, L. R. (2003). Numerical approach to simulating turbulent flow of a viscoelastic polymer solution. Journal of Computational Physics, 187(1), 1-21.
- ✓ Virk, P. S. (1971). An elastic sublayer model for drag reduction by dilute solutions of linear macromolecules. Journal of Fluid Mechanics, 45(03), 417-440.
- ✓ Virk, P. S. (1975). Drag reduction fundamentals. AIChE Journal, 21(4), 625-656.
- ✓ Wallin, S., & Johansson, A. V. (2000). An explicit algebraic Reynolds stress model for incompressible and compressible turbulent flows. Journal of Fluid Mechanics, 403, 89-132.
- ✓ Walker, D. T., & Tiederman, W. G. (1990). Turbulent structure in a channel flow with polymer injection at the wall. Journal of Fluid Mechanics, 218, 377-403.
- ✓ Warner Jr, H. R. (1972). Kinetic theory and rheology of dilute suspensions of finitely extendible dumbbells. Industrial & Engineering Chemistry Fundamentals, 11(3), 379-387.
- ✓ Warholic, M. D., Massah, H., & Hanratty, T. J. (1999). Influence of drag-reducing polymers on turbulence: effects of Reynolds number, concentration and mixing. Experiments in Fluids, 27(5), 461-472.
- ✓ White, C. M., & Mungal, M. G. (2008). Mechanics and prediction of turbulent drag reduction with polymer additives. Annual Review of Fluid Mechanics, 40, 235-256.
- ✓ Wei, T., & Willmarth, W. W. (1992). Modifying turbulent structure with drag-reducing polymer additives in turbulent channel flows. Journal of Fluid Mechanics, 245, 619-641.
- ✓ Xi, L., & Graham, M. D. (2010). Active and hibernating turbulence in minimal channel flow of Newtonian and polymeric fluids. Physical Review Letters,104(21), 218301.
- ✓ Yu, B., & Kawaguchi, Y. (2005). DNS of fully developed turbulent heat transfer of a viscoelastic drag-reducing flow. International Journal of Heat and Mass Transfer, 48(21), 4569-4578.

✓ Zhou, Q., & Akhavan, R. (2003). A comparison of FENE and FENE-P dumbbell and chain models in turbulent flow. Journal of Non-Newtonian fluid mechanics, 109(2), 115-155.